Department of Materials

Development of 9 wt.% Cr Steels for Next Generation Power Plant

Ryan MacLachlan

Department of Materials

Loughborough University

A doctoral thesis submitted in partial fulfilment

of the requirements for the award of

Doctor of Philosophy

August 2014

ACKNOWLEDGEMENTS

I would like to thank my project supervisor Professor Rachel Thomson for her guidance, encouragement, inspiration and friendship throughout this project. In addition I would also like to thank Dr. Mark Jepson and Dr. Geoff West for their continuous support throughout this project.

I would like to acknowledge the support of the Technology Strategy Board (Project Number TP11/CAT/6/I/BP074G) and the following companies: Alstom Power Ltd, E.ON, Doosan Babcock, Goodwins Steel Castings and the National Physical Laboratory for their continuous valuable contributions to the project.

I would like to acknowledge Alstom Power Ltd and Doosan Babcock who have carried out the creep testing presented within this research and E.ON for conducting the creep data analysis.

I would also like to thank Mr. S. Doak and all the members of Loughborough Materials Characterisation Centre (LMCC). I am extremely grateful to all the staff from LMCC who have provided support and invaluable technical support whilst using the microscopes within the Centre.

I would like to thank all of the staff within the Department of Materials and all the students within the Energy Materials Research Group who have helped me over the course of this project and also created an enjoyable working environment.

Finally I am extremely grateful to Mary Tierney for her constant source of encouragement and patience, and my parents for their enthusiasm and support.

ABSTRACT

There is a need to increase the thermal efficiency of coal fired power plants. High chromium ferritic steels have historically been used to manufacture steam pipes, tube and headers. Over the last forty years there has been a continuous development of the 9 – 12 wt. % chromium martensitic alloys which has allowed the service temperature to be increased from 510°C – 550°C[1]. There is now a high demand for Ultra Super Critical coal fired power plants which operate at 650°C and hence have an increased thermal efficiency. The aim of this research project was to develop a MarBN steel (Martensitic Steel Strengthened with Boron and Nitrides) with an optimised composition in order to allow MarBN to be used at 650°C. In order for MarBN to be used within high temperature applications it is vital to understand how microstructural changes can have an impact on their creep strength. This is a key area that the present research has focused upon. The long term creep strength of 9 wt. % chromium ferritic steels is derived from the stability of the microstructure over its service life, which has a direct relationship to the stability of the precipitates and the lath structure within the microstructure.

In order to develop MarBN, thermodynamic calculations were initially used to model the phases predicted to be present. The key experimental work focussed on understanding how the pre-service normalising and tempering heat treatments affected the phases observed to be present within the microstructure. Further experimental work was subsequently carried out to understand how the microstructure of MarBN changes as a function of isothermal ageing, and similarly how small changes in the chemical composition can affect the number, size and distribution of phases observed to be present during long term isothermal ageing.

Thermodynamic calculations were performed to optimise the composition of MarBN. The chemical composition of standard MarBN was used as an initial input into Thermocalc, which was subsequently used to predict the phases present. A stability study was carried out by adjusting a number of elements at the expense of iron, then subsequently analysing the effect on the stability of phases, such as M_2B, $M_{23}C_6$, Laves Phase and Z phase. The thermodynamic calculations were also used to predict the formation and dissolution temperatures of a number of phases, such as delta ferrite and boron nitride. The thermodynamic calculations were used as an aid to develop an optimised composition of MarBN. The phases which are beneficial within the system were maximised, whereas the

phases which are thought to be detrimental to the creep properties were minimised. In total eight alloys were manufactured based on the thermodynamic calculations and were subsequently creep tested.

In order to maximise the creep properties of the MarBN alloys manufactured during this research, the pre-service normalising and tempering heat treatments were optimised. This was carried out using advanced microstructural characterisation which was verified with the use of short term creep tests. It has been observed that boron nitride is widely present after normalising at 1150°C. The processing conditions were observed to have a significant impact on the area percentage of this phase. It has been identified that a high temperature normalising heat treatment can be used to reduce the amount of boron nitride, which indicates that boron can be dissolved back into solution. Upon tempering, a higher number density of $M_{23}C_6$ carbides was observed when boron was in solution. Furthermore the normalising temperature was observed to have a direct impact on the type of MX carbonitrides precipitated during tempering. When boron is in solution there was observed to be a distribution of both vanadium nitride (VN) and niobium carbide (NbC). In comparison, when no boron was in solution, only NbC was observed to be present. Short term creep tests indicate that superior creep properties can be obtained when boron is within solution.

In order to predict the degradation of MarBN in service, long term isothermal ageing was carried out in order to study the evolution behaviour of $M_{23}C_6$, Laves phase, BN, M_2B and the martensitic matrix. After long term ageing (10,000 hours) EBSD was used to characterise the grain structure, and the martensitic laths were observed to coarsen marginally. It was observed that the number density of $M_{23}C_6$ precipitates increased during short term ageing, and the precipitates were found to subsequently coarsen during long term ageing. When boron was in solution there was an increased number density of finer $M_{23}C_6$ precipitates precipitated during short term ageing. In addition, during long term ageing the coarsening rate of the $M_{23}C_6$ carbides was observed to be reduced. Laves phase was observed to coarsen as a function of isothermal ageing and be independent of the nature of the boron addition within the alloy.

The effect of cobalt on the phases observed to be present within the microstructure after a pre-service normalising and tempering heat treatment was investigated. The characterisation has shown that increasing the cobalt content increases the hardness and also the number density of $M_{23}C_6$ precipitates. Long term isothermal heat treatments were carried out on

samples with different cobalt contents. It was observed that after 10,000 hours the number density and size of $M_{23}C_6$ precipitates were similar in both alloys. EBSD analysis was carried out to study the degradation of the martensitic microstructure. Cobalt was not found to influence the degradation of the microstructure after long term isothermal ageing.

Finally, the ability to manufacture MarBN on a commercial scale was demonstrated. The project has shown that the properties of MarBN can be achieved using a chemical composition range and has highlighted that nitrogen is the key element which needs to be controlled during the steel making process. Furthermore an 8 tonne melt was manufactured using an Argon oxygen decarburization steel making technique here after known as (AOD), which is one of the most common melting processes used to manufacture other 9 wt. % chromium steels such as P91 and P92. The demonstration casting has provided evidence that the properties obtained on a small scale can be replicated in an industrial environment. The demonstrator tube designed as an integral part of this project has recently been installed in an operating power plant.

PUBLICATIONS

Part of this work has been published, or is due to be published in the near future, details are shown below:

R.C. MacLachlan, J.J. Sanchez-Hanton and R.C. Thomson, "*The effect of simulated post weld heat treatment temperature overshoot on microstructural evolution in P91 and P92 power plant steels"*, Presented at the 6th International Conference on Advances in Materials Technology for Fossil Power Plants La Fonda, Santa Fe, New Mexico, USA, August 31st – September 3rd, 2010

Li, L., MacLachlan, R. C., Jepson, M. A. E., & Thomson, R. C. (2013). Microstructural Evolution of Boron Nitride Particles in Advanced 9Cr Power Plant Steels. *Metallurgical and Materials Transactions A: Physical Metallurgy and Materials Science*,*44*(7), 3411-3418

R.C. MacLachlan, C. Dyson, L. Li and R.C. Thomson, *"The Influence of Cobalt on Microstructural Evolution in 9 wt.% Cr Power Plant Steels"* presented at Energy Materials: High Temperature Materials Conference, Loughborough University, 2012 and to be submitted to Metallurgical and Materials Transactions A, 2014

R.C. MacLachlan and R.C. Thomson, *"Effect of Pre-Service Heat Treatments on the Creep Strength of MarBN alloys"*, In preparation for submission to Materials Science and Engineering: A

CONTENTS

Chapter One

INTRODUCTION

1.1 Background

During recent years there have been a number of significant drivers to improve the efficiency and subsequent emissions of fossil fuelled power plants. A standard subcritical coal fired power plant operates at an efficiency of ~37%, whereas a supercritical power plant operates at a higher efficiency of ~42%[1]. In order to improve the efficiency, the steam temperature within the system increases from 580°C to 600°C which subsequently results in an increased steam pressure of between 25 and 30 MPa (250 – 300 bar)[1]. Supercritical power plants reduce the amount of harmful emissions emitted into the environment because less fuel is burnt to generate the same amount of electricity[2]. There is on-going demand to reduce emissions that are produced from fossil fuelled power plants; one such mechanism is the implementation of carbon capture and storage technology, hereafter known as CCS. Although CCS can provide a significant reduction in the emissions released into the environment, the system also consumes a significant amount of energy from the power plant. This enhances the driver for a higher efficiency coal fired power plant.

The demand for new power plants has fluctuated as a function of time, as shown in Figure 1.1. The demand is thought to be influenced by economic, political and technological advances. Over the last forty years key events such as the US boom, China boom, and Global boom have all had an influence on the number of new power plants ordered, as shown in Figure 1.1. There is currently a significant decrease in the demand for new power plants, which has been influenced by the global recession.

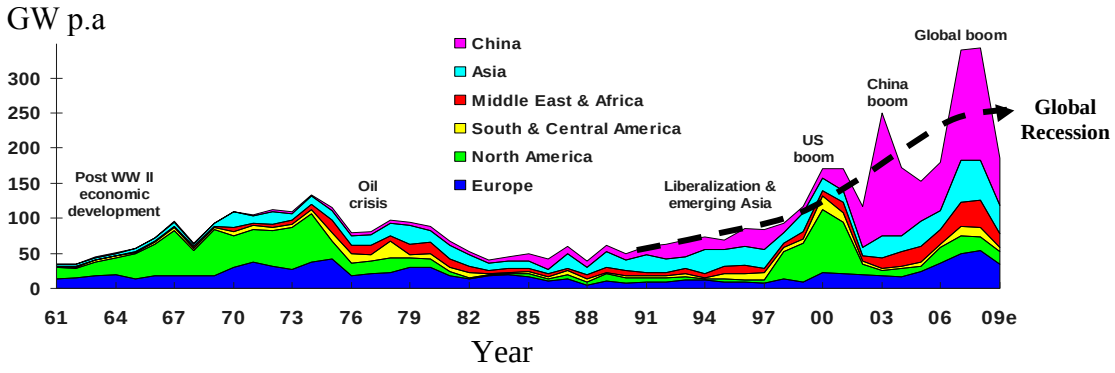

Figure 1.1: *A graph showing the amount of new power plant orders in GW p.a, as a function of time and region.*[3]

The technology each country uses to generate electricity can vary significantly depending on the country's political policies and also the resources available a particular country. The overall wealth of the country can also have an influence on the generation method. In China there is widespread construction of subcritical coal fired power plants because this allows electricity to be generated using a relatively simple and well understood technology and there is a suitable supply of coal.

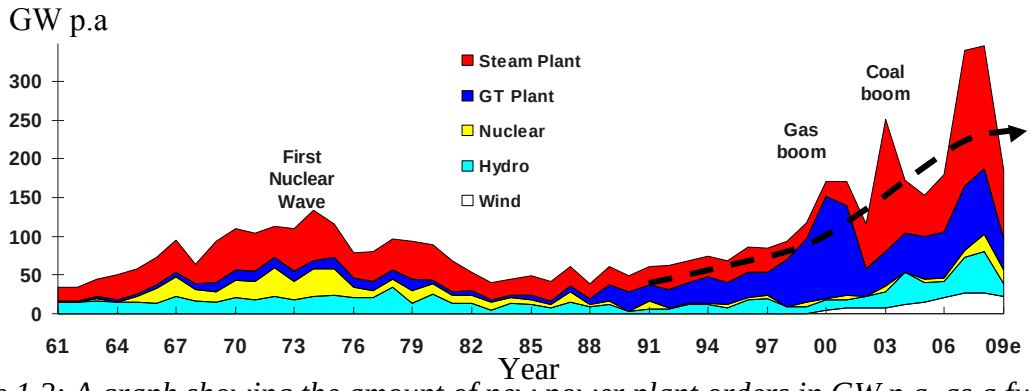

Figure 1.2: A graph showing the amount of new power plant orders in GW p.a, as a function of time and technoldgy.[3]

Figure 1.2 shows a graph of the new power plants ordered as a function of time and technology; it is evident that there is a significant proportion of new power plants manufactured using renewable technology. However, there is still a considerable proportion (~75%) of the new power plants still being manufactured using steam technology.

1.2 Supercritical Fossil Fuel Technology

There is a demand for next generation fossil fuelled power plants to be manufactured which are more efficient. To increase the efficiency of such power plant the steam temperature and pressure are required to be increased[4]. One of the options is to use supercritical fossil fuel technology. Fossil fuel power plants typically use the Rankine cycle for the generation of electricity from coal, as shown in Figure 1.3. The Rankine cycle shows a closed loop system in which a fuel is burned to produce heat, which in turn produces steam. The steam then drives the turbine to produce mechanical energy, which is then converted into electrical energy using an alternator[5]. The efficiency of the Rankine cycle is limited by the pressure of

the fluid within the system. The theoretical efficiency of such a cycle is 63%, whereas the typical efficiency of a coal fired power plant is ~35%.

In a supercritical power plant the operating pressure is higher than the critical pressure of the fluid. This results in an increased efficiency of the Rankine cycle due to the increased pressure within the system.

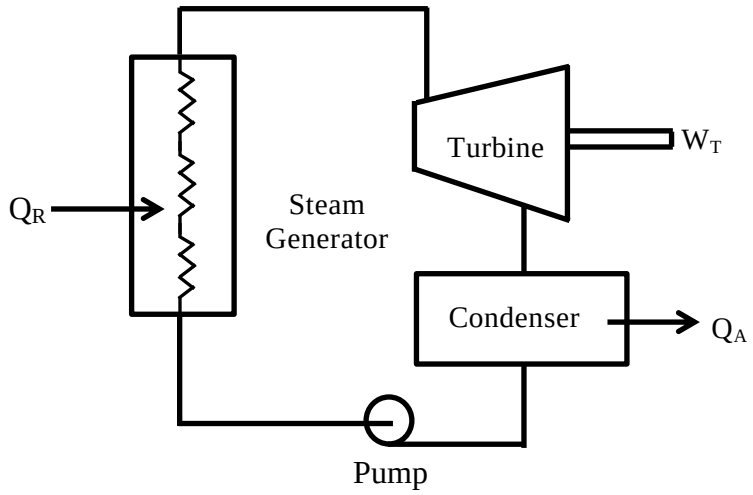

W_T = Work transferred from Working Fluid, in Turbine
Q_R = Heat Transferred to Working Fluid, in Steam Generator
Q_A = Heat Rejected by Working Fluid, in Condenser

Figure 1.3: A schematic diagram of the Rankine Cycle, after Selwin Rajadurai.[6]

1.3 The Need for Improved Materials

9 wt. % Cr steel grades P91 and P92 are the current materials used for the steam boiler tubing within a modern coal fired power plant. These alloys cannot be safely operated at the steam temperature required for supercritical technology to be used. This is the key reasons why supercritical fossil fuel technology is not used in European countries. One solution is to develop or modify an alloy to ensure the plant can be safely operated at a higher service temperature and operating pressure. Over the last forty years there has been a continuous development of the 9 – 12 wt. % chromium martensitic alloys which has allowed the service temperature to be increased from 510°C – 550°C[1]. Section 1.4 provides a review of the development of 9 – 12 wt. % chromium steels over the last forty years.

1.4 Previous Development of 9 – 12% Cr Martensitic Steels

9 – 12% wt. % chromium ferritic alloys are used for boiler tubing within subcritical power plants. Ferritic alloys have similar rupture strength and oxidation resistance to that of

austenitic stainless steel. However, the main reason there is continuous development in ferritic alloys is because the coefficient of thermal expansion has been shown to be ~50%[7] lower in comparison to austenitic alloys.

The development of ferritic alloys has been on-going since the first 9 – 12% wt.% chromium steel was used, denoted as P9. The next major development was P91 in the 1970's at Oak Ridge National Laboratory. The development of P91 was carried out by modifying a 9 wt. % chromium steel classed as grade P9. This change was achieved by the addition of 0.2 wt. % niobium, 0.06 wt. % niobium and 0.05 wt. % nitrogen[1]. Since the development of P91, a number of alloys have been developed such as P92, E911 and the newly developed 9Cr-3W-3Co-V-Nb-B-N alloy, known as MarBN steel.

The next major development was in 1991 and this was obtained by modifying grade 91 steel. This grade was developed in Japan by Nippon steel and was classed as grade 92 steel. The increased creep properties were achieved by the addition of 1.8 wt. % tungsten and a reduction of molybdenum to 0.5 wt. %[1].

Further improvements in the alloy design are required to allow ultra-supercritical power plants to operate safely at the target operating temperature of 650°C. The National Institute for Materials Science (NIMS, Japan) have recently developed a 9Cr-3W-3Co-V-Nb-B-N alloy that provides improved creep properties and therefore indicates that this material could be a candidate material for such applications[8].

The development of 9 wt. % chromium steels has allowed power plants to operate at a higher service temperature and the plant to operate at higher efficiencies. The development of P91 allowed the service temperature to be increased from 545°C to 585°C[1]. P92 allowed the maximum service temperature to be increased further from 585°C to 610°C.

9 – 12 wt. % chromium steels have a complex microstructure. They have been reported to comprise of a martensitic matrix, which contains a high dislocation density[9]. The steels are strengthened by solid solution strengthening with molybdenum and tungsten[10]. The most recent alloys developed such as P92 have additions of niobium, vanadium and chromium which on tempering produce carbide and nitride precipitates[9]. $M_{23}C_6$ precipitates are chromium rich which have been reported to be found on the prior austenite and lath boundaries[2]. Vanadium nitride (VN) and niobium carbide (NbC) have been reported to be significantly smaller precipitates, which precipitate within the martensitic laths[11].

The addition of boron into 9 – 12 wt. % has been reported to enrich the volume near the $M_{23}C_6$ carbides and therefore reduce the coarsening rate of $M_{23}C_6$. Decreasing the rate at which the $M_{23}C_6$ carbides coarsen is thought to improve the long term microstructural stability[7]. The disadvantage of the boron addition is that it is a strong nitride former and large boron nitride particles can form. The boron and nitrogen contents need to be carefully optimised to ensure that boron nitride is not precipitated throughout the microstructure[12]. The precipitation of boron nitride can offset the beneficial effect of the boron and nitrogen addition and can decrease the creep properties of the steel[8].

1.5 Project Overview

A number of R & D projects have been launched in Japan, the USA and Europe to overcome the issue that there is no current material that can be used for the steam tubing within a fossil fuelled power plant at a reasonable cost[13]. The UK has also initiated a project with the aim of developing MarBN steels for its use in a ultra-supercritical power plant. The project is called IMPACT (Innovative Materials, Design and Monitoring of Power Plant to Accommodate Carbon Capture) funded by the Technology Strategy Board. The programme is a collaboration of a number of companies; Doosan Power Systems, EON New Build & Technology, Goodwin Steel Castings, Alstom Power and the National Physics Laboratory together with Loughborough University.

This research project has formed part of the IMPACT project, which since January 2011 developed an optimised chemical composition of MarBN steel and has assessed its mechanical properties at high temperature. Microstructural characterisation has been carried out throughout the project to aid the development of the chemical composition and alloys heat treatment parameters. During the project a commercial scale casting was manufactured to assess whether such alloys can be manufactured on a commercial scale using an Argon Oxygen Decarburization (AOD) process. Finally a MarBN tube has been manufactured during the project and will be installed into a coal fired power plant to assess its degradation over time in the near future.

The IMPACT project has been split into seven work packages; 1 Materials Development, 2 Materials Production, 3 Welding Development, 4 Materials Testing and Assesment, 5 Component Monitoring Technologies, 6 Welding Design and 7 Component Demonstration. The work reported in this thesis is split across a number of work packages, but provides a detailed explanation about the alloy development and microstructural characterisation.

1.6 Organisation of the Thesis

The thesis has been divided into ten chapters. Chapter 2 consists of a literature review of 9 – 12 wt. % Chromium steels. The literature review focuses on reviewing the previous alloy development and the physical metallurgy of 9 – 12 wt. % chromium ferritic martensitic steels.

Chapter 3 discusses the experimental procedures used during this research. The chapter describes the chemical compositions of the steels developed. The chapter also provides a detailed description of all the heat treatments carried out and microstructural techniques used throughout the project, together with a detailed description of the instrument parameters used.

In Chapter 4, a study has been carried out using thermodynamic calculations to determine the optimum chemical composition of a MarBN alloy. The optimum chemical composition was determined by maximising the beneficial phases predicted to be present and minimising the detrimental phases. The first part of the study focusses on investigating the effect of alloying elements on the stability of the phases predicted to be present. The second part of the chapter focusses on investigating the effect of chemical compositions on the formation of delta ferrite and boron nitride.

Chapter 5 quantifies the phase transformations using dilatometry and other experimental techniques of a number of optimised MarBN alloys developed in Chapter 4 using thermodynamics. The chapter discusses measurements of the Ac_1, Ac_3 and Ms transformation temperatures and compares the results to the thermodynamic calculations.

Chapter 6 focuses on optimising the pre-service normalising and tempering heat treatment using one of the optimised MarBN alloys (GAM 3). Microstructural characterisation was carried out as a function of both normalising and tempering. The investigation focussed on characterising the precipitates present within the microstructure such as $M_{23}C_6$ and MX. Key attention was paid to the precipitation and dissolution of boron nitride as a function of the normalising temperature.

Chapter 7 has focussed on investigating the long term microstructural evolution of an optimised MarBN alloy (GAM 3), in conjunction with both a standard and optimised normalising heat treatments. The effect of the boron addition on the stability of precipitates such as $M_{23}C_6$ and Laves phase has been investigated. The stability of the matrix has also been investigated as a function of ageing. Creep tests were carried out as a function of both

normalising and tempering; the results have been compared to the microstructural characterisation.

Chapter 8 focusses on understanding the effects of the cobalt addition within a MarBN alloy. The effect of a small change in cobalt (0.4 wt. %) has been investigated. The microstructure has been characterised after a pre-service normalising and tempering heat treatment and after long term ageing.

In Chapter 9 the implications of the research on the commercialisation of MarBN has been reviewed. An 8 tonne MarBN casting was manufactured to demonstrate the ability for this alloy to be manufactured on a commercial scale. Microstructural characterisation has been carried out on this casting. Heat treatments were carried out to study the effects such as a slow cooling on the precipitation of phases precipitated within the microstructure.

Chapter 10 presents the conclusions from this research and makes suggestions as to further work to be carried out in the future.

Chapter Two

LITERATURE REVIEW

2.1 Phases Present in Chromium Steels

The iron – carbon equilibrium diagram is shown below in Figure 2.1. The figure shows that the alloy can contain various structures depending on the temperature and carbon concentration. The phase diagram shows that below the eutectoid temperature of 723°C the phase that exists is ferrite (α), which has a body centred cubic (BCC) structure[14]. As the alloy is heated above the eutectic temperature of 723°C austenite (γ) forms, which has a face centred cubic (FCC) structure. This transformation leads to a decrease in the alloys volume at the Ae_1 phase transformation[14] because ferrite has a BCC crystal structure. A BCC crystal structure can pack two atoms per unit cell as the transformation to austenite occurs a change to a FCC crystal structure takes place, an FCC unit cell can pack four atoms and therefore a decrease in volume occurs because the density of the atoms per unit cell changes.

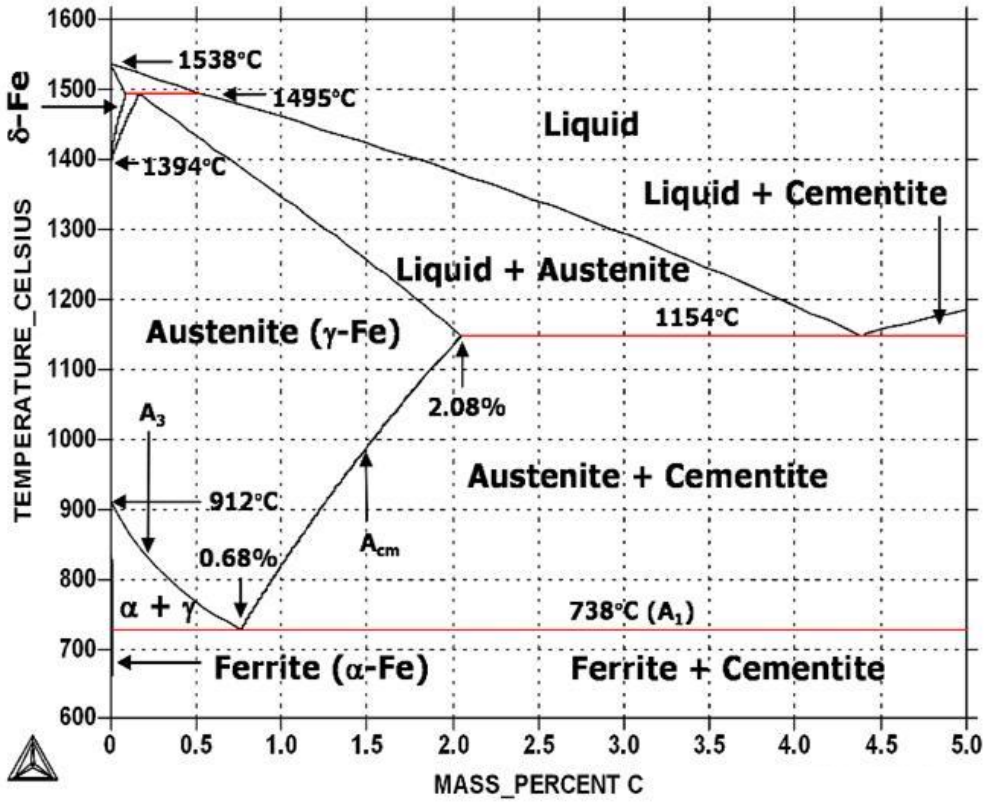

Figure 2.1: The Iron-Carbon Phase Diagram.[15]

The solubility of carbon in each phase field is very different. The austenite phase field has a maximum carbon solubility of ~2% at 1147°C, whereas the ferrite phase field has a significantly lower carbon solubility of ~0.02% at 723°C[14]. The delta ferrite region has a very restricted carbon solubility of less than 0.1%, although this is temperature dependant, as shown in Figure 2.1.

The iron – carbon phase diagram shown in Figure 2.1 shows the phase transformations that will occur under equilibrium conditions. The Ae_1 transformation occurs when iron transforms from $\alpha + Fe_3C$ to $\gamma + \alpha$. This occurs at the eutectoid temperature of 723°C in an iron – carbon binary system. The Ae_3 transformation occurs when the phase transforms from $\gamma + \alpha$ to γ in the binary system, where the transformation temperature is approximately 910°C. The Ae_4 transformation occurs when the phase transforms from γ to δ ferrite. This occurs at 1390°C in the iron – carbon binary system[14].

The iron – carbon equilibrium diagram shows the phases that exist if only iron and carbon are present. 9 wt. % chromium steels such as P91, P92 and MarBN used for steam pipe work in a power plant contain a wide range of elements, as shown in Table 2.1. Additional elements are added to improve the corrosion resistance and creep strength of the material. The addition of other elements has a major effect on the microstructure and resulting mechanical properties. The phase transformation temperatures such as Ae_1, Ae_3 and Ae_4 will be significantly different from the iron carbon binary system.

The Fe - 0.1%C - Cr equilibrium diagram shown in Figure 2.2 shows that various phases are predicted to be present under equilibrium conditions, when the system has a carbon composition of 0.1% wt. %. The system shows that various phases are predicted to exist and are a function of the temperature and chromium content. The chromium content within the steel has a major effect on the corrosion resistance and the achievable mechanical properties[16]. Figure 2.2 shows that the addition of chromium into an Fe-0.1%C-Cr system has been found to change the transformation temperatures considerably from the iron-carbon binary system.

Table 2.1: Elemental Compositions of P92, P91 and MarBN. The compositions for P91 and P92 were from Vallourec & Mannesmann tubes, the chemical composition is shown in weight %, balance Fe.[17]

	C	**Si**	**Mn**	**P**	**S**	**Cr**	**Mo**	**Ni**	**Al**
P91, Specified Composition	0.08 - 0.12	0.2 - 0.5	0.3 - 0.6	0.04 Max.	0.03 Max.	8.0 - 9.5	0.85 - 1.05	0.4 Max.	0.04 Max.
P92, Specified Composition	0.07 - 0.13	0.5 Max	0.3 – 0.6	0.02 Max.	0.05 Max.	8.5 – 9.5	0.3 – 0.6	0.4 Max.	0.04 Max.
Standard MarBN	0.08	0.5	0.46	0.009	0.005	8.92	0.12	0.16	0.005
	B	**Co**	**Cu**	**Nb**	**Sn**	**V**	**W**	**N**	
P91, Specified Composition	-	-	-	0.06 - 0.1	-	0.18 - 0.25	-	0.03 - 0.07	
P92, Specified Composition	-	-	-	0.04 - 0.09	-	0.15 - 0.25	1.5 - 2.0	0.03 - 0.07	
Standard MarBN	135 ppm	2.93	0.11	0.10	0.005	0.19	3.09	0.015	

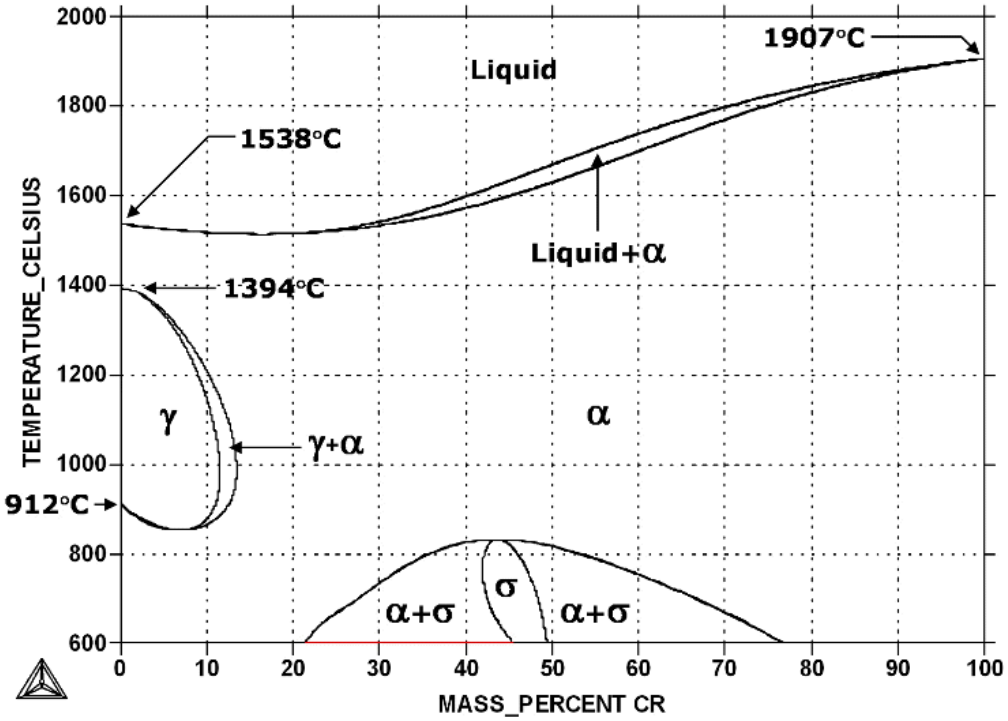

Figure 2.2: Equilibrium diagram for Fe - 0.1%C - Cr system.[15]

The Fe - 0.1%C - Cr equilibrium diagram can be used to explain the normalising and tempering heat treatments for a 9 wt. % chromium steel, such as that of grade 92 and MarBN steels. The phase diagram predicted under equilibrium conditions shows that between 820°C and 1200°C there is a very large γ (austenite) phase region[18]. The standard normalising heat

treatment for grade 92 steel is between the temperature range of 1040°C and 1080°C. MarBN steels have previously been normalised by NIMS at 1150°C[17]. The justification for increasing the normalising temperature from 1050°C to 1150°C is that there is a reduction in the number of tungsten borides precipitated within the microstructure, which therefore enables more boron to be in solution[19]. The normalising temperatures for P92 and MarBN are both within the austenite phase field shown in Figure 2.2. During the normalising heat treatment the steel is fully austenised and upon cooling the austenite initiates the transformation to martensite. This transformation is explained in detail in section 2.3.1.

2.2 Alloying Additions

2.2.1 Chromium (Cr)

Chromium is a very important element in 9 – 12 wt. % chromium steels. The weight percentage of this element in grade 92 steel is between 8.50 – 9.50 wt. %. The high chromium content improves the oxidation resistance of the steel[10], however it has been reported that the oxidation resistance of these steels may need to be improved further for use in an ultra supercritical power plant that will operate with a steam temperature in excess of 600°C[8].

One of the main carbides present within 9 – 12 wt. % chromium steels is the chromium based carbide $M_{23}C_6$. The chromium based carbides preciptate predominantly on the prior austenite grain boundaries and lath boundaries. They exert a pinning force on the lath boundaries that provides stabilisation during creep[20]. A small change in the chromium content within the steel can significantly change the number and size of $M_{23}C_6$ carbides present and therefore change the creep resistance of the steel.

The martensite start temperature has been reported to decrease as the chromium content is increased[10].

2.2.2 Carbon (C)

Carbon is required in 9 – 12 wt. %% chromium steels to preciptate carbides such as $M_{23}C_6$ and MX carbonitrides such as NbC, during the normalising and tempering heat treatments[21]. The preciptates provide one of the key strengthening mechanisms required to provide excellent creep resistance in ferritic alloys. Increasing the carbon content has been reported to increase the amount of preciptates such as $M_{23}C_6$ and MX[21]. Carbon occupies the intersitial sites in ferrite and austenite and the solubility of carbon is higher in austenite[14]. Carbon plays

a significant role in the diffusionless martensite transformation, as discussed further in section 2.3.1.

2.2.3 Tungsten (W)

Tungsten is present in grade 92, with a weight percentage of 1.5 – 2.0 wt. %. The MarBN alloy developed by NIMS contains 3 wt. % of tungsten [22]. Tungsten has been found to play a key role in increasing the creep resistance of P92. The addition of tungsten in P92 has been found to increase the creep strength by approximately three times[10].

Tungsten strengthens the alloy by solid solution strengthening due to their much larger atomic sizes in comparison to that of iron[13,23]. Tungsten also strengthens the alloy by dislocation hardening and precipitation strengthening. The dislocation hardening strengthening mechanism is affected by tungsten because the element lowers the martensite start temperature which helps form a fine sub grain structure; the boundaries are subsequently pinned by $M_{23}C_6$ precipitates.

A proportion of tungsten atoms in the steel will form Fe_2W, an intermetallic compound otherwise known as Laves phase. Fe_2W particles are often larger than $M_{23}C_6$ and also consume tungsten atoms which would otherwise be contributing to solid solution strengthening. Laves phase can provide some strengthening during short term creep exposure, however the precipitates coarsen during long term exposure, which will result in a decrease in the long term creep properties[24].

Tungsten helps produce a fine grain structure and reduces the coarsening of the $M_{23}C_6$ carbides[24]. The temperature at which martensite starts to form is lowered with the addition of tungsten.

2.2.4 Boron (B)

A very small addition of boron was used in grade 92, the level of boron utilised was between 1 and 60 ppm[17]. A higher addition of boron was reported to be present in MarBN steels. Abe *et al.*[7] have investigated the effect of the boron level between 0 and 139 ppm in a tempered martensitic 9Cr-3W-3Co-0.2V-0.05Nb steel which was subsequently creep tested at 650ºC. The longest times to rupture were reported to be associated with the higher boron addition of 139 ppm, as shown in Figure 2.3.

The addition of boron has been known for a number of years to increase the creep strength of high chromium ferritic heat resistant steels[12]. However the mechanism in which the creep

strength is improved is not fully understood at the present time. The current theory of how boron improves the creep strength is through improved microstructural stability. The boron addition is thought to reduce the coarsening rate of the $M_{23}C_6$ carbides in the vicinity of the prior austenite grain boundaries. Decreasing the coarsening rate of the $M_{23}C_6$ helps maintain a fully martensitic microstructure and prevent the recovery of the microstructure, because fine $M_{23}C_6$ carbides are pinning the grain boundaries.

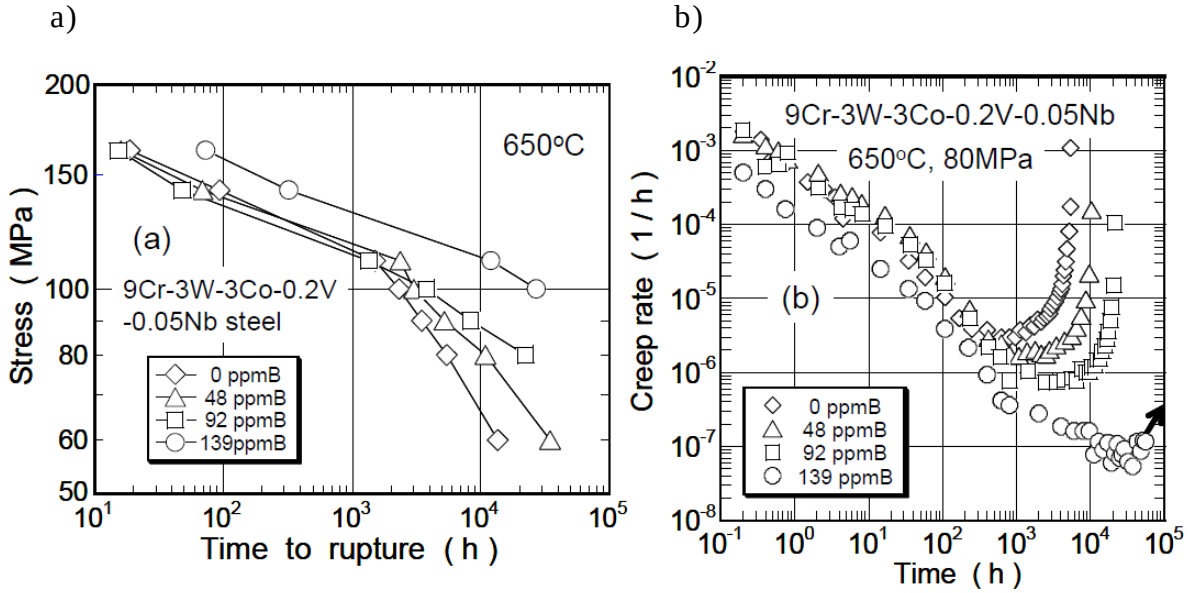

Figure 2.3: The effect of the boron level in a tempered martensitic 9Cr-3W-3Co-0.2V-0.05Nb steel when creep tested at 650ºC[7]*, a) shows stress versus time to rupture and b) shows the creep rate versus time.*

The main mechanism reported in literature explaining how a boron addition can prevent the coarsening of the carbides, is that the addition of boron is interacting with the vacancies located at the interface between the $M_{23}C_6$ carbides and the matrix[7,25]. This is thought to slow down diffusion and therefore decreases the rate of Ostwald ripening. This mechanism is discussed in further detail in section 2.3.2.

Hattestrand *et al.*[25] have investigated a number of MarBN steels with the use of atom probe to identify the location of boron within the microstructure. It has been reported that very small amounts of boron remain dissolved within the matrix; instead the majority of the boron was found to be present in only the $M_{23}C_6$ precipitates. Precipitates which were reported to be close to a prior austenite grain boundary had a higher boron content in comparison to precipitates which were formed within subgrains. This is a significant finding because it identifies that the mechanism which provides the increased creep properties in MarBN is not fully understood.

Boron has been reported to form boron nitride inclusions[12,26]. The precipitation of boron nitride inclusions is thought to offset the beneficial effect of both the boron and nitrogen additions[11]. Boron nitride inclusions have been reported to grow to a size of several micrometres in diameter. The precipitation of coarse boron nitride inclusions results in a reduced amount of soluble boron; this reduces the amount of soluble boron which can be located at the interface of the $M_{23}C_6$ carbides. The precipitation of boron nitride will also decrease the amount of nitrogen that can be used to form strengthening nitrides and carbonitrides[26].

2.2.5 Cobalt (Co)

Cobalt was used within grade 92 steel, with a weight percentage of approximately 0.3 – 0.6 wt. %[17]. The MarBN alloy recently developed by NIMS, utilises 3 wt. % cobalt, whereas researchers and steel makers in Europe believe 1 wt. % cobalt is adequate to provide sufficient creep strength[27]. Cobalt is a very expensive element and is currently more expensive than any other element used in MarBN at present this time, there is no clear evidence in current literature to determine the optimum amount of cobalt. The addition of 3 wt. % cobalt in other alloys such as P911, has increased the time to failure in creep tests by a factor of 3 – 5 times[28].

Cobalt is an austenite stabilising element and is therefore used to suppress the formation of delta ferrite, during high temperature normalising heat treatments[13,29]. Cobalt is the only alloying element in MarBN that increases the Ms temperature. Increasing the Ms temperature helps reduce the amount of residual austenite present after a normalising heat treatment.

Thermodynamic simulations carried out by Helis *et al.* [29] showed that varying the cobalt from 1 – 3 wt. % produced very little change in the level of $M_{23}C_6$ and MX predicted to be present. This indicates that cobalt is present within solution and not within precipitates such as $M_{23}C_6$ and MX. Helis *et al.* [29] has also reported that an increased precipitation of both $M_{23}C_6$ and MX carbonitrides was observed in 3 wt. % and 5 wt. % cobalt steels in comparison to those with 0 wt. % and 1 wt. % cobalt as shown in Figures 2.4 - 2.5.

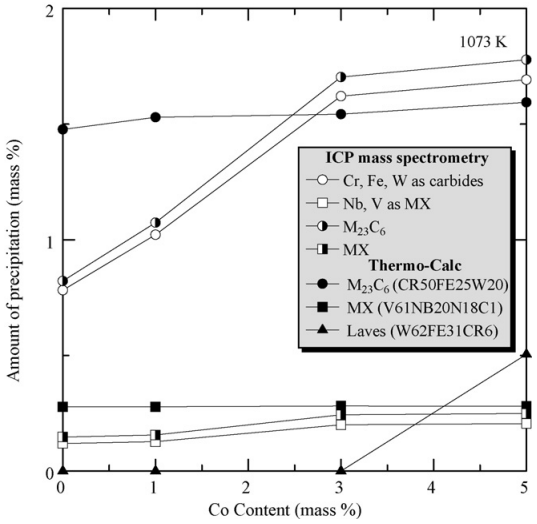

Figure 2.4: A plot showing the amount of precipitation in mass % of MX, $M_{23}C_6$ and Laves phase using ICP mass spectrometry and also using thermodynamic predictions using Thermo-calc. [29]

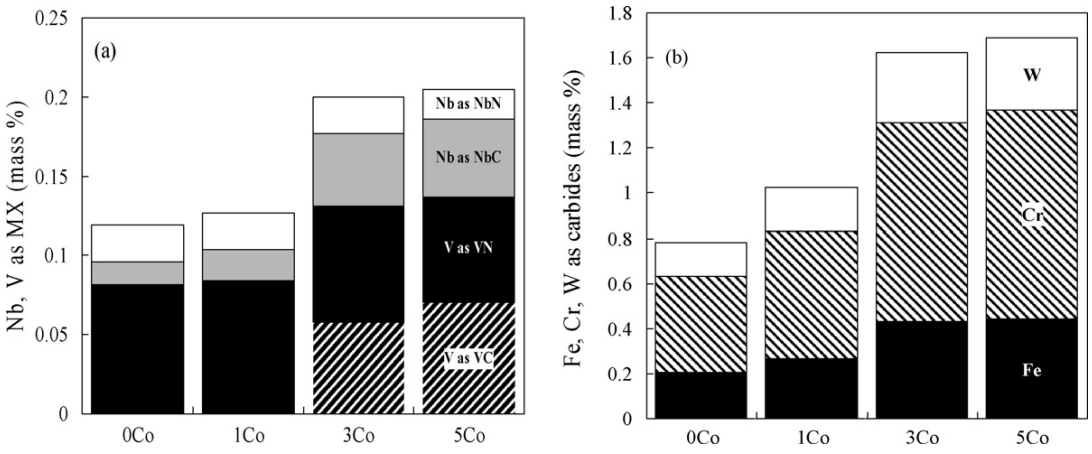

Figure 2.5: A graph showing quantitative values of metallic elements in precipitates for steels with different amount of Cobalt. (a) Nb and V as MX forming elements; (b) Fe, Cr,W, as carbides. [29]

Ageing heat treatments up to 4,000 hours on P911, with a 3 wt. % cobalt addition have been reported in literature [28]. The results indicate that the cobalt addition has been reported to reduce the rate of coarsening of the $M_{23}C_6$ carbides and Laves phase. The addition of cobalt has been found to decrease the rate of diffusion and therefore decrease the rate of Oswald ripening which subsequently reduces the carbide coarsening[28]. Reducing the coarsening rate of the carbides allows the carbides to pin the grain boundaries and preserve the fine martensitic microstructure for longer time periods.

2.2.6 Vanadium (V)

Vanadium is used in grade 92 and MarBN steel. Vanadium is one of the primary elements required to form the carbonitrides such as vanadium nitride (VN) [30]. Vanadium has a high affinity for carbon and nitrogen and therefore can precipitate as vanadium nitride. Vanadium has a high solubility in austenite and therefore remains in solution during the normalising heat treatment[21]. Vanadium has a low solubility in austenite, which ensures that vanadium rich MX carbonitrides do not grow easily during creep at high temperature[9].

2.2.7 Niobium (Nb)

Niobium is used in very small quantities in grade 92 and MarBN steel, between 0.04 – 0.09 wt. %. Niobium has a high affinity for carbon and therefore precipitates as niobium carbide (NbC). This type of precipitate has a low density and is finely dispersed throughout the microstructure predominantly on the lath and block boundaries[31].

2.2.8 Nitrogen (N)

Nitrogen is a key element in 9 wt. % Cr steels used for precipitation strengthening of fine MX carbonitrides in the tempered condition. Nitrogen is used in grade 92 in small quantities between 0.03 – 0.07 wt.%[17]. In standard MarBN the level of nitrogen is reduced to 0.015 wt. %[11]. MarBN steels have the addition of boron, which literature indicates may decrease the rate of coarsening rate of the $M_{23}C_6$ carbides. However coarse boron nitrides can precipitate in some situations which can have a detrimental impact on the creep properties of the steel[12].

Semba *et al.* [22] reported that a small change in the nitrogen content can have a significant effect on the creep strength of the steel, as shown in Figure 2.6. An excess addition of nitrogen has been shown to decrease the creep properties. Semba *et al.* [22] has observed coarse boron nitride particles in conjunction with a nitrogen content of 650 ppm, the precipitation of boron nitride could prevent the formation of vanadium nitride particles during the tempering heat treatment and hence decrease the effectiveness of the nitrogen addition[12]. Utilising a lower nitrogen addition of 70 ppm indicates from literature that all the nitrogen is dissolved into the matrix and prevents the formation of coarse boron nitride particles[22].

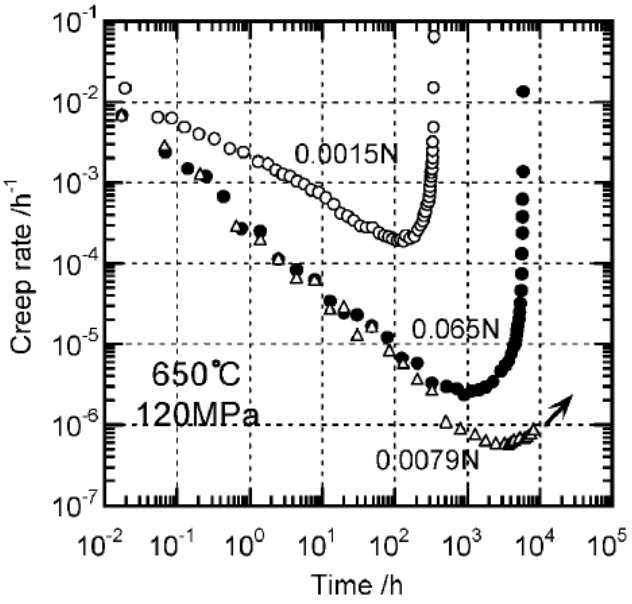

Figure 2.6: A graph that shows the effect of nitrogen on the creep rate versus time curves of a 9Cr-3W-3Co-V-Nb-0.014B steel. [22]

The nitrogen content in MarBN requires careful consideration. Increasing the nitrogen content may decrease the amount of effective boron which is dissolved in the $M_{23}C_6$ precipitates, due to the precipitation of boron nitride. This will also result in less vanadium nitrides being precipitated than a lower nitrogen steel[22].

2.2.9 Silicon (Si)

Silicon is added into 9 wt. % Cr steels to improve the oxidation resistance at high temperatures[16]. The disadvantage of adding silicon into the steel is that the element is a ferrite former. Therefore the chance of forming delta ferrite during the normalising heat treatment is more likely and therefore the creep strength of the material could be significantly reduced if the percentage of silicon is too high within the steel.

2.3 Microstructure of P92

2.3.1 Martensite

Martensite has a characteristic lath structure, which results in a very high hardness of approximately 450 HV_{10} after a normalising heat treatment[17]. The transformation to martensite is formed by a sudden shear in the austenite lattice due to the carbon atoms within the crystal structure, this results in a change in the crystal structure from a face centred cubic to a body centred tetragonal, the transformation is a diffusion less transformation.

The transformation occurs when the steel is cooled from a temperature above the Ae_1/Ac_1 transformation temperature. The martensitic transformation occurs because austenite is present within the steel above the Ae_1/Ac_1 temperature, which initiates the transformation to martensite[32].

The transformation to martensite in 9 – 12 wt. % chromium steels occurs athermally. The transformation begins at the martensite start temperature (Ms) which is approximately ~400^{o}C for grade 92 steel[17]. The transformation of martensite should continue to transform until the martensite finish temperature (Mf), which is approximately 100^{o}C for grade 92 steel[17]. The temperature at which the martensite starts to form decreases as the carbon content is increased.

The transformation from ferrite to austenite causes the carbon atoms to diffuse into the octahedral sites within the FCC structure. The carbon atoms, which have a diameter of 1.54 Å, can either occupy the tetrahedral or octahedral sites. These sites have a diameter of 0.568 Å or 1.044 Å respectively within the FCC lattice[14]. Since the size of the octahedral sites are closest to the size of the carbon atoms these sites are preferred. However the larger size of the carbon atoms compared to the octahedral sites causes strain on the surrounding atoms.

The BCC lattice has more octahedral and tetrahedral sites per unit cell compared to the FCC unit cell. The BCC lattice has three possible octahedral sites located at $\frac{1}{2}[100]$ $\frac{1}{2}[010]$ and $\frac{1}{2}[001]$ and six possible octahedral sites, due to the number of potential sites being higher the size of the individual sites is reduced. The atom size which can be contained with the tetrahedral and octahedral sites without causing distortion within the BCC lattice is 0.733 Å or 0.391 Å respectively. Within the BCC lattice carbon atoms prefer to occupy the octahedral positions; this causes considerable distortion within the lattice, as shown in Figure 2.7.

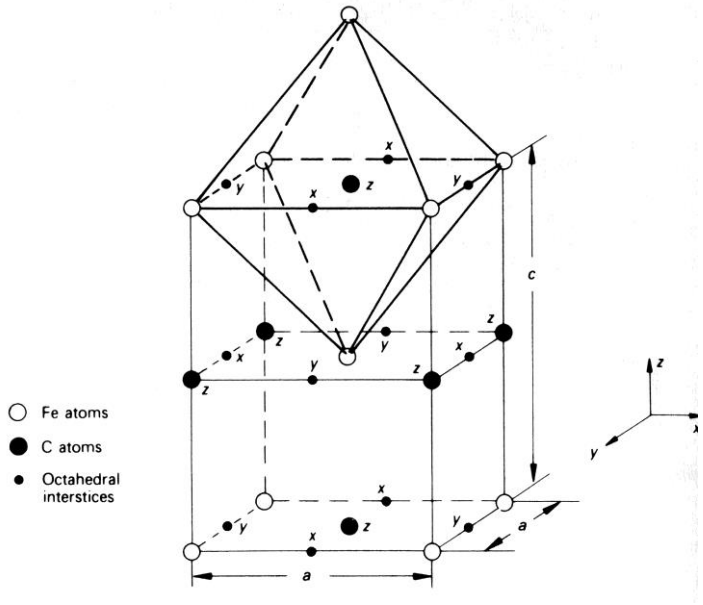

Figure 2.7: A schematic diagram of a martensite body-centred tetragonal lattice.[14]

As described above within the FCC and BCC lattice the carbon atoms prefer to occupy the octahedral sites, within the FCC lattice six iron atoms are positioned around each interstitial atom which forms a regular octahedron. In the BCC lattice when interstitial atoms occupy the z positions a non-regular octahedron is formed, which causes increased distortion within the lattice in the z direction. The martensitic transformation is diffusionless and therefore the carbon atoms do not have time to move to other sites. The interstitial atoms that occupy the z positions within the BCC lattice cause a distortion within the unit cell, this consequently changes the structure from BCC to body cantered tetragonal (BCT).

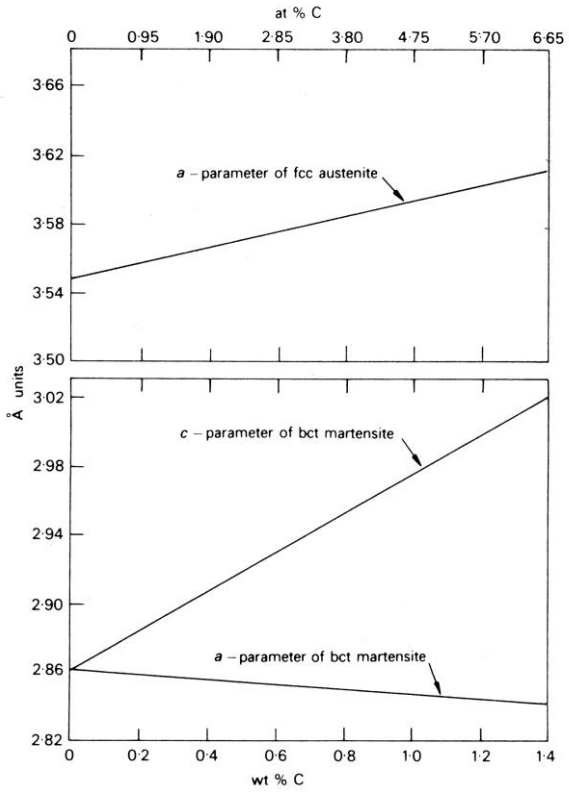

Figure 2.8: A graph showing the effect of carbon on the lattice parameters of austenite and of martensite.[14]

Figure 2.8 shows the change in the a and c parameters as the carbon content is changed. The figure shows schematically the distortion of the crystal structure as the carbon content is changed. The diagram shows that when no carbon is present the structure will be BCC, however as the carbon content is increased the tetragonality of the martensite increases.

The Bain model produced in 1924 can be used to describe the orientation change which occurs in martensite. The model shows how the FCC crystal structure can be transformed into BCT with minimum atomic movement. The model shows that within two face centred cubic cells a body centred tetragonal cell can be drawn, as shown in Figure 2.9. The transformation requires distortion on the two FCC unit cells which is a decrease of approximately 20% in the z axis and an expansion of approximately 12% in the x and y axes.

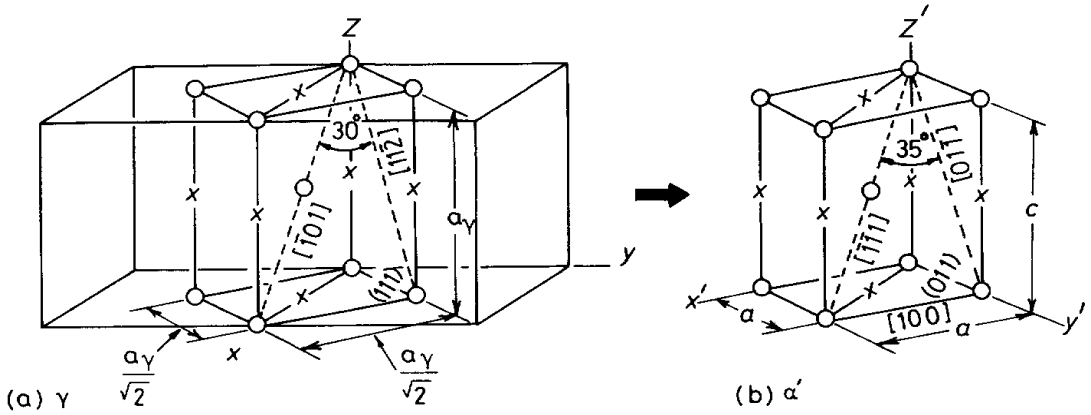

Figure 2.9: A schematic diagram of the Bain model. [14]

2.3.2 Preciptates

9 – 12 wt. % chromium steels have excellent resistance to creep properties and are strengthened by carbides, carbonitrides and intermetallic compounds which precipitate in the matrix and at grain boundaries. Precipitates present within the microstructure stabilise free dislocations and helps reduce the rate of sub grain structure recovery[11].

The stress required to pass a dislocation through a precipitate can be described using the Orowan mechanism, as given in Equation 1.

$$\sigma_{or} = \frac{0.8\,MGb}{\lambda} \qquad \textit{Equation 1}$$

Where, M = Taylor factor (3), G = Shear modulus, b = burgers vector, λ = mean inter-particle spacing.

A number of different types of precipitates have been reported to be present in 9 – 12 wt. % chromium steels; $M_{23}C_6$, M_6C, M_7C_3, MX and M_2X, where M denotes a metallic element and X is carbon or nitrogen. Table 2.2 shows the approximate volume percent, diameter, inter-particle spacing and estimated Orowan stress for each type of precipitate.

Table 2.2: A summary of the volume percent, diameter and inter particle spacing of each type of preciptate in 9 – 12 wt. % chromium steels.[11]

Particle	Volume Percent, %	Diameter, nm	Spacing, nm	Orowan Stress, MPa
$Fe_2(W,Mo)$	1.5	70	410	95
$M_{23}C_6$	2.0	50	260	150
MX	0.2	20	320	120

Figure 2.10 shows a schematic diagram indicating the location of where the three types of particles described above are precipitated within the microstructure. The $M_{23}C_6$ carbides are present on the grain and sub boundaries. The MX precipitate is significantly finer than the $M_{23}C_6$ carbide and is found within the sub grains. Laves phase is not present after the normalising and tempering heat treatment and starts to precipitate on grain and sub grain boundaries after long term exposure in excess of 10,000 hours[33].

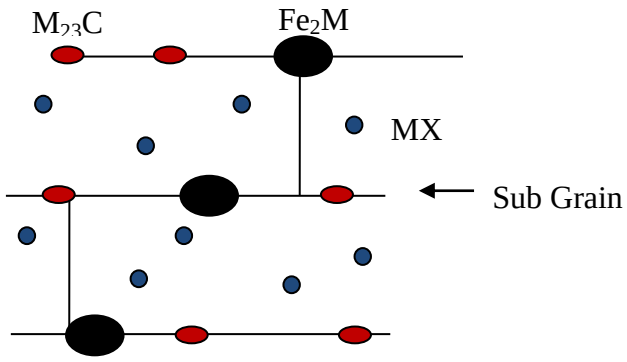

Figure 2.10: A schematic diagram indicating the location of precipitates in high Cr ferritic steel, after Maruyama et al.[20]

2.3.3 $M_{23}C_6$ Carbide

$M_{23}C_6$ is a chromium based carbide. In MarBN based steels it has been reported that the chromium based carbide can be found as $M_{23}(C,B)_6$ [12]. The carbide precipitates preferentially on the prior austenite grain boundaries, ferrite subgrain boundaries and on dislocations inside subgrains[9]. The carbides have been reported to be significantly larger (100 to 300 nm) when they have been precipitated on the PAGB's, instead of inside the grains when they are typically smaller (50 – 70 nm)[11].

The carbide precipitates during the tempering heat treatment. It has also been shown by other authors that the carbide will continue to precipitate or coarsen during service within a power plant or during creep tests at an elevated temperatures[9,11].

The $M_{23}C_6$ carbide acts as an obstacle within the microstructure to dislocation movement as it pins the grain boundaries. The precipitates have been reported to stabilise the microstructure and supressing the recovery of the lath structure [34,35]. However coarsening of the carbides occurs during long term ageing; this has been reported to be one of the factors that cause the recovery of the microstructure, which in turn causes the onset of accelerated creep.

The addition of boron into 9 – 12% chromium steels has been reported by Abe *et al.* [2] to have an effect on $M_{23}C_6$ carbides. It has been reported that boron provides stabilisation of the $M_{23}C_6$ carbides due to enrichment of boron. High temperature normalising is reported to increase the enrichment of the carbides, which is postulated due to the dissolution of borides. Furthermore the $M_{23}C_6$ near the prior austenite grain boundaries were found to have a higher enrichment of boron in comparison to those within the grains.

The coarsening rate is affected by a number of factors according to the theory of Ostwald ripening, which are the diffusion coefficient, solid solubility and interfacial energy. However the above parameters cannot be used to explain the decrease in the coarsening rate of the $M_{23}C_6$ carbides. Therefore the current understanding in literature is that as a small carbide goes into solution and carbon atoms occupy the interstitial sites in the matrix which leaves vacancies. The vacancies migrate through matrix and occupy sites near the interface of a growing $M_{23}C_6$ carbide. The theory is that boron atoms occupy the vacancies at the interface and therefore local change cannot be accommodated.

The addition of tungsten into the alloy has been found by other researchers to suppress the coarsening rate of $M_{23}C_6$ carbides. The mechanism in which tungsten decreases the coarsening rate is not yet fully understood[36].

The rate in which the $M_{23}C_6$ carbides coarsen has been found by Abe *et al.* [22] to be much greater in the vicinity of the PAGB's, this is due to enhanced diffusion along the prior austenite boundaries.

2.3.4 MX Carbonitrides

The MX carbonitrides have been reported to precipitate within the sub grains along dislocations in the matrix[37,9,21]. The MX precipitates are typically 2 to 20 nm and are therefore considerably smaller than the $M_{23}C_6$ precipitates. MX carbonitrides have been reported to be very stable and not coarsen easily at high temperatures. The carbonitrides are very stable at high temperatures because the precipitates are mainly composed of niobium and vanadium, whose solubility is low in the ferrite phase field.

MX carbonitrides are a key precipitate required to ensure excellent creep properties are achieved. The MX carbonitrides provide an obstruction to dislocation movement, this type of precipitate is more effective than $M_{23}C_6$ because it does not coarsen as fast during creep [38,39].

There are four main types of MX particles, reported to be present in P92[10]: -

1 - Coarse primary NbX particles

2 - Fine platelet VX particles

3 - Fine spherical NbX particles

4 - VX wings are also formed on the NbX particles

A significant number of researchers[21,40,41,29,42] have investigated the types of MX preciptates in P9, P91 and P92. However, there is a lack of information regarding the types of preciptates present in the newly developed MarBN alloy. P92 has a nitrogen content in the range of 300 – 700 ppm[17], in comparison MarBN has a considerably lower nitrogen content of approximatly 150 ppm[7] which could affect the types of preciptates present within the microstructure.

In previous alloys such as P91 and P92, the formation mechanism of the four types of MX particles is very different. The coarse primary NbX particles are formed during the normalising heat treatment. The fine platelet VX particles and fine spherical NbX particles are formed during the tempering heat treatment. Finally the VX wings are formed on the NbX particles during creep tests and service exposure.

2.3.5 Boron Nitride

The addition of boron into MarBN can lead to the formation of boron nitride inclusions, which has been reported to offset the beneficial effect of the boron and nitrogen additions if both additions are not carefully controlled. The inclusions have been reported to be present on the grain boundaries.

The solubility product of boron nitride at the normalising temperature of 1050°C – 1150°C has been reported by Sakuraya *et al.* [26] to be:-

$$Log[\%B] = -2.45\, log[\%N] - 6.81 \qquad \textit{Equation 2.1}$$

Where $[\%B]$ *and* $[\%N]$ *are the concentration of dissolved boron and nitrogen, respectively in mass %.*

The work by Sakuraya *et al.* [26] indicates that boron nitride form at high temperature during the normalising heat treatment. Figure 2.11 shows a graph of the solubility product described by Equation 2.1.

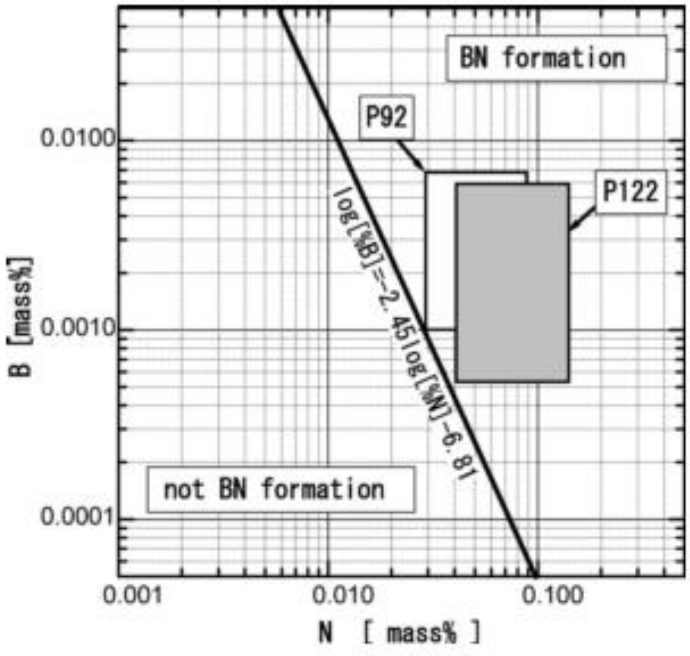

Figure 2.11: A phase diagram of the product solubility generated by Sakuraya et al. [26] *to show the concentration of boron and nitrogen required to precipitate coarse boron nitrides.*

Sakurya *et al.* [26] has investigated the effect of boron nitride precipitation and dissolution behaviour in P122. Coarse boron nitride particles were observed to be present in P122 when the steel is normalised between 1150°C and 1200°C. It has been reported that boron nitride inclusions can be dissolved by normalising the steel at 1200°C to 1250°C and then subsequently quenching the samples.

P122 was reported to have a nitrogen content between 540 ppm - 664 ppm[26] and therefore has a significantly higher nitrogen content than is reported to be present in standard MarBN. This will have an effect on the precipitation of boron nitride throughout the microstructure. Sakuraya *et al.* [26] have reported that the effect of subsequent processing can have an effect on the formation of boron nitride. It has been reported in P122 that after hot rolling where the steel is cooled slowly from 1250°C large boron nitride groups can form up to 30 µm in diameter depending on how slow the cooling rate is, as shown in Figure 2.12.

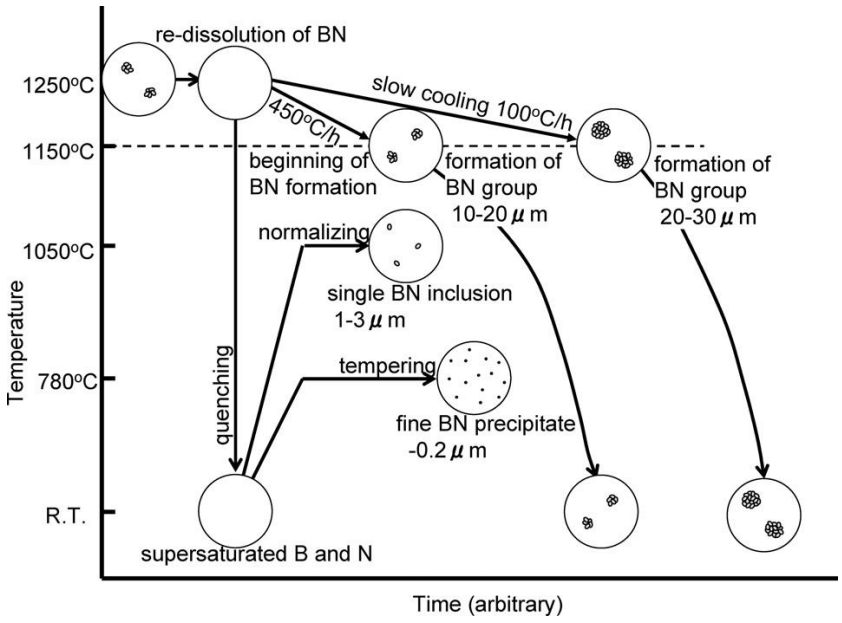

Figure 2.12: A schematic diagram of boron nitride formation in P122 steel under various heat treatments.[26]

2.3.6 Laves Phase

Laves phase (Fe_2M) is an intermetallic compound. There are two main variations of this compound; Fe_2W and Fe_2Mo[10]. The intermetallic compound is not present immediately after the tempering heat treatment but the intermetallic compound has been reported to precipitate on grain boundaries and sub boundaries during long term exposure within service[43,33,10].

Studies carried out by other authors have shown that MX is the most stable precipitate, followed second by the chromium based carbide $M_{23}C_6$[33]. Laves phase in comparison has been reported to have the largest size and also has the fastest growth rate in comparison to the MX and $M_{23}C_6$ carbide[33].

The preciptation of Laves phase results in a loss of solid solution strengthening due to the reduction of tungsten and molybdenum. The lath widths have been found to coarsen over the duration of the creep process which is caused by the migration of lath boundaries as well as absorbing free disclocations. The loss of strength from solid solution strengthening is compensated by the preciptation of fine Laves phase particles which are effective at pinning the grain boundaries during the early stage of creep process[44]. Abe *et al.*[11] have postulated that the preciptation of Laves phase in the early stage of the creep process decreases the minimum creep rate. However as the Fe_2W particles coarsen, this has been reported to promote the acceleration of the creep rate[20] as shown in Figure 2.13. Therefore the precipitation of Fe_2W has a very insignificant effect in improving the creep properties.

The creep test temperature has been shown to have an effect on the creep rate. At a temperature of 823 K (550°C) the precipitation of Fe_2W is low and therefore the creep rate decreases slightly. As the test temperature is elevated to 973 K (700°C) this was found by Abe *et al.* [20] to result in large Fe_2W particles which cause a significant decrease in the creep rate and also promotes the acceleration of the creep rate, as shown in Figure 2.13.

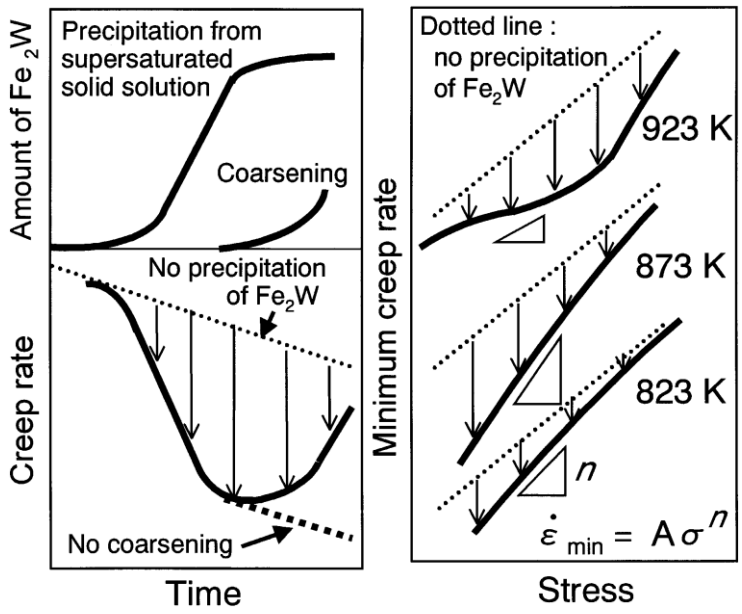

Figure 2.13: A graph showing the effect of fine precipitation and subsequent coarsening of Fe_2W on the subsequent creep rate.[20]

The size of Laves phase is of particular importance, this has been reported to cause a change in fracture mechanism. Coarse Laves phase is widely known to be present after long term exposure in P92. Once the particles coarsen to a critical size of 130 nm, creep cavities are nucleated at the interface of the Laves phase[33]. The formation of creep cavities along grain boundaries has been reported to trigger a brittle intergranular fracture.[45]

2.3.7 Z Phase

The preciptation of Z – phase is commonly found within 9 – 12 wt. % chromium steels after long term exposure in the temperature range of 600ºC to 700ºC[41]. The chemical composition of the compex nitride is Cr(V,Nb)N and has been linked within literature as one of the main causes for the microstructual degradation that is associated with the decrease in long term creep properties[46]. This is due to Z phase preciptating as large particles in excess of 600 nm[47], the large particles do not contribute to the preciptation strengthening within an alloy. The preciptation of Z phase has been shown by numerous authors to consume small MX

carbonitrides, which have a similar chemical composition (V,Nb) (C,N) which are major contributors to the overal creep strength of the alloy[48].

Cipolla *et al.* [41] has shown using a thermodynamic model that at the service temperature of 500 to 600°C Z phase is the most stable nitride. Therefore in this temperature range Z phase will attempt to replace all of the finely dispersed MX carbonitrides preciptated during the pre-service normalising and tempering heat treatments.

The chemical composition of Z – phase is Cr(V,Nb)N, a modified version of Z –phase which is primarily a CrV based nitride has been reported to preciptate in 9 – 12 wt. % chromium steels. Chromium therefore has a major influence on the driving force for Z phase formation, 12 wt. % chromium steels have been found to have Z phase preciptated after a few thousand hours, whereas similar preciptation in a 9 wt. % chromium steels is predicted to take 100,000 hours. The modified Z phase has been reported to contain limited amounts of Nb and Fe[41]. The crystal structure of the modified Z phase has been reported to be mainly tetragonal with lattice parameters of a = 0.286 nm and c = 0.739 nm as shown in Figure 2.14, the structure is also associated with alternating layers of VN and Cr.

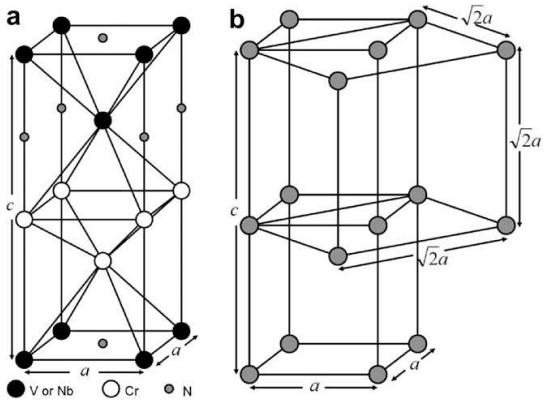

Figure 2.14: A schematic of two crystal structures a) A tetragonal crystal structure that is associated with z phase b) A hybrid crystal structure where cubic and tetragonal crystal structures coexist. The hybrid crystal structure is the proposed crystal structure of modified Z-phase. [41]

At the present time there are a number of mechanisms which have been used to explain the precipitation of Z phase and help understand why the phase is so slow in comparison to the MX precipitates.

Two of the latest mechanisms have been studied by Danielsen *et al.* [46] using a 12 wt. % chromium based alloy. The first mechanism highlights that the alloying elements required to precipitate Z phase are present within the matrix and that pre-existing MX carbonitrides are a

nucleation site for Z phase. The MX particles have been reported to be a nucleation site for Z phase because of its semi coherent interface, which helps reduce the interfacial energy as shown in Figure 2.14. After the nucleation of Z phase the phase is thought to continue to coarsen by the consumption of adjacent MX particles, through diffusion in the matrix, as shown in Figure 2.15.

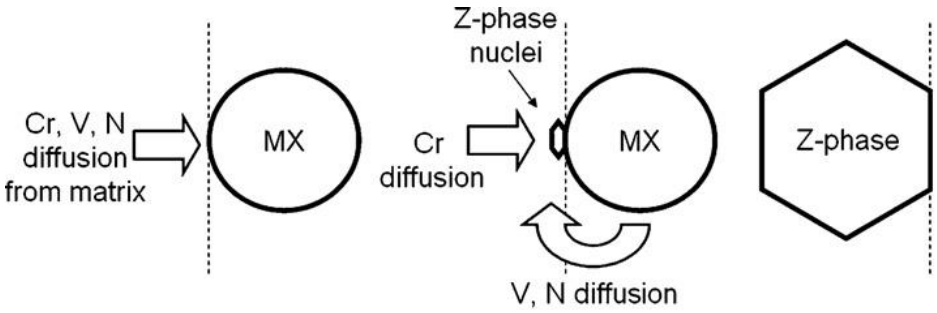

Figure 2.15: A schematic diagram illustrating the formation of Z-phase by nucleation of MX.[46]

Danielsen *et al.* [46] has also reported a second mechanism which can be used to understand the precipitation of a modified Z–phase structure. It is thought that a transformation from MX to Z phase occurs due to the diffusion of chromium after exposure at 600°C to 650°C. MX particles have a cubic crystal structure with a lattice parameter of 0.416 nm and have a composition of (V,Nb)N. As chromium diffuses into the MX particles the composition gradually changes to Cr(V,Nb)N and the lattice parameter is reduced to 0.405 nm. The atoms have been reported to order themselves into vanadium nitride and chromium layers. A schematic diagram of this process is shown in Figure 2.16.

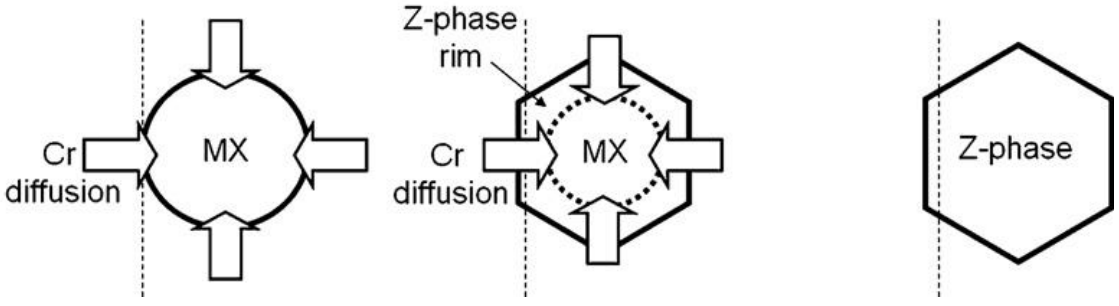

Figure 2.16: A schematic diagram illustrating the transformation from MX to Z-Phase.[46]

2.4 Heat Treatments

A 9 wt. % chromium steel is given a two stage heat treatment before it enters service within a power plant. The two stage process consists of normalising and tempering. On previous alloys such as P91 and P92 the normalising stage consists of heating the steel up to ~1050^{o}C and holding for approximately one hour before quenching the steel to room temperature to form martensite[17]. This is followed by tempering, which consists of heating the steel up to 750^{o}C and holding for approximately two hours before cooling to room temperature[17].

There is a distinct lack of information within the literature about the optimised heat treatment for MarBN alloys.

2.4.1 Normalising

The typical normalising heat treatment for 9 - 12 wt. % chromium steels such as P91 and P92 is carried out at approximately 1040^{o}C to 1080^{o}C for one hour[17]. When the material is heated up to the normalising temperature a transformation from ferrite (BCC) to austenite (FCC) occurs. The heat treatment allows the $M_{23}C_6$ carbides that exist within the steel to be dissolved back into solution[37]. In MarBN the normalising heat treatment is carried out at approximately 1150°C, which has led to an increase in the prior austenite grain size [49].

The Fe - 0.1%C - Cr equilibrium phase diagram is shown in Figure 2.2. The figure shows there is a wide austenite field however; as the normalising temperature is increased there is a greater chance of delta ferrite being precipitated within the microstructure. A number of austenite stabilising elements such as cobalt and copper are added in order to reduce the chance of delta ferrite forming during the normalising heat treatment[10]. As the material is cooled from 1050^{o}C to room temperature the microstructure transforms fully into a non-equilibrium phase martensite with a BCT crystal structure.

There is extensive information within the available literature about the effect of the normalising heat treatment on the microstructure and mechanical properties of previous 9 wt. % chromium steel alloys such as P91 and P92.

A normalising temperature of approximately 1050^{o}C in grade 92 steel has been found to produce an optimum microstructure[50,37,51]. Ennis *et al.* [1] have shown that when the material undergoes a low normalising temperature of approximately 970°C, the microstructure produced is fully martensitic; which has a high dislocation density and small amounts of retained austenite present at the lath boundaries. When normalised using a low normalising

temperature (~970°C) the $M_{23}C_6$ carbides are not all dissolved back into solution and needle like $M_{23}C_6$ carbides are formed as shown in Figure 2.17. At the standard normalising temperature of 1050°C a fully martensitic microstructure is produced and all the $M_{23}C_6$ carbides are fully dissolved back into the solution. The MX precipitates are also present within the material which will impede the austenite grain growth.

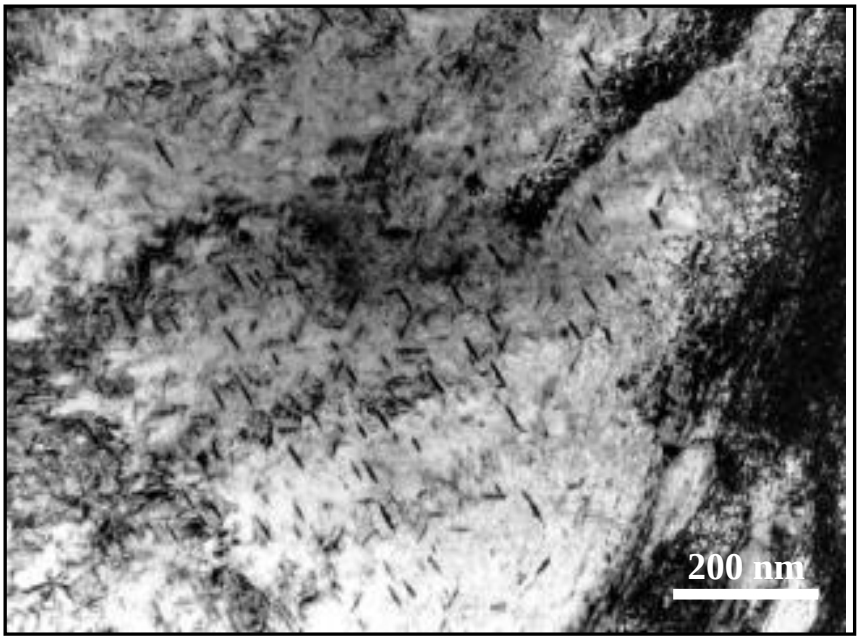

Figure 2.17: Transmission electron micrograph of P92 after austenitising at 970°C for 2 hours showing needle like Fe-rich M_3C particles.[1]

The lath width has been reported to increase as the normalising temperature increases [1]. The lath width at 970°C in grade 92 was reported to be 0.38 nm, which increases to 0.58 nm when the steel is normalised at a temperature of 1145°C[37]. The variation in the lath width occurs due to the decrease in the volume fraction of MX carbides present at the different normalising temperatures. At a lower normalising temperature there is a higher volume of MX carbides present, which impedes austenite grain growth. As the normalising temperature is increased the volume of MX carbides decreases and therefore the laths can grow in width more easily[37].

The rate of cooling from the normalising temperature has been shown to have a significant consequence on the microstructure produced. When a sufficiently slow cooling rate is used there is a possibility that pro eutectoid ferrite can be present within the microstructure[50].

It has been reported by Ennis *et al.* [1] that when grade 92 is normalised in the temperature range of 970°C to 1070°C there is no detrimental effect on the creep properties of the steel. There has been very little change in the creep properties reported because at both

temperatures of 970°C and 1070°C the heat treatments are within the austenite phase region and therefore upon cooling they will both form martensite.

2.4.2 Tempering

The tempering heat treatment consists of heating the material within the temperature range of 750°C to 780°C and holding for two hours before cooling to room temperature. The tempering heat treatment is within the ferrite region of the phase diagram and therefore allows the carbides to precipitate homogenously throughout the microstructure. The tempering heat treatment also helps to promote the formation of $M_{23}C_6$ and MX carbides, which improve the mechanical properties of the steel[52] .

During the tempering heat treatment the carbon atoms are re-distributed, which can affect the dislocation density within the material. A lower tempering temperature of 715^{o}C can result in a higher dislocation density in comparison to a higher tempering temperature. When the tempering temperature is increased beyond 835°C there is a 75% reduction in the dislocation density. The TEM micrographs shown in Figure 2.20 show the effect of the tempering temperature on the recovery and dislocation density.

The amount of carbides within the steel has a major impact on the creep strength of the material as they impede dislocation movement. During the tempering process the $M_{23}C_6$ carbides are precipitated on the prior austenite grain boundaries, sub grain boundaries and within the martensite laths. The fine MX carbides which are present within the microstructure have a very important role in increasing the mechanical properties of the steel. The M(C,N) carbides which are not dissolved during the normalising heat treatment act as nucleation sites for V-wing precipitates during the tempering process[21].

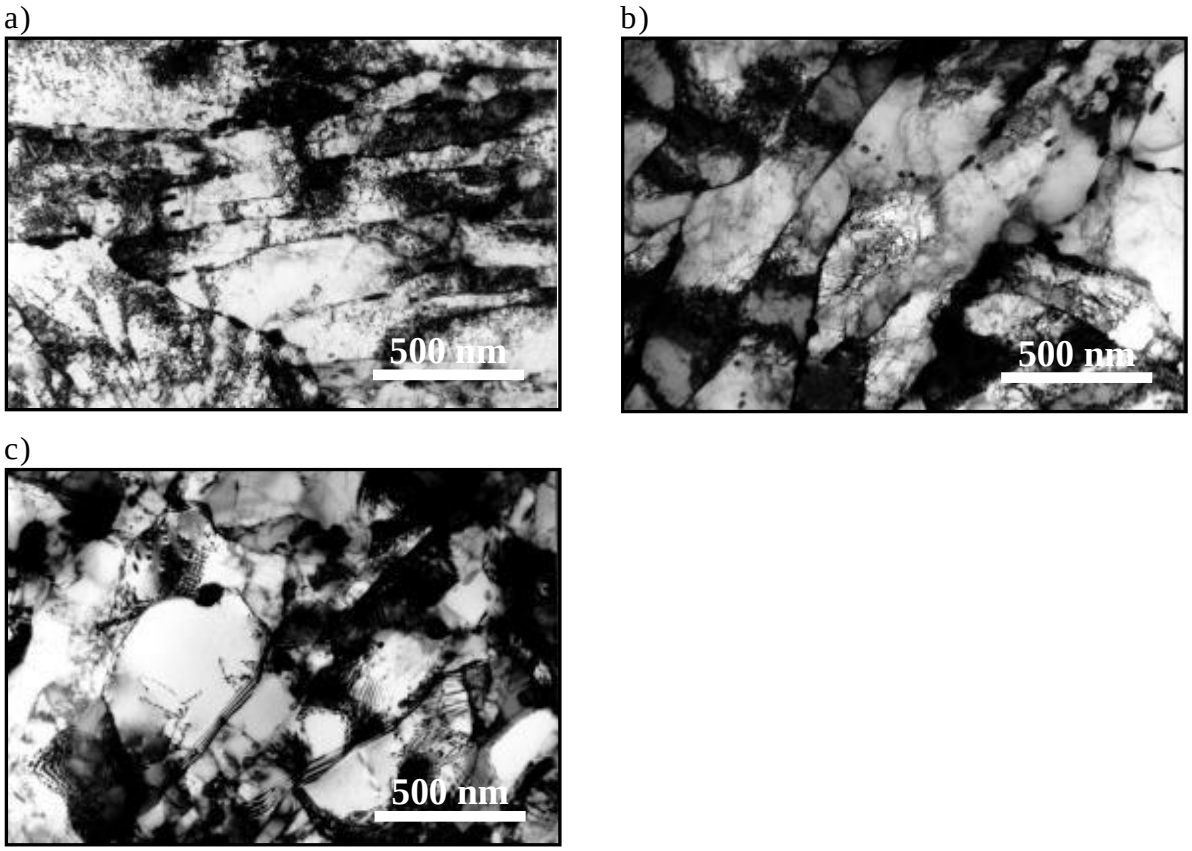

Figure 2.18: Transmission electron micrographs of P92 austenitised for 2 hr at 1070°C and tempered at a) 715°C and b) 775°C and c) 835°C for 2 hrs.

Table 2.3 shows the mechanical properties of grade 92 steel when normalised at 1070°C and tempered in the temperature range of 715°C to 835°C. The data shows that using a low tempering temperature results in a higher ultimate tensile strength (UTS) and higher 0.2% proof stress. The proof stress and UTS are considerably higher at room temperature, than at an elevated temperature. The tempering heat treatment promotes the formation of the $M_{23}C_6$ and MX carbides. It has been reported that the formation of the carbides at a lower tempering temperature results in an increase in the mechanical properties of the steel.

Table 2.3: The mechanical properties of P92 in conjunction with a normalising temperature of 1070°C, and a tempering temperature ranging from 715°C to 835°C.[1]

		0.2% Proof Stress, MPa			**Ultimate Tensile Strength, MPa**			**Elongation, %**		
Normalising, °C	**Tempering, °C**	**25 °C**	**600 °C**	**650 °C**	**25 °C**	**600 °C**	**650 °C**	**25 °C**	**600 °C**	**650 °C**
1070	715	792	482	400	911	495	410	18.3	26.8	28.3
1070	775	513	331	279	683	356	285	25.1	31.8	38.9
1070	835	480	314	269	661	342	282	26.2	35.1	37.2

When the tempering heat temperature is too high and exceeds the α + carbides phase region, the heat treatment will be within the γ phase region. Therefore carbides such as $M_{23}C_6$ and MX will not be precipitated during this heat treatment and instead will be dissolved back into the matrix[48]. Furthermore austenite will be formed during the heat treatment and upon cooling un-tempered martensite will be formed. A reduction in the amount of $M_{23}C_6$ and MX carbides reduces the amount of grain boundaries that are pinned by carbides. This will therefore have a significant effect on the creep properties of the alloy.

A study by Tamura *et al.* [53] investigating the effect of the precipitation behaviour of vanadium nitride during tempering, has shown that vanadium nitride precipitates on dislocations in the early stage of tempering but then temporarily re dissolve and finally re precipitate again. It is postulated that the reason for the re-dissolution of vanadium nitride particles is due local climbing of dislocations or the generation of local stresses which causes the MX particle to become unstable and thus dissolves into solution. It has been reported by Shen *et al.* [54] that two types of vanadium nitride with the same crystal structure but with different chemical compositions co-exist in a tempered condition.

2.4.3 Continuous Cooling Transformation Diagram

The continuous cooling transformation (CCT) diagram is shown in Figure 2.19 for grade 92 steel. The diagram shows the phases that will be present when the material is cooled at a continuous cooling rate from the austenising temperature of approximately 1050^{o}C to room temperature.

When the steel is cooled from the normalising temperature very fast a complete transformation to martensite takes place [13]. When an intermediate cooling rate is used of 17°C/min to 4°C/min the transformation passes through the austenite + carbides region. However upon further cooling a complete transformation to martensite occurs. When a very slow cooling rate is used in excess of 0.85°C/min, the transformation will occur from austenite to pro eutectoid ferrite[17].

The CCT diagram, shown in Figure 2.19, shows there is a relationship between the hardness of the steel and the cooling rate from the normalising temperature. Figure 2.19 shows that using a very fast cooling rate results in a hardness of ~441 HV_5. As the cooling rate is decreased, the hardness has been shown to steadily decrease. When a very slow cooling rate is used this results in ferrite being formed and the hardness has been shown to rapidly decrease to ~263HV_5[17].

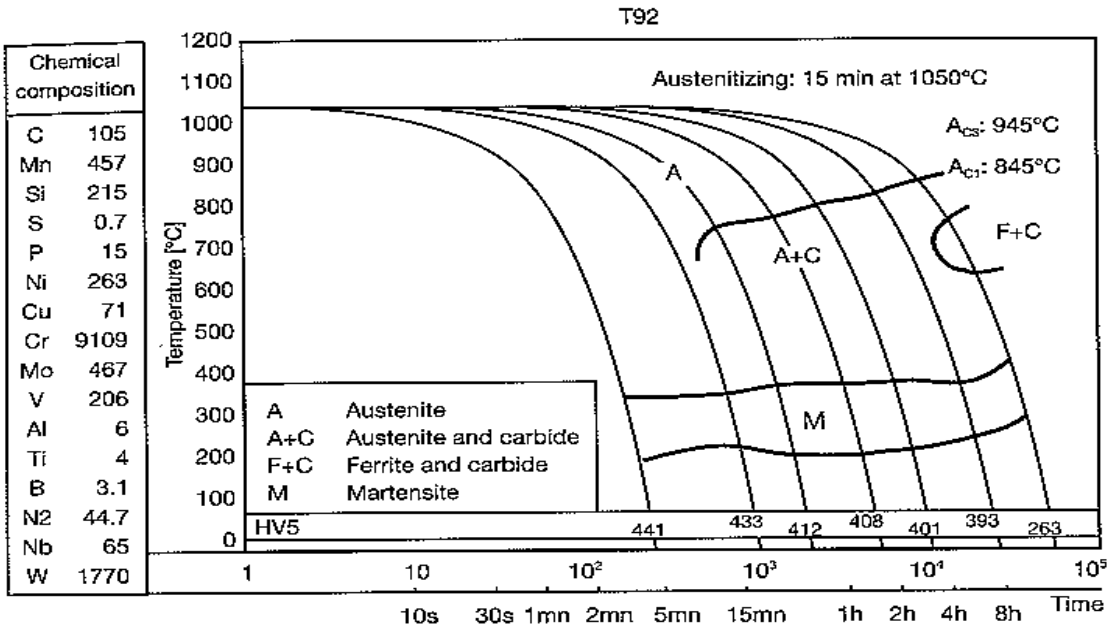

Figure 2.19: A CTT Diagram for T/P92, showing the effect of cooling from an austenising temperature of 1050°C to room temperature.[17]

2.5 Principles of Creep

Creep deformation is an irreversible process and describes the material deformation which occurs as a result of long term exposure to a stress and elevated temperature. The temperature is typically greater than 0.4Tm of the melting point of the material. Creep tests are commonly carried out at a constant tensile strength and temperature for experimental convenience. Figure 2.20 shows schematically the creep curves produced under constant tensile load and constant temperature and also shows their associated creep rates.

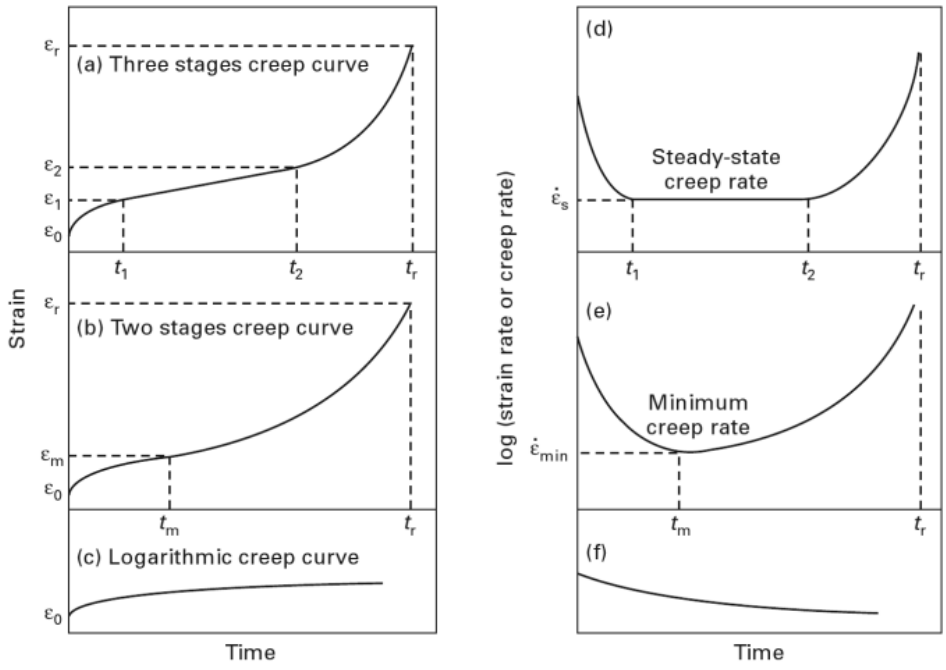

Figure 2.20: Creep curves of engineering steels under constant tensile load and constant temperature. The figure also shows the associated creep rates as a function of time for each stage of the creep process.

Figure 2.20 shows the three stages to the creep process which are primary (transient), secondary (steady state) and tertiary (rupture). During primary creep there has been reported to be a decrease in the number of free mobile dislocations. In the secondary stage, there is a balance between the rates in which dislocations are generated, which contribute to hardening and the recovery of the microstructure and also contribute to softening of the material. The tertiary stage is the final creep stage where the creep rate increases with time, until the time of rupture. The increase in creep rate can be attributed to an increase in stress or associated with microstructure evolution during the creep process.

Creep can take place by six mechanisms at an elevated temperature depending on the temperature and stress. The six mechanisms are (1) defect-less flow, (2) glide motion of dislocations, (3) dislocation creep, (4) volume diffusion flow, (5) grain boundary diffusion flow and (6) twinning. Figure 2.21 shows the relationship between the creep mechanism, the test temperature and stress. The figure shows that coble creep is the dominant mechanism at a lower stress, whereas dislocation creep is the dominant mechanism at an intermediate stress.

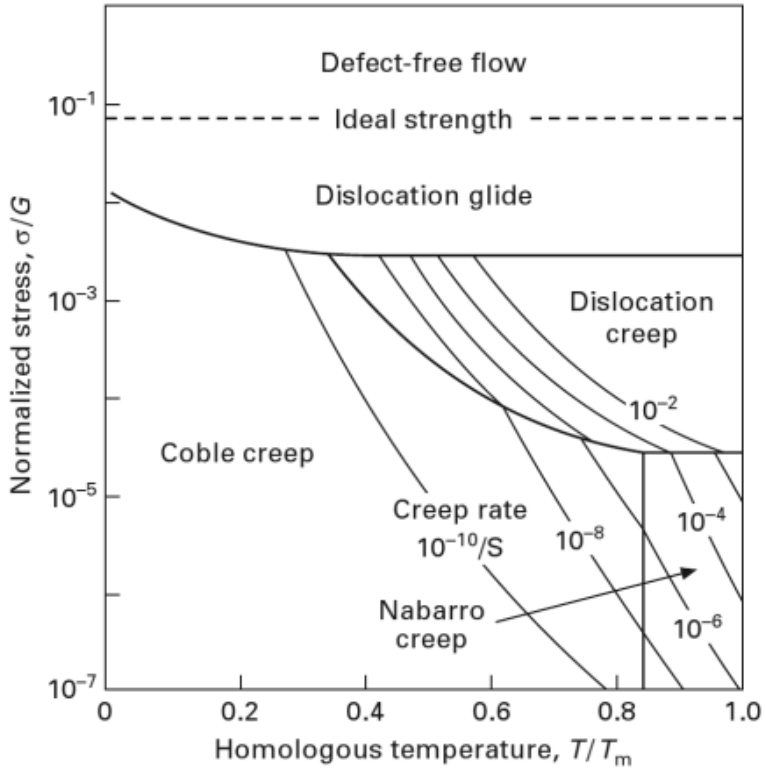

Figure 2.21: A schematic diagram, displaying a deformation mechanism map with contours of constant creep rate.

2.6 Thesis Objectives

This chapter has reviewed the key literature of 9 – 12 wt. % chromium steels. The chapter has shown why chromium steels need to be developed and what developments have taken place over the last four decades.

The main thesis objective is to optimise the composition of MarBN to further improve the creep properties attained from such an alloy. The aim is to optimise all of the elements using thermodynamic calculations, and validate the model using experimental observations.

Both the normalising and tempering heat treatment parameters will be investigated, in light of improving the creep properties of the alloy. The effect of such a heat treatment on the long term properties will also be investigated.

Finally, the key objective of this research project is to optimise the composition and pre-service heat treatment of MarBN, to determine if the alloy can be used at a higher service temperature in order to increase the efficiency of coal fired power plants.

Chapter 3

EXPERIMENTAL PROCEDURES

3.1 Materials

The materials examined in this work were 9 wt. % chromium steels and during this project a number of steels have been manufactured. In total eleven small scale trial melts were manufactured, before a final 8 tonne validation melt was manufactured. The initial eleven melts were manufactured to optimise the compositions of the new alloy based on short term creep tests and microstructural information, before the final 8 tonne melt was manufactured. The chemical compositions of the steels examined are shown in Tables 3.1 and 3.2. The chemical analysis was carried out by a third party lab; Optical Emission Spectroscopy (OES) spectroscopy was utilised to determine the chemical composition of all the elements excluding carbon, sulphur and nitrogen. Carbon and sulphur were determined using LECO analysis and nitrogen was analysed using an inert gas fusion method. The rationale behind the composition of each of the steels manufactured can be found in Chapter 4.

Three batches of steels were manufactured during this project. The first and second batch of steels consisted of four melts each manufactured at Goodwin Steel Castings Ltd, using a standard air melt casting method. The 3rd batch of steels consisted of two melts which were manufactured at Tata Steel using a vacuum melting technique. The aim of the 1st batch and 2nd batch was to optimise standard MarBN steel and to understand what effect changing the tungsten, cobalt, boron and nitrogen has on the resulting microstructure and short term creep properties. The 3rd batch consisted of two steels which were manufactured to understand what effect niobium has on the microstructure and short term creep properties. This series of melts was manufactured using a vacuum melting technique because it was easier to control the nitrogen content within the steel.

The 1st and 2nd batches of steels were manufactured using a single one tonne melt as the starting point which was subsequently poured into four individual melts. Chemical additions were made directly into the furnace in an incremental manner between the pouring of each melt. Two tapered plates of approximately 300 mm x 300 mm x 15 – 40 mm were manufactured for each melt, as shown in Figure 3.1. The materials manufactured by this technique were classified as ‘Goodwin’s air melts’ (GAM). The steels have been supplied by

Goodwin Steel Castings in the as cast condition and also in a normalised and tempered condition.

Table 3.1: Chemical composition of the 1st batch of steels manufactured by Goodwin Steel Castings denoted as GAM 1 – 4, Weight %, balance Fe.

	C	Si	Mn	P	S	Cr	Mo	Ni	Al
GAM 1	0.09	0.29	0.38	0.006	0.006	8.67	<0.01	0.06	0.01
GAM 2	0.09	0.31	0.46	0.007	0.007	8.70	<0.01	0.06	0.01
GAM 3	0.09	0.46	0.54	0.007	0.006	8.65	<0.01	0.06	0.02
GAM 4	0.09	0.43	0.50	0.008	0.006	8.62	<0.01	0.06	0.02

	As	B (ppm)	Co	Cu	Nb	Sn	V	W	N (ppm)
GAM 1	<0.01	110	1.06	0.01	0.05	<0.01	0.22	0.96	190
GAM 2	<0.01	100	3.18	0.01	0.06	<0.01	0.22	2.51	200
GAM 3	<0.01	180	2.84	0.01	0.06	<0.01	0.22	2.49	200
GAM 4	<0.01	90	2.85	0.01	0.07	<0.01	0.21	3.13	210

Table 3.2: Chemical composition of the 2nd batch of steels manufactured by Goodwin Steel Castings denoted as GAM 5 – 8, Weight %, balance Fe.

	C	Si	Mn	P	S	Cr	Mo	Ni	Al
GAM 5	0.085	0.36	0.59	0.007	0.003	9.01	0.12	0.17	0.023
GAM 6	0.084	0.39	0.55	0.006	0.004	8.83	0.12	0.16	0.012
GAM 7	0.083	0.45	0.51	0.008	0.005	8.72	0.12	0.16	0.020
GAM 8	0.082	0.50	0.46	0.009	0.005	8.92	0.12	0.16	0.005

	As	B (ppm)	Co	Cu	Nb	Sn	V	W	N (ppm)
GAM 5	0.003	135	1.06	0.12	0.10	0.005	0.21	0.98	90
GAM 6	0.003	145	1.55	0.11	0.11	0.005	0.20	2.07	130
GAM 7	0.003	195	2.78	0.11	0.10	0.005	0.19	2.60	160
GAM 8	0.003	135	2.93	0.11	0.10	0.005	0.19	3.09	150

Figure 3.1: A photograph of GAM 1 – 4 plates cast at Goodwin Steel Castings Ltd. Photograph courtesy of R. Leese (Goodwin Steel Castings Ltd).

The normalising heat treatment was carried out by heating the material up to 1150°C and holding for two hours before cooling to room temperature by forced air cooling. This was followed by a conventional tempering heat treatment which consisted of heating the material to 780°C and holding for three hours before cooling to room temperature using forced air cooling. This combination of normalising and tempering is termed the 'heat treated' condition.

A selection of the steels, GAM 2, 3, 5 and 6, were rolled at Tata Steel Ltd. The rolling process consisted of soaking the steels at 1225°C for two hours before the ingots were hot rolled to an approximate thickness of 60 mm. The rolled steels were then re-soaked at 1225^{o}C for a further 30 minutes before a final rolling process took place which reduced the thickness of the plates to approximately 20 mm.

The 3rd batch of steels was manufactured by Tata Steel and their chemical compositions are shown in Table 3.3. This batch of steels were cast into 125 kg ingots using an induction vacuum technique as it was deemed easier to achieve a low nitrogen content in the steel. The ingots were subsequently hot rolled to a thickness of 25 mm. The rolling process used in the 3rd batch of steels was identical to the parameters described above. The materials were supplied in the as-cast and as-rolled condition to allow the heat treatments to be optimised.

Table 3.3: Chemical composition of the 3rd batch of steels manufactured by Tata Steel, Weight %, balance Fe.

	C	Si	Mn	P	S	Cr	Mo	Ni	Al
VS5018	0.10	0.54	0.55	0.01	0.016	9.43	0.07	0.06	0.009
VS5019	0.09	0.49	0.53	0.01	0.021	9.14	0.07	0.06	0.007

	As	B (ppm)	Co	Cu	Nb	Sn	V	W	N (ppm)
VS5018	-	140	2.85	0.03	0.04	-	0.22	2.51	70
VS5019	-	140	2.80	0.03	0.04	-	0.22	2.49	90

A large scale, 8 tonne melt, was subsequently manufactured with a final optimised composition, as shown in Table 3.4. The melt was manufactured in an optimised composition for MarBN steels to provide material for subsequent analysis and fabrication into other components, and also to simple assess whether such alloys can be made on a commercial scale using an AOD process. This alloy was manufactured using an argon oxygen decarburization (AOD) technique. A number of different components were manufactured from the 8 tonne melt; 1 x O2 Ingot (2900 kg), 1 x Bonnet casting (3500 kg), 6 x 6″ ingots, 5 x weld test plates and 8 x test plates.

The samples were supplied in the as-cast form to enable the heat treatment to be optimised.

Table 3.4: Chemical composition of the 8 tonne melt manufactured by Goodwin Steel Castings using an AOD process during the IMPACT project, Weight %, balance Fe.

	C	Si	Mn	P	S	Cr	Mo	Ni	Al
8 T Melt	0.10	0.42	0.53	-	-	8.81	-	-	0.007

	As	B (ppm)	Co	Cu	Nb	Sn	V	W	N (ppm)
8 T Melt	-	110	3.10	-	0.067	-	0.22	2.50	170

Figure 3.2: A series of photographs showing the manufacturing process and component moulds of the 8 tonne melt manufactured during the IMPACT project.

3.2 Sample Locations

Due to the large scale nature of the cast plates it was deemed impossible to characterise the microstructure at all locations within the plate. Therefore a number of sampling locations were chosen to study if there was any variation in the microstructure, as shown in Figure 3.3. This study identified that there was very little difference in the macro microstructures observed to be present. However, caution was applied when extracting samples to ensure the samples were not removed from the edge of the plate and on the centre line of the casting.

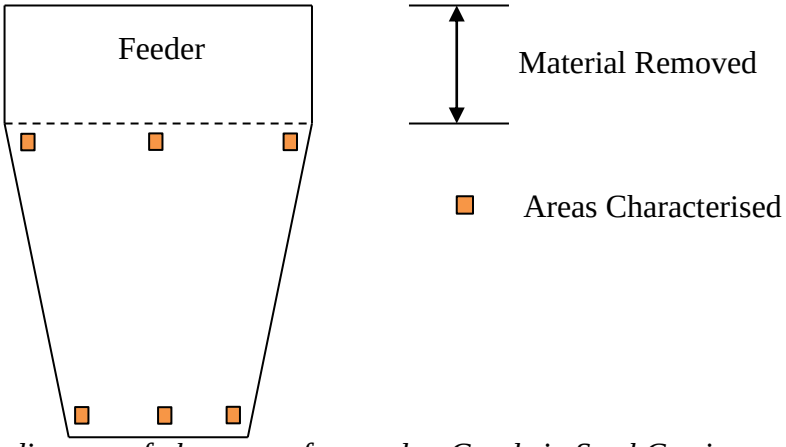

Figure 3.3: A schematic diagram of plate manufactured at Goodwin Steel Castings, showing the locations of samples for characterisation from within the plate.

3.3 Optical Microscopy

Samples were prepared for microscopical analysis using the following techniques. First samples were sectioned using a Struers Accutom cutting machine with a Struers alumina slitting (50A15) disc, which exposed the surface which needed to be examined. The sample was mounted in conductive Bakelite resin followed by grinding using SiC grinding disks from 240 grit to 1200 grit. Water was used as a coolant throughout the grinding process. The samples were then polished to a 1 µm finish using three polishing cloths; Struers Largo, Dac and Floc with diamond suspensions of 9 µm, 3 µm, and 1 µm respectively.

Chemical etching was used to reveal the grain structure using Vilella's reagent (1 g picric acid, 100 ml ethanol, 5 ml hydrochloric acid) [55]. Etching was carried out by immersing the mounted sample into the etchant for approximately 30 seconds, followed by rinsing in methanol and drying.

The samples were analysed using an inverted optical microscope (Reichert-Jung MeF3) which was used to examine the microstructure of the samples using a range of magnifications. The images were captured in a digital format using a Fujitsu HC-300Z digital camera and image capture software, Q-Capture.

3.4 Hardness Testing

Hardness testing was used to measure the materials resistance to plastic deformation using a Vickers macro hardness testing machine.

The Vickers hardness testing process consists of forcing a diamond indenter with a geometry of 136° between opposite faces into the surface of the sample, as shown in Figure 3.4 a). This produced an indentation which could be measured using an optical microscope, as shown in Figure 3.4 b). The diameters could then be converted into a hardness value using Equation 3.1 as shown below.

a) **b)**

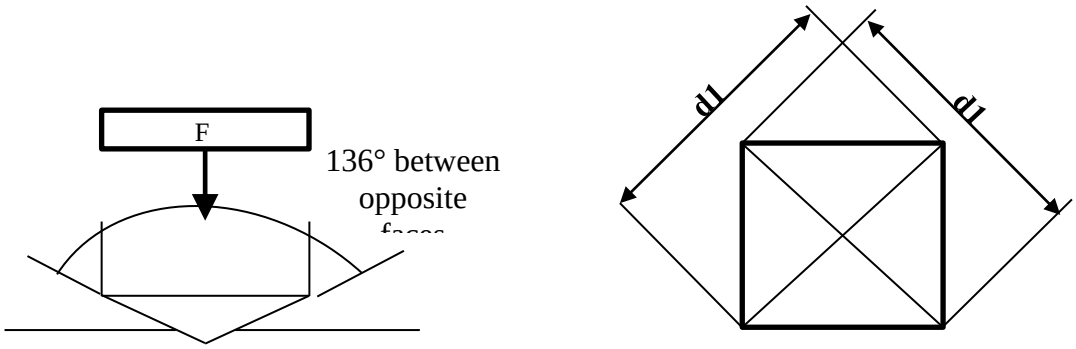

Figure 3.4: A schematic diagram of the Vickers hardness testing process.[56]

$$HV = \frac{2FSin\frac{136^\circ}{2}}{d^2} \qquad \textit{Equation 3.1}\ [56]$$

Macro hardness testing was carried out using a Mitutoyo AVK-C2. The samples were first prepared as described in Section 3.3, to ensure a flat surface was produced prior to the indentation. A diamond indenter was used with a load of 10 kg and the indenter was forced into the material for 15 seconds. After this time, the diameters of the indent were measured using an optical microscope and the measurements were then converted into a hardness value using Equation 3.1. Five measurements were taken, ensuring that there was at least 2.5 x the diameter of the indent from either the edge of the sample or another indentation.

3.5 Creep Testing

Creep testing was conducted during the project by E.O.N and Doosan Babcock and the testing was carried out in accordance to ASTM E139-11. The tests were performed using a constant tensile force and temperature. The specimens used were manufactured in accordance to ASTM E139-11 and were of a circular cross section without a notch. All tests were conducted until the sample ruptured.

The tests were carried out at a constant temperature of 675°C, and were predominantly tested at three standard stresses (142 MPa, 127 MPa and 113 MPa) on each alloy.

3.6 Heat Treatments

A number of heat treatments were carried out throughout the duration of this project on GAM 1 – 8 using both a dilatometer and laboratory furnaces. Figure 3.5 shows a flow diagram of all the heat treatments carried out on the GAM materials.

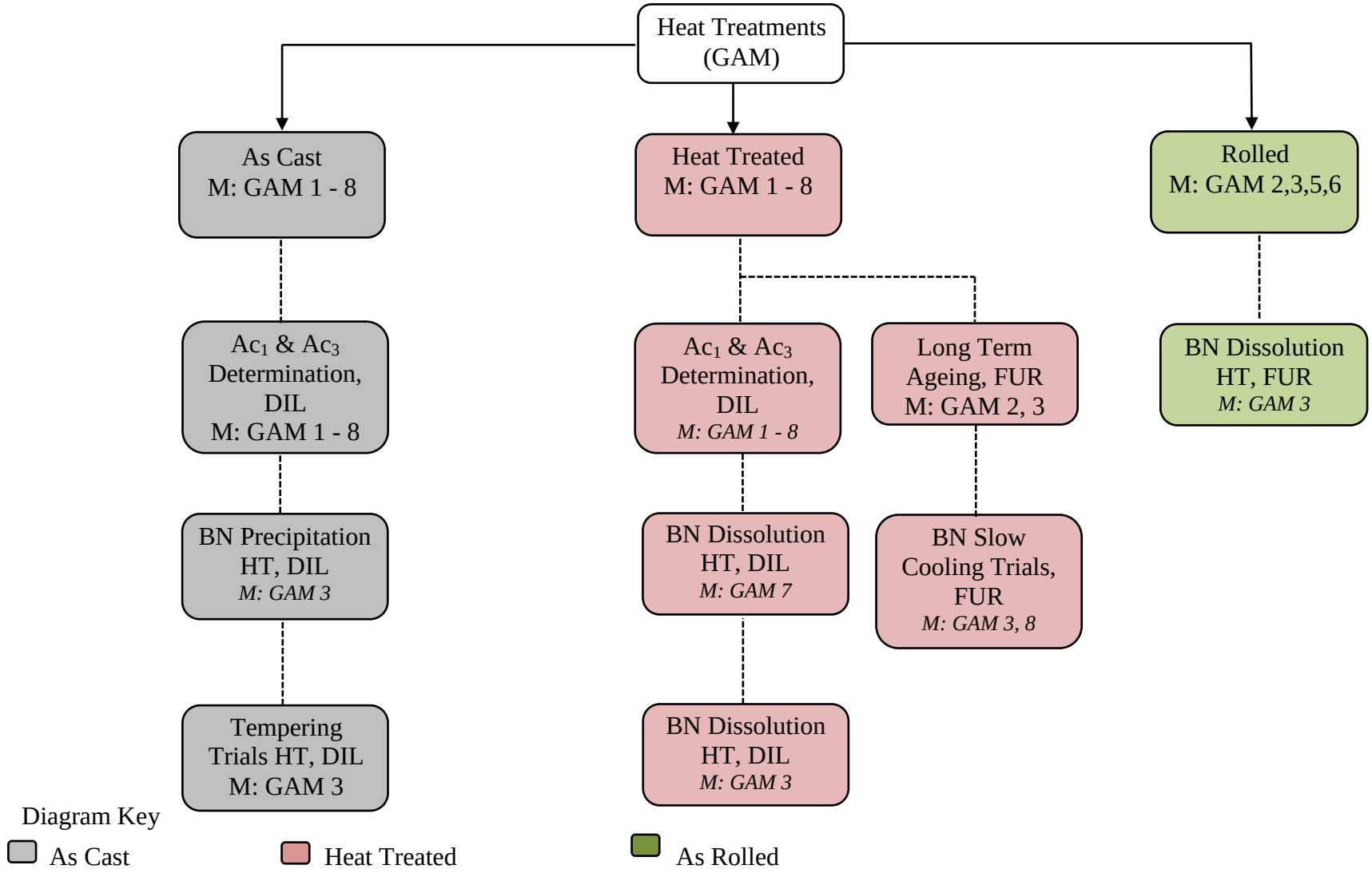

DIL = Heat treatment carried out in the dilatometer FUR = Furnace Heat Treatment

Figure 3.5: A flow diagram illustrating the heat treatments carried out on the Goodwins Air Melts (GAM) throughout the IMPACT project.

3.6.1 Dilatometer Heat Treatments

A variety of heat treatments were carried out using a Bähr-Thermoanalyse Dilatometer DIL 805, as shown in Figure 3.6. The dilatometer was used to carry out heat treatments because of its ability to control the heating rates and cooling rates applied to the sample to a very high accuracy. The change in length was monitored to accuracies of up to 0.1 µm[57]. The samples used for heat treatments were machined into cylinders of 10 mm (length) x 5 mm (diameter). Two types of rods were used to support the samples within the dilatometer; alumina or silica rods. Silica rods were used up to an operating temperature of 1000°C above these temperatures alumina rods were used. The sample was supported in the dilatometer by two alumina / silica rods which are spring loaded. The sample was heated using induction heat from the radio frequency coil, which was generated using a high frequency generator.

Figure 3.6: A photograph of a Bähr-Thermoanalyse Dilatometer DIL 805.[57]

All of the samples were heated in a vacuum of 10 x 1.3^{-2} Pa to prevent decarburization and oxidation occurring on the surface of the sample. Very fast cooling rates were achieved within the dilatometer with the use of helium gas which was carefully controlled by the dilatometer system to obtain the correct cooling rate.

The data produced from the dilatometer were analysed using the WinTA 7.0 thermo analysis software package. This software package can be used to produce graphs with different parameters such as relative and differential change in length, time, and temperature.

3.6.2 Influence of Heating Rate on the Ac_1 & Ac_3 Transformation Temperatures

A study was carried out to determine if the heating rate effects the Ac_1 and Ac_3 temperatures determined for GAM 1 – 8. During this study the samples were held between two silica rods and heated in a vacuum to 600°C at a rate of 580°C/min and then were heated further from 600°C to 1000°C at a number of different heating rates. The heating rates used varied from

3.3°C/min to 100°C/min. The samples were then quenched to room temperature at a rate of 90°C/sec with the use of helium gas.

3.6.3 Ac_1 & Ac_3 Determination

The Ac_1 and Ac_3 transformation temperatures were subsequently determined for GAM 1 - 8. The samples were held between two silica rods and were rapidly heated to 600°C at a rate of 580°C/min and then were heated further from 600°C to 1000°C at a rate of 6.6°C/min (60 minutes). This was followed by a quench to room temperature at a rate of 90°C/sec. All the heating was carried out under a vacuum and the quench was carried out with the use of the helium gas.

3.6.4 Boron Nitride Precipitation Heat Treatments

Heat treatments were carried out to determine at which temperature boron nitride precipitates. The samples were held between two alumina rods and were heated to a peak normalising temperature of 1000°C, 1150°C, 1175°C, 1200°C and 1225°C. The samples were heated up to the normalising temperature in 10 minutes and therefore the samples normalised at a lower temperature had a marginally faster heating rate than those samples normalised at a higher temperature, the heating rate was between 98°C – 120°C/min for all samples analysed. The samples were held at the normalising temperature for 10 minutes before cooling to room temperature at a rate of 90°C/sec, as shown in Figure 3.7.

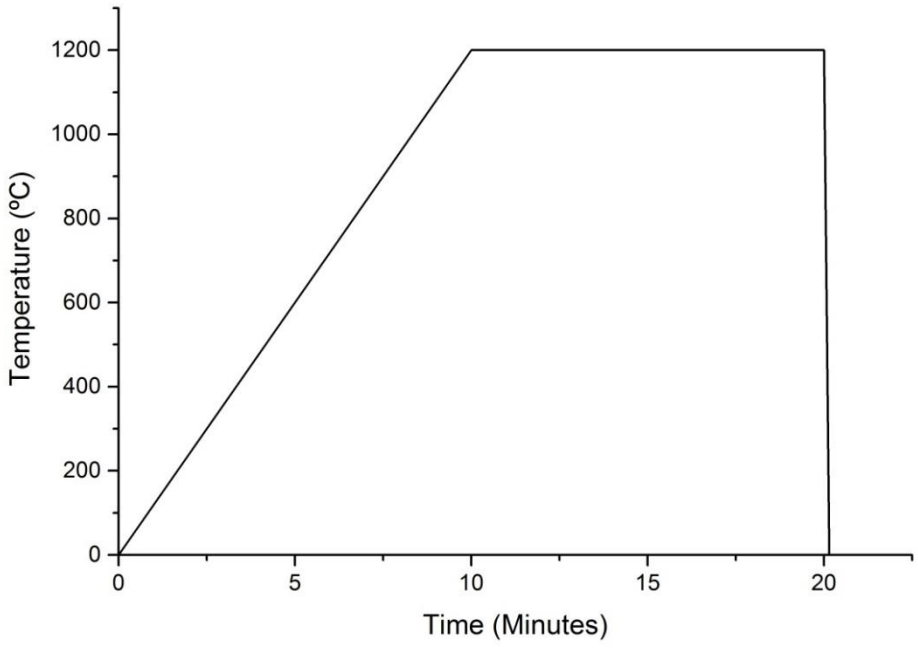

Figure 3.7: A schematic diagram of the heating profile used for the normalising trials to examine the precipitation of boron nitride in GAM 2 and GAM 3 (As-Cast).

3.6.5 Boron Nitride Dissolution Heat Treatments

Heat treatments were carried out to determine at what temperature boron nitride could be dissolved. GAM 2 and GAM 3 were previously heat treated at Goodwin Steel Castings Ltd the steels were all found to have boron nitride present, therefore it is critical to understand if and how boron nitride can be dissolved in order to optimise the materials creep properties. The samples were previously heat treated at Goodwin Steel Castings Ltd, as described in Section 3.10. The samples were held between two alumina rods and then heated at a steady rate of 120°C/min to a normalising temperature of 1200°C. The samples were held at 1200°C for 30 minutes before cooling to room temperature at a rate of 90°C/sec; this is shown by the red line in Figure 3.8. The black line represents the heat treatment previously carried out at Goodwin Steel Castings Ltd.

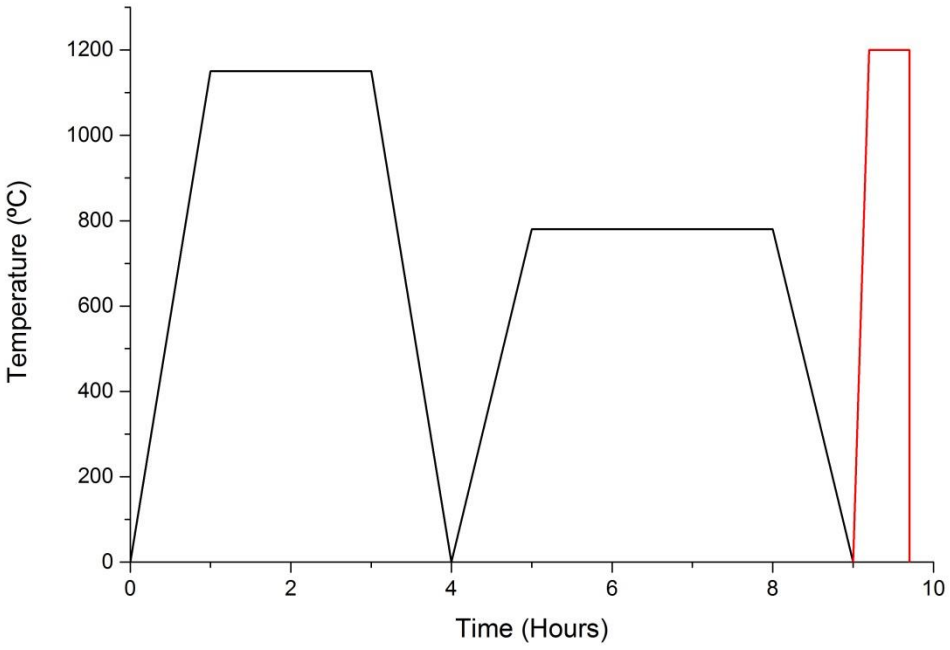

Figure 3.8: A schematic diagram of the heating profile used for the normalising trials to examine the dissolution of boron nitride in GAM 2 and GAM 3, which was previously been heat treated at Goodwin Steel Castings Ltd and shown by the black line.

Further heat treatments were carried out in order to investigate the effect of the cooling rate on the precipitation of boron nitride. Subsequent high temperature heat treatments were designed to prevent the precipitation of boron nitride and therefore may increase the creep properties of the steels. However, it is very important that the cooling rate is investigated to determine if large components with a slower cooling rate could be used in conjunction with a higher normalising temperature to prevent the precipitation of boron nitride.

The heat treatments were carried out on GAM 3; the samples which were previously heat treated at Goodwin Steel Castings Ltd as described above in section 3.1. Two samples were heated at a steady rate of 120°C/min to a normalising temperature of 1200°C. The samples were held at 1200°C for 10 minutes before cooling to room temperature at two different cooling rates. One sample was cooled to room temperature at a rate of 90°C/sec and another was cooled at a slower rate of 6°C/min. A schematic diagram of the heat treatments are shown in Figure 3.9; this figure does not show the previous heat treatment carried out at Goodwin Steel Castings Ltd.

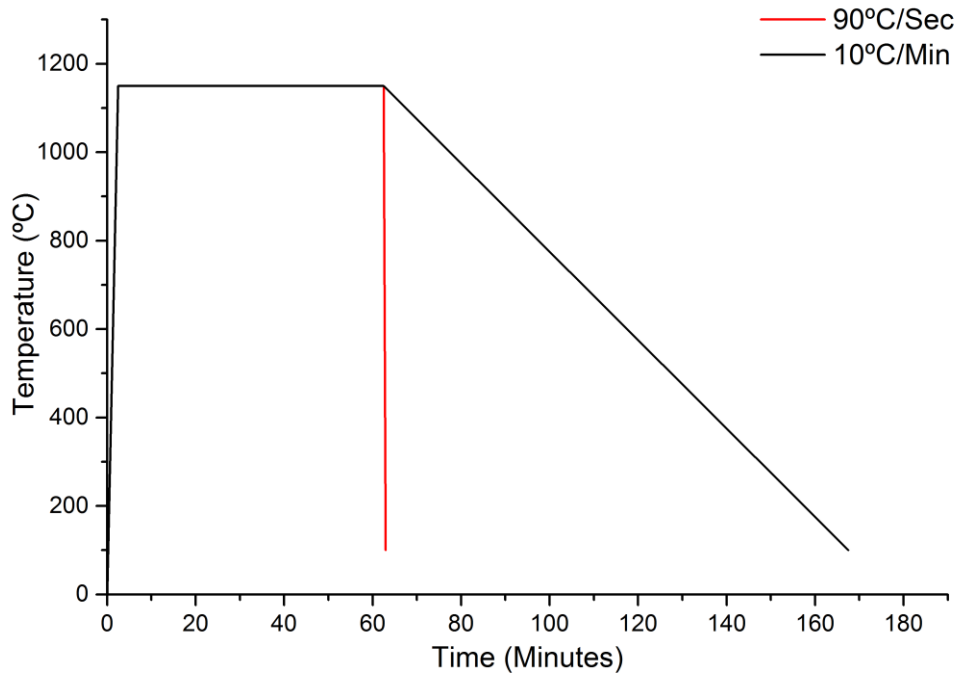

Figure 3.9: A schematic diagram of the heating profile used to examine the effect of the cooling rate in conjunction with high temperature normalising. The trials were carried out on GAM 3 using two cooling rates of 90°C/sec and 10°C/min.

3.6.6 Furnace Boron Nitride Dissolution Heat Treatments

Furnace heat treatments were carried out to verify the heat treatments carried out in the dilatometer on a slightly larger scale, using samples of approximately 1 cm x 1 cm x 1 cm. The heat treatments carried out in the furnace were to investigate the dissolution of boron nitride. The aim of the heat treatments carried out in the furnace was to determine if a similar heat treatment could be used to that carried out in the dilatometer, and therefore to consider their applicability to larger section castings.

The heat treatments were carried out in a Carbolite CWF1300 5l chamber furnace to reproduce the heat treatments that were carried out in the dilatometer. The as cast samples

had been previously heat treated using the standard normalising and tempering conditions. The furnace was pre-heated to 1200^{o}C and then the samples were placed into the furnace and held at this temperature for 1 to 6 hours, and then they were removed from the furnace and left to air cool. This heat treatment is shown schematically in Figure 3.10 by the red line; the black line indicates the previous normalising and tempering heat treatment.

The heat treatments carried out in the furnace investigated a number of different product forms. Heat treatments were carried out on the cast and rolled condition.

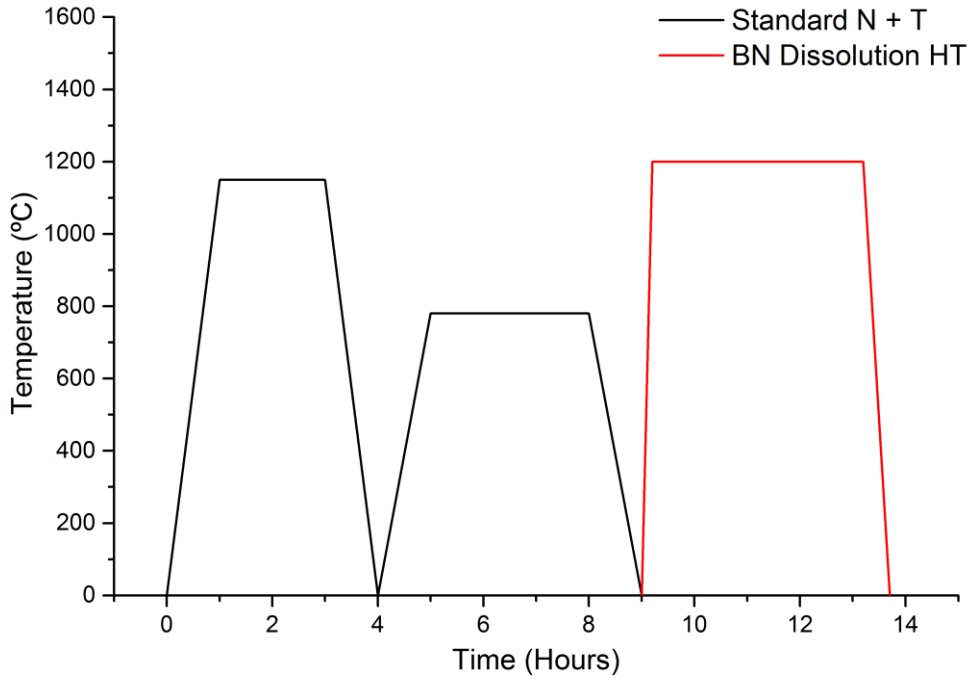

Figure 3.10: A schematic diagram of the heating profile used to attempt to dissolve boron nitride. The heat treatment was carried out on both GAM 2 and 3 in the cast and rolled condition. The black line shows the heat treatment previously carried out at Goodwin Steel Castings Ltd.

3.6.7 Tempering Trials

Heat treatments were carried out using the dilatometer on GAM 3 to determine the effect of the tempering temperature on the resulting microstructure and mechanical properties. The samples were heated at a steady rate of 120°C/min to a normalising temperature of 1150°C and then held at 1150°C for 30 minutes before cooling to room temperature at a rate of 90°C/sec. The samples were then held at the tempering temperature for 60 minutes before cooling to room temperature at a rate of 90°C/sec. The samples were then tempered at temperatures ranging from 660°C - 820°C in 20ºC increments. The samples were heated at a steady rate of 120°C/min to the designated tempering temperature.

An additional series of heat treatments were carried out to study the effect of the tempering temperature, however, these heat treatments were carried out in conjunction with a higher temperature normalising heat treatment. The same parameters as above were used however instead of heating the samples up to 1150°C, the samples were heated up to 1200°C.

3.6.8 Ageing

Long term ageing heat treatments were carried out on GAM 1 – 8 within a Carbolite CWF1300 5l chamber furnace. The heat treatments were carried out to understand the degradation of the initial microstructure. The materials were subjected to ageing up to 18,000 hrs at two different temperatures, 650ºC and 675ºC. The ageing temperatures were chosen because they are both above the expected service temperature. In addition, at 650ºC there is a wide range of data available in literature on comparable 9% Cr power plant steels. The materials were also aged at 675ºC because this is the creep test temperature within the IMPACT project and was chosen by the consortium to accelerate the degradation of the microstructure and hence decrease the time to failure to allow results to be obtained over an appropriate timescale.

The standard normalising and tempering heat treatment was used for the ageing heat treatments on GAM 1 – 8. GAM 3 was aged both at the standard normalising temperature of 1150°C, in addition to an optimised normalising heat treatment of 1200°C for 2 hours. Both series of samples were tempered at 780°C for three hours prior to ageing at lower temperatures.

3.5.9 Summary of Heat Treatments Used Throughout the IMPACT Project

Table 3.5: A summary of the objective and heat treatment profile of each heat treatments used throughout the IMPACT project.

Heat Treatment	Objective of The Heat Treatment	Summary of the Heat Treatment	Equipment Used	Samples Heat Treated
Influence of Heating Rate on Ac_1 & Ac_3	These heat treatments were carried out to determine if the heating rate has an influence on the Ac_1 & Ac_3 transformation temperatures.	Samples were heated to 600°C very quickly and then were heated further from 600°C – 1000°C at a number of different heating rates (3.3°C/min – 100°C/min)	Dilatometer	GAM 3
Ac_1, Ac_3 & Ms Determination	These heat treatments were carried out to determine the Ac_1, Ac_3 & Ms transformation temperatures.	The samples were heated to 600°C very quickly and then heated from 600°C – 1000°C at a rate of 6.6°C/min followed by a quench to room temperature	Dilatometer	GAM 1 - 8
BN Precipitation Trials	This heat treatment was carried out to determine to identify at which temperature boron nitride preciptates.	The samples were heated steadily to the normalising temperature, then subsequently held at the normalising temperature for 10 minutes. The normalising temperature ranged from 1000°C – 1225°C.	Dilatometer	GAM 2, 3
BN Dissolution Heat Treatment Trials	A series of heat treatments were carried out using a dilatometer to identify at what temperature boron nitride could be dissolved.	GAM 7 was used in the normalised and tempered condition. The samples were steadily heated up to the normalising temperature of 1200C. Two samples were heat treated which were normalised for 10 & 30 minutes respectively.	Dilatometer	GAM 7
BN Dissolution (Furnace)Trials	A number of heat treatments were carried out on a slightly larger scale to verify the previous heat treatment on GAM 2 & GAM 3 in the rolled condition.	A series of heat treatments were carried out on GAM 2 & GAM 3 in the rolled condition which had previously received a standard normalising and tempering heat treatment. The sampeles were then normalised at 1200°C and held for between 1 to 6 hours.	Furnace	GAM 2, 3
Tempering Trials	A series of heat treatments were carried out to identify the effect of tempering on the resulting microstructure and mechanical properties.	During this series of heat treatments the samples were initially normalised at 1150°C and then susequently tempered at a range of temperatures ranging from 660°C to 820°C.	Furnace	GAM 3
Ageing Trials	Ageing heat treatments were carried out to understand the evolution and degradation of the intial microstructure as a function of time.	The samples previously received a standard normalising and tempering heat treatment. The samples were then isothermally aeged at 650°C and 675°C for upto 15,000 hours.	Furnace	GAM 2, 3

3.7 Thermodynamic Calculations

The software package Thermocalc was used to predict the phases that would be present under equilibrium conditions in the material by the use of the elemental composition data over specific temperature ranges. The software package uses a mathematical model that allows the Gibbs free energy data in a multiphase system to be used. The software uses a series of calculations to calculate the true Gibbs energy minimisation within a system and hence can calculate the equilibrium volume fraction of a particular phase to be present[58]. The thermodynamic database used for the calculations was TCFE version 6.2[59].

Phase stability calculations were performed in the temperature range of 500°C to 1500°C a 5°C step size. The software used a global minimisation when carrying out the calculations, the software automatically determined the miscibility gaps of the phases predicted to be present at equilibrium. In addition the software automatically determined the phases predicted to be present at equilibrium and no phases were removed. The calculations were performed using a range of elements (Fe, C, Si, Mn, Cr, Mo, Ni, Al, B, N, Nb, V, W, Co), however, impurity elements such as P, S, As, Sn, Pb and Sb were neglected during the calculations.

3.8 Scanning Electron Microscopy

The scanning electron microscope used in this work was a LEO-1530VP Field Emission Gun Scanning Electron Microscope (FEGSEM).

The electron microscope works using an electron beam which is directed at the surface of the material to be examined and when the electrons interact with surface of the material this causes various secondary emissions to be produced from the specimen.

There are three main types of secondary emissions which are produced; secondary electrons, backscattered electrons and X-Rays. When primary electron beam interacts with the surface of the material primary electron beam penetrates to a certain depth, which is known as the interaction volume, which is approximately 1 μm for X-Rays [60].

Typically, a secondary electron signal originates from an area which may be marginally larger than the incident beam, and therefore has a low sampling volume. This results in secondary electrons having a smaller sampling volume and hence secondary electrons have the best spatial resolution in comparison to backscattered electrons and X-Rays. Secondary electrons are typically the electrons with energies below 50 eV. The brightness of the signal captured by the detector can be related to the number of secondary electrons detected.

Backscattered electrons typically have energies above 50 eV and are produced from elastic interactions between the incident electron beam and the sample. In comparison secondary electrons are produced from inelastic interactions. This type of signal can be used to identify compositional differences within the sample because elements with a high atomic number have a greater tendency for elastic scattering. Areas which have a lower atomic number have a greater tendency for inelastic scattering and as a result produce secondary electrons and less backscattered electrons. The differing production rates of backscattered electrons results in elements with a higher atomic number, appearing brighter in the image than elements with a lower atomic number [61].

Characterisation of various samples was carried out using the settings shown in Table 3.5.

Table 3.6: The experimental parameters used on a LEO-1530VP used to characterise the steels.

Imaging Mode	Accelerating Voltage	Aperture	Working Distance
Secondary Electron Imaging	10 kV	30 µm	~10 mm
Backscattered Imaging	20 kV	120 µm	~ 10 mm

A LEO-1530VP FEGSEM was also utilised to acquire a number of images which were subjected to further analysis, to quantify a particular phase. Three types of phases were quantified using the FEGSEM; Laves phase, boron nitride and tungsten borides. Specific settings were used to acquire the relevant images, which are described in section 3.8.

3.9 Quantification of the Phases within the Microstructure using an Scanning Electron Microscope

3.9.1 Quantification of Laves Phase

Laves phase has been quantified with the use of a backscatter detector. This technique has allowed Laves phase to be quantified and has provided data on the number and size of Laves phase precipitates.

The backscatter detector has been utilised because the particles were significantly brighter than the matrix, which allowed the phase to be isolated and quantified. Laves phase is significantly brighter than the matrix because the majority of the phase is comprised of tungsten which is a significantly heavier than iron, and therefore more elastic scattering takes place which produces more backscattered electrons.

A series of five images were collected using the settings described in Table 3.6. The images were taken with a magnification that provided a field of view of 48 µm x 36 µm. The images produced were analysed using the ImageTool software package version 3.0. The software package was used to threshold the images and automatically find particles, and subsequently analyse the distribution of particles. The minimum particle size was set to 70 nm in the ImageTool software package, therefore any particles less than this were not quantified.

This technique provides a reliable method for characterising Laves Phase within the microstructure. The average particle size was approximately 250 nm and therefore all the particles are larger than the minimum particle size determined by ImageTool.

3.9.2 Quantification of Boron Nitride

Boron nitride was quantified in a number of samples. Image analysis software has been utilised to quantify the number and size of the borides present within the microstructure.

A series of images were collected using a secondary electron detector in this case, the boron nitride particles were significantly darker than the matrix and therefore there was a distinct contrast differential between the boron nitride particles and the matrix.

An accelerating voltage of 5 kV was used, in conjunction with a working distance of 12 mm and an aperture of 60 µm. The images were taken at a magnification of 2,400x providing a field of view of 160 µm x 107 µm.

The images produced using the FEGSEM were subsequently analysed using the ImageTool software package version 3.0. The software package was used to threshold the images and automatically find particles, and analyse the distribution of particles. The minimum particle size was set to 70 nm in the ImageTool software package, therefore any particles that were found less than 70 nm were not analysed.

This technique has been identified as a reliable method for determining the size of $M_{23}C_6$ precipitates. The $M_{23}C_6$ precipitates were observed to be within the range of 95 nm – 120 nm and therefore all the particles are larger than the minimum particle size determined by ImageTool.

3.9.3 Quantification of Tungsten Borides (W_2B)

Tungsten borides were observed to be primarily present in the as cast condition of GAM 1 – 8. Quantification of tungsten borides was therefore carried out in the as cast condition. Images were obtained with a backscatter detector, which allowed the tungsten borides to be independently quantified and provided data on the number and size of the precipitates present within the microstructure.

A series of micrographs were collected using the settings described in Table 3.6; images were acquired with a field of view of 250 µm x 250 µm. The micrographs were quantified using the same method described in section 3.9.2, however, the minimum particle size was set to 1 µm.

3.10 Focussed Ion beam Microscopy

An FEI Nova 600 Nanolab dual beam field emission gun scanning electron microscope and ion beam system (FIBSEM) was used for advanced microstructural characterisation. The microscope was used to characterise the grain structure and carbide population using ion beam imaging. The FIBSEM was also equipped with an EDAX Hikari electron backscatter diffraction analytical system, which was used for quantification of the grain structure. In addition an Energy Dispersive X Ray (EDX) system was used to determine the chemical composition of precipitates and inclusions present within the microstructure.

The focussed ion beam can be used to destructively remove material through a process known as sputtering. When the ion beam is operated using a low current, the secondary ions can be used for imaging. If the system is operated using a higher current the system is capable of milling samples to produce site specific TEM samples [62]. Within this study the FIBSEM has primarily been used to image the precipitates present within the microstructure.

3.10.1 Examining Second Phase Particles

The secondary ions emitted from the sample were used to form an image. The contrast of the image was observed to change as the ion beam exposure was increased. When the ion beam exposure was low the composition contrast mechanism is produced from conductivity of the matrix and the non-conductive secondary phases present. As the ion beam exposure is increased, the contrast in the image is produced from channelling contrast which can show changes in crystallographic orientation [62].

The sample preparation for ion beam imaging was similar to that described in section 3.3. However, instead of chemically etching the samples using Villela's reagent the samples were further polished with a 0.02 µm colloidal silica suspension for 15 minutes.

The parameters chosen for ion beam imaging were carefully selected to optimise the images produced. Images were acquired using a low ion beam exposure to generate a good compositional contrast between the particles and matrix to allow quantification of the precipitates to be carried out. The settings used were a magnification of 7,500 x which produced a field of view of 17 µm x 16 µm. An accelerating voltage of 30 kV was used in conjunction with a current of 50 pA. The gallium beam was rastered across the sample at a speed of 150 µm s^{-1}.

Ion beam images were also produced using a higher ion beam exposure to enhance the channelling contrast to allow grain structure to be observed. The gallium beam was rastered across the sample at a speed of 150 µm s^{-1}.

The contrast of Laves phase and $M_{23}C_6$ was found to be very similar in the ion beam images and therefore it is difficult to quantify the particles independently. Therefore, in order to separate the two phases a XeF_2 gas etch was used to temporarily reduce the contrast of Laves phase. The gas etch was used in conjunction with an accelerating voltage of 30 kV and current of 50 pA. The gallium beam was rastered across the sample at a speed of 150 µm s^{-1} in conjunction with the gas etch. After the gas etch is removed, the contrast of Laves phase particles returns to the original levels, once the ion beam is rastered across the samples surface.

3.10.2 Energy-dispersive X-Ray (EDX) Analysis

EDX analysis was carried out to determine the chemical composition of the particles and inclusions present within the steel samples. The EDX system works by analysing the X-Rays that are emitted from the sample. When the surface of the carbides is bombarded with an electron beam this causes some of the inner shell electrons to be ejected, which results in electrons subsequently transferring from a higher electron shell to a lower electron shell. This process emits an x-ray; the energy of the x-ray photon can be used to identify the corresponding element.

EDX analysis was carried out on particles, inclusions and other defects that were present in the steel. An EDAX Apollo XL Silicon drift detector, with a 30 mm^2 sensor was used

throughout this study. It was possible to detect boron using this detector when some optimised settings were utilised. The optimised settings consisted of an accelerating voltage of 5 kV along with an aperture size of 120 µm and an amp time of 12.8 µs. The settings were verified with the use of a boron carbide power, which clearly shows the boron and carbon peaks as shown in Figure 3.11. For EDX spot analysis alternative settings were used to increase the count rate; the voltage was increased to 20 kV, an aperture of 120 µm and an amp time of 50 µs was used.

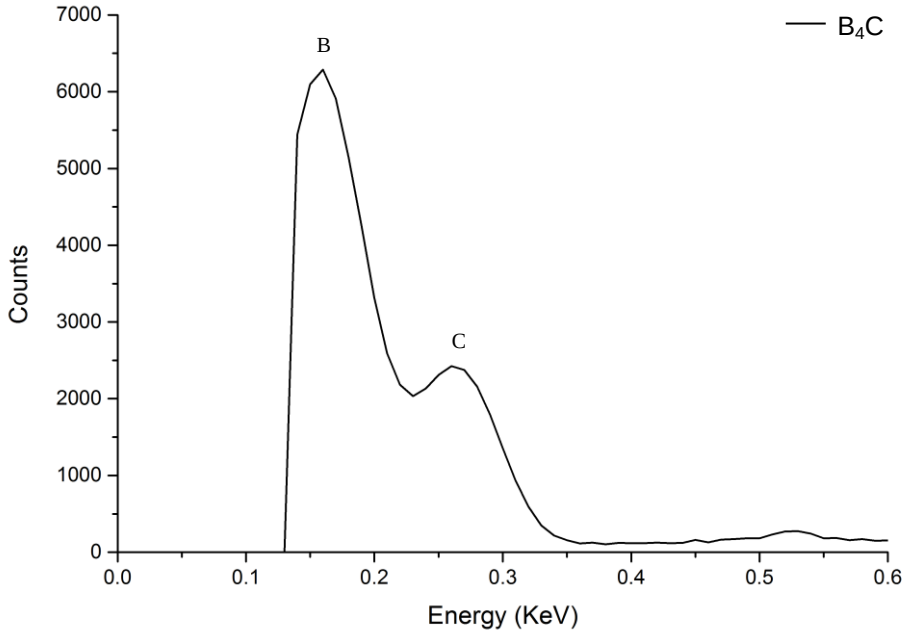

Figure 3.11: A spectrum produced using an EDAX Apollo XL silicon drift EDX detector of a standard B_4C powder.

3.10.3 Electron Backscatter Diffraction (EBSD)

EBSD has been used throughout this study, primarily to examine the microstructure and the degradation of the microstructure as a function of ageing; this was carried out by quantifying the rotation angle of the boundaries and total length within a given area.

The EBSD setup requires the sample to be pre-tilted at 70° and an incident electron beam is directed at the sample. A phosphor screen is fluoresced by electrons from the sample to produce a diffraction pattern. A CCD camera captures the diffraction patterns, and a computer collects and analyse the diffraction patterns. Electronic hardware is used to control the beam, to allow an area to be scanned. A schematic diagram of this process is shown in Figure 3.12.

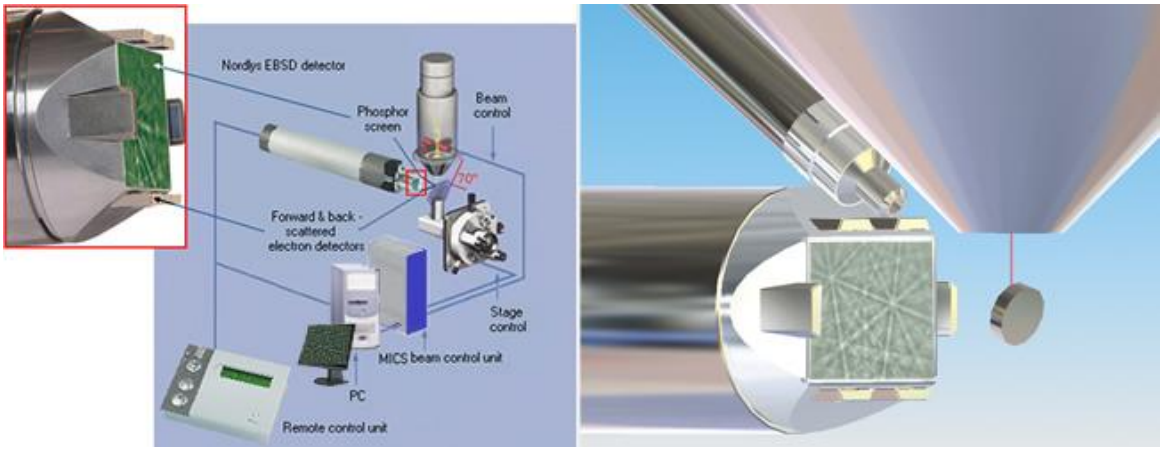

Figure 3.12: A schematic diagram of the experimental set up of an EBSD system.[63]

The incident electron beam is directed at the sample. Upon interacting with the sample the atoms in the material are inelastically scattered and a number of the electrons form a divergent source of electrons close to the surface of the sample. A number of the electrons may satisfy Bragg's equations, as shown in Equation 3.2.

$$n\lambda = 2dsin\theta \qquad \text{Equation 3.2}$$

where; n is an integer, λ is the wavelength of the electrons, d is the spacing of the diffracting plane and θ is the angle of incidence of the electrons on the diffracting plane.

When the electrons satisfy Bragg's law, they are diffracted to form a pair of two large cones relating to each diffracting plane, as shown in Figure 3.13. The pair of cones are then used to form an image on the fluorescent screen and the regions where the intensity of electrons is higher will result in characteristic Kikuchi bands being formed [64].

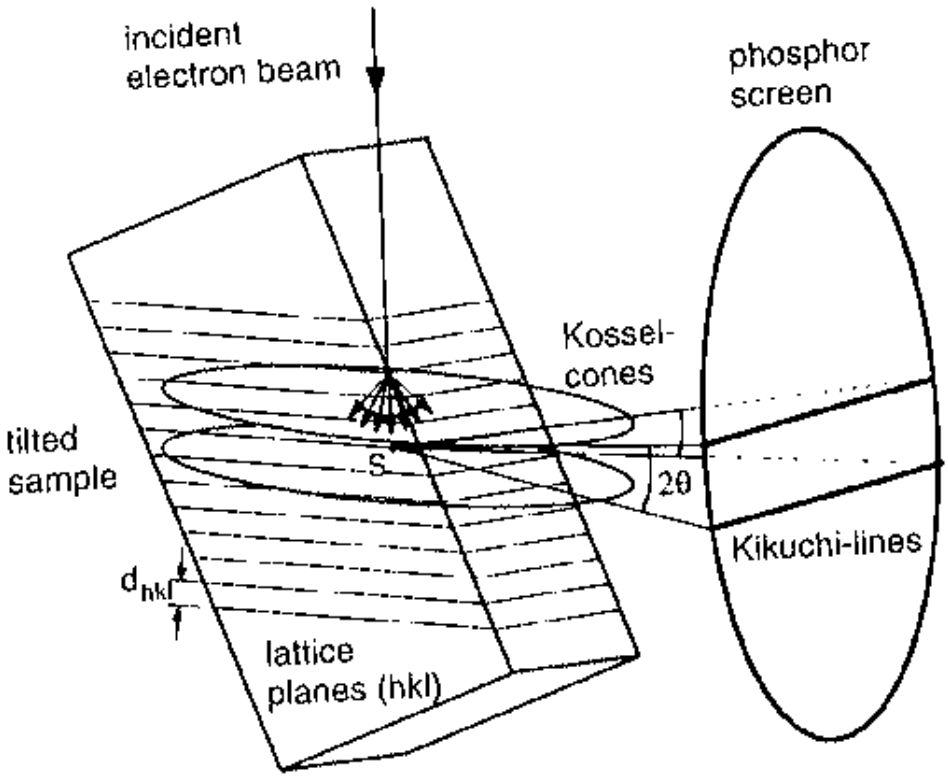

Figure 3.13: A schematic diagram showing the formation of the electron backscattered diffraction pattern. [65]

The sample preparation for EBSD was similar to that described in section 3.3; the samples were first polished from 12 µm to 1 µm. However, instead of chemically etching, the samples were further polished with a 0.02 µm colloidal silica suspension for 30 minutes. The colloidal silica polish was carried out to ensure that all areas were free of mechanical deformation.

An FEI Nova 600 Nanolab dual beam field emission gun scanning electron microscope (FIBSEM) equipped with an EDAX Hikari electron backscatter diffraction (EBSD) analytical system has been used throughout this study. The sample was mounted on a tilted holder at 70° with respect to the horizontal. An accelerating voltage of 20 kV was used in conjunction with an aperture size of 50 µm, providing a nominal beam current of 24 nA.

Areas of 100 µm x 100 µm were typically selected for indexing. The prior austenite grains within MarBN steel were observed to be over 300 µm in diameter and therefore only a portion of one grain was selected. A study was carried out to determine if there was an area to area variation within a single prior austenite grain, as discussed in section 7.1.2. Maps were indexed using a step size of 0.15 µm, which produced EBSD maps containing ~500,000 points. The study has shown that the variation within a single prior austenite grain is

relatively small. This therefore identifies that a small area of 100 µm x 100 µm can be used to analyse the grain structure because in order to produce results with a higher accuracy approximately 20 prior austenite grains would need to be analysed which would require an analysis area of approximately 6mm x 6mm which is not practice using this technique.

The backscattered diffraction patterns obtained were indexed with Orientation Information Microscopy software (OIM) using a ferritic iron structure TSL data database file provided by EDAX. The data was subsequently analysed with the use of the OIM software package. The mis-orientations of the grain boundaries were used to quantify the data. Two types of angles were analysed, low angle boundaries with a mis-orientation between 2° and 15°, and high angle grain boundaries classified as those with a mis-orientation between 15° to 180°.

3.11 Transmission Electron Microscopy (TEM)

A JEOL 2000FX transmission electron microscope was used throughout the microstructural investigations as a complementary technique to examine features that could not be resolved using a FEG-SEM. Carbon extraction replicas were used throughout this study to investigate the different types of precipitates observed to be present without interference from the ferrous matrix.

3.11.1 Specimen Preparation Carbon Extraction Replicas

Carbon extraction replicas were used to characterise the second phase particles within the microstructure. This type of sample was used because the particles are removed from the ferritic matrix, which when the samples are analysed using EDX any influence from the matrix is removed.

To produce the carbon replicas the samples were first polished to a 1 µm finish. The samples were lightly chemically etched using Villela's reagent for approximately 10 seconds. The chemical etch removes the matrix and surface contamination, but does not attack the particles. A thin carbon film with a thickness of 20 – 30 nm was subsequently deposited on the etched surface. The coating was deposited using a Quorum Q150T ES carbon Evaporator, in conjunction with a vacuum of approximately 10^{-5} Pa.

After the carbon film was deposited, the coating surface was scored using a razor blade into squares of 3 mm. The carbon film was removed from the surface using an electrolytic etch of 10% HCl in methanol solution, with a voltage of 1 – 3 V and a current of 30 – 50 mA. After the electrolytic etch the samples were rinsed in methanol, before finally immersing the

samples into distilled water. The samples were immersed at an angle of 45°, which helped to remove the carbon film from the surface of the sample. The carbon films then floated on the water and were collected with tweezers onto copper mesh grids.

Figure 3.14 shows a schematic diagram of the preparation process to produce carbon extraction replicas.

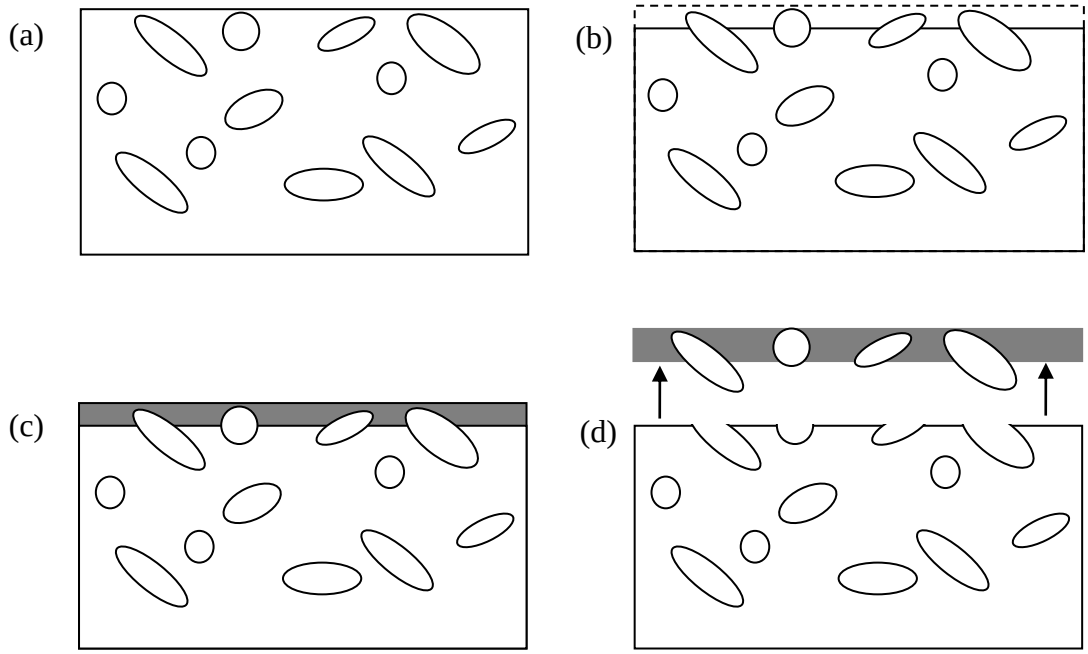

Figure 3.14: A schematic diagram showing the preparation process required to produce carbon extraction replicas; a) shows the a schematic of the particles within the polished sample, b) after etching, c) after a thin carbon film is deposited and d) after the electrolytic etch to extract the particles.

3.11.2 TEM Microstructural Characterisation using Imaging and EDS

Microstructural characterisation was performed on carbon replicas using a bright field mode. The microscope was operated using an accelerating voltage of 200 kV. The images were subsequently digitally acquired using an Erlangshen ES500W digital camera.

Energy Dispersive X-Ray Spectroscopy (EDS) was used determine the chemical composition of the precipitates present on the carbon extraction replicas. When the sample is bombarded with electrons, characteristic x rays are produced in a similar to manner to those produced in an SEM discussed in section 3.9.2. The EDX analysis was carried out using a JEOL 2000FX TEM in conjunction with an Oxford Instruments Inca EDS system. To ensure statistically valid data a minimum of 20 measurements were carried out on each type of precipitate per sample using a live time of 60 seconds.

3.12 Summary

This chapter has described the different characterisation techniques that were used in detail and explained the settings required to reproduce the experimental work. The materials used in this research, together with details of all of the heat treatments applied have been discussed. The use of advanced electron microscopy techniques to determine and quantify specific features within the microstructure has been described. Subsequent chapters will demonstrate how the experimental work has been used to design, develop and evaluate a new generation of MarBN steels.

Chapter 4

THERMODYNAMIC MODELLING

4.1 Introduction

Thermodynamic modelling is a very important technique which was used in the early stages of this project to optimise the chemical composition of a MarBN alloy. Thermodynamic calculations allowed a prediction to be made on the type and amount of each phase predicted under equilibrium conditions for a given chemical composition. This chapter consists of four sections; the first section focusses on a systematic study investigating the effect of alloying elements on the phase stability and delta ferrite formation temperature. The second section focusses on investigating the boron and nitrogen composition required to predict boron nitride. The third part of the chapter outlines the requirements for a new MarBN alloy and provides the rationale behind the optimised compositions for the new alloys manufactured. The fourth section compares the thermodynamic calculations of the compositions aimed for in comparison to the actual compositions of the alloys manufactured.

4.2 Thermodynamic Predictions for the Phases in MarBN

Thermodynamic calculations were performed using the chemical composition of a standard MarBN alloy, denoted as NPM1 investigated by Mayr *et al.* [66] as shown in Table 4.1.

The calculations predicted the weight percentage of the phases present as a function of temperature. The calculations were performed using a step size of 5°C within a temperature range of 500°C to 1500°C.

Table 4.1: The chemical composition of a MarBN base (VS4863) used for the thermodynamic calculations during the stability study. The compositions are shown in wt. %, balance Fe.

	C	**Si**	**Mn**	**P**	**S**	**Cr**	**Mo**	**Ni**	**Al**
MarBN-1 VS4863	0.885	0.295	0.465	0.015	0.005	9.045	0.055	0.165	0.0075

	As	**B (ppm)**	**Co**	**Cu**	**Nb**	**Sn**	**V**	**W**	**N (ppm)**
MarBN-1 VS4863	-	130	2.975	0.11	0.062	-	0.23	3.02	145

Figure 4.1 shows the phase diagram predicted using thermodynamic calculations and the chemical composition of standard MarBN, as shown in Table 4.1. The data are shown on a logarithm scale to allow the major and secondary phases to be plotted on the same graph. The phase diagram shows that between 500°C and 1500°C three major transformations occur. Ferrite (α) is predicted to be the stable phase between 500°C and 800°C; at 800°C austenite (γ) starts to form at the expense of ferrite. The transformation to austenite finishes at 850°C and then becomes the stable phase between 850°C to 1250°C. At 1250°C both delta ferrite and liquid are predicted to form at the expense of austenite. The mass percentage of delta ferrite is precicted to increase until 1415°C. Between 1415°C and 1488°C liquid is predicted to form at the expense of delta ferrite. Liquid is predicted to be stable beyond 1485°C.

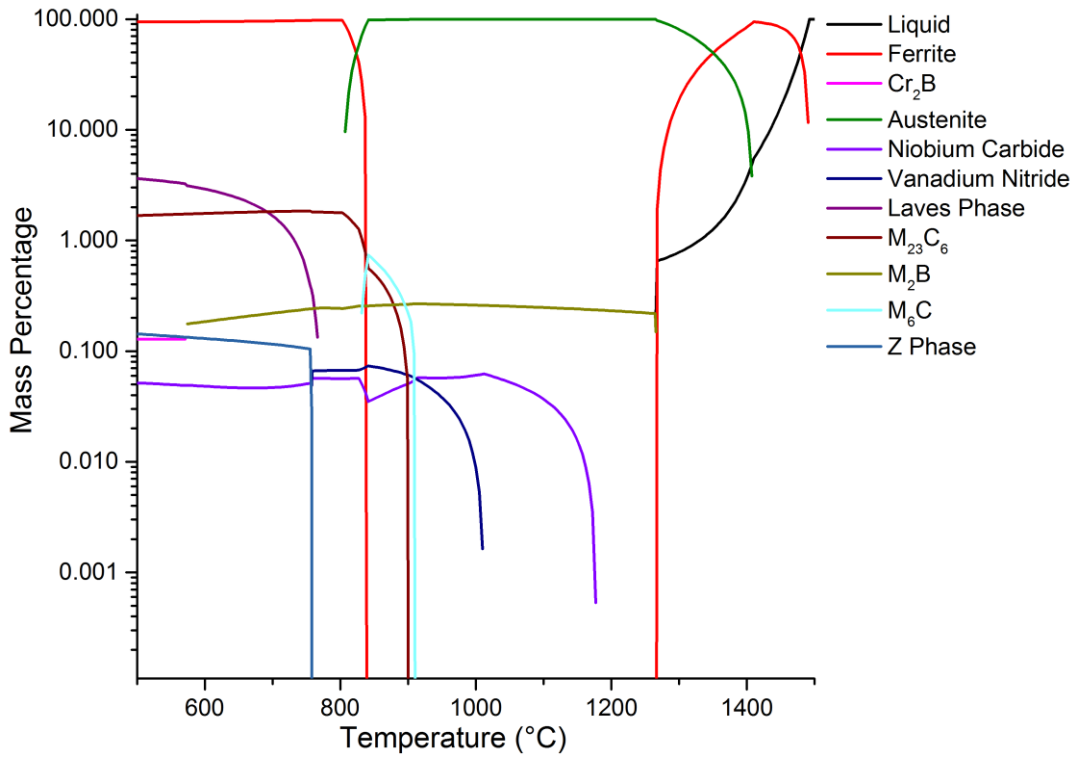

Figure 4.1: A phase diagram predicted using thermodynamic calculations showing the mass percentage of phases present against temperature, calculated using the chemical composition of standard MarBN shown in Table 4.1.

The phase diagram predicts the phases present at equilibrium conditions. The phases observed to be present during microstructural characterisation may be different after normalising and tempering which do not represent equilibrium conditions. For example, after normalising at 1150°C a complete transformation to austenite takes place, and then upon cooling to room temperature using a relatively fast cooling rate a non-equilibrium transformation takes place to martensite [14].

Figure 4.1 also shows that a number of secondary phases are predicted to be present. The phases predicted are niobium carbide (NbC), vanadium nitride (VN), Laves phase, $M_{23}C_6$, M_2B, M_6C and Z Phase. A review of the effect of each phase on the creep properties of the steel was provided in section 2.3.2.

The major addition to MarBN alloys when compared to conventional 9 wt.% Cr steels is the addition of boron, which has been shown by Abe *et al.* [2] to significantly improve the creep properties at 650°C and eliminate type IV cracking in welds. Abe *et al.* [11,31,67] . report that the addition of boron is able to reduce the rate in which the $M_{23}C_6$ carbides coarsen during ageing, which improves the creep properties of the steel.

Boron is predicted to be distributed in two phases Cr_2B and W_2B. Cr_2B is thermodynamically stable between 500°C and 600°C, W_2B is thermodynamically stable between 600°C and 1300°C. A carbide (M_6C) is predicted to be present between 800°C and 900°C. Figure 4.2 shows the chemical composition of each of the phases present as a function of temperature.

a) Ferrite

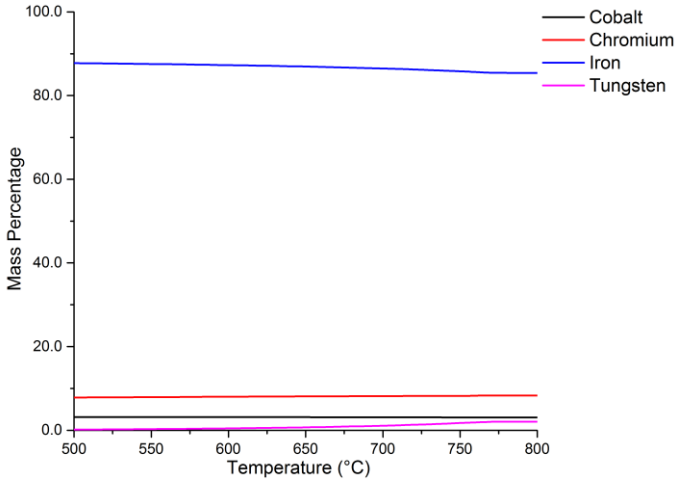

b) Austenite

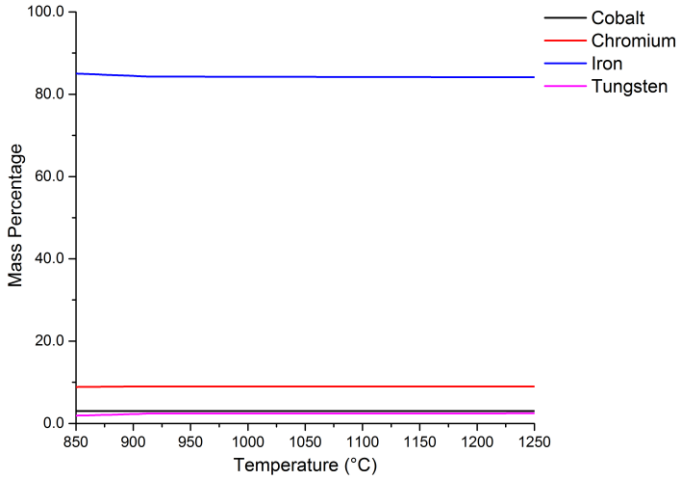

c) Cr_2B

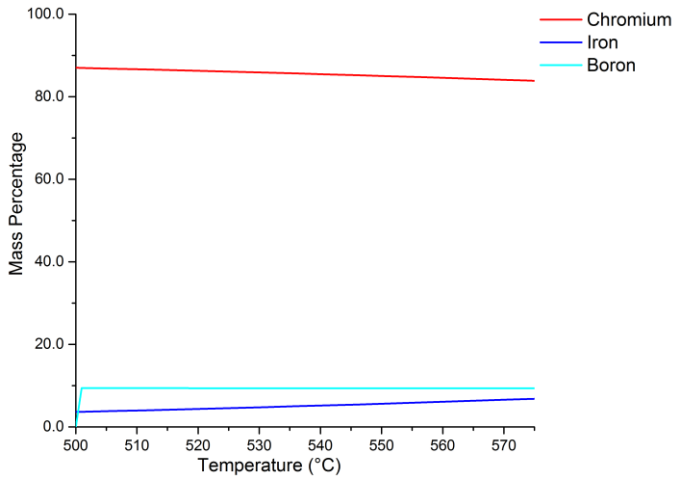

d) Niobium Carbide

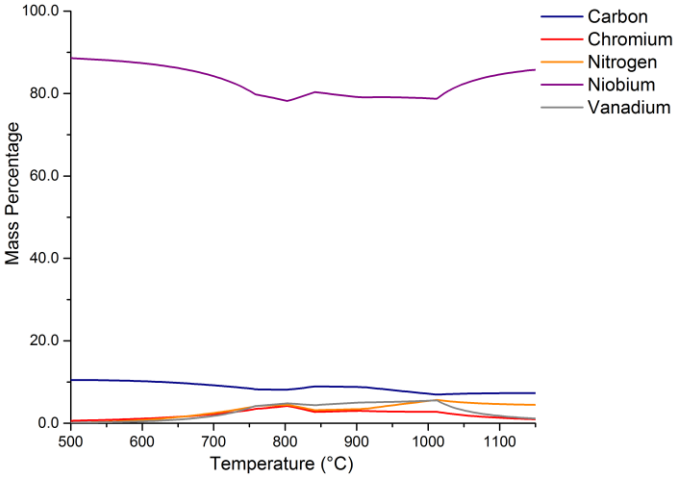

e) Vanadium Nitride

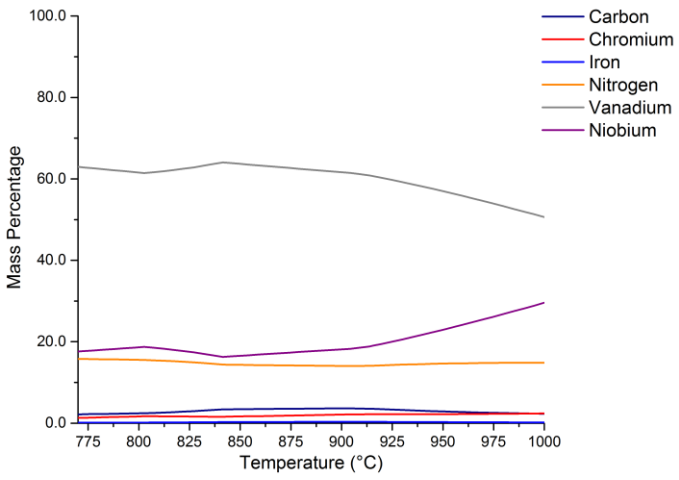

f) Laves Phase

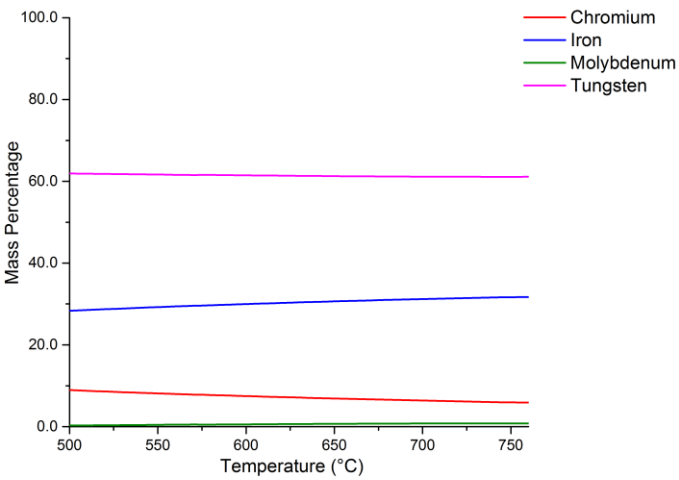

g) $M_{23}C_6$

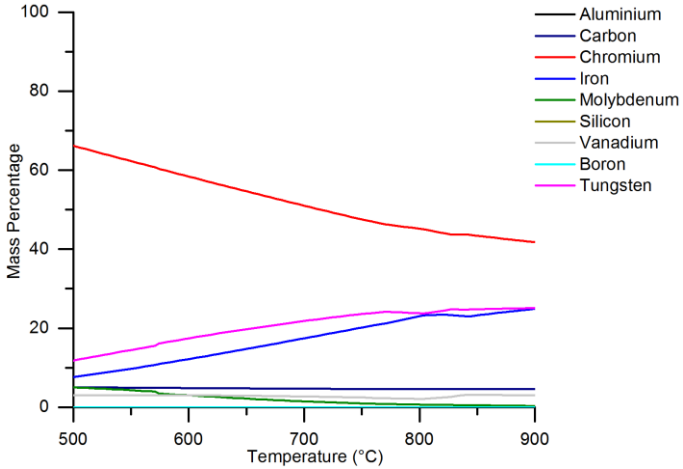

h) M_2B

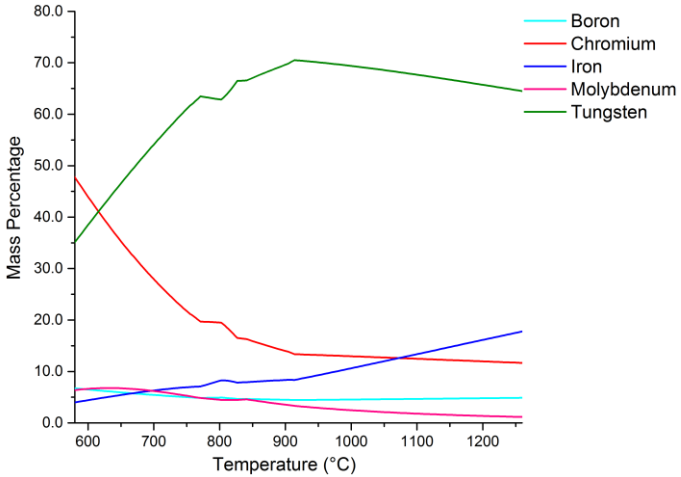

i) M_6C

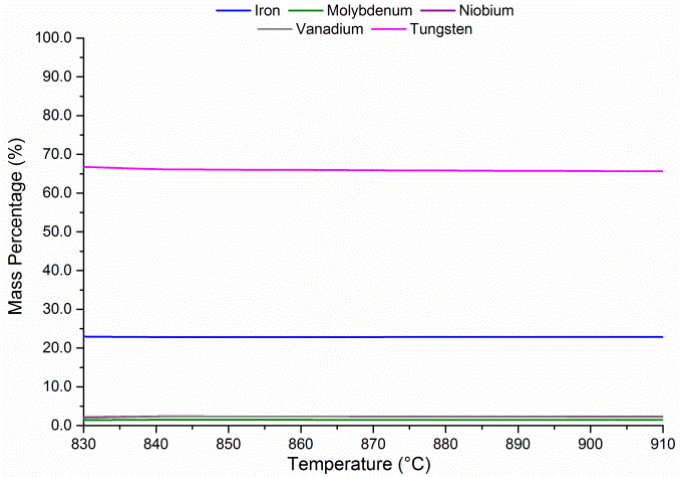

j) Z Phase

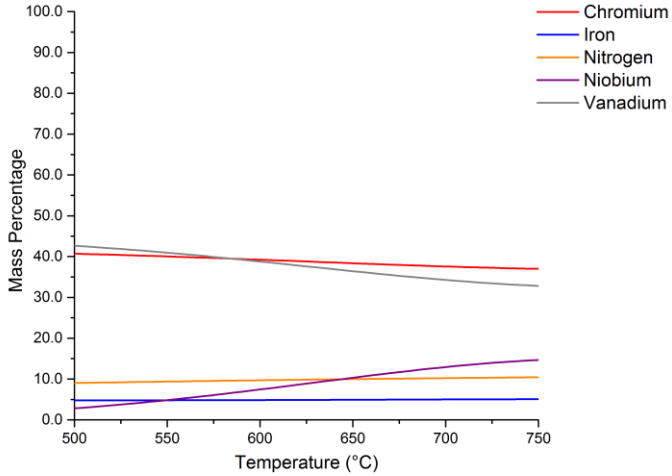

Figure 4.2: A series of graphs showing the chemical composition of each of the phases predicted using thermodynamic calculations in MarBN as a function of temperature a) ferrite, b) austenite, c)Cr_2B, d)NbC, e) VN, f) Laves phase, g) $M_{23}C_6$, h) M_2B, i) M_6C and j) Z phase.

4.3 Sensitivity Study

A sensitivity study was carried out on a MarBN alloy to determine the effects of each alloying element within the alloy. The literature review in Section 2.2 has reported that the amount of each type of phase can significantly influence the overall creep properties of the alloy. Therefore it is vital to understand how the key elements within the alloy can affect the phase stability. The elements investigated within the stability study are C, Mn, Al, B, Co, N and W.

The sensitivity study has focussed on investigating the phase stability and also subsequent delta ferrite formation temperatures. During the study one alloying element was changed by up to ± 30% of the original composition at the expense of iron.

4.3.1 Effect of Nitrogen

The nitrogen content in standard MarBN is 145 ppm, which is significantly lower than that in P92 steels, which is reported to be approximately 400 to 500 ppm[17]. The study has shown that the amount of vanadium nitride at 780ºC and Z Phase at 600ºC increases as the nitrogen content increases. This indicates that the amount of vanadium nitride predicted is lower in MarBN in comparison to P92.

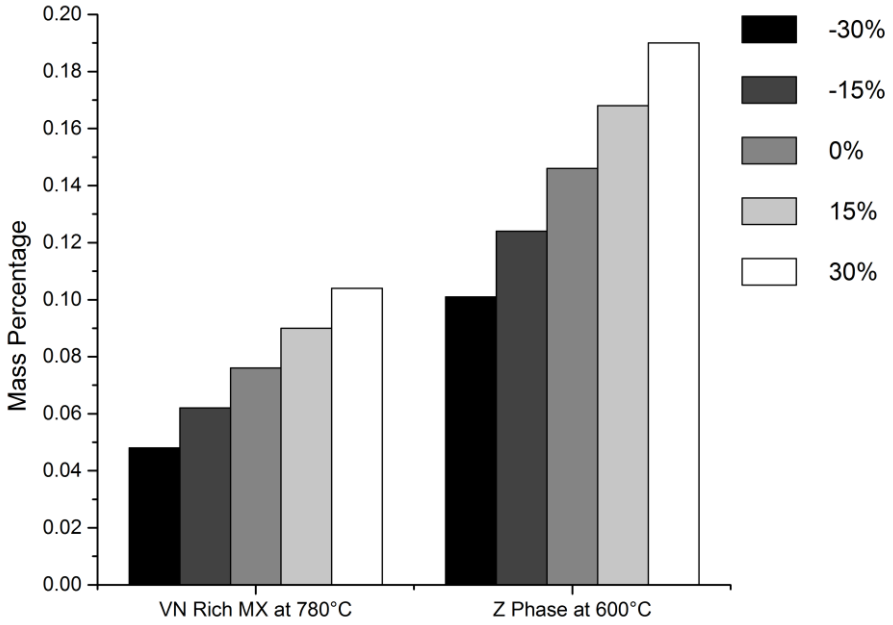

Figure 4.3: A graph showing the effect of nitrogen on the mass percentage of vanadium nitride (MX carbo-nitride) and Z phase predicted in MarBN.

Thermodynamic calculations have been used to predict the mass percentage of vanadium nitride and Z phase as a function of nitrogen content. The results show that there is a clear

correlation between increasing the nitrogen content and the increased mass percentage of each of these phases. The nitrogen content needs to be carefully controlled as an increased precipitation of vanadium nitride could have a beneficial effect on improving the creep properties, whereas the increased mass percentage of Z phase is likely to produce detrimental creep properties in the long term.

4.3.2 Effect of Boron

Boron has been reported by *Abe et al* [2]. to significantly improve the creep properties in 9 wt. % chromium steels. The key theory to explain the role of the boron addition in MarBN alloys is when boron is in solution the coarsening rate of the $M_{23}C_6$ carbides can be reduced. However, boron has a strong affinity for nitrogen and therefore can form boron nitride if the nitrogen content is not carefully controlled, which can offset the beneficial effect of the nitrogen addition [26]. Thermodynamic calculations have also predicted that a small amount of boron can be dissolved within the $M_{23}C_6$ carbide as shown in Figure 4.2 g).

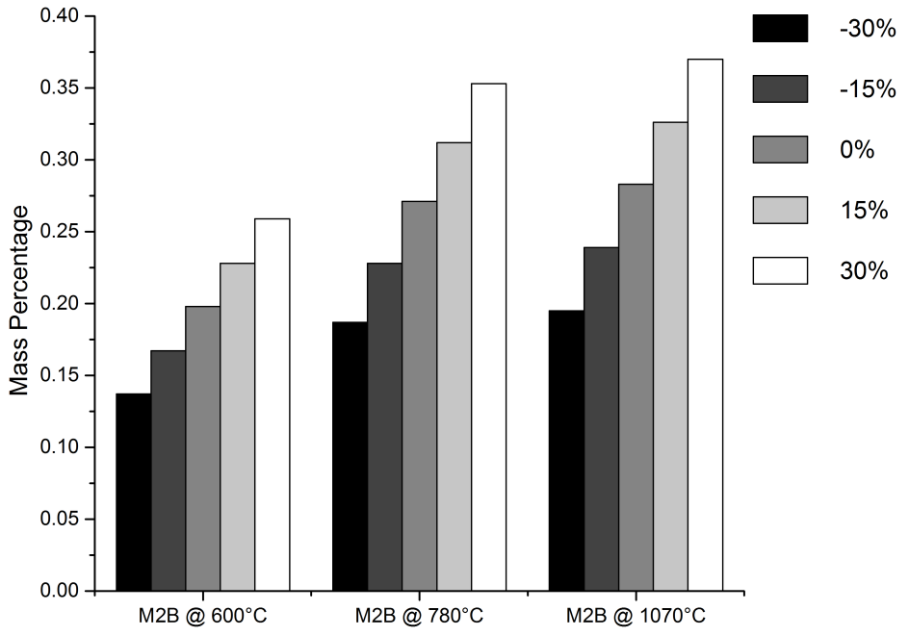

Figure 4.4: A graph showing the effect of boron on the predicted mass percentage of W_2B at 600°C, 780°C and 1070°C.

The precipitation of W_2B can reduce the amount of boron within solution. A sensitivity study has been undertaken to investigate the effect of the boron addition on the precipitation of W_2B at 600°C, 780°C and 1070°C. Figure 4.4 shows the predicted mass percentage of M_2B at 600°C, 780°C and 1070°C as a function of boron content; it is evident that as the boron content increase the amount of M_2B increases proportionally.

4.3.3 Effect of Carbon

Figure 4.2 shows that in MarBN alloys, carbon is predicted to be present within Laves phase, $M_{23}C_6$, NbC and M_6C. A sensitivity study investigated the effect of the carbon content on the mass percentage of Laves phase, $M_{23}C_6$ and M_6C. Figure 4.5 shows the effect of the carbon content on the mass percentage of Laves phase and $M_{23}C_6$ at 600°C. The predicted mass percentage of Laves phase decreases gradually as the carbon content is increased; in contrast the mass percentage of $M_{23}C_6$ increases as the carbon content is increased.

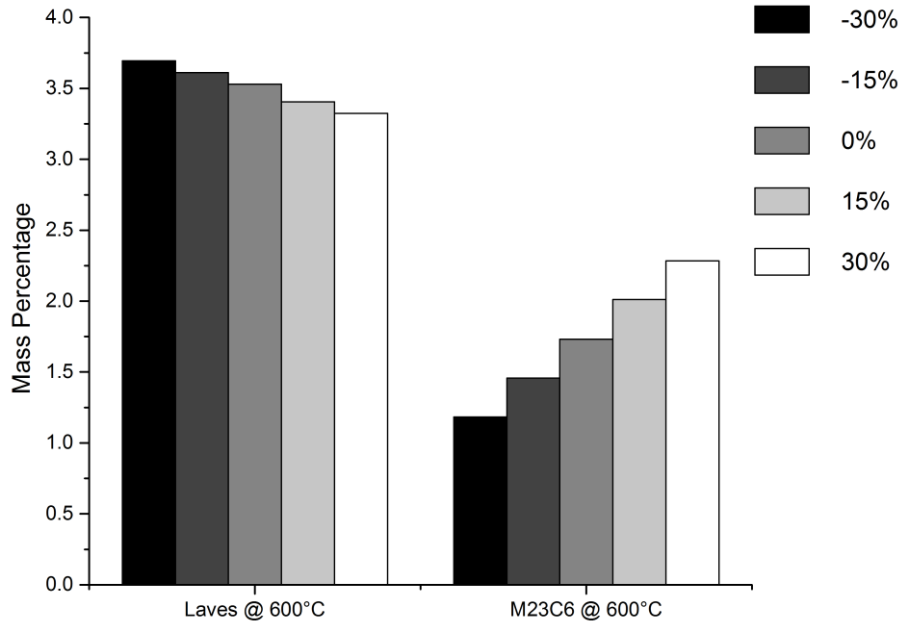

Figure 4.5: A graph showing the effect of the carbon content on the predicted mass percentage of Laves phase and $M_{23}C_6$ at 600°C.

Figure 4.6 shows the effect of carbon on the dissolution temperature of niobium carbide. It is evident that increasing the carbon content in the alloy increases the stability of this phase, which results in a higher dissolution temperature of this phase.

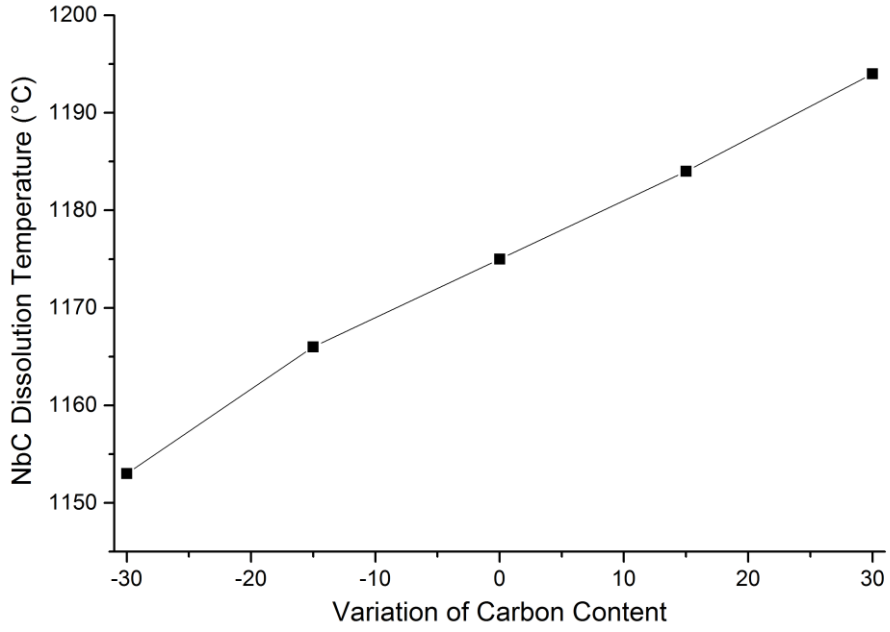

Figure 4.6: A graph showing the effect of the carbon content on the dissolution temperature of niobium carbide within MarBN.

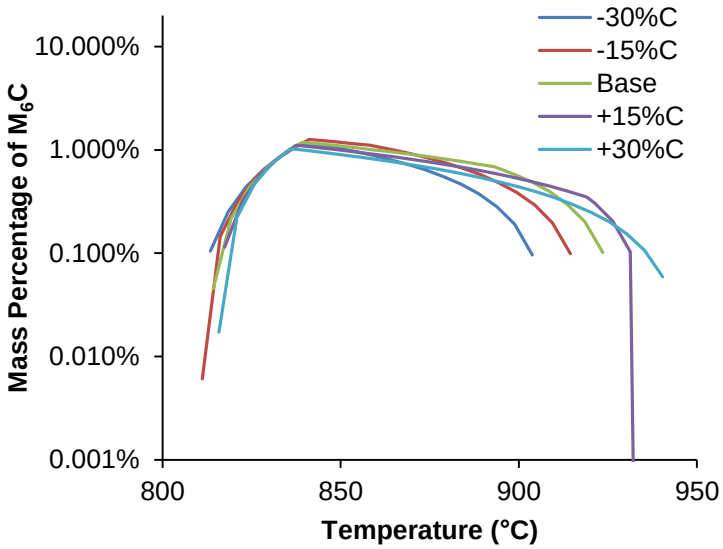

Figure 4.7: A graph showing the effect of the carbon content on the predicted formation of M_6C at 600°C.

4.3.4 Effect of Tungsten

Figure 4.2 shows the chemical composition of the phases predicted to be present in standard MarBN. There are two phases predicted which have a significant concentration of tungsten which are Laves phase and M_6C, as shown in Figure 4.2 f) and i) respectively.

During the stability study the effect of tungsten on the mass percentage of Laves phase under equilibrium conditions has been investigated. The results predict that as the tungsten content is increased the mass percentage of Laves phase increases at 600°C.

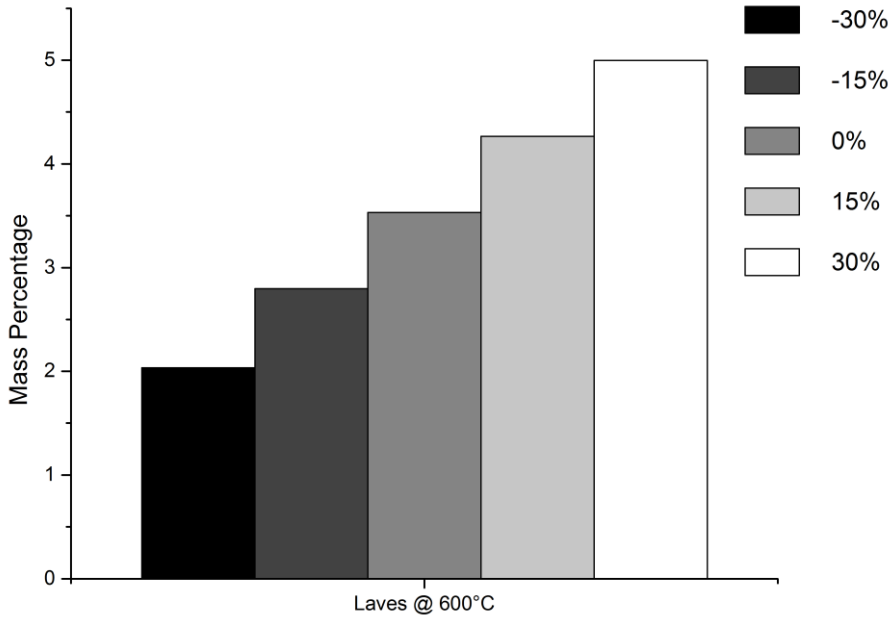

Figure 4.8: A graph showing the effect of the tungsten content on the predicted mass percentage of Laves phase at 600°C.

The effect of the tungsten content on the mass percentage of the M_6C phase has also been investigated. Thermodynamic predictions have shown that as the tungsten content is increased, the temperature range in which Laves phase and M_6C was predicted to be stable over increased. In addition to this the mass percentage of Laves phase and M_6C also increased as a function of tungsten content, as shown in Figure 4.9 a).

M_6C is a carbide and therefore the precipitation of this phase will reduce the amount of carbon available to precipitate other strengthening carbides such as NbC. This is important because NbC is known to be an important strengthening carbide in 9 wt. % chromium steels.

Therefore, a stability study has also investigated the effect of the presence of M_6C, on the mass percentage of NbC phase. Figure 4.9 a) and b) shows the predicted mass percentage of M_6C and NbC respectively at a range of tungsten contents. Figure 4.9 a) and b) show that as the tungsten content is increased, M_6C is predicted to be stable over a wider temperature range, which results in a suppression of NbC over the temperature range which M_6C is also stable over.

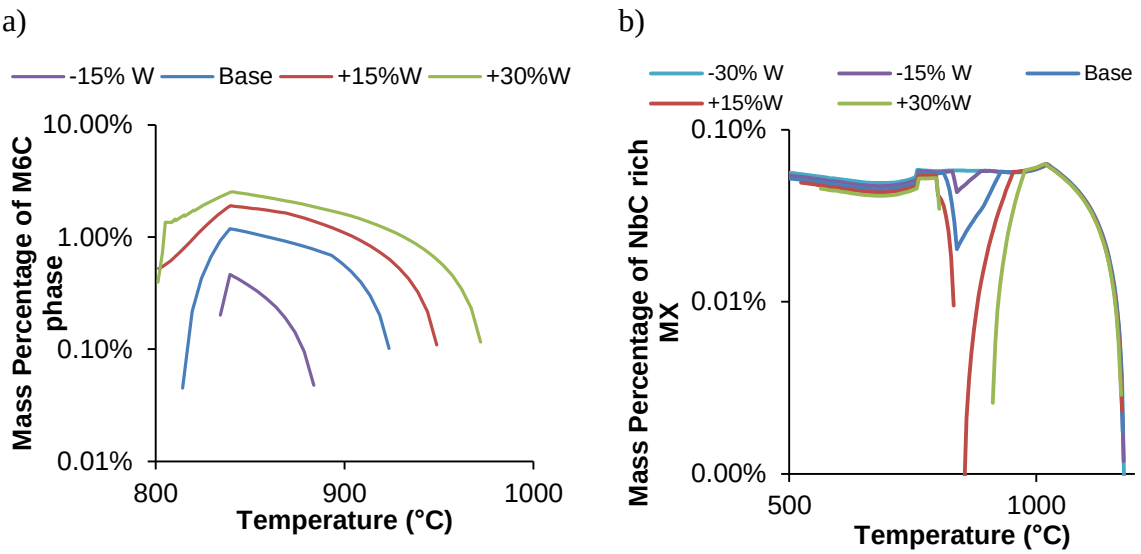

Figure 4.9: A graph showing the effect of the tungsten content on a) the mass percentage of M_6C as a function of temperature and b) on the effect of tungsten on the formation of NbC.

4.3.5 Effect of Alloying Elements on the Delta Ferrite Formation Temperature

Thermodynamic calculations were carried out to investigate the effect of the chemical composition of C, Mn, Al, B, Co, N and W on the delta ferrite formation temperature. Each element was changed independently by ±30% at the expense of iron. Figure 4.10 shows the results; it is evident that increasing the percentage of cobalt and carbon leads to an increase in the delta ferrite formation temperature and are therefore austenite stabilising elements. In comparison, increasing the tungsten content is predicted to result in a decrease in the delta ferrite temperature and therefore is a ferrite stabilising element. The addition of Al, B, Mn and N were predicted to have very little impact on the delta ferrite formation temperature.

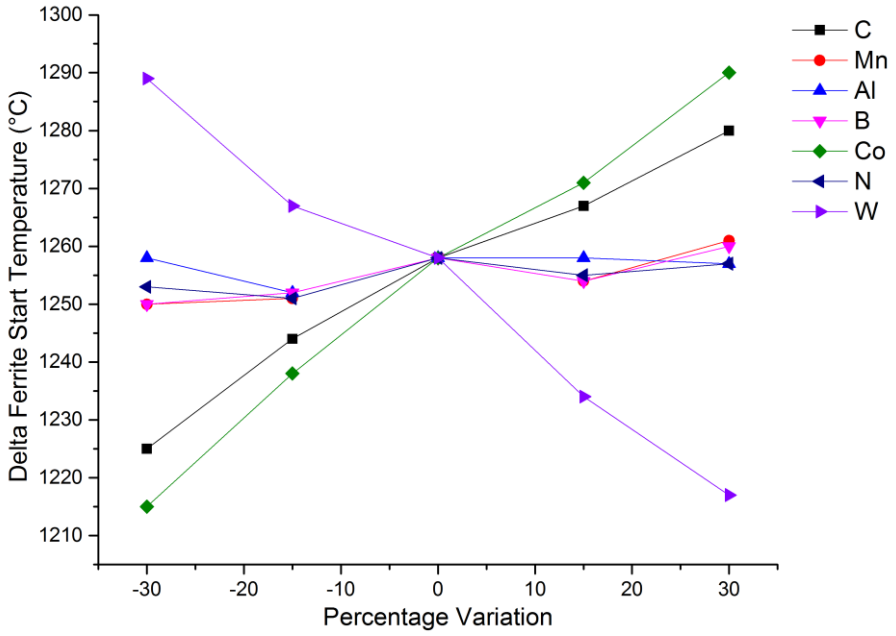

Figure 4.10: A graph showing the effect of C, Mn, Al, B, Co, N and W on the predicted delta ferrite formation temperature.

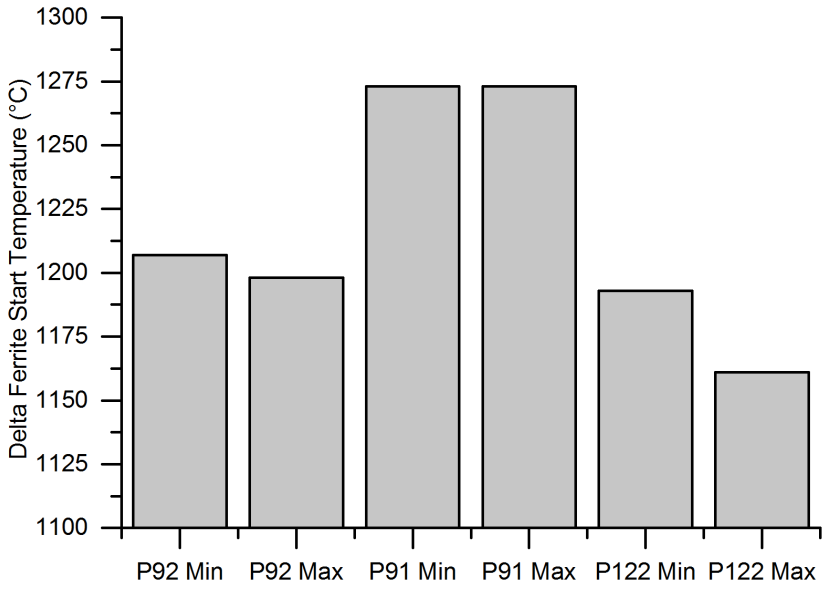

Figure 4.11: A graph showing the predicted delta ferrite start temperatures of a number of commercial 9 wt. % chromium steels such as P91, P92, P122 and the newly developed MarBN alloy.

Figure 4.11 shows the predicted delta ferrite start temperature for P91, P92, P122 and the newly developed MarBN alloy. It is vital that the delta ferrite start temperature is above 1250°C to ensure that during rolling no delta ferrite is precipitated, as this has been reported to have a detrimental effect on the creep properties of the alloy. The delta ferrite temperature has been predicted to decrease from P91 to P92, which is thought to be due to the addition of 1.8 wt. % tungsten [1]. The MarBN composition developed by the NIMS has a composition of

3W-3Co-B-N-V-Nb in which the addition of tungsten will lower the delta ferrite start temperature and therefore this has had to be balanced with the addition cobalt in order to raise the delta ferrite start temperature.

4.4 Effect of Boron and Nitrogen on the Formation of Boron Nitride

The MarBN alloy utilises the addition of boron to improve the creep properties. The boron addition is thought to reduce the coarsening rate of the $M_{23}C_6$ carbides [11,22]. Nitrogen is a key element in 9 wt. % chromium steels as it helps promote strengthening phases such as vanadium nitride. The addition of boron can have a detrimental effect as it can form boron nitride which can offset the beneficial effects of both the boron and nitrogen additions [12,26].

Therefore, it is essential that both the boron and nitrogen additions are carefully optimised to ensure boron nitride is not precipitated. A systematic study has been carried out with the use of thermodynamic calculations to predict the boron and nitrogen levels required to prevent the precipitation of boron nitride. The thermodynamic calculations were carried out in conjunction with a MarBN base alloy composition, as shown in Table 4.1. The boron and nitrogen contents were both varied at the expense of iron. If boron nitride was predicted to be stable between 1050°C to 1150°C a red diamond was plotted on Figure 4.12; if boron nitride was not predicted to be present a square grey point was plotted. The figure shows that when the boron content was between 0.0001 wt. % and 0.4 wt. %, the nitrogen content needs to be below 0.016 wt. % to ensure that boron nitride is not predicted to be present. If the boron content is below 0.0001 wt. % the nitrogen content is required to be below 0.1 wt. % to ensure boron nitride is not predicted to be present. The figure also shows there is a clear boundary where boron nitride is predicted, and it is therefore deemed that near this boundary the boron and nitrogen compositions are at a higher risk to boron nitride formation.

The thermodynamic calculations performed within this section have been compared to the boron nitride solubility product developed by Sakuraya *et al.* [12], as shown in Figure 4.13. A comparison has shown that the two methods demonstrate a good agreement in predicting boron nitride, however some small variations were observed. The solubility product shows that boron nitride can be precipitated using a lower nitrogen content of 0.005 wt. % and high boron content of 0.05 wt. %.

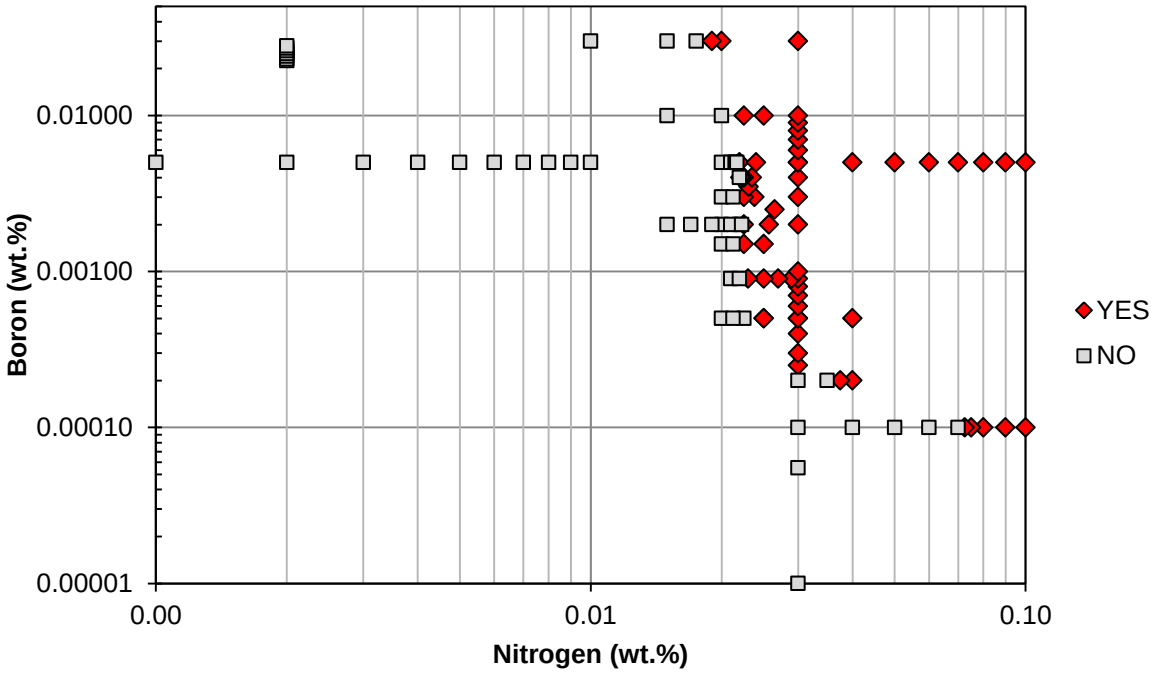

Figure 4.12: A graph showing a series of individual thermodynamic calculations carried out in conjunction with a MarBN base at a temperature of 1150ºC to show the maximum boron and nitrogen level before boron nitride is predicted to be precipitated.

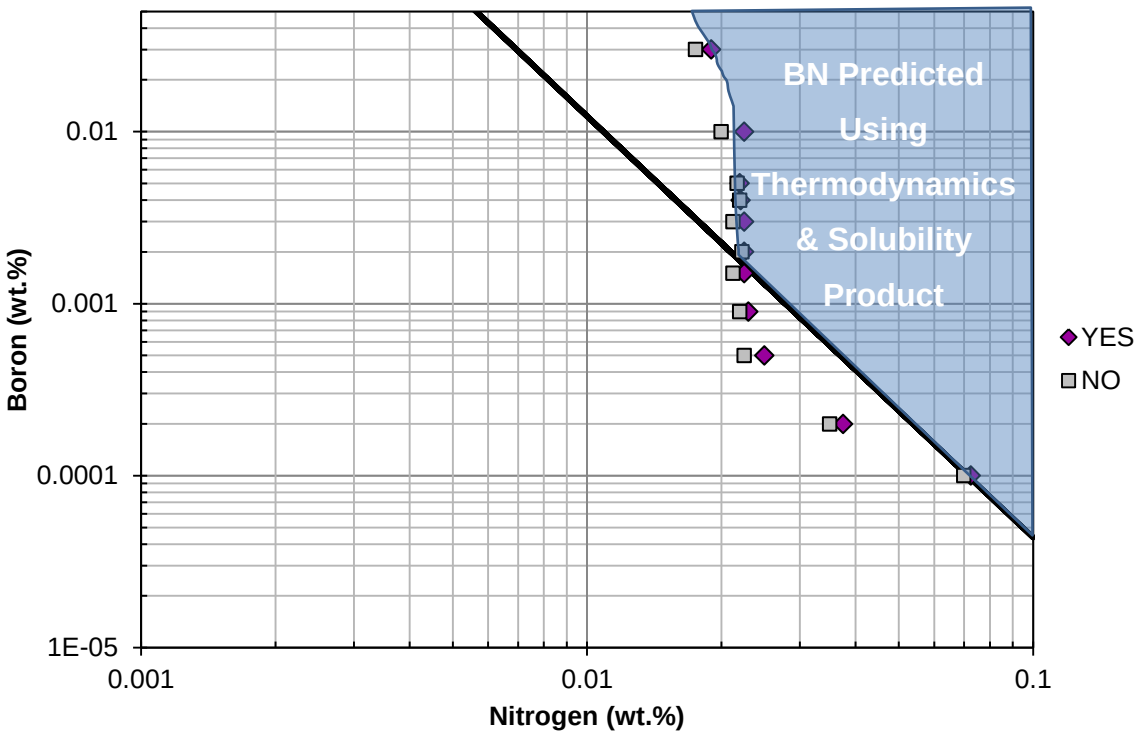

Figure 4.13: A graph showing the boron and nitrogen content required to prevent the precipitation of boron nitride (determined using thermodynamic calculations at a temperature of 1150ºC), and the black solid line shows the BN solubility line determined by Sakurya et al.

The thermodynamic predictions provide essential information to understand the precipitation behaviour of boron under equilibrium conditions. These data will help provide essential information to maximise the boron and nitrogen contents to help optimise the creep strength of MarBN. The thermodynamic calculations will need to be validated with the use of experimental trial melts manufactured with different boron and nitrogen contents.

4.5 Effect of Alloying Elements on Phase Stability of Z Phase

Z phase has been predicted to be present in MarBN as shown in Figure 4.1, and the predicted chemical composition of this complex nitride is shown in Figure 4.2 j). Z phase is one of the main phases that is associated with the decrease of long term creep properties.

Z phase has a composition of Cr(V,Nb)N and has been reported to precipitate as large particles which consume smaller MX carbonitrides after long term ageing at the service temperature [47,68].

A systematic thermodynamic study has been carried out to identify if the mass percentage of Z phase can be reduced or eliminated by changing the chemical composition of chromium, niobium and nitrogen. The thermodynamic calculations were performed using a MarBN base composition. The elements (chromium, niobium and nitrogen) were independently modified at the expense of iron.

4.5.1 Effect of Chromium on the Phase Stability of Z Phase

The chromium content was changed between 6.25 wt. % and 11.0 wt. %. Figure 4.14 shows the effect of the chromium content on the mass percentage of Z phase predicted. In order to significantly change the amount of Z phase predicted the chromium content is required to be reduced to less than 6.25 wt. %. The high chromium addition is added into 9 wt. % chromium steels to improve the oxidation resistance; reducing the chromium level to approximately 6 wt. % will not provide the required oxidation resistance for such application and therefore it is expected that Z phase will be predicted for these steel compositions.

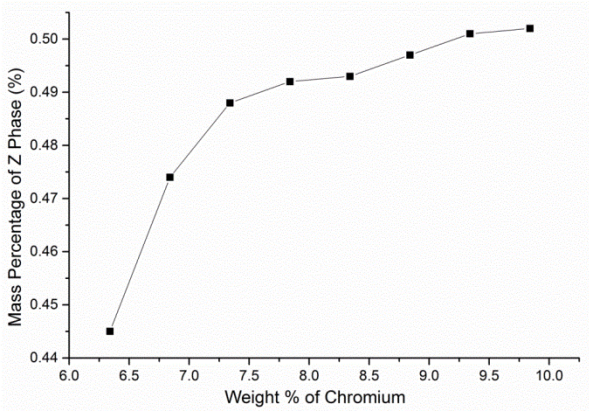

Figure 4.14: A graph showing the effect of the chromium content on the predicted mass percentage of Z Phase.

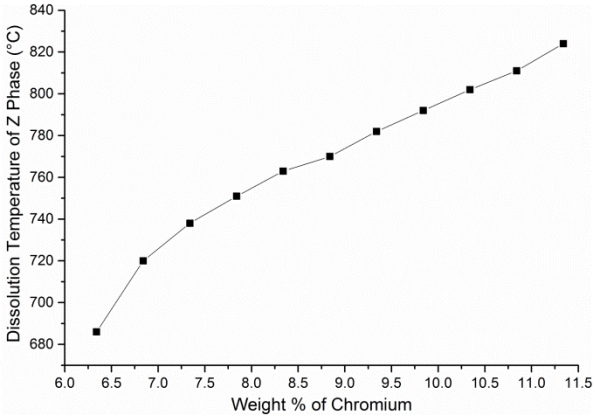

Figure 4.15: A graph showing the effect of the chromium content on the dissolution temperature of Z Phase.

The dissolution temperature of Z phase as a function of chromium content has also been investigated. The dissolution temperature was predicted to decrease in a linear manner as the chromium content was decreased; however, the changes in the dissolution temperature were small. Thermodynamic calculations were carried out using a chromium content of 6.5 wt. %, and the dissolution temperature was still above the service temperature of 650°C for ultra-super critical applications, indicating that it is likely to be present in these steel compositions.

4.5.2 Effect of Nitrogen on the Phase Stability of Z Phase

Thermodynamic calculations were performed to study the effect of the nitrogen content on the phase stability of Z phase. During this study the nitrogen content was changed from 0.20 wt. % to 0.50 wt. % at the expense of iron.

The predictions show that nitrogen is one of the key elements that can affect the mass percentage of Z phase predicted. The dissolution temperature of Z phase has been investigated as a function of nitrogen content, as shown in Figure 4.17. The figure shows that the dissolution temperature of Z phase decreases as a function of nitrogen content. The thermodynamic calculations indicate that the dissolution temperature of Z phase is above the service temperature when the nitrogen content is reduced to 200 ppm.

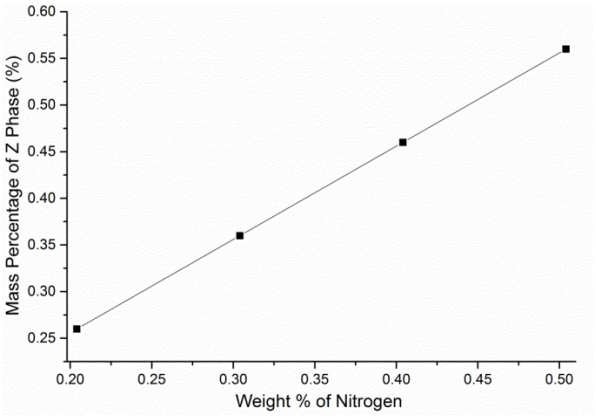

Figure 4.16: A graph showing the effect of the nitrogen content on the mass percentage of Z phase predicted.

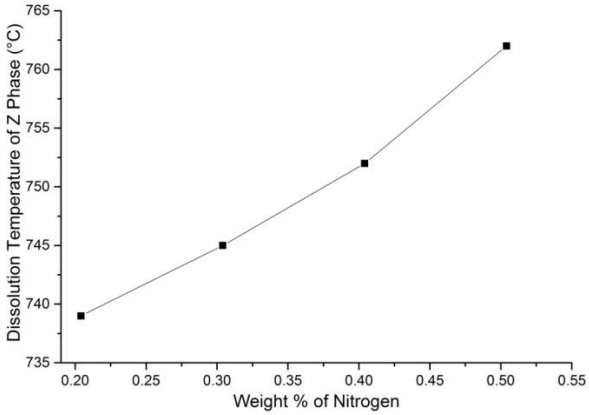

Figure 4.17: A graph showing the effect of the nitrogen content on the dissolution temperature of Z phase.

4.5.3 Effect of Niobium the Phase Stability of Z Phase

The effect of niobium on the phase stability of Z phase has been predicted with the use of thermodynamic calculations, in a similar manner to the previous calculations investigating the effect of chromium and nitrogen. Thermodynamic calculations were carried in conjunction with a niobium content from 0 wt. % to 0.9 wt. %. The mass percentage of Z phase was predicted to decrease as the niobium content was decreased. Niobium was not predicted to have a significant effect on the mass percentage of Z phase; the calculations indicate Z phase will form when niobium is completely removed.

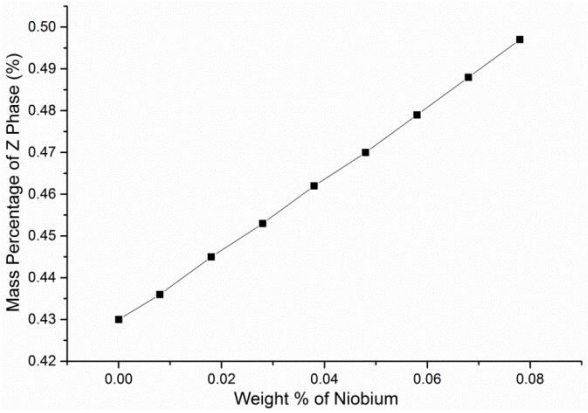

Figure 4.18: A graph showing the effect of the niobium content on the mass percentage of Z phase predicted.

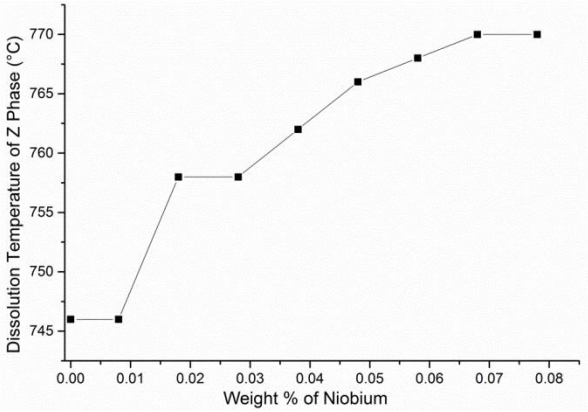

Figure 4.19: A graph showing the effect of the niobium content on the dissolution temperature of Z phase.

The predictions indicated that a reduction in the niobium content would have only a small effect on reducing the dissolution temperature of Z phase. The dissolution temperature was

predicted to be above the service temperature even when the niobium content was reduced to 0 wt. %.

4.6 Strategy Used to Develop a Series of Optimised MarBN Alloys

The aim of the IMPACT project was to develop and manufacture a series of MarBN alloys, which have optimised creep properties. Results from the thermodynamic calculations in the earlier part of this chapter have therefore been used to help optimise the steel. The thermodynamic calculations have been used in this process to maximise the phases which provide a beneficial effect to creep, whilst the phases which are detrimental to creep have been minimised. A summary of the phases which are thought to have a beneficial or detrimental effect to the creep properties are shown in Table 4.3.

Table 4.2: A summary of the beneficial and detrimental phases predicted to be present in a MarBN alloy.

Effect on Mechanical Properties	**Phase**
Beneficial	$M_{23}C_6$, Vanadium Nitride and Niobium Carbide
Detrimental	Boron Nitride, Aluminium Nitride, Delta Ferrite, M_6C, Z Phase, Laves Phase

The delta ferrite temperature was another key factor in the design of such alloys; it was required to produce a steel with a delta ferrite start temperature above the rolling temperature of 1250°C. In addition to this, the steels were also required to have a suitable prior austenite grain size, and have a martensite finish temperature above room temperature.

During the IMPACT project a number of MarBN alloys were designed with the use of thermodynamic calculations. Four melts were initially designed and were manufactured at Goodwin Steel Castings using a standard air melting technique. The four alloys each had different objectives, one melt was designed to determine if a MarBN alloy could be manufactured at low cost, two further variants were designed to optimise the composition of MarBN further and a final steel was manufactured with the standard MarBN composition in order that a comparison could be carried out.

4.6.1 Development of a Low Cost MarBN Alloy

The costs of 9 – 12 wt. % chromium steels are increasing due to the addition of alloying elements to achieve improved creep properties required to increase the service temperature. Cobalt and tungsten are two of the most expensive elements and can have a significant effect on the overall price of the alloy.

In the first alloy variant the concentrations of cobalt and tungsten were reduced to 1.0 wt. %, as indicated by the green columns in Table 4.4. The boron and nitrogen additions were also modified to ensure that boron nitride is not predicted to be present when normalised at 1150°C or tempered at 780°C.

The calculated phase diagram computed from the composition of the low cost variant is shown in Figure 4.20. The figure shows that this melt may be problematic due to the relatively low tungsten addition and the high boron addition which are likely to retain the liquid to lower temperatures and also suffer from hot working problems.

Table 4.3: Chemical composition of the low cost MarBN variant and the original MarBN alloy in wt. %, balance Fe.

	C	**Si**	**Mn**	**Cr**	**Mo**	**Ni**	**Al**	**B**	**Co**	**N**	**Nb**	**V**	**W**
Standard MarBN	0.09	0.40	0.50	9.0	0.10	0.10	0.015	0.012	3.0	0.013	0.06	0.22	3.0
Low Cost Variant	0.09	0.40	0.50	9.0	0.10	0.10	0.015	0.012	1.0	0.013	0.06	0.22	1.0

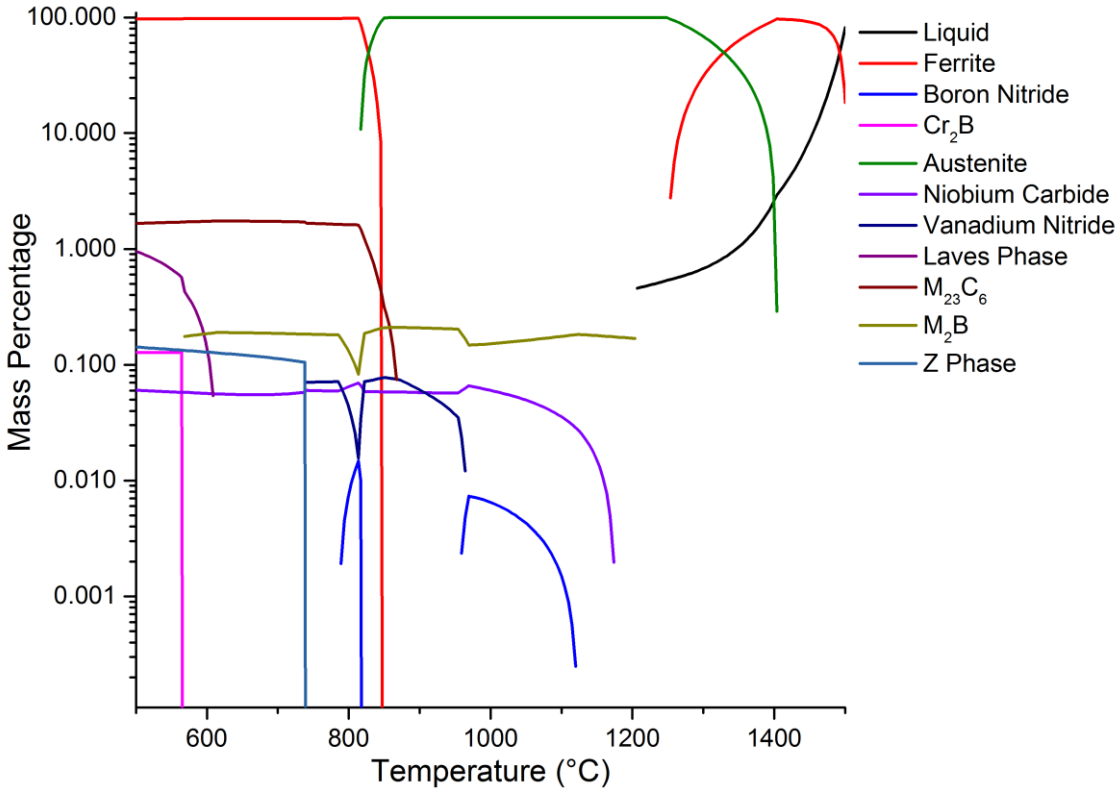

Figure 4.20: A graph showing the phases predicted using thermodynamic calculations as a function of temperature for the low cost MarBN variant.

4.6.2 Development of an Optimised MarBN Composition

Two alloys were designed with the use of thermodynamic calculations to optimise the MarBN alloy. Table 4.4 shows the chemical composition of the two optimised MarBN compositions, in addition to the composition of standard MarBN for comparison. The key changes to the chemical composition have been made to three elements boron, nitrogen and tungsten which are highlighted by the green columns.

Table 4.4: A table showing the chemical composition of the two optimised MarBN variants and the composition of standard MarBN in wt. %, balance Fe.

	C	**Si**	**Mn**	**Cr**	**Mo**	**Ni**	**Al**	**B**	**Co**	**N**	**Nb**	**V**	**W**
Standard MarBN	0.09	0.40	0.50	9.0	0.10	0.10	0.015	0.012	3.0	0.013	0.06	0.22	3.0
Optimised – 1	0.09	0.40	0.50	9.0	0.10	0.10	0.015	0.012	3.0	0.013	0.06	0.22	2.6
Optimised – 2	0.09	0.40	0.50	9.0	0.10	0.10	0.015	0.020	3.0	0.016	0.06	0.22	2.6

The stability study indicated that tungsten was found to increase the amount of Laves phase predicted to be present and also decrease the delta ferrite start temperature. The tungsten content was therefore reduced to 2.6 wt. % in both optimised compositions, to raise the delta ferrite finish temperature above 1250°C and supress the formation of Laves phase and M_6C. Figure 4.21 shows the mass percentage of Laves phase for the standard composition and the two optimised MarBN compositions. Figure 4.22 shows the predicted mass percentage of M_6C for the standard MarBN composition and the two optimised compositions.

The aim was to keep the boron and nitrogen content similar to the MarBN alloy designed by Abe *et al.* [22] The boron and nitrogen additions in the optimised composition have been designed to avoid the precipitation of boron nitride. The phase diagram predicted using thermodynamic calculations and the composition of the first optimised alloy; Optimised-1 is shown in Figure 4.23.

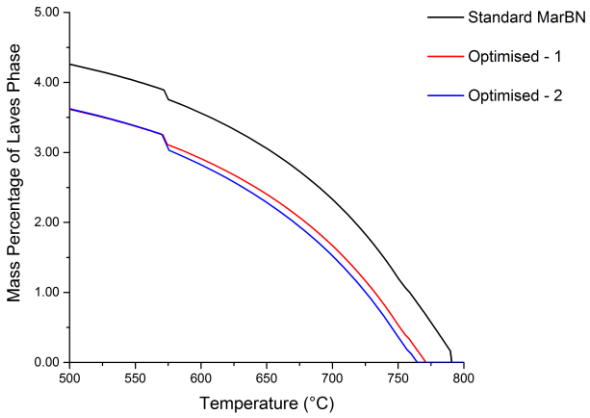

Figure 4.21: A graph showing a comparison of the mass percentage of Laves phase predicted in standard MarBN and the two optimised MarBN compositions, shown in Table 4.5.

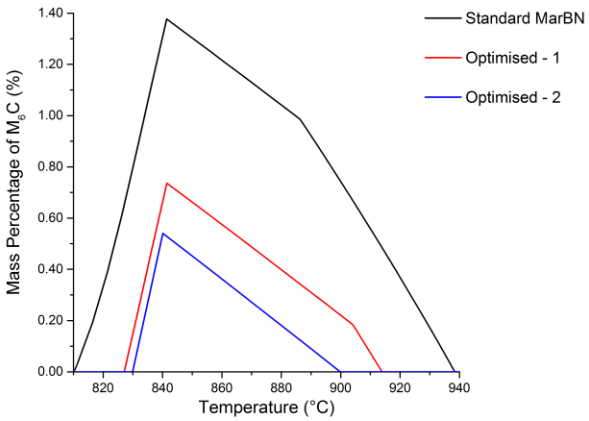

Figure 4.22: A graph showing a comparison of the mass percentage of M_6C predicted in standard MarBN and the two optimised MarBN compositions, shown in Table 4.5.

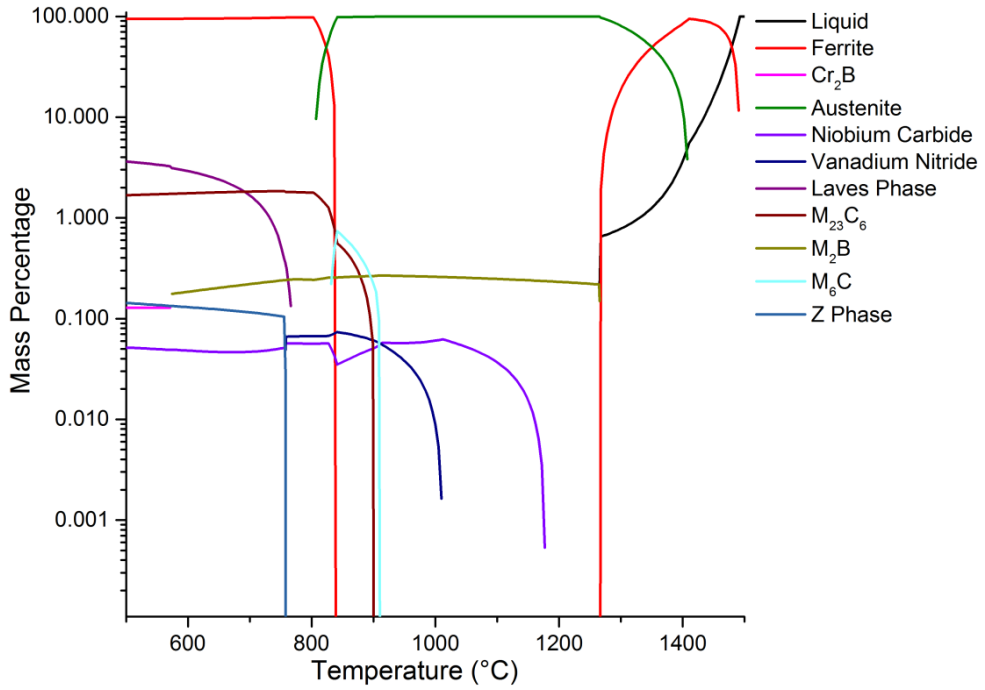

Figure 4.23: A graph showing the phases predicted using thermodynamic calculations as a function of temperature for the Optimised-1 variant.

A second optimised MarBN alloy was designed to maximise the boron and nitrogen additions, whilst avoiding the formation of boron nitride. The increased addition of nitrogen was designed to promote the formation of vanadium nitride MX precipitates. Figure 4.24 shows the predicted mass percentage of vanadium nitride for the standard composition and also for the Optimised-2 composition. The phase diagram predicted using thermodynamic calculations and the composition of Optimised-2 is shown in Figure 4.25.

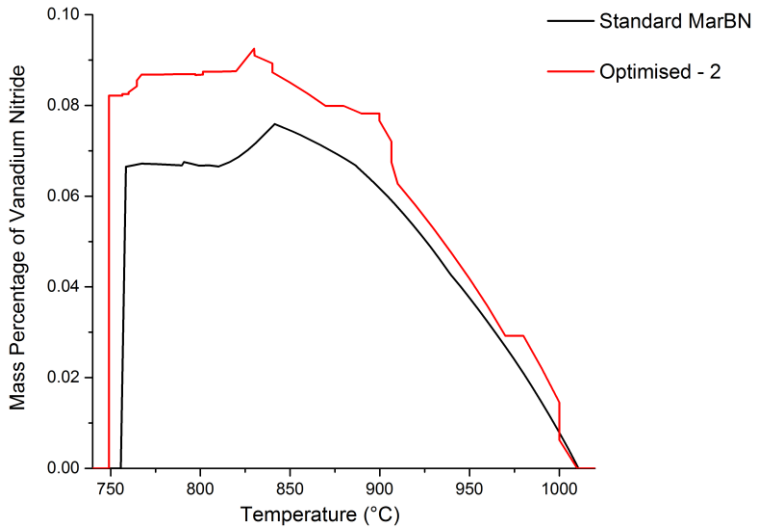

Figure 4.24: A graph showing a comparison of the mass percentage of vanadium nitride predicted in standard MarBN and the Optimised-2 MarBN composition, shown in Table 4.5.

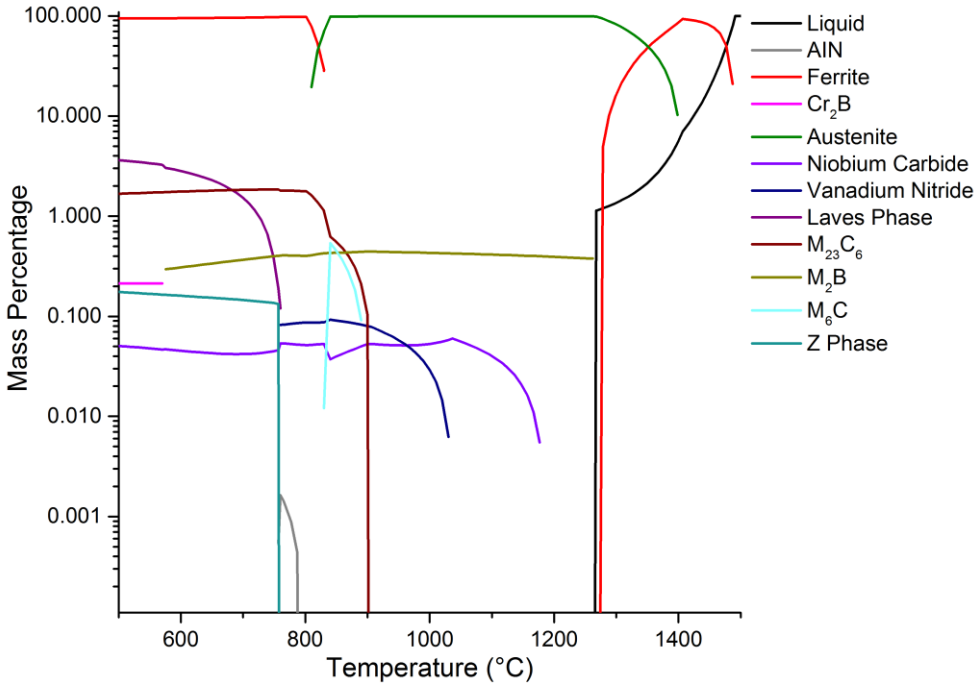

Figure 4.25: A graph showing the phases predicted using thermodynamic calculations as a function of temperature for the Optimised-2 variant.

4.7 Compositions of the Steels Manufactured in the First Batch and the Influence on the Phases Predicted to be Present

The chemical compositions of the alloys designed for manufacture were carefully determined using thermodynamic calculations to optimise the phases predicted. Unfortunately, when the alloys were manufactured the ability to control the chemical composition to a high degree of accuracy was not possible for a number of elements using a standard air melting technique.

The alloys manufactured during the first batch have been given the following nomenclature to provide a reference system throughout the thesis:

- "Low Cost MarBN" denoted as GAM 1;
- "Optimised – 1 MarBN" denoted as GAM 2;
- "Optimised – 2 MarBN" denoted as GAM 3;
- "Standard MarBN" denoted as GAM 4;

Table 4.5: A summary of the target and actual compositions of the steels manufactured during the first batch in wt. %, balance Fe.

	C	Si	Mn	Cr	Mo	Ni	Al	B	Co	N	Nb	V	W
Target Composition													
Low Cost MarBN	0.09	0.40	0.5	9.0	0.1	0.1	0.015	0.012	1.0	0.013	0.06	0.22	1.0
Optimised – 1	0.09	0.40	0.5	9.0	0.1	0.1	0.015	0.012	3.0	0.013	0.06	0.22	2.6
Optimised – 2	0.09	0.40	0.5	9.0	0.1	0.1	0.015	0.020	3.0	0.016	0.06	0.22	2.6
Standard MarBN	0.09	0.40	0.5	9.0	0.1	0.1	0.015	0.012	3.0	0.013	0.06	0.22	3.0
Measured Composition													
GAM 1	0.09	0.29	0.38	8.67	<0.01	0.06	0.01	0.011	1.06	0.019	0.05	0.22	0.96
GAM 2	0.09	0.31	0.46	8.70	<0.01	0.06	0.01	0.010	3.18	0.020	0.06	0.22	2.51
GAM 3	0.09	0.46	0.54	8.65	<0.01	0.06	0.02	0.018	2.84	0.020	0.06	0.22	2.49
GAM 4	0.09	0.43	0.50	8.62	<0.01	0.06	0.02	0.009	2.85	0.21	0.07	0.21	3.13

The phase diagrams calculated using the aim composition of GAM 1 – 3 are shown in Figures 4.20, 4.23 and 4.25. In addition phase diagrams were calculated using the actual chemical composition of the alloys manufactured, as shown in Figures 4.26 – 4.29. In the case of GAM 1, variations were observed to be present between the phases predicted to be present using the aim and actual composition. The nitrogen content was 60 ppm higher in the alloy manufactured; this led to boron nitride predicted to be present over a wider temperature range of ~900°C - 1230°C, furthermore the mass percentage of vanadium nitride was increased due to the higher nitrogen addition, as shown in Figure 4.26.

In the case of GAM 2, the major variations between the aim composition and the composition of the alloy manufactured was an increased nitrogen content of 70 ppm, and an increased cobalt addition of 0.18 wt. % and a reduction of 0.09 wt. % tungsten. The change in the chemical composition led to the prediction of boron nitride and an increase in the mass percentage of vanadium nitride predicted to be present. The change in the cobalt and tungsten alloying additions was demonstrated to have very little effect on the phases predicted to be present as shown in Figure 4.27. The change in the alloying elements in GAM 3 was similar to that of GAM 2; this led to an increase in the precipitation of boron nitride, aluminium nitride, and an increase in the mass percentage of vanadium nitride.

The precipitation of boron nitride and aluminium nitride is thought to have a detrimental effect on the creep properties of the alloys. Short term creep testing and microstructural characterisation were therefore carried out on GAM 1 to 4 to understand the effect of both boron nitride and aluminium nitride.

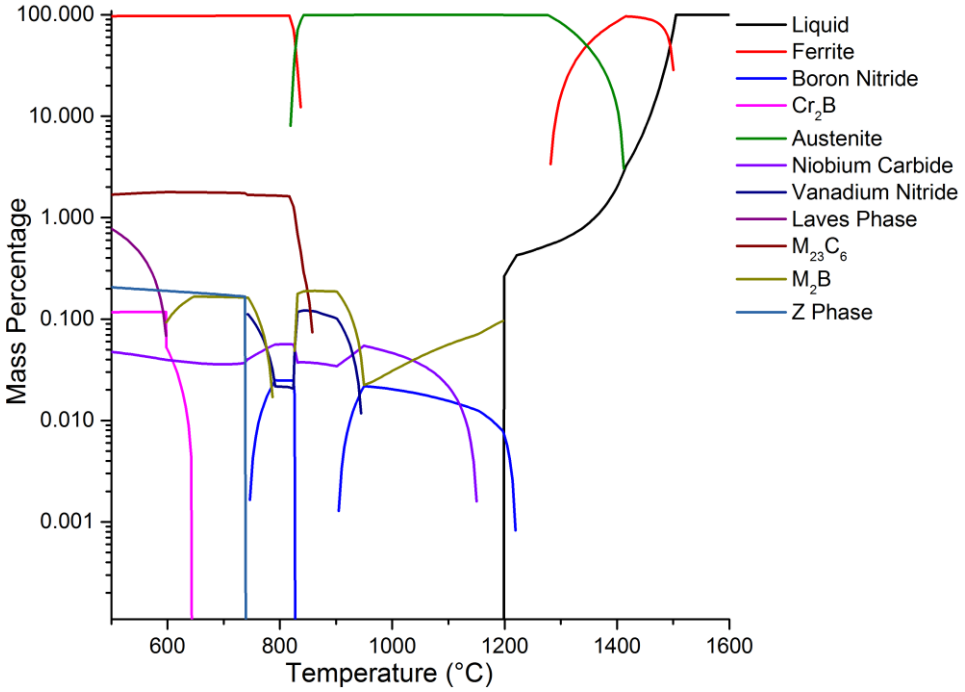

Figure 4.26: A graph showing the phases predicted using thermodynamic calculations as a function of temperature for the composition of GAM 1, as shown in Table 4.6.

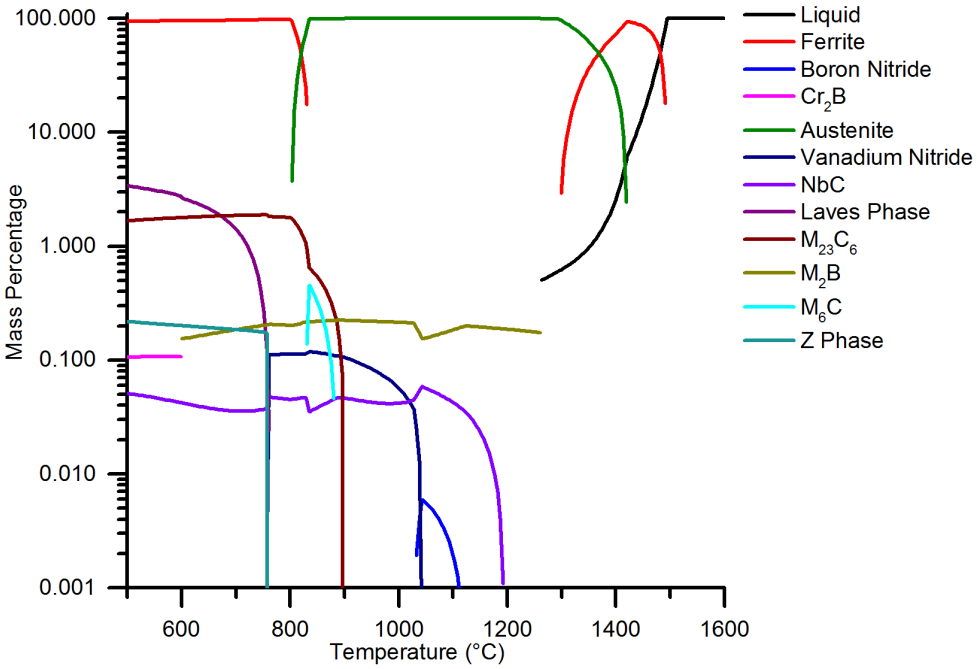

Figure 4.27: A graph showing the phases predicted using thermodynamic calculations as a function of temperature for the composition of GAM 2, as shown in Table 4.6.

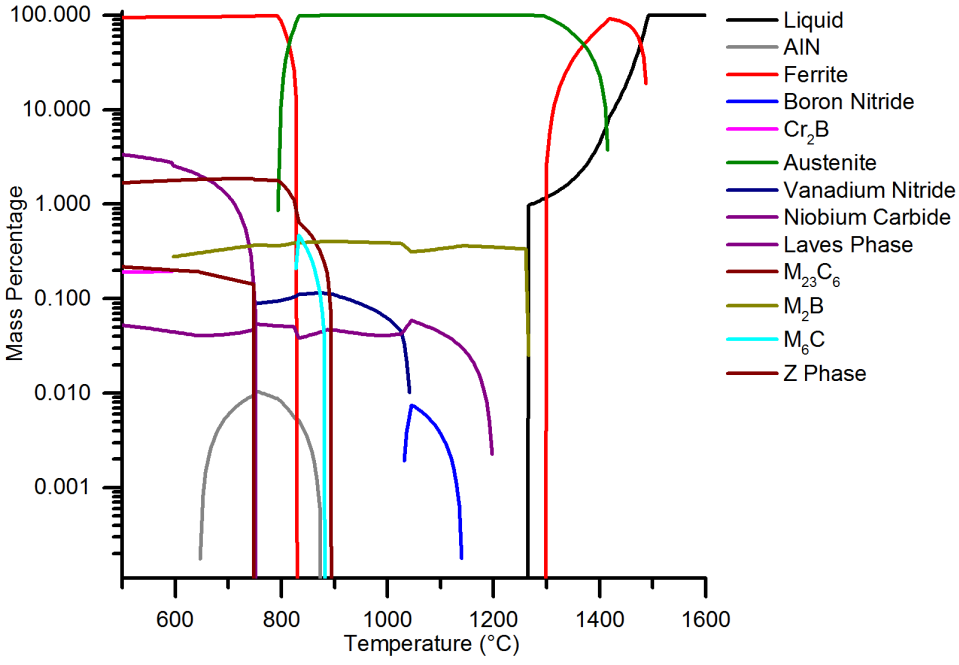

Figure 4.28: A graph showing the phases predicted using thermodynamic calculations as a function of temperature for the composition of GAM 3, as shown in Table 4.6.

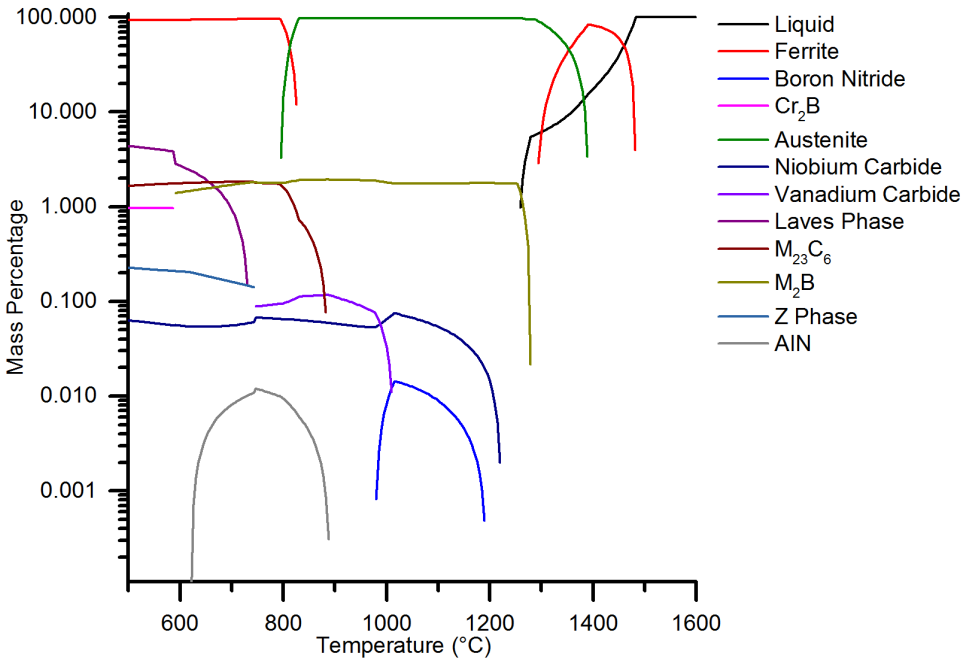

Figure 4.29: A graph showing the phases predicted using thermodynamic calculations as a function of temperature for the composition of GAM 4, as shown in Table 4.6.

4.8 Compositions of the Steels Manufactured in the Second Batch and the Influence on the Phases Predicted to be Present

The steels manufactured during the first batch were deemed out of specification due to the nitrogen content being significantly higher than the target composition, which consequently led to the formation of boron nitride and aluminium nitride.

The steels were therefore manufactured a second time by Goodwin Steel Castings using a different casting technique. An argon purging technique was utilised during the pouring stage to limit the nitrogen pick up from the atmosphere.

GAM 2 was predicted to have boron nitride present over a small temperature range of approximately 1020°C to 1100°C with a maximum mass percentage of 0.00008. Due to the presence of a very small boron nitride peak, this alloy was not re-manufactured, and the opportunity was taken to manufacture a different alloy with another optimised composition using a lower cobalt content.

The effect of cobalt on the long term creep properties in MarBN has not been reported within literature. Microstructural characterisation has been reported by Helis *et al.* [29] with the cobalt content between 1 to 4 wt. % in a 9 wt. % chromium martensitic steel. The cobalt content has

been reported to affect the number density of the $M_{23}C_6$ and MX carbonitrides however its effect on the creep properties is currently unknown.

The optimised composition was denoted as Optimised – 3; the aim of this composition was to investigate the effect of a lower cobalt and tungsten addition. The cobalt addition was reduced to 1.5 wt. %. This low cobalt content was predicted using thermodynamic calculations to lower the start of the delta ferrite transformation, however in order to ensure that the delta ferrite temperature was above 1250°C, the tungsten content was reduced to 2 wt. %, which was predicted in turn to raise the delta ferrite start temperature. Decreasing the tungsten content from 3 wt. % in standard MarBN was found to significantly decrease the mass percentage of Laves phase predicted to be present. M_6C was not predicted to be present when the tungsten content was reduced to 2 wt. %.

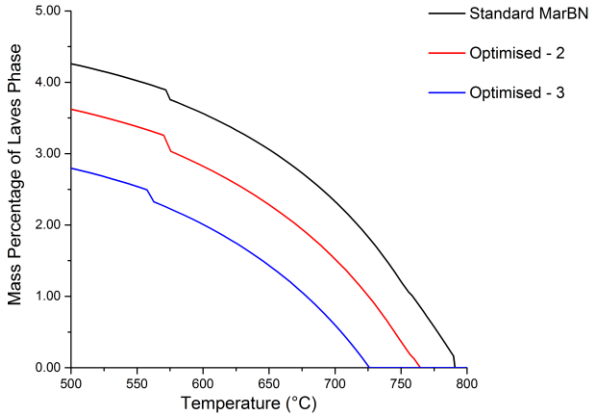

Figure 4.30: A graph showing a comparison of the mass percentage of Laves phase predicted in standard MarBN and Optimised-2 and Optimised-3 MarBN compositions.

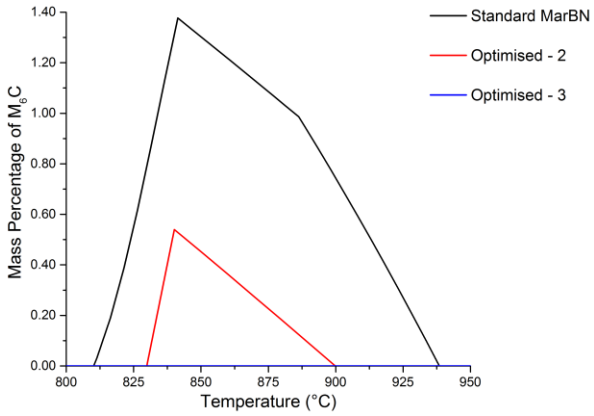

Figure 4.31: A graph showing a comparison of the mass percentage of M_6C predicted in standard MarBN and Optimised-2 and Optimised-3 MarBN compositions.

The composition of the alloys manufactured during the second batch are shown in Table 4.7. The alloys have been given the following nomenclature to provide a reference system throughout the thesis:

- "Low Cost MarBN" denoted as GAM 5;
- "Optimised – 3 MarBN" denoted as GAM 6;
- "Optimised – 2 MarBN" denoted as GAM 7;
- "Standard MarBN" denoted as GAM 8;

Table 4.6: A summary of the target and actual compositions of the steels manufactured during the second batch in wt. %, balance Fe.

	C	Si	Mn	Cr	Mo	Ni	Al	B	Co	N	Nb	V	W
Target Composition													
Low Cost MarBN	0.09	0.40	0.5	9.0	0.1	0.1	0.015	0.012	1.0	0.013	0.06	0.22	1.0
Optimised – 2	0.09	0.40	0.5	9.0	0.1	0.1	0.015	0.020	3.0	0.016	0.06	0.22	2.6
Optimised - 3	0.09	0.40	0.5	9.0	0.1	0.1	0.015	0.012	1.5	0.013	0.06	0.22	2.0
Standard MarBN	0.09	0.40	0.5	9.0	0.1	0.1	0.015	0.012	3.0	0.013	0.06	0.22	3.0
Measured Composition													
GAM 5	0.085	0.36	0.59	9.01	0.12	0.17	0.023	0.0135	1.06	0.009	0.10	0.21	0.98
GAM 6	0.084	0.39	0.55	8.83	0.12	0.16	0.012	0.0145	1.55	0.013	0.11	0.20	2.07
GAM 7	0.083	0.45	0.51	8.72	0.12	0.16	0.020	0.0195	2.78	0.016	0.10	0.19	2.60
GAM 8	0.082	0.50	0.46	8.92	0.12	0.16	0.005	0.0135	2.93	0.015	0.10	0.19	3.09

The nitrogen content of the second batch of steels manufactured, were within a reasonable tolerance of the aim specification. There was observed to be a small variation in a number of other elements which has affected the phases predicted to be present. The chemical composition of GAM 5 was very similar to that of the Low Cost MarBN aim composition and therefore the phase diagram is very similar to that shown in Figure 4.23.

In the case of GAM 6 a change in specification was specified and therefore the cobalt and tungsten additions were significantly below the specification. The thermodynamic calculations have shown indicated that the variation has a small decrease in the mass percentage of Laves phase. The nitrogen content (130 ppm) and the boron content (145 ppm) were both below specification; this led to a reduction in the mass percentage of vanadium nitride predicted to be present.

The chemical composition of GAM 7 was broadly similar to the specification. There was a marginal increase in the chemical composition of boron and nitrogen, but this was observed to have very little effect on the mass percentage of the nitrogen containing phases predicted to be present. There was observed to be an increase of 0.60 wt. % tungsten, which has led to an increase in the mass percentage of Laves phase.

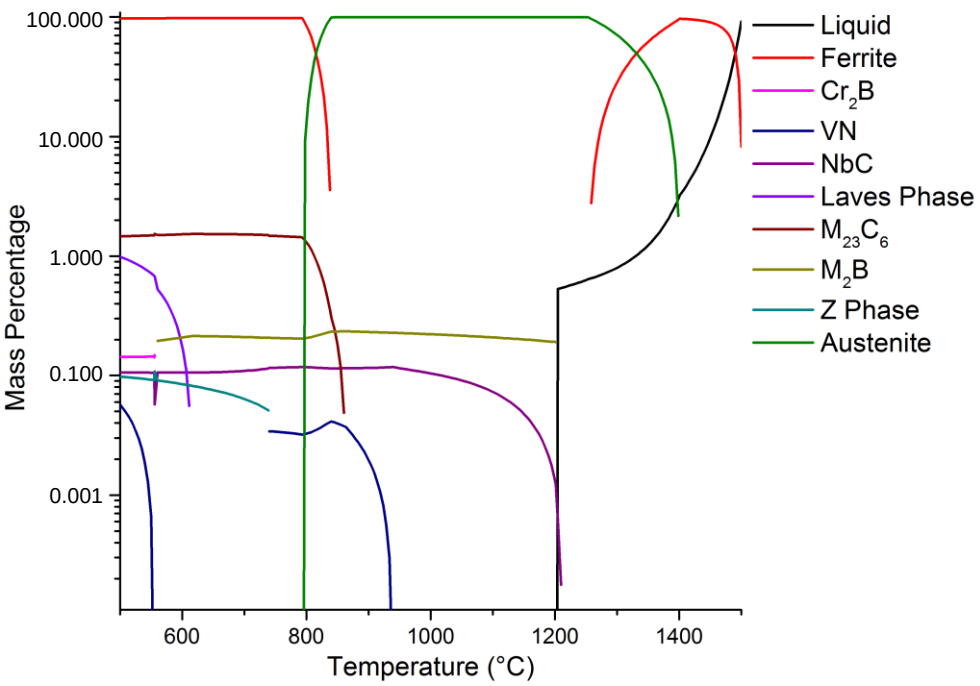

Figure 4.32: A graph showing the phases predicted using thermodynamic calculations as a function of temperature for the composition of GAM 5, as shown in Table 4.7.

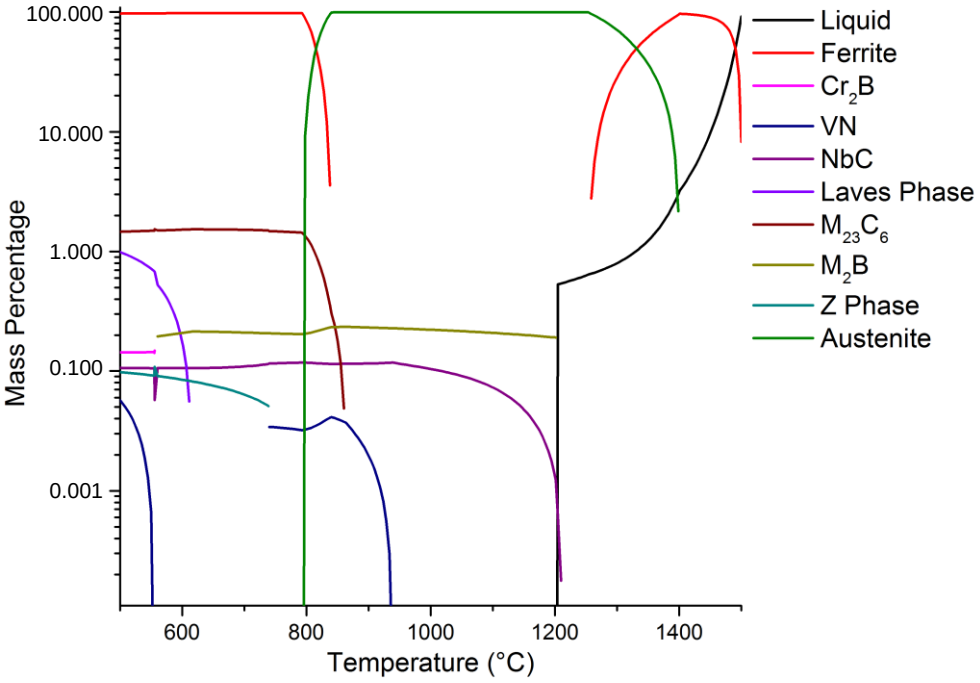

Figure 4.33: A graph showing the phases predicted using thermodynamic calculations as a function of temperature for the composition of GAM 6, as shown in Table 4.7.

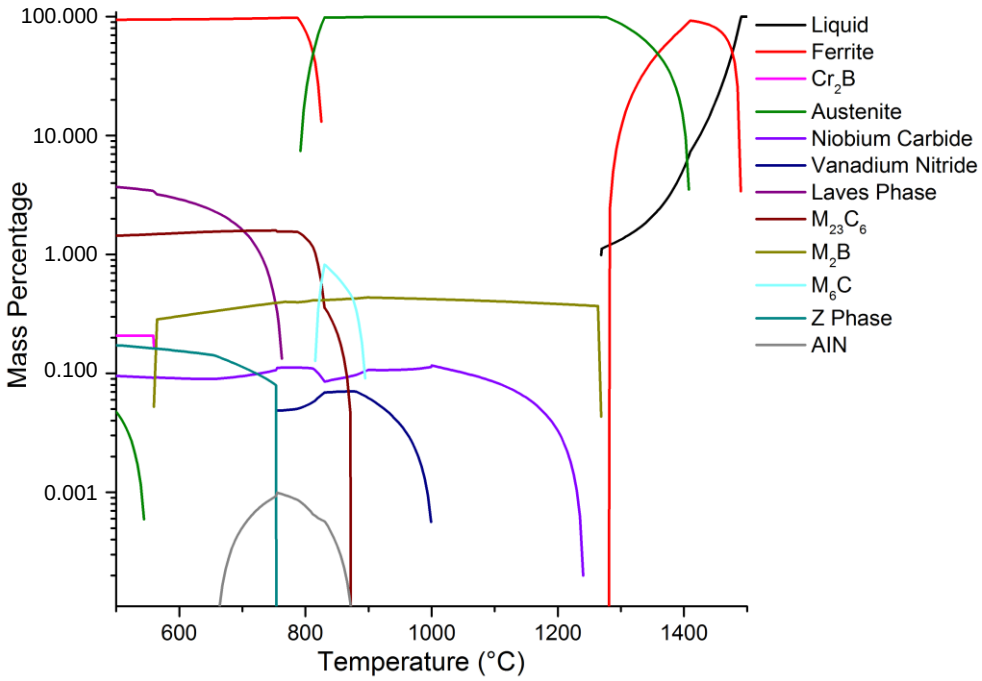

Figure 4.34: A graph showing the phases predicted using thermodynamic calculations as a function of temperature for the composition of GAM 7, as shown in Table 4.7.

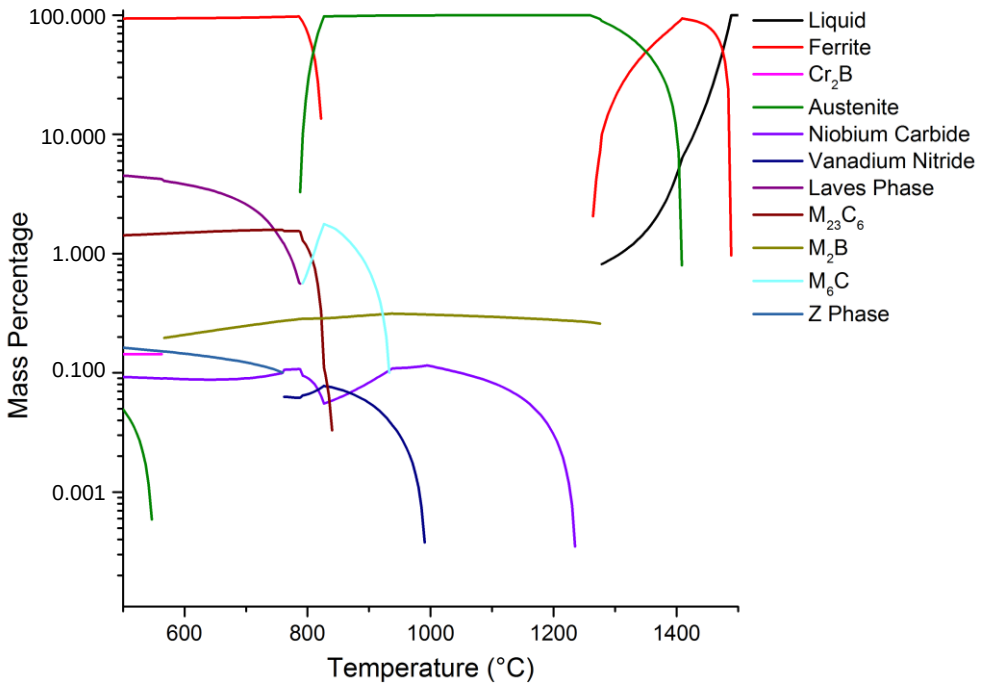

Figure 4.35: A graph showing the phases predicted using thermodynamic calculations as a function of temperature for the composition of GAM 8, as shown in Table 4.7.

4.9 Summary

This chapter has presented a study carried out using thermodynamic calculations to investigate the effect of the key alloying elements on the phases predicted in a MarBN alloy. This information was subsequently used to optimise the chemical composition of a number of MarBN alloys. Eight alloys were manufactured, and characterised with the use of electron microscopy and were subsequently mechanically tested, as discussed in later chapters.

A sensitivity study was carried out on B, C, N, Al and W. The key findings from the stability study showed the following:

- **Nitrogen –** was found to promote the formation of VN, Z Phase and Aluminium Nitride;
- **Carbon –** was predicted to increase the mass percentage of $M_{23}C_6$, whilst supressing the amount of Laves phase predicted to be present and the NbC dissolution temperature was predicted to increase as a function of carbon content;
- **Tungsten –** was predicted to promote the formation of Laves phase and M_6C, whilst suppressing the formation of M_6C;
- **Boron –** was predicted to promote the formation of BN and M_2B;

In addition to studying the stability of individual phases predicted, the calculations were used to identify the delta ferrite formation temperatures. The results show that cobalt and carbon can increase the delta ferrite temperature, whilst tungsten can reduce the delta ferrite temperature and that these elements must be carefully balanced.

The addition of boron can promote the formation of boron nitride, which has been reported to offset the beneficial effect of both elements independently. A systematic study was carried out using thermodynamic calculations to determine the limits of the boron and nitrogen additions without predicting boron nitride to be present. The following rules were obtained; if the boron addition is between 0.0001 wt. % and 0.04 wt. %, the nitrogen addition should be kept below 0.016 wt. %. In contrast, if the boron addition is below 0.0001 wt. % the nitrogen addition should be kept below 0.1 wt. %.

Thermodynamic calculations have been carried out to investigate the effect of chromium, niobium and nitrogen on the phase stability of Z phase. The thermodynamic calculations indicate that a marginal change in the phase stability of Z phase can be obtained by

optimising the chemical composition. The calculations indicate that it is not possible to remove this Z phase without significantly changing the overall composition of the alloy.

The thermodynamic calculations carried out to date have helped understand the effect of individual alloying elements on the stability of phases predicted. This information has been subsequently interpreted to predict the likely effect on the mechanical properties of the alloy. A series of optimised compositions were manufactured based on the stability of phases predicted to be present.

Chapter 5

DETERMINATION OF PHASE TRANSFORMATIONS IN MarBN

5.1 Introduction

MarBN steels undergo a number of phase transformations as a function of temperature. It is of paramount importance to understand at what temperature the phase transformations occur at in order to produce optimum creep properties. A number of phase transformations have been reported for previous 9 wt. % chromium steels such as P91 and P92. The key phase transformation temperatures reported are Ac_1, Ac_3, Ac_4 and Ms. The Ac_1 transformation temperature for P92 has been reported to be between 800°C to 835°C, whilst the Ac_3 temperature is between 900ºC to 920ºC and the Ms is approximately 400ºC. To date no phase transformation temperatures have been reported for MarBN steels specifically.

In order to measure the Ac_1, Ac_3 and Ms transformation temperatures, a Baehr-Thermoanalyse dilatometer DIL 805 was used. The dilatometer allowed the change in length to be accurately monitored as the sample was heated up or cooled down. This therefore allowed the temperature at which the phase transformation occurred to be determined. The Ac_4 temperature is typically too high in 9 wt. % steels to measure with the use of a dilatometer and therefore a differential scanning calorimetry (DSC) was used to measure this phase transformation temperature.

An initial study was carried out to investigate the effect of the heating rate on the phase transformation temperatures measured. A series of heating rates between 3.3°C/min and 100°C/min were used and the Ac_1, Ac_3 and Ms phase transformations were measured. A suitable heating rate was then selected and the phase transformation temperatures were determined for all of the GAM alloys (1 – 8). This information has allowed the phase transformation temperatures to be correlated with the chemical composition of the steels and the thermodynamic predictions. The temperature at which the phase transformations occur can be very important when choosing the correct normalising, tempering and post weld heat treatment temperatures.

5.2 The Effect of the Heating Rate on the Ac_1 & Ac_3 Phase Transformations

A study investigating the effect of the heating rate on the Ac_1 and Ac_3 transformation temperatures was carried out. For this study, all the heat treatments were carried out on GAM 3 in the as-cast condition. The Ac_1, Ac_3 and Ms transformation temperatures were measured using a Baehr-Thermoanalyse dilatometer DIL 805.

The heating profile used to determine the Ac_1 and Ac_3 transformation temperatures is shown in section 3.5.2. The Ac_1 and Ac_3 temperatures were measured upon heating the sample to 1000°C. The Ms temperatures were measured upon cooling the sample to room temperature.

The Ac_1 transformation is the temperature at which austenite starts to be present within the material. At the Ac_1 temperature a transformation occurs from ferrite to austenite, and the two phases have different crystal structures. Ferrite has a body centred cubic (B.C.C) crystal structure and austenite has a face centred cubic (F.C.C) crystal structure. The packing of atoms within each unit cell is different; a F.C.C unit cell can pack four atoms, whereas a B.C.C can only pack two atoms per unit cell and there is a significant difference between the lattice parameters of the two phases.

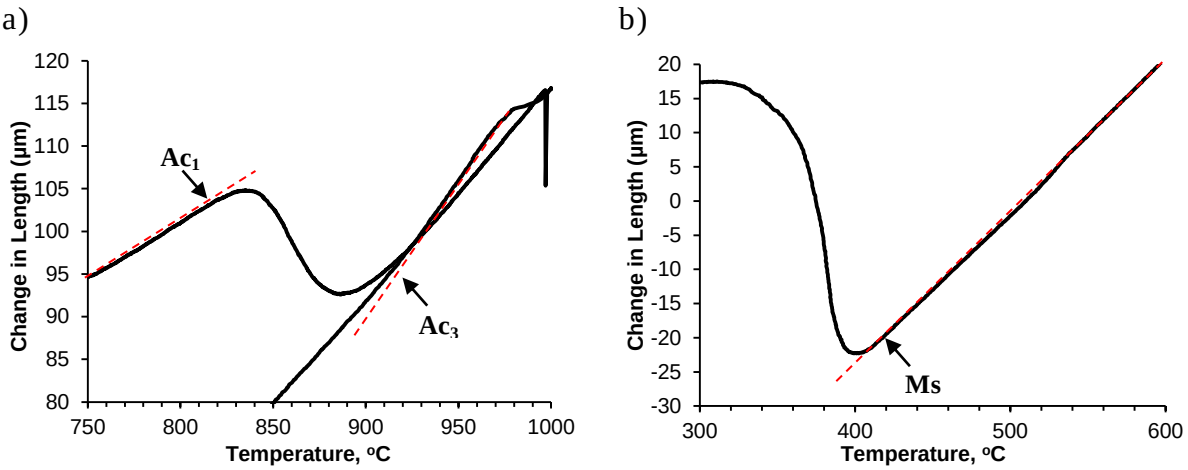

Figure 5.1: The change in length of GAM 3 as a function of temperature when subjected to a heating rate of 100°C/min. a) shows the Ac_1 and Ac_3 transformation and b) shows the Ms transformation.

Figure 5.1 a) shows that at approximately 820°C there is a decrease in the samples length corresponding to the Ac_1 temperature.

The Ac_3 transformation temperature is the temperature where no ferrite remains within the material. Therefore, this transformation temperature can be determined as the temperature at which the change in length deviates from a linear expansion between 900°C to 1000°C.

The Ms transformation temperature is the temperature at which martensite starts to form within the material. Martensite has a body centred tetragonal (B.C.T) crystal structure. At the Ms temperature, an increase in the sample's length was observed as shown in Figure 5.1.

A summary of the transformation temperatures measured using the dilatometer produced using heating rates from 3.3°C/min to 100°C/min are shown in Table 5.1 and graphically in Figure 5.2, Figure 5.3 and Figure 5.4 for the Ac_1, Ac_3 and Ms temperatures respectively.

Analysis of the Ac_1 transformation temperatures has shown that the temperatures measured can vary by approximately 7°C, when the heating rate is changed between 100°C/min to 3.3°C/min. All the results are within a scatter of ± 7°C, and therefore within the error expected using this particular technique. The transformation temperatures produced using a heating rate of 3.3°C/min and 33.4°C/min, were found to be 4 – 5°C higher than the mean value of the Ac_1 transformation temperatures measured in the stability study.

The Ac_3 temperatures are shown in Figure 5.3, the transformation temperatures were found to be stable throughout the heating rate range of 100°C/min to 4°C/min. A mean transformation temperature of 921°C was produced over the eight different heating rates carried out. All the Ac_3 temperatures were found to be within ± 6°C. There was however a significant reduction in the Ac_3 transformation temperature observed at 3.3°C/min, which is thought to be an anomalous result.

The Ms transformation temperatures were found to remain constant, with the majority of the martensite start temperatures between 420°C and 425°C. Two anomalous results were observed to be present after a heating rate of 5°C/min and 100°C/min.

In summary the study investigating the effect of the heating rate on GAM 3 in the as cast condition between heating rates of 4°C/min and 100°C/min shows some variation in the Ac_1, Ac_3 and Ms transformation temperatures measured. However when the data was analysed between 3.4°C/min to 8.3°C/min stable transformation temperatures were produced.

Table 5.1: A summary of results for the study investigating the effect of heating rate on the Ac_1, Ac_3 and Ms transformation temperatures in GAM 3, at heating rates between 3.3°C/min and 100°C/min.

Heating Rate (°C/min)	**Ac_1 Temperature (°C)**	**Ac_3 Temperature (°C)**	**Ms Temperature (°C)**
100.0	821	920	413
50.0	823	926	420
33.4	826	918	423
16.0	823	920	424
8.3	820	923	422
5.6	822	921	430
4.1	821	922	424
3.3	827	900	422

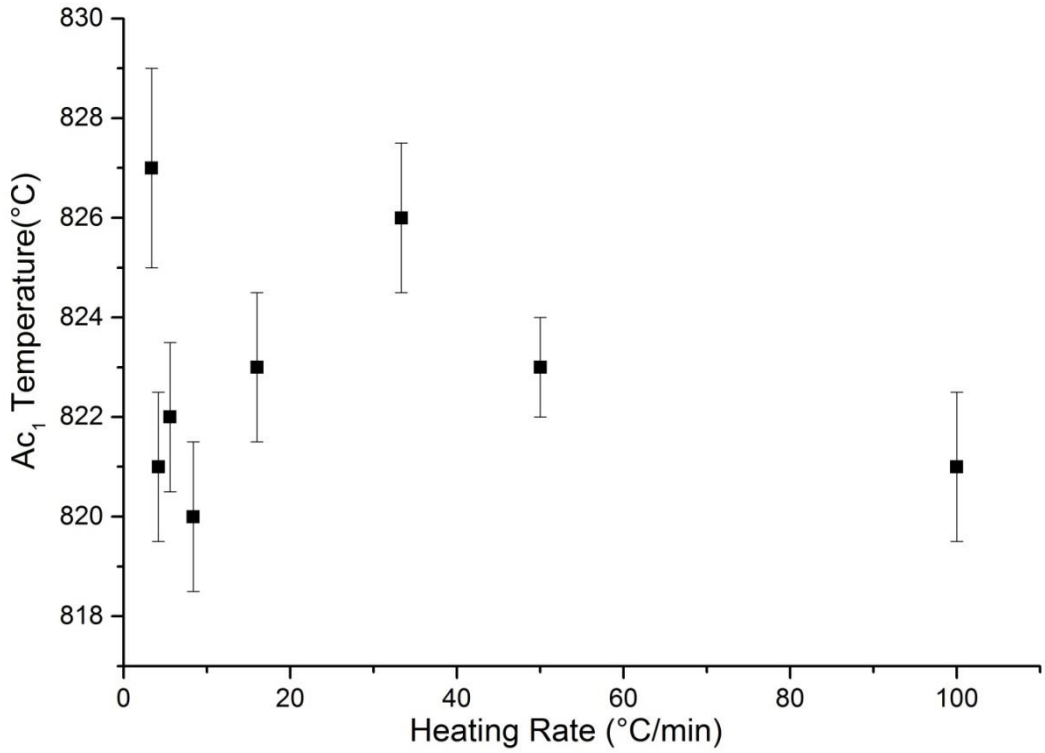

Figure 5.2: A graph showing the change in the Ac_1 transformation temperature in GAM 3 when the material was subjected to heating rates varying from 100°C/min to 3.0°C/min.

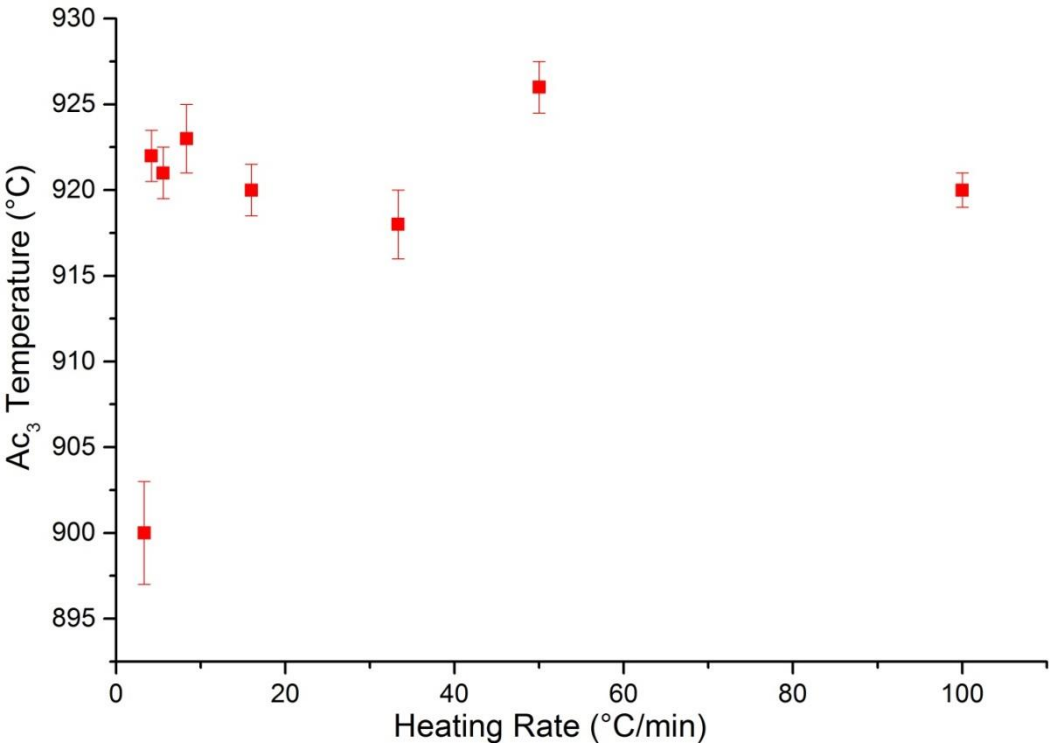

Figure 5.3: A graph showing the change in the Ac_3 transformation temperature in GAM 3 when the material was subjected to heating rates varying from 100°C/min to 3.0°C/min.

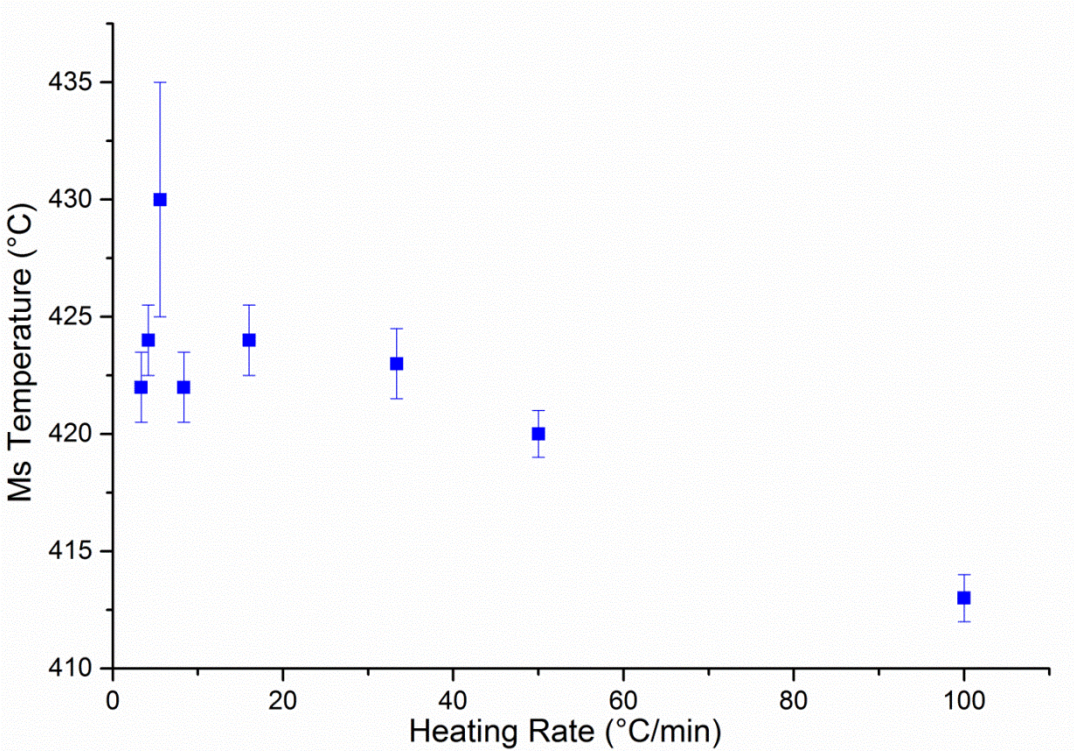

Figure 5.4: A graph showing the change in the Ms transformation temperature in GAM 3 when the material was subjected to heating rates varying from 100°C/min to 3.0°C/min.

5.3 Ac_1 & Ac_3 Determination of GAM 1 – 8

The Ac_1 and Ac_3 transformation temperatures were measured using a Baehr-Thermoanalyser dilatometer 805. A similar heat treatment to the previous study carried out to investigate the effect of the heating rate on the Ac_1, Ac_3 and Ms transformation temperatures was used to determine the transformation temperatures. The materials tested were GAM 1 – 8 in the as-cast condition and normalised and tempered condition (N1150°C T780°C). The heating profile used to determine the Ac_1 and Ac_3 temperatures is described in section 3.6.3.

A summary of the Ac_1, Ac_3 and Ms transformation temperatures measured for GAM 1 – 8 using a dilatometer are shown in Table 5.2, 5.3 and 5.4. Figures 5.5 – 5.7 shows a graph of the Ac_1, Ac_3 and Ms temperatures for both the as-cast and heat treated conditions. The figures show that there is no simple relationship between the transformation temperatures measured for the first batch of steels (GAM 1 – 4) and the second batch of steels (GAM 5 – 8).

The aim was to modify the chemical composition of GAM 6 and keep the chemical composition of the remaining melts (GAM 5, GAM 7 and GAM 8) identical but only change the nitrogen content. Unfortunately small changes in the chemical composition were observed to be present which has led to a fluctuation in the transformation temperatures measured. The Ac_1 and Ac_3 temperature were observed to be lower for the second round of steels manufactured. The overall decrease in the transformation temperatures measured is thought to be due to an increase in nickel and copper, which are austenite stabilising elements.

The results show that the Ac_1 temperatures are approximately 10 to 15°C higher in the heat treated condition in comparison to the as-cast condition. The transformation temperatures are thought to be higher in the heat treated condition because the transformation is controlled by the rate of carbon diffusion as the thermodynamic driving force for the formation of austenite increases as there is an increase in the amount of available carbon. However within MarBN steels after a tempering heat treatment carbon is present within $M_{23}C_6$ carbides, which must dissolve in order to release the carbon and therefore increase the Ac_1 temperature measured. The Ac_3 temperatures were typically found to be very similar in both the as-cast condition and heat treated condition of each melt.

The martensite start temperatures were observed to be very similar for all GAM melts in the as-cast condition. The transformation temperatures were observed to be slightly higher in the heat treated condition, in comparison to the as-cast condition.

Table 5.2:A summary of the Ac_1, Ac_3 and Ms transformation temperatures for GAM 1 – 8.

	Composition	**Ac_1 As Cast**	**Ac_1 Heat Treated**
GAM 1	9Cr-1W-1Co-V-Nb	830 ± 2	833 ± 2
GAM 2	9Cr-2.5W-3.2Co-V-Nb	825 ± 3	832 ± 2
GAM 3	9Cr-2.5W-2.8Co-V-Nb	820 ± 2	838 ± 2
GAM 4	9Cr-3W-2.8Co-V-Nb	834 ± 3	N/A
GAM 5	9Cr-1W-1Co-V-Nb	813 ± 3	827 ± 2
GAM 6	9Cr-2W-1.5Co-V-Nb	821 ± 2	840 ± 2
GAM 7	9Cr-2.6W-2.7Co-V-Nb	820 ± 3	831 ± 1
GAM 8	9Cr-3W-2.9Co-V-Nb	825 ± 3	833 ± 2

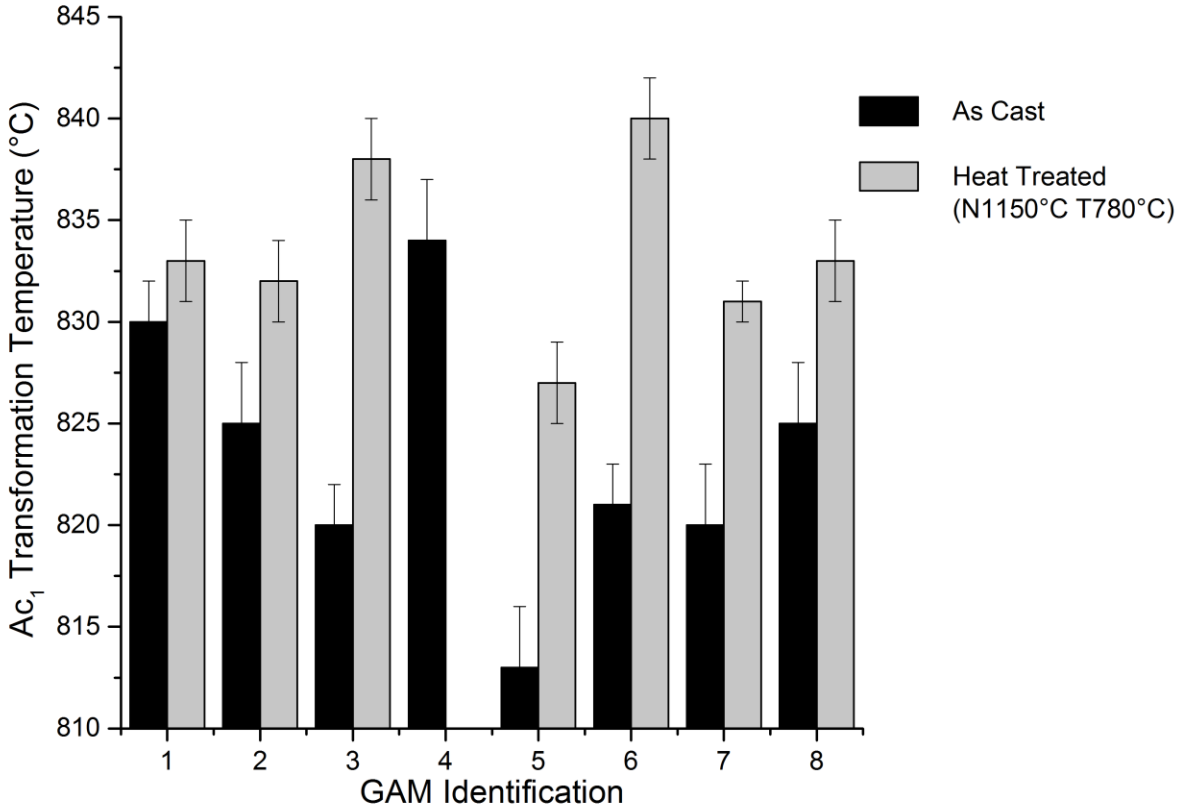

Figure 5.5: A graph showing the Ac_1 transformation temperatures measured for GAM 1 – 8. The transformation temperatures were measured for two different microstructural starting conditions; As-cast (Black) and the heat treated condition (Grey).

Table 5.3: A summary of the Ac_1, Ac_3 and Ms transformation temperatures for GAM 1 – 8.

	Composition	**Ac_3 As Cast**	**Ac_3 Heat Treated**
GAM 1	9Cr-1W-1Co-V-Nb	911 ± 3	900 ± 3
GAM 2	9Cr-2.5W-3.2Co-V-Nb	908 ± 3	912 ± 3
GAM 3	9Cr-2.5W-2.8Co-V-Nb	916 ± 3	914 ± 3
GAM 4	9Cr-3W-2.8Co-V-Nb	923 ± 2	N/A
GAM 5	9Cr-1W-1Co-V-Nb	910 ± 2	914 ± 2
GAM 6	9Cr-2W-1.5Co-V-Nb	923 ± 5	934 ± 2
GAM 7	9Cr-2.6W-2.7Co-V-Nb	910 ± 2	912 ± 2
GAM 8	9Cr-3W-2.9Co-V-Nb	916 ± 3	914 ± 3

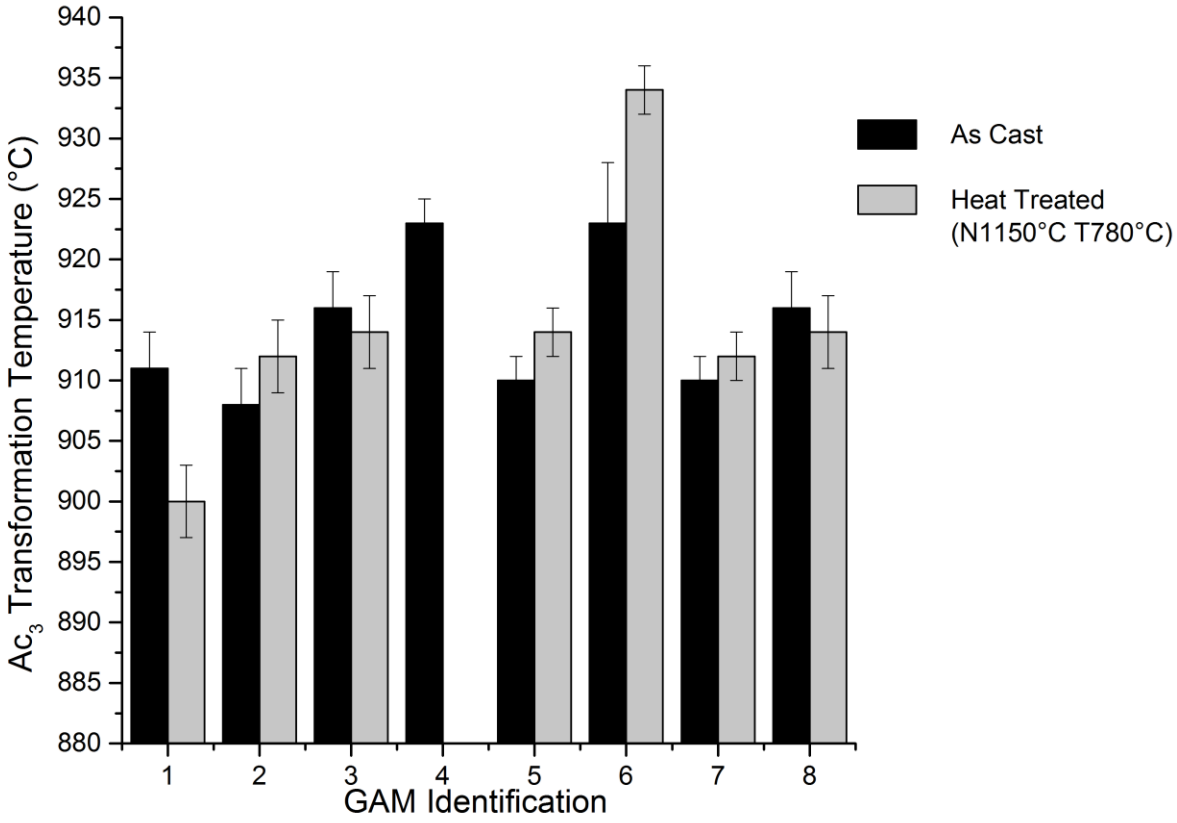

Figure 5.6: A graph showing the Ac_3 transformation temperatures measured for GAM 1 – 8. The transformation temperatures were measured for two different microstructural starting conditions; As-cast (Black) and the heat treated condition (Grey).

Table 5.4: A summary of the Ac_1, Ac_3 and Ms transformation temperatures for GAM 1 – 8.

	Composition	**Ms As Cast**	**Ms Heat Treated**
GAM 1	9Cr-1W-1Co-V-Nb	426 ± 3	437 ± 3
GAM 2	9Cr-2.5W-3.2Co-V-Nb	425 ± 2	414 ± 3
GAM 3	9Cr-2.5W-2.8Co-V-Nb	416 ± 3	425 ± 3
GAM 4	9Cr-3W-2.8Co-V-Nb	417 ± 3	N/A
GAM 5	9Cr-1W-1Co-V-Nb	419 ± 4	428 ± 3
GAM 6	9Cr-2W-1.5Co-V-Nb	415 ± 4	435 ± 3
GAM 7	9Cr-2.6W-2.7Co-V-Nb	421 ± 3	439 ± 4
GAM 8	9Cr-3W-2.9Co-V-Nb	415 ± 3	405 ± 3

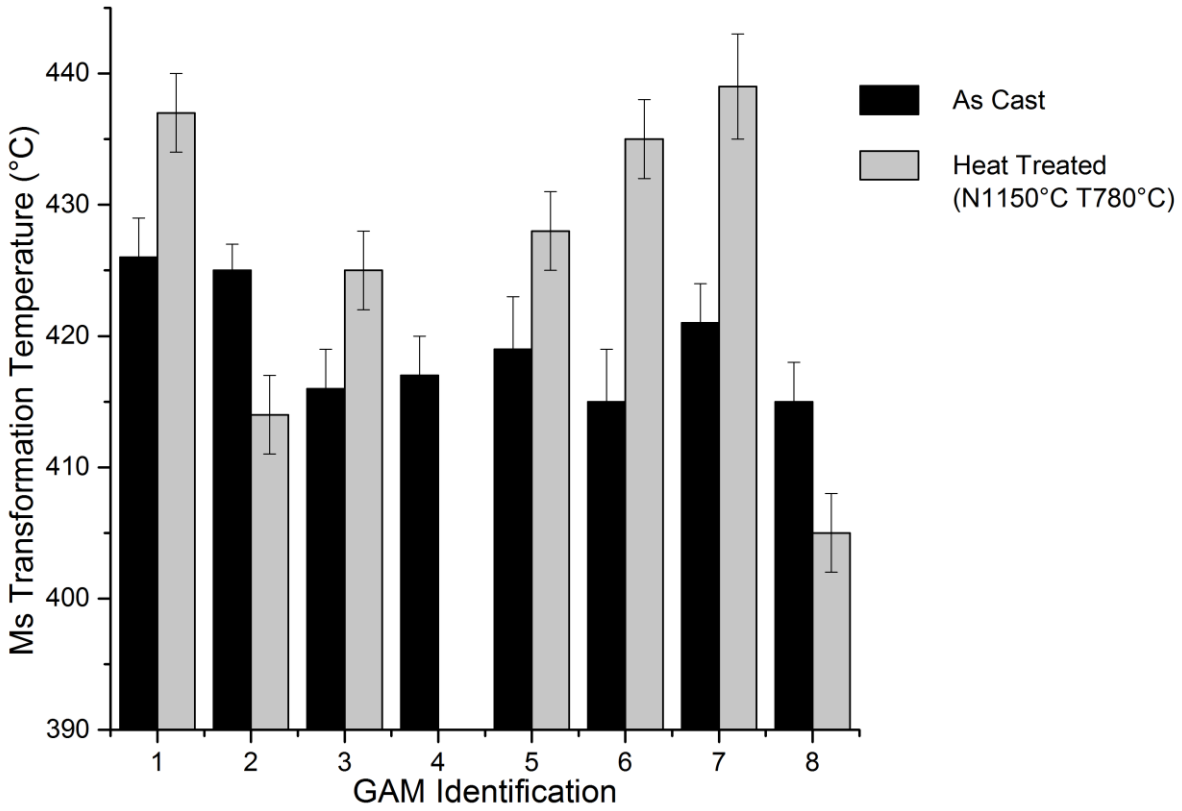

Figure 5.7: A graph showing the Ms transformation temperatures measured for GAM 1 – 8. The transformation temperatures were measured for two different microstructural starting conditions; As-cast (Black) and the heat treated condition (Grey).

The chemical variation between the first and second rounds of steels has been analysed. The variation in the transformation temperatures are shown in Table 5.5, 5.6 and 5.7. The largest variation was observed between GAM 2 and GAM 6, and indeed the chemical composition of the two steels was significantly different due to a reduction in cobalt and tungsten by

1.63 wt. % and 0.44 wt. % respectively. Cobalt is an austenite stabilising element, which results in a higher Ac_1 transformation temperature. Tungsten is a ferrite stabilising element and therefore results in a decrease in the Ac_1 transformation temperature. A far greater reduction in cobalt was observed compared to the increase in ferrite stabilising elements. This caused an overall decrease in the Ac_1 temperature.

The second largest variation was observed between GAM 3 and GAM 7, which was found to be -11^{o}C and 4^{o}C for the Ac_1 and Ac_3 transformation temperatures respectively. There was a small increase in ferrite stabilising elements molybdenum, tungsten and chromium which resulted in a higher Ac_1 and Ac_3 temperature. There was also a decrease in the amount of austenite stabilising elements such as manganese and cobalt, which would also result in a higher Ac_1 and Ac_3 temperature. There were also some changes in nickel, copper, silicon and vanadium which resulted in a decrease in the Ac_1 and Ac_3 temperatures. However, the increase in the Ac_1 transformation temperature was dominated by the increase in ferrite stabilising elements and a decrease in austenite stabilising elements.

Table 5.5: A summary table of the Ac_1 temperatures for the first and second batches of GAM melts.

	Ac_1 Temperature (°C) (Steel 1, 2, 3, 4)	**Ac_1 Temperature (°C) (Steel 5, 6, 7, 8)**	**Temperature Variation (°C)**
GAM 1 / 5	830	827	3
GAM 2 / 6	825	840	-15
GAM 3 / 7	820	831	-11
GAM 4 / 8	834	833	1

Table 5.6: A summary table of the Ac_3 temperatures for the first and second batches of GAM melts.

	Ac_3 Temperature (°C) (Steel 1, 2, 3, 4)	**Ac_3 Temperature (°C) (Steel 5, 6, 7, 8)**	**Temperature Variation (°C)**
GAM 1 / 5	911	914	-3
GAM 2 / 6	908	934	-26
GAM 3 / 7	916	912	4
GAM 4 / 8	923	914	9

Table 5.7: A summary table of the Ms temperatures for the first and second batches of GAM melts.

	Ms Temperature (^{o}C) (Steel 1, 2, 3, 4)	**Ms Temperature (^{o}C) (Steel 5, 6, 7, 8)**	**Temperature Variation (^{o}C)**
GAM 1 / 5	426	425	1
GAM 2 / 6	425	432	-7
GAM 3 / 7	416	433	-17
GAM 4 / 8	417	417	0

A comparison of the thermodynamically predicted transformation temperatures (Ae) and experimentally measured transformation temperatures (Ac) is shown in Table 3.8 and Table 5.9, for the Ae_1/Ac_1 and Ae_3/Ac_3 temperatures respectively. The comparison shows that between the Ae_1 and Ac_3 temperatures there was a variation of approximately 20°C to 50°C, and between the Ae_3 and Ac_3 there was a higher variation of approximately 70°C to 90°C. A graph showing the variation between the Ae_1/Ac_1 and Ae_3/Ac_3 is shown in Figure 5.9.

The main reason for the variation between the thermodynamically predicted values and the experimental values is that the thermodynamic predictions do not take into account the kinetics of the transformation. Reaction kinetics are very important for the transformation from ferrite to austenite, because the rate at which austenite forms is controlled by the rate of carbon diffusion. However, the majority of the carbon is in the form of $M_{23}C_6$ carbides which results in the reaction being slow, as the $M_{23}C_6$ carbides have to be dissolved, to release carbon to allow the transformation to austenite. Therefore a higher transformation temperature is seen experimentally.

Table 5.8: A summary of the thermodynamically predicted Ae_1 transformation temperatures and the experimentally measured Ac_1 transformation temperatures measured using the dilatometer.

Material	**Ae_1 Temperature (^oC)**	**Ac_1 Temperature (^oC)**	**Variation (^oC)**
GAM 1	814	830 ± 2	-16
GAM 2	801	825 ± 3	-24
GAM 3	793	820 ± 2	-27
GAM 4	794	834 ± 3	-40
GAM 5	792	827 ± 2	-35
GAM 6	799	840 ± 2	-41
GAM 7	787	831 ± 1	-44
GAM 8	786	833 ± 2	-47

Table 5.9: A summary of the thermodynamically predicted Ae_3 transformation temperaturse and the experimentally measured Ac_3 transformation temperatures measured using the dilatometer.

Material	Ae_3 Temperature (°C)	Ac_3 Temperature (°C)	Variation (°C)
GAM 1	840	911 ± 3	-71
GAM 2	835	908 ± 3	-73
GAM 3	832	916 ± 3	-84
GAM 4	830	923 ± 2	-93
GAM 5	840	914 ± 2	-74
GAM 6	854	934 ± 2	-80
GAM 7	830	912 ± 2	-82
GAM 8	827	914 ± 3	-87

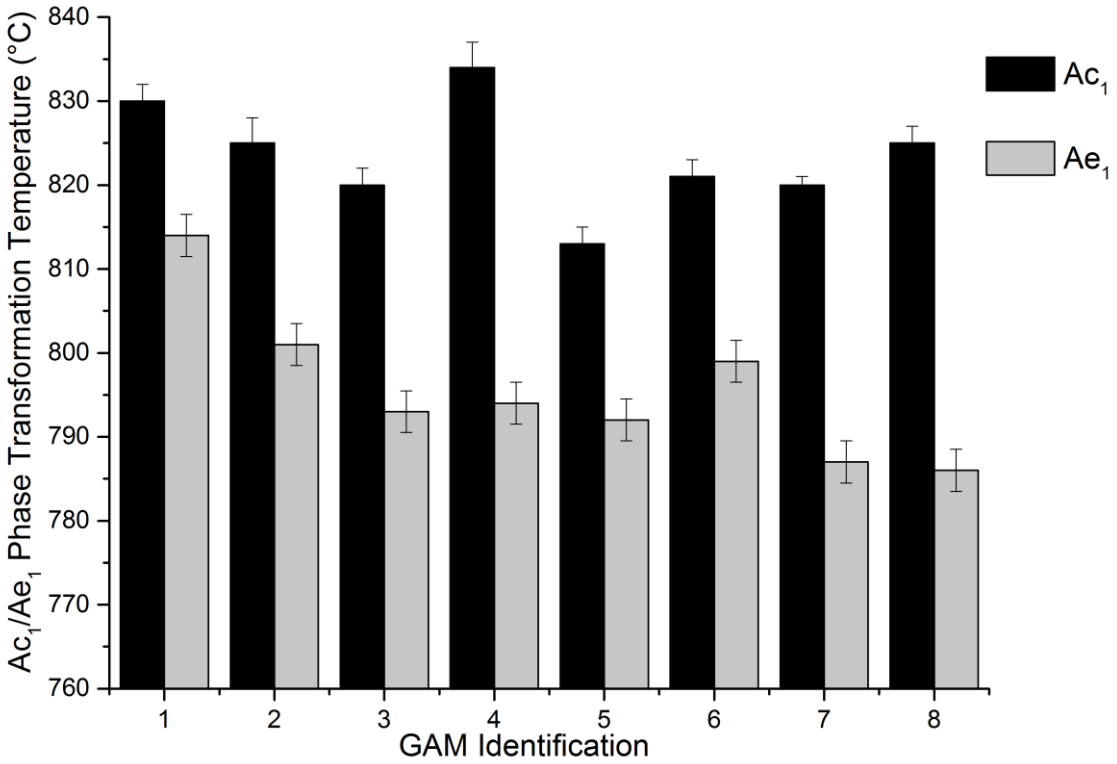

Figure 5.8: A graph showing a comparison between the Ae_1/Ac_1 phase transformation temperatures.

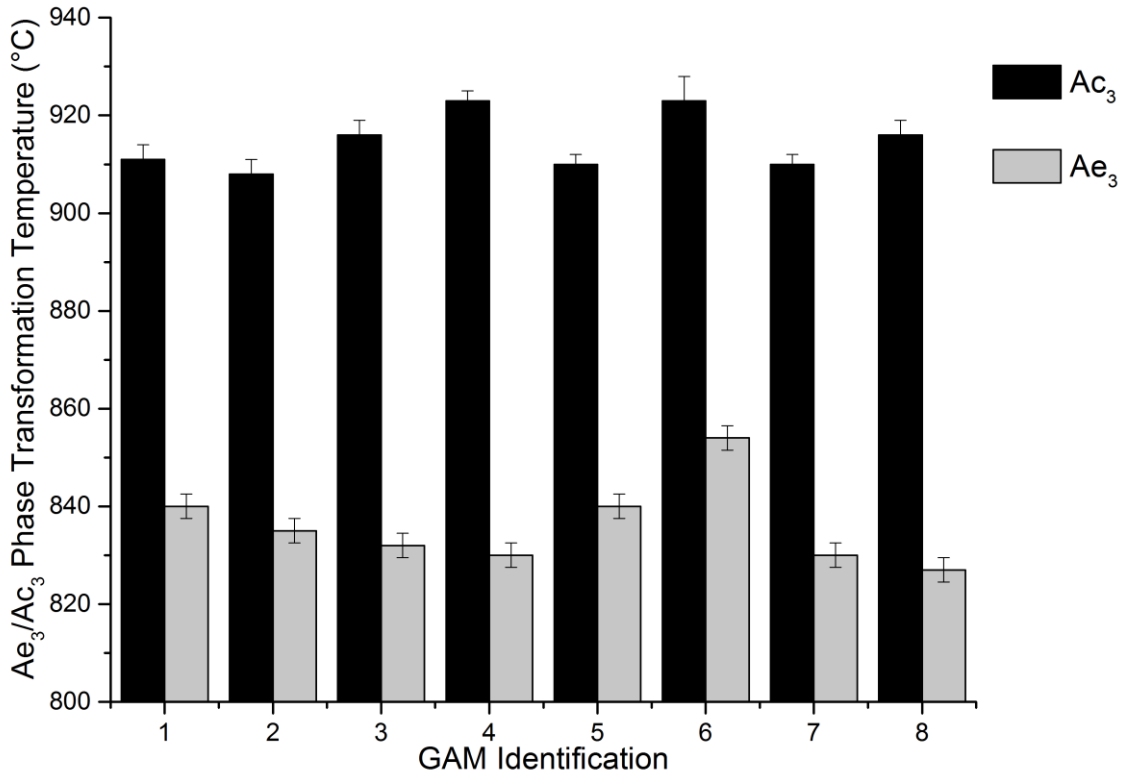

Figure 5.9: A graph showing a comparison between the Ae_3/Ac_3 phase transformation temperatures.

5.4 Determining Phase Transformations Using Differential Scanning Calorimetry

Differential Scanning Calorimetry (DSC) was used as a technique to measure the Ac_4 transformation temperature and liquid formation temperature. This technique has been carried out on GAM 3 as this melt is of particular interest to the IMPACT consortium due to its very good creep properties. Thermodynamic calculations predict that the delta ferrite start temperature (Ac_4) is 1295°C and the liquid formation temperature is 1260°C. The thermodynamic calculations have predicted a low liquid formation temperature, which could have serious implications during hot rolling which is typically carried out at 1250°C. The delta ferrite temperature in comparison has been predicted to be higher than the liquid formation temperature.

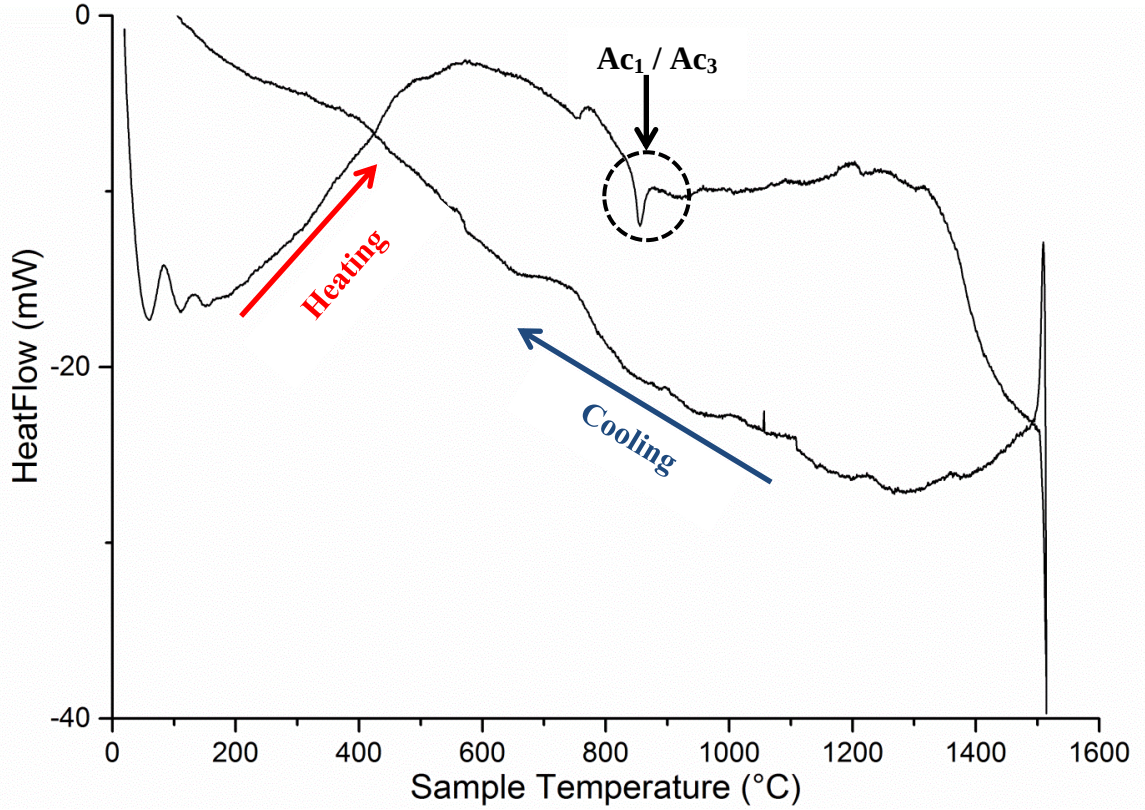

Figure 5.10: A DSC curve produced from GAM using a Seteram Evolution 1600°C. The curve shows heat flow against the sample temperature.

GAM 3 has been analysed using a DSC up to a 1500°C, as shown in Figure 5.10. The result clearly shows that when heating the sample up to 1500°C the Ac_1 and Ac_3 transformation temperature are observed to be present. Figure 5.10 shows that the heat flow is relatively constant between approximately 900°C – 1300°C indicating no phase transformation takes place during this temperature range. At approximately 1300°C there is a significant decrease in the heat flow of the sample, this continues to the maximum operating temperature of the DSC (1500°C). This indicates that a phase transformation maybe taking place, however, it is inconclusive without being able to run the sample to a higher temperature.

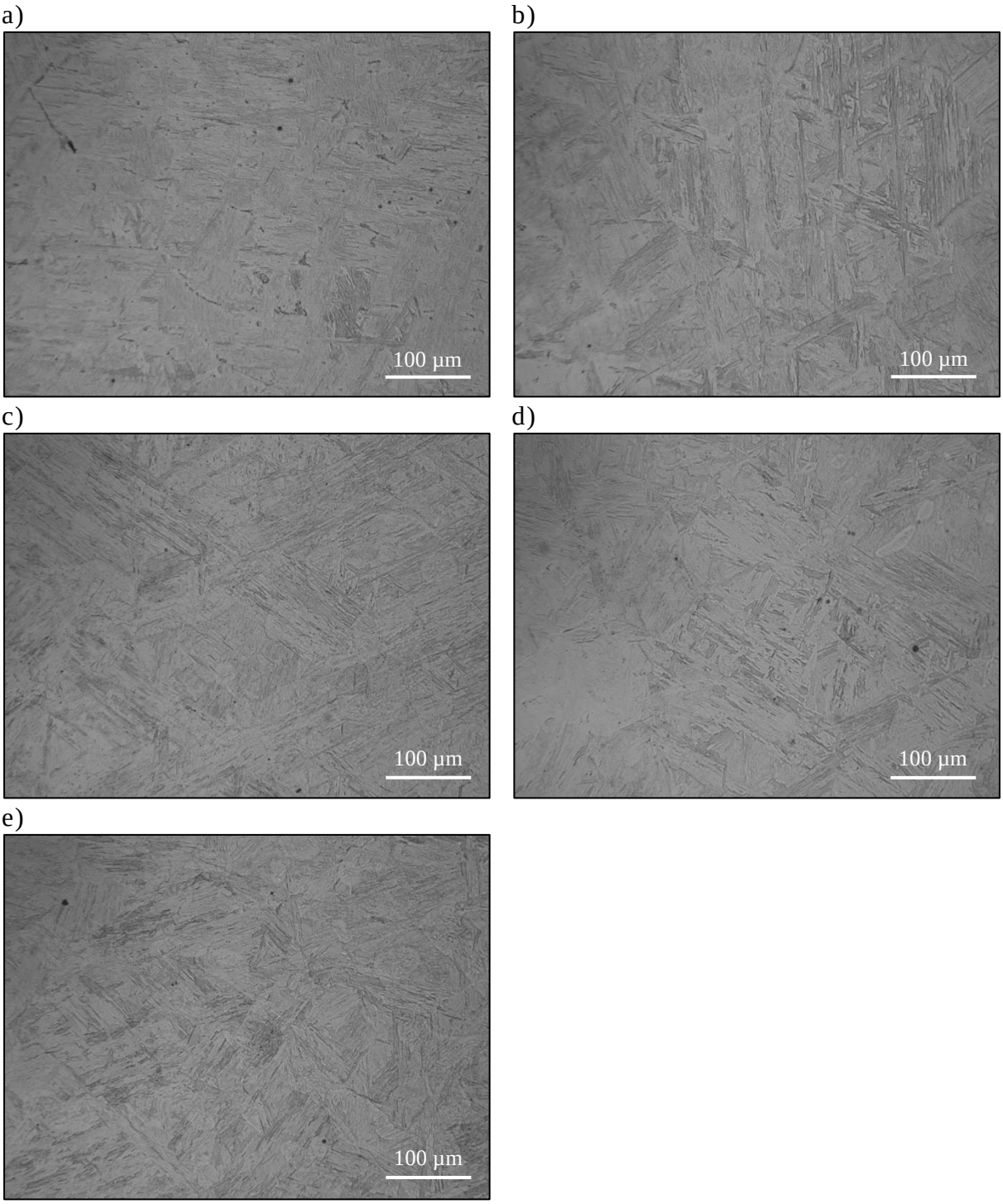

Figure 5.11: A series of optical micrographs of GAM 3 produced after a normalising for 1 hour at a) 1100°C, b) 1150°C, c) 1175°C, d) 1200°C and e) 1225°C.

A series of normalising heat treatments were carried out within a furnace to verify the DSC results and show that no phase transformations occur between 1100°C to 1225°C. The micrographs in Figure 5.11 show that after normalising at 1100°C to 1225°C the microstructures are all fully martensitic. After normalising at 1100°C, large precipitates are observed to be present predominantly on the prior austenite grain boundaries. These

precipitates have identified with the use of EDX to be W_2B precipitates. Delta Ferrite was not observed to be present using optical microscopy, as shown in Figure 5.11.

Although no conclusive transformation temperatures can be interpreted from the DSC results regarding the Ac_4 and liquid formation temperature, the information provided about the phase stability between 900°C and 1300°C provides reassurance that this material can be hot rolled at 1250°C without delta ferrite or liquid forming within the microstructure. The normalising trials carried out confirm the DSC results that the Ac_4 phase transformation does not take place within the temperature range of 1100°C to 1225°C.

5.5 Effect of Cooling Rate on the Formation of Martensite

Previous 9 wt. % chromium steels have shown that, upon continuous cooling from the normalising temperature, it is possible to precipitate ferrite and carbides as shown on the CCT diagram in Figure 2.19. The precipitation of pro-eutectoid ferrite within the microstructure is detrimental to the creep properties and it is therefore imperative to understand if this phenomenon occurs in MarBN and if so, what critical cooling rate is required to produce such a microstructure.

A series of cooling trials were carried out after normalising at 1200°C on GAM 1 and GAM 4. Two cooling rates were used 0.8°C/min and 0.2°C/min, 0.2°C/min was deemed the slowest cooling rate utilised within industry. Optical microscopy was used to examine the microstructures, as shown in Figure 5.12. The microstructures show that all the structures are martensitic which implies if ferrite can be precipitated upon cooling; a cooling rate slower than 0.2°C/min must be used.

The industrial implication of this work is that large scale castings take several days to cool down from the normalising temperature. It is important to understand how critical small changes such as the cooling rate make to the microstructure and subsequent creep properties. If detrimental phases precipitate, this could have significant consequences on the commercialisation and adoption by industry of such an alloy.

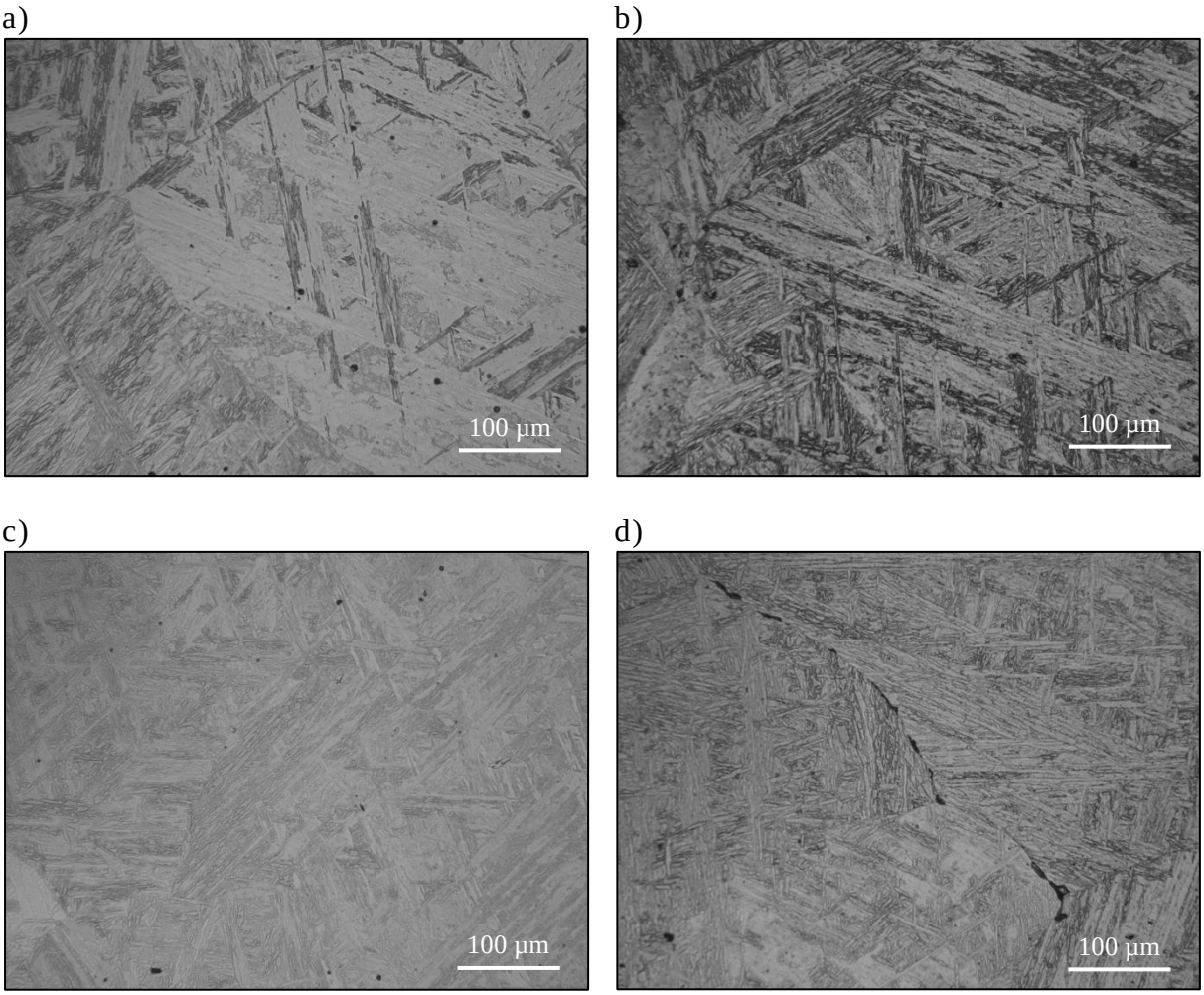

Figure 5.12: A series of optical micrographs produced after normalising GAM 1 and GAM 4 at 1200°C and cooling at 0.8°C/min and 0.2°C/min. a) GAM 1 0.8°C/min b) GAM 1 0.2°C/min c) GAM 4 0.8°C/min d) GAM 4 0.2°C/min.

5.6 Summary

The phase transformations that exist in MarBN alloys (GAM 1 – 8) have been measured and described in this chapter of the thesis. A dilatometer was used to measure the Ac_1, Ac_3 and Ms transformation temperatures. The Ac_4 and liquid formation temperatures were estimated with the use of a DSC on GAM 3, and optical microscopy was used to confirm the DSC results.

A study investigating the effect of the heating rate on the transformation temperatures in GAM 3 in the as-cast condition was carried out. During the study the samples were heated up to 1000°C, at a heating rates between 100°C/min to 3.3°C/min. The transformation temperatures have shown some small fluctuations, however, all the Ac_1 and Ac_3 transformation temperatures are all within a scatter of 6°C.

The transformation temperatures were determined for GAM 1 – 8, using a heating rate of 8.3°C/min. The transformation temperatures were measured in both the as-cast and heat treated conditions. The results show that there is no simple correlation between the transformation temperatures measured for the first batch of steels and the second batch of steels. The aim was to keep the chemical compositions the same (except GAM 2 / GAM 6) however small changes in the compositions have been observed which has led to a small fluctuation in the transformation temperatures.

The results show that the Ac_1 and Ac_3 temperatures are approximately 10 to 15°C higher in the heat treated condition in comparison to the as-cast condition. The transformation temperatures are thought to be higher in the heat treated condition because of the effect of dissolving the $M_{23}C_6$ carbides. The Ms temperatures were found to be very constant in both the as-cast and heat treated condition, with the Ms temperature found to be marginally higher in the heat treated condition.

The measured transformation temperatures (Ac) have been compared with the thermodynamically predicted temperatures (Ae). Comparing Ac_1/Ae_1 shows that the Ac_1 temperatures are approximately 20°C to 50°C higher than the thermodynamically predicted transformation temperatures. The Ac_3 transformation temperatures were observed to be 70°C to 90°C higher than the thermodynamically predicted transformation temperatures. The main reason for the variation between the thermodynamically predicted transformation temperatures and the measured transformation temperatures is that the thermodynamic predictions do not take into account kinetics of the transformation.

DSC was used to estimate the Ac_4 transformation temperature and liquid formation temperature in GAM 3. GAM 3 has been analysed using DSC up to 1500°C and the results show that the heat flow is stable between 900°C to 1300°C and therefore do not indicate any phase transformations within this temperature range. The heat flow decreases after 1300°C indicating a phase transformation may be taking place, however the final result is inconclusive due to the temperature limitations of the DSC. Optical microscopy has been used to understand if any phase transformations occur between 1000°C to 1225°C; the results indicate that there is no precipitation of delta ferrite or evidence of liquation.

In previous 9 wt. % chromium alloys such as P92, it has been possible to create a ferrite and carbide structure by using a sufficiently slow cooling rate. There is a concern that when manufacturing large scale commercial alloys it is important to understand what critical

cooling rate is required to produce such a microstructure. Therefore, cooling rate trials have been carried out on GAM 1 and GAM 4. The structures were found to be fully martensitic when a cooling rate of 0.2°C/min was used, which is believed to be slower than any cooling rate used when heat treating industrial castings.

Chapter Six

THE EFFECT OF PRE SERVICE HEAT TREATMENTS ON THE INITIAL MICROSTRUCTURE

6.1 Introduction

In this chapter the effects of optimising the pre service heat treatment on a 9Cr-3W-3Co steel has been investigated. The material used throughout this chapter was GAM 3 (9Cr – 3Co – 3W - B), this particular alloy was characterised in a number of different conditions. The chapter has been divided into three main sections. The first section focuses on characterising GAM 3 in the standard normalised and tempered condition (N1150ºC T780ºC), in both the cast and rolled variants. This characterisation provides a detailed understanding of the microstructure after a standard normalising and tempering heat treatment. The second section of this chapter investigates the effect of the normalising temperature on the resulting microstructure. The final section investigates the effect of the tempering temperature on the resulting microstructure.

The normalising and tempering optimisations in this chapter were based on microstructural observations and characterisation. Chapter 7 evaluates the mechanical properties and the long term microstructural evolution, of both the standard and optimised heat treatments.

6.2 Starting Microstructure

The samples examined within this chapter of the thesis are GAM 3 and their chemical composition is shown in Table 3.1. This variant of MarBN was chosen to investigate the effect of pre service heat treatments on the initial microstructure. The reason this alloy was chosen was because it was designed with the use of thermodynamic calculations to have the highest boron (180 ppm) and nitrogen (150 ppm) level without predicting that boron nitride was likely to be present. This series of melts were produced using an induction air melting process. During this process it was difficult to manufacture a melt with the target nitrogen content of 150 ppm and consequently the final nitrogen content of the melt was 200 ppm. Thermodynamic calculations have predicted, using the composition of the final melt that under equilibrium conditions there will be a small boron nitride stability window with a maximum mass percentage of 0.007% predicted to be present between the temperature range of 1030°C - 1130°C as shown in Figure 6.4. Boron nitride has been reported by a number of

researchers to be a coarse nitride which can offset the beneficial effect of both the boron and nitrogen additions[12].

GAM 3 was characterised in both the cast and rolled conditions and both products received a standard normalising and tempering heat treatment for MarBN materials. The heat treatment consisted of normalising at 1150°C for two hours, followed by air cooling to room temperature. After cooling to room temperature the steels received a tempering heat treatment at 780°C for three hours. A number of ingots were cast, and were subsequently hot rolled to a thickness of ~25 mm. Prior to rolling, the ingot was preheated to 1225°C and full details of this heat treatment can be found in Section 3.5.

The standard normalising temperature for P92 has been reported to be approximately 1070°C. MarBN alloys have been reported to require a higher normalising temperature, because W_2B precipitates have been reported not to be fully dissolved at the lower normalising temperature of 1050°C, whereas at a higher normalising temperature of 1150°C no W2B preciptates were reported to be present. Therefore this indicates that at a lower normalising temperature of 1050°C, there is a reduction in the amount of soluble boron available which is designed to be present in order to reduce the coarsening rate of the $M_{23}C_6$ carbides[69].

Figures 6.1 a) and b) show the initial microstructure of GAM 3 in the cast and rolled conditions respectively and both variants were heat treated using standard normalising and tempering parameters for MarBN alloys. Both micrographs show a tempered martensitic, containing prior austenite and lath boundaries.

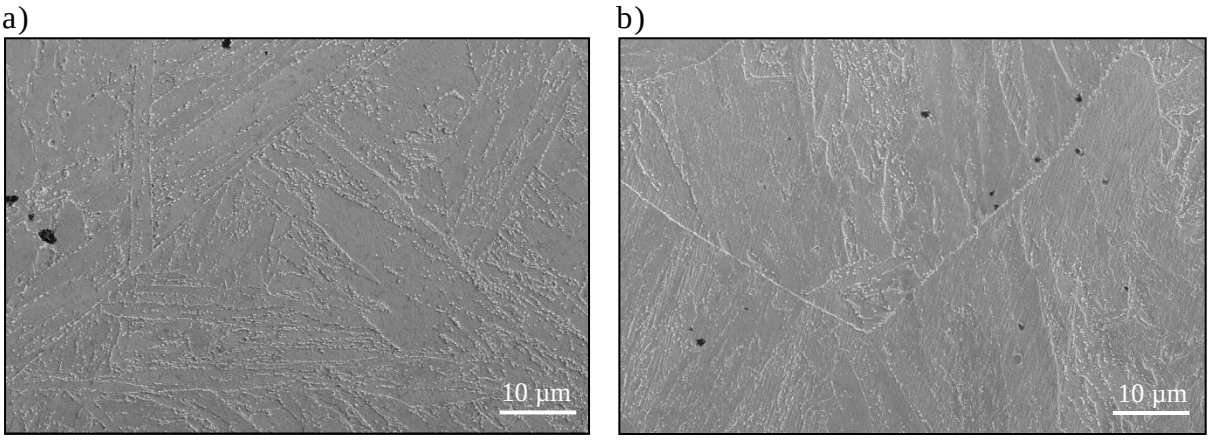

Figure 6.1: Two SEM micrographs of GAM 3 in different product forms a) the cast variant and b) the rolled variant. Both samples received a standard normalising and tempering heat treatment, at 1150°C for 2 hours and 780°C for 3 hours respectively.

Figure 6.2 shows two micrographs produced with the use of ion beam imaging, which shows that the microstructure contains a number of precipitates. The precipitates have been observed to be present on the lath boundaries, which are consequently pinning the boundaries. Carbon extraction replicas were used to identify the precipitates present within the microstructure and the large precipitates were identified to be chromium rich $M_{23}C_6$ precipitates, as shown in Figure 6.3. The microstructure also contained a number of smaller NbC (MX) precipitates which were observed to be present using TEM, as shown in Figure 6.3. The hardness of GAM 3 after a standard normalising and tempering heat treatment in the cast and rolled condition was found to be 256 HV_{10} and 233 HV_{10} respectively. The prior austenite grain size was measured using optical microscopy after a standard normalising and tempering heat treatment in both the cast and rolled variant of GAM 3 and the grain size was found to be 677 µm ± 105 and 187 µm ± 22 respectively.

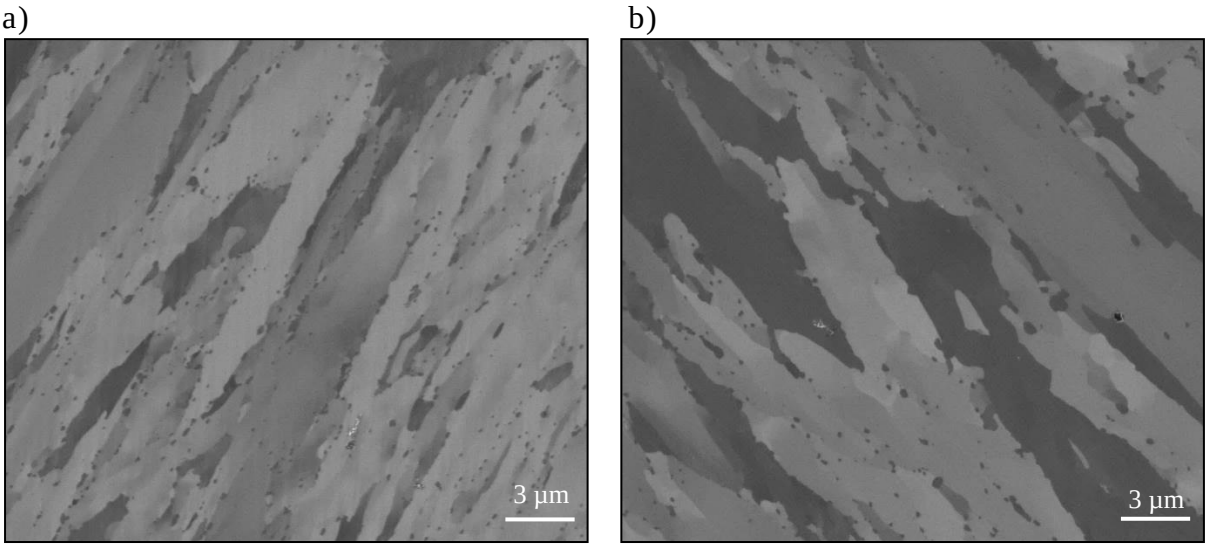

Figure 6.2: Micrographs of GAM 3 produced using ion beam imaging in two different product forms a) the cast variant and b) the rolled variant. Both samples received a standard normalising and tempering heat treatment, at 1150°C for 2 hours and 780°C for 3 hours respectively.

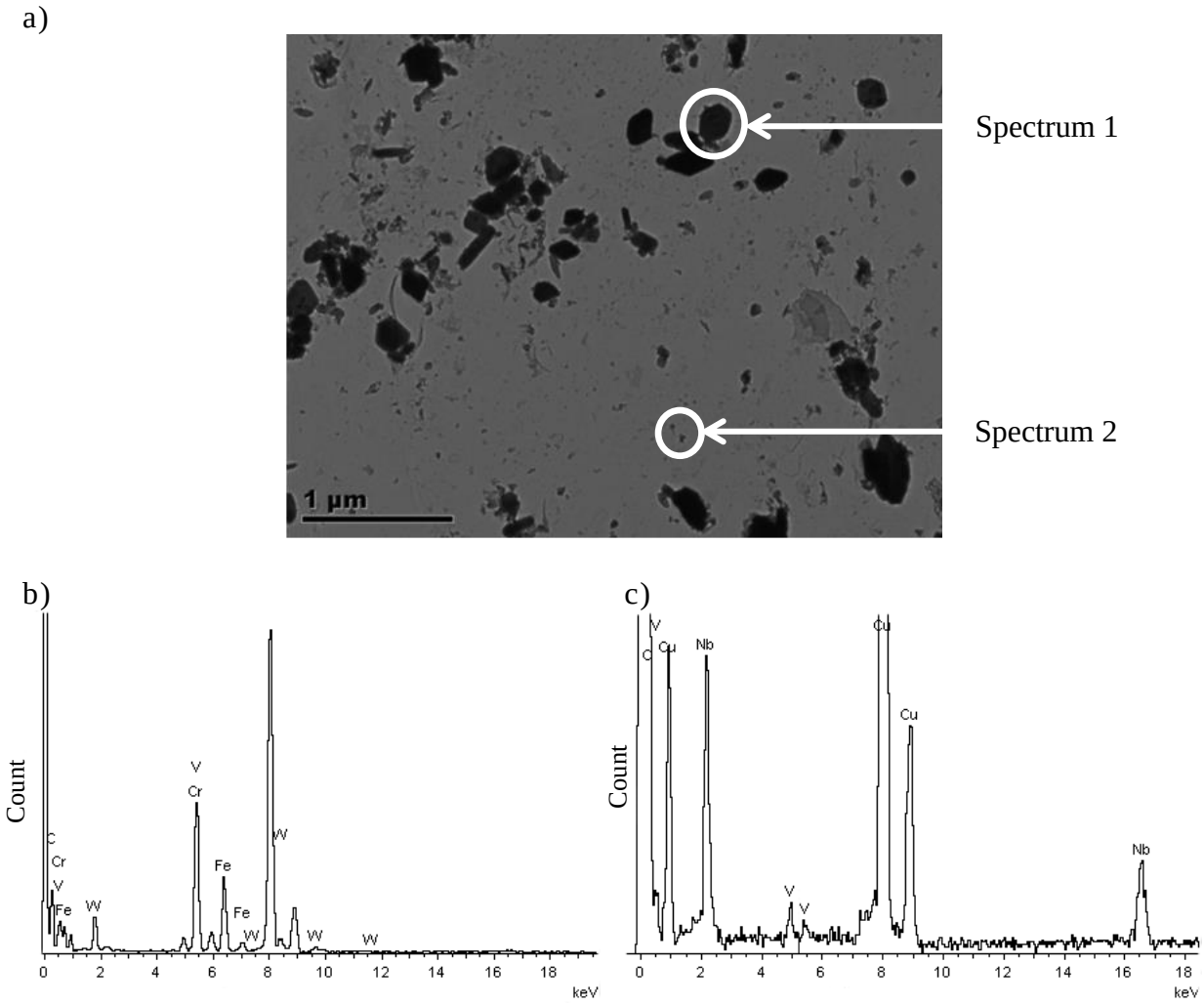

Figure 6.3: A carbon extraction replica of GAM 3 after a standard normalising and tempering heat treatment (N1150C T780C). Two EDS spectra show different types of precipitates present in the standard condition. Spectrum b) shows a typical EDS profile of a $M_{23}C_6$ precipitate and spectrum c) shows a typical EDS spectrum of a NbC precipitate.

6.3 Identification of Boron Containing Phases

Thermodynamic calculations were carried out under equilibrium conditions using the chemical composition of GAM 3, as shown in Table 3.1. Two boron containing phases were predicted to be present; M_2B and boron nitride. Figure 6.4 shows the predicted phase diagram of the boron containing phases and the liquid phase predictions under equilibrium conditions. Boron nitride was predicted to be present between 1030ºC - 1130ºC and M_2B was predicted to be present from 605ºC to the liquid formation temperature of 1260ºC. The chemical compositions of M_2B and BN have been predicted using thermodynamic calculations. M_2B was found to be rich in tungsten, chromium and iron over the temperature range of 800ºC - 1200ºC, as shown in Figure 6.5. Boron nitride was found to have similar levels of both boron and nitrogen as shown in Figure 6.6.

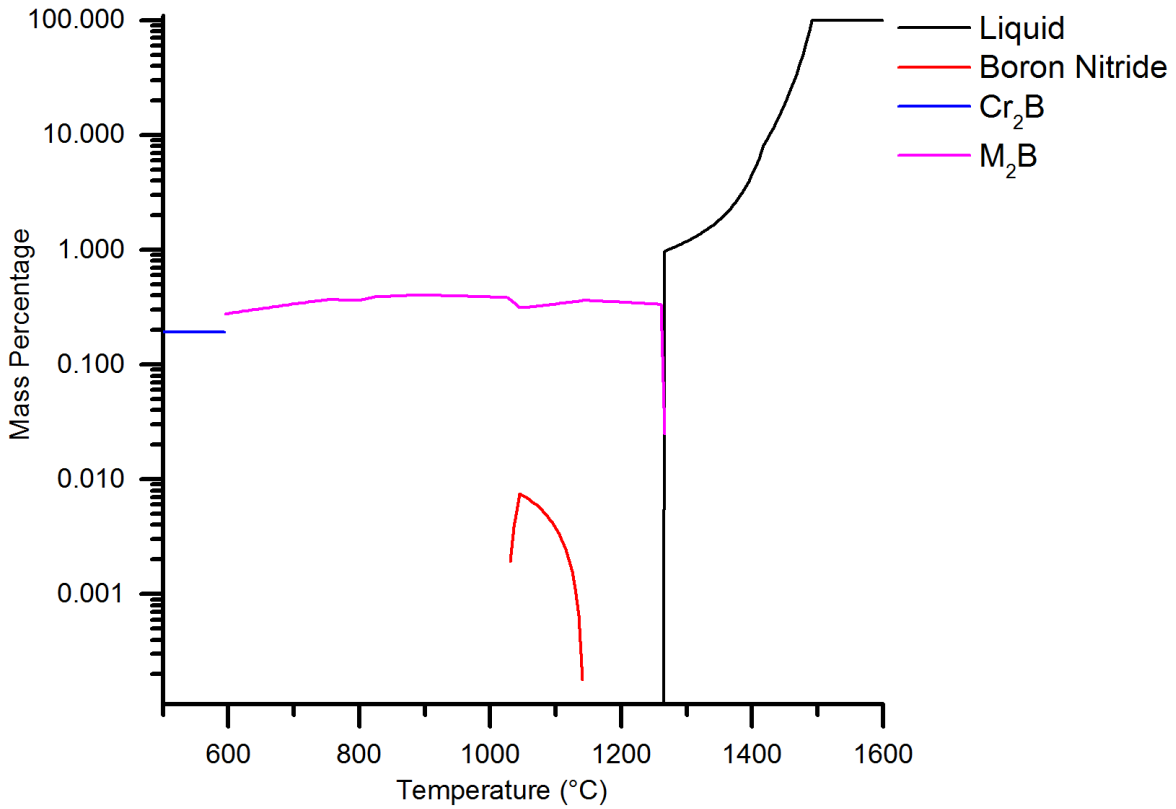

Figure 6.4: A phase diagram showing the boron containing phases predicted to be present at thermodynamic equilibrium. Calculations were performed using the actual composition of GAM 3.

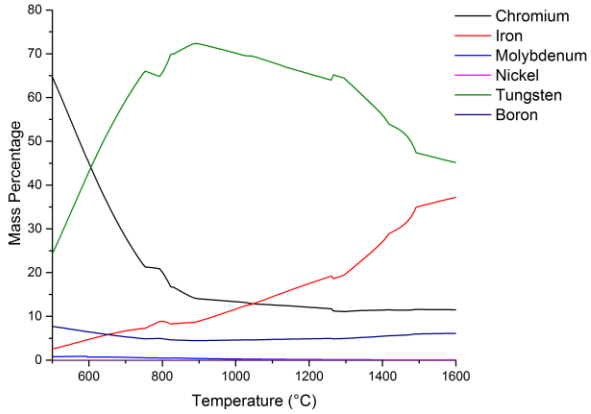

Figure 6.5: A graph showing the predicted chemical composition of W_2B in GAM 3 at thermodynamic equilibrium.

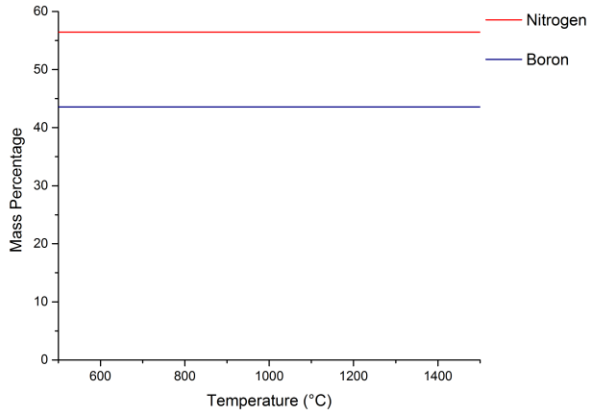

Figure 6.6: A graph showing the predicted chemical composition of BN in GAM 3 at thermodynamic equilibrium.

The secondary electron micrograph shown in Figure 6.7 shows two different types of particle which have different contrast in the backscatter image. The particles have been denoted as particles 'A' and 'B' and EDS point analysis was performed on both particles. Figure 6.8 shows a spectrum generated from particle A, which shows a boron and nitrogen peak

providing conclusive evidence that the particle is consistent with it being boron nitride. Figure 6.8 also shows a spectrum generated from a B_4C powder and subsequent analysis shows that the intensity of the boron peak in the B_4C powder is higher. This is consistent with the higher concentration of boron in the B_4C powder compared to that in boron nitride particle.

EDS point analysis was carried out on particle 'B' and the spectrum is shown in Figure 6.9. It can be observed from the spectrum that there are four clear peaks, tungsten, iron, chromium and boron, which confirms this particle is a tungsten boride. Although boron has been identified to be present from the spectrum, the amount of boron has not been quantified. Table 6.1 shows a comparison between the measured chemical composition of a W_2B particle after normalising and tempering and the thermodynamic predictions. It is evident from comparing the elements predicted to be present using thermodynamic calculations and those observed to be present using EDS that similar elements are present.

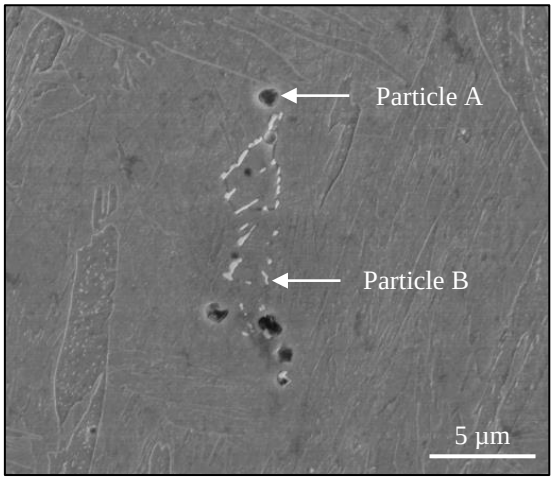

Figure 6.7: A backscatter electron micrograph of GAM 3 in the cast variant, showing two types of particles present labelled as 'A' and 'B'. Both samples received a standard normalising and tempering heat treatment.

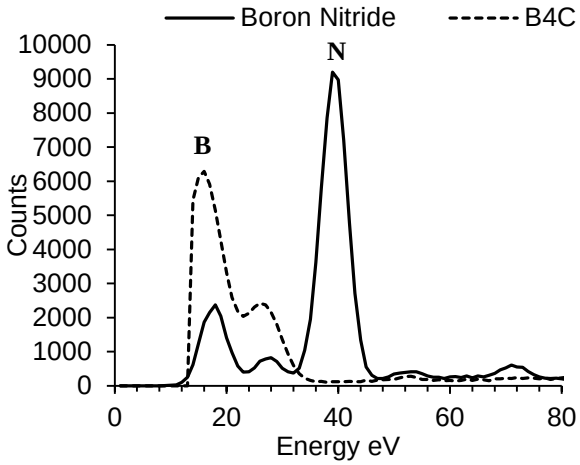

Figure 6.8: An EDS Spectrum of particle A (solid line) in the cast variant of GAM 3. The sample received a standard normalising and tempering heat treatment. The dotted line shows an EDS spectrum of a B_4C powder analysed separately.

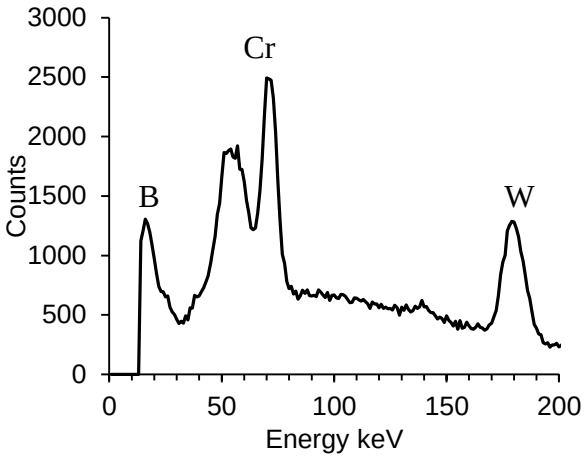

Figure 6.9: An EDS Spectrum of particle B (solid line) in the cast variant of GAM 3. The sample received a standard normalising and tempering heat treatment.

Table 6.1: A comparison between the actual and thermodynamically predicted chemical composition of W_2B. The predicted composition was calculated under equilibrium conditions using ThermoCalc and the measured composition was determined using EDS analysis.

	Weight, % balance Fe				
	B	**W**	**Fe**	**Cr**	**Mo**
Thermodynamic Predictions	4.9%	65.0%	8.4%	21.0%	0.5%
Actual Composition	*	61 %	22%	17%	0%

* Boron peak observed to be present in the spectrum; however, it has not been quantified

GAM 3 was examined in the 'as-cast' condition prior to the normalising and tempering heat treatment. In the as-cast condition there was found to be a large number of coarse tungsten borides throughout the microstructure, as shown in Figure 6.10 a). The precipitation of tungsten borides has been associated with a reduction in the creep properties within literature. This has been reported to be caused by two factors, the precipitation of tungsten borides reduces the amount of soluble boron able to be located near the $M_{23}C_6$ interface which it has been claimed can reduce the coarsening rate of the $M_{23}C_6$ carbides. In addition the precipitation of W_2B reduces the amount of tungsten that is utilised for solid solution strengthening. After normalising at 1150°C, only a small number of W_2B borides were found to be present within the microstructure, however coarse boron nitride precipitates were observed to be present, as shown in Figure 6.10 b). In the 'as-rolled' condition a small

number of tungsten borides were observed to be present, however, widespread precipitation of boron nitride was also observed and the precipitates were observed to be elongated in the rolling direction. Li *et al.*[19] have reported that normalising at 1150°C reduces the number of tungsten borides compared with normalising MarBN at the standard normalising temperature for P92 of 1050°C. The change in the number of W_2B borides has been reported to have a significant impact on the creep properties of the alloy.

Boron nitride is considered to be a harmful phase in boron strengthened advanced 9 wt. % Cr power plant steels because the formation of boron nitride reduces the effect of boron and nitrogen strengthening simultaneously. Boron nitride has been identified to be present in GAM 3 after a standard heat treatment and therefore it is important to quantify the number and size of the borides present in the standard condition. Quantification of this phase will provide statistical data to choose an optimum heat treatment, in order to optimise the creep properties of the alloy.

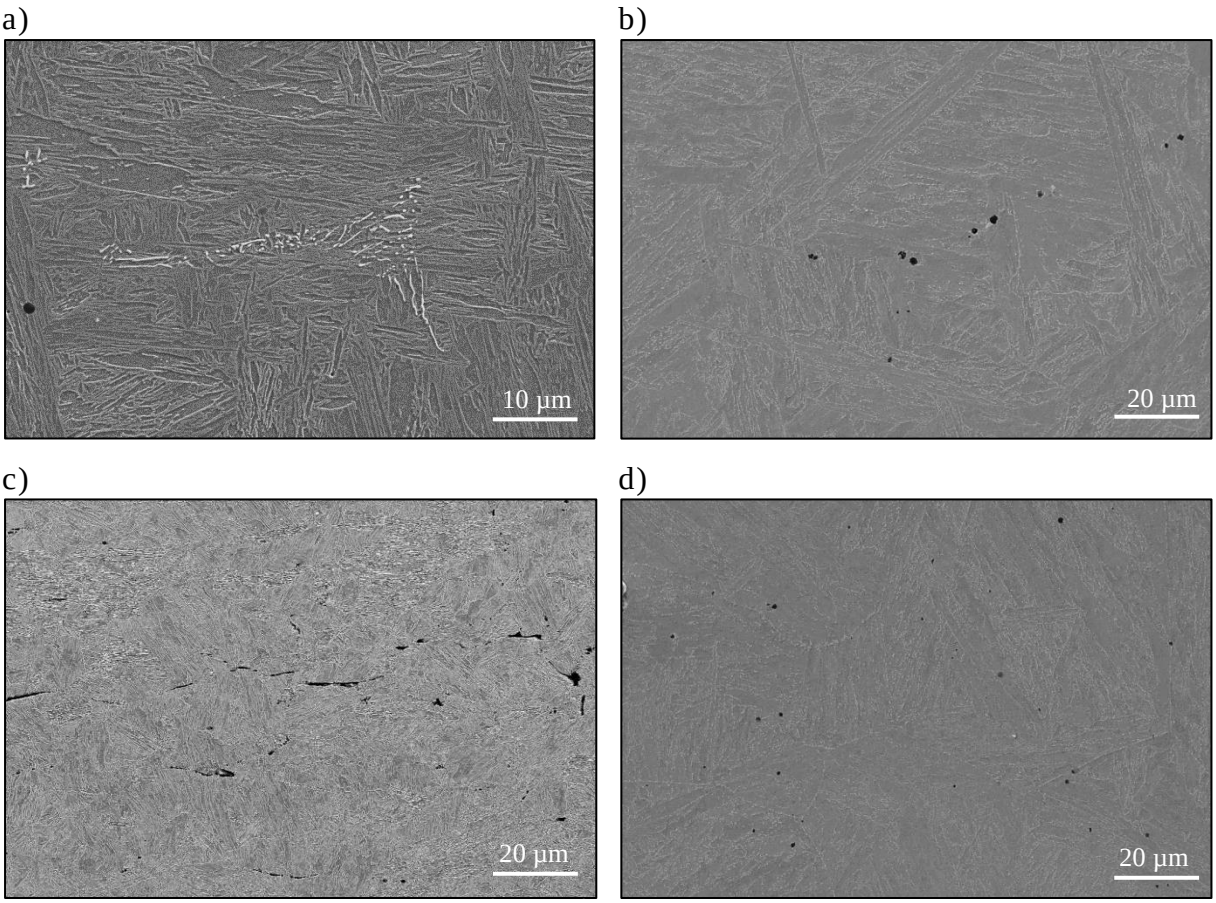

Figure 6.10: A series of SEM micrographs of GAM 3 in a number of conditions a) as-cast, b) cast HT (N1150°C T780°C) c) as-rolled, d) rolled HT (N1150°C T780°C).

Quantification of boron nitride has been carried out on images collected in secondary electron mode using the experimental procedure described in section 3.9.2. Figure 6.11 a) shows an SEM image with two boron containing phases present; boron nitride and tungsten boride, in addition to a number of intermetallic inclusions. Figure 6.11 b) shows the processed image which has independently isolated the boron nitride particles from the matrix and other types of precipitates. The processed image shows the boron nitride particles in different colours; this represents the different sizes of particles.

a)

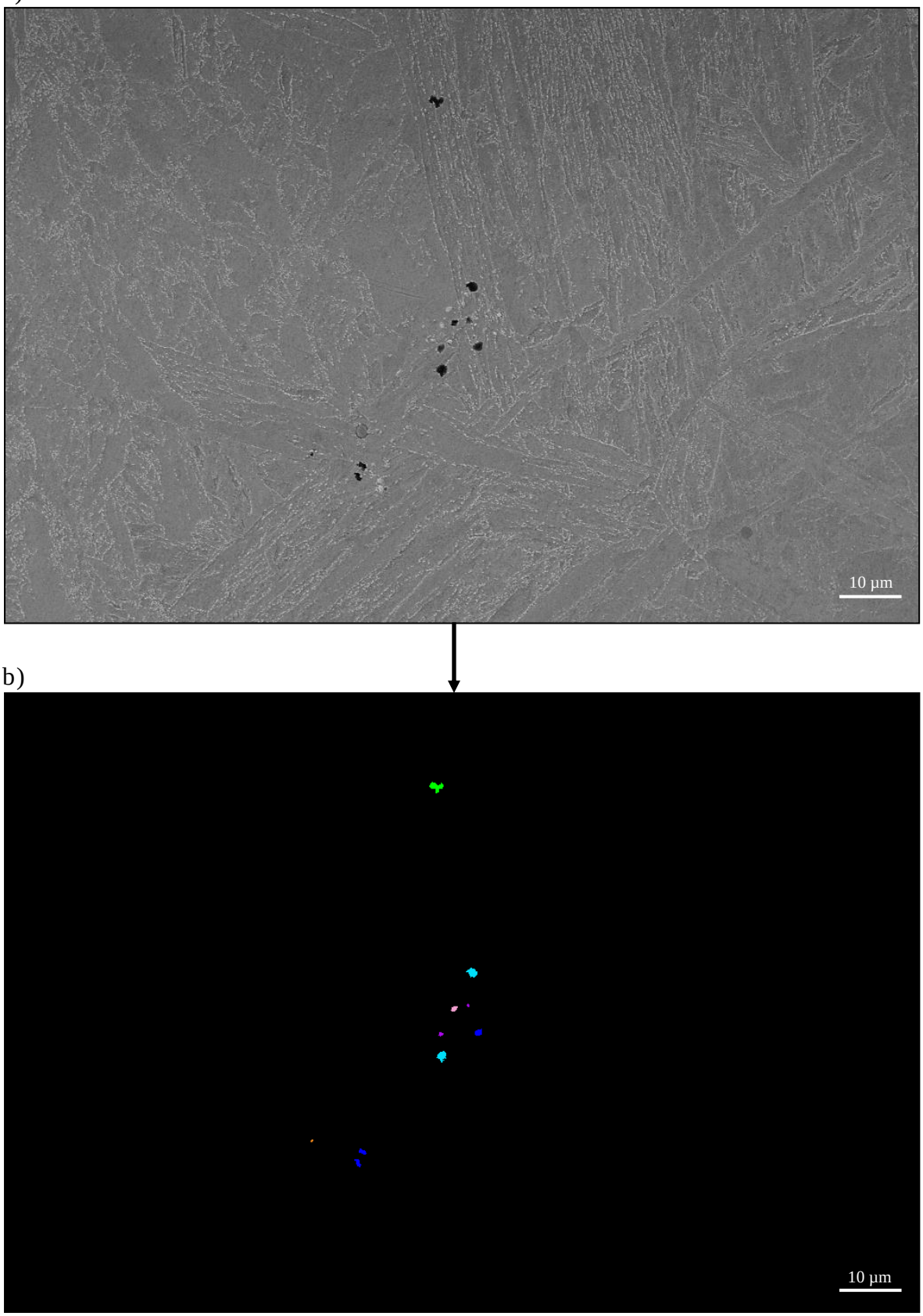

Figure 6.11: Ilustrates the image processing technique used to quantify boron nitride particles. a) An SEM micrograph which contain a number of secondary phases, b) shows the processed image of only the boron nitride particles identified using ImageTool.

The amount of boron nitride present has been quantified in a number of conditions; as-rolled, rolled N1150°C T780°C and as-cast and cast N1150°C T780°C. The variant with the highest area percentage of boron nitride was the as-rolled condition. After the rolled steel was normalised and tempered, the area percentage of boron nitride was found to decrease to ~0.030%. In the as-cast variant no boron nitride was observed to be present, however after normalising and tempering at the standard condition (N1150°C T780°C) boron nitride was observed to be present in small quantities. The area percentage of boron nitride observed to be present in the cast heat treated condition was ~0.007%.

It is therefore postulated that in the cast variant, boron nitride is precipitated during the normalising heat treatment at 1150°C. However in the rolled variant, boron nitride is thought to precipitate during the initial rolling process. At the start of the rolling process the steel temperature was observed to be 1225°C and throughout the rolling process the temperature will decrease. This will consequently lead to the alloy being processed within the range of 1030°C – 1150°C when boron nitride has been observed to be precipitated. The rolling process is a two stage process, as discussed in section 0.2. This is thought to result in an increase in the amount of boron nitride precipitated within the microstructure.

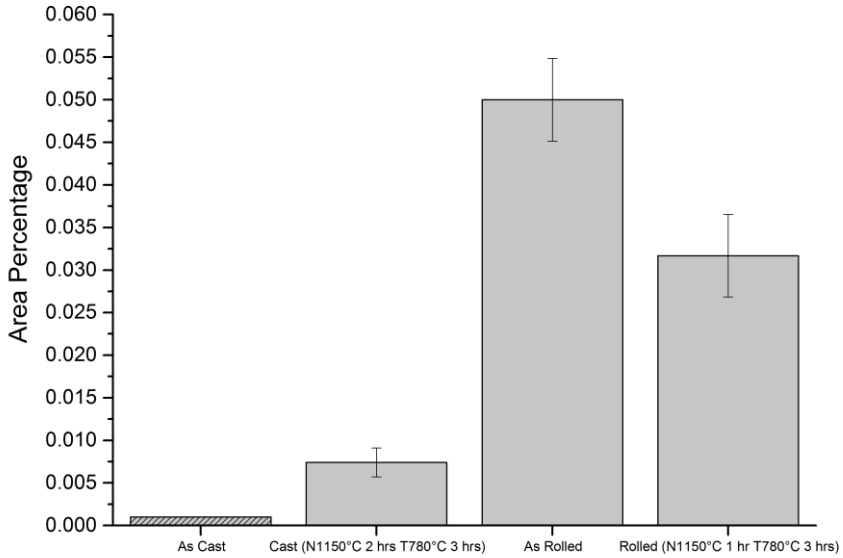

Figure 6.12: A graph showing the area percentage of boron nitride in the cast and rolled variants. Both variants were analysed after received a standard normalising and tempering heat treatment (N1150°C T780°C).

6.4 Optimising the Normalising Temperature

Understanding at what temperature boron nitride is precipitated will help develop a heat treatment that results in a microstructure which is free of boron nitride. A series of normalising heat treatments were carried out on GAM 3 in the as-cast condition. The heat treatments were carried out using a dilatometer which can closely control and monitor the thermal cycles. During this investigation various samples were normalised at 1000ºC, 1150ºC, 1175ºC, 1200ºC and 1225ºC. The samples were subsequently cooled from the normalising temperature to room temperature at 90°C/sec.

Figure 6.13 presents a series of secondary electron micrographs, showing the microstructure of the cast samples when normalised in the range of 1000°C – 1225°C. The secondary electron images show a number of particles present; the lighter particles have been identified as W_2B and the darker particles have been found to be boron nitride. The results from the normalising trials show that boron nitride is precipitated within the temperature range of 1000ºC - 1150ºC, as shown in Figure 6.13 a) and b). However, when GAM 3 was normalised at 1175ºC - 1200ºC no boron nitride was found to be precipitated, as shown in Figure 6.13 c), d) and e).

Quantification of the area percentage of boron nitride has been carried out at a range of normalising temperatures, as shown in Figure 6.14. Quantification has shown that normalising at 1000ºC resulted in an area percentage of ~0.030% boron nitride present. Normalising at 1150ºC was found to result in a decrease in the area percentage of boron nitride to approximately ~0.020%. As the normalising temperature was increased to 1175°C no boron nitride particles were observed to be present.

The experimental results were found to be very similar to the thermodynamic calculations, which predict that boron nitride will be present between 1031ºC - 1130ºC in GAM 3. Normalising GAM 3 at 1150°C resulted in the precipitation of boron nitride; however no boron nitride was observed when the steel was normalised at 1175ºC. There was found to be a small variation of approximately 45ºC between the experimental results and the thermodynamic predictions for GAM 3.

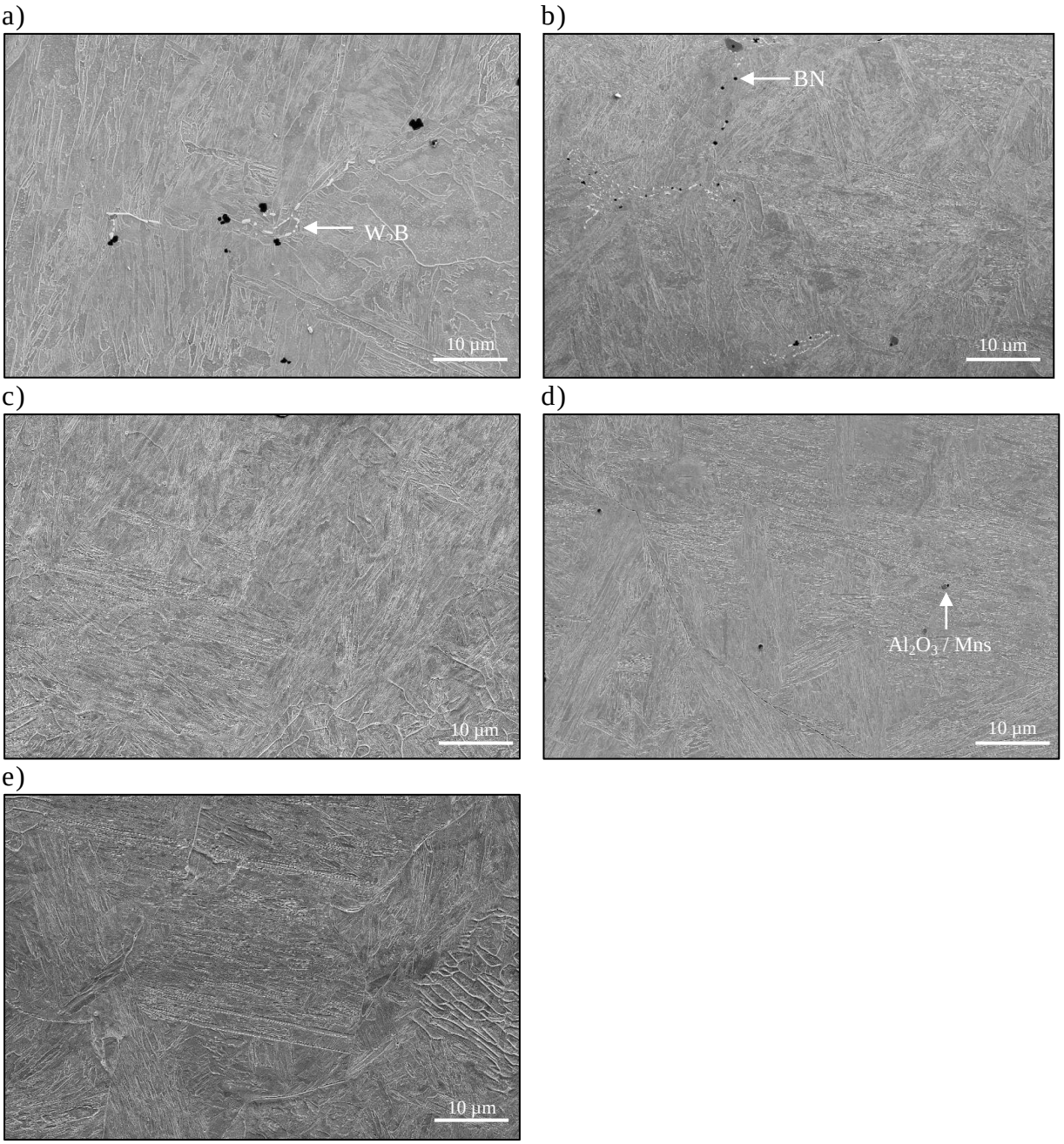

Figure 6.13: A series of SEM micrographs of GAM 3 showing the microstructures resulting from different normalising temperatures. The cast variant was normalised for 15 minutes in a dilatometer using a sample size of 10 mm at the following temperatures a) 1000°C, b)1150°C, c)1175°C, d)1200°C, e)1225°C.

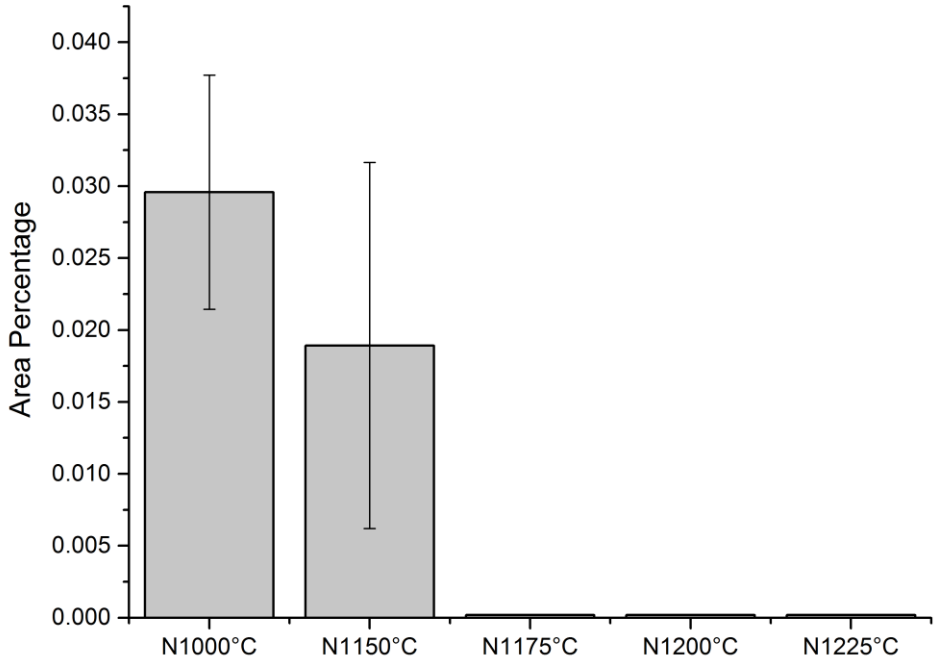

Figure 6.14: A graph showing the area percentage of boron nitride after GAM 3 was normalised using a dilatometer for 15 minutes at temperatures ranging from 1000°C to 1225°C.

Increasing the normalising temperature can have implications on the prior austenite grain size and the martensitic lath width. Figure 6.15 shows the effect of the grain growth of the prior austenite size (PAGB) as a function of normalising temperature. When the normalising temperature was increased from 1000ºC to 1150ºC, the prior austenite grain size was found to increase from 86 µm ± 10 to 194 µm ± 20 respectively. The increase in grain size is postulated to be due to the partial dissolution of niobium carbide. Thermodynamic calculations have predicted that niobium carbide has an average mass percentage of 0.4% in the temperature range of 500°C – 1050°C. The carbide is predicted to dissolve between 1050°C – 1200°C. As the normalising temperature was increased from 1150ºC to 1200ºC, no further significant change in the grain size was observed. An extended normalising heat treatment carried out at 1200ºC for four hours, showed that the prior austenite grain size was very similar to that with a normalising heat treatment carried out at 1200ºC for one hour. It should be noted that the prior austenite grain size of the cast MarBN used in this work was significantly larger than that in conventional P91/P92 steels.

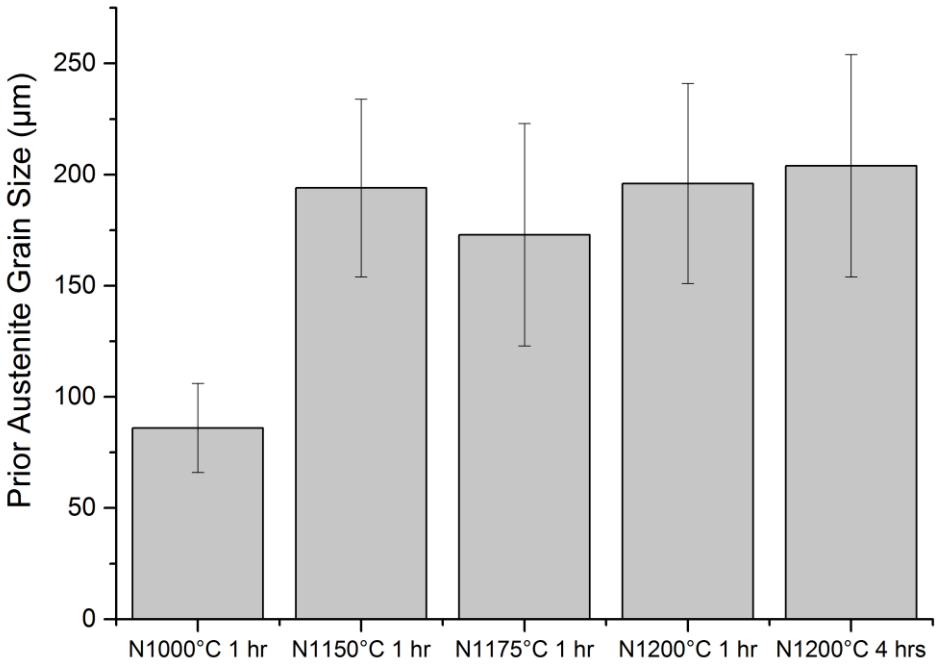

Figure 6.15: A graph showing the prior austenite grain size of the cast variant of GAM 3 after the samples were normalised for one hour in the temperature range of 1000°C – 1200°C within a chamber furnace. The figure also shows an additional measurement which was carried out after normalising at 1200°C for 4 hours.

6.4.1 Dissolution of Boron Nitride

Boron nitride was observed to be present in the cast condition after a standard normalising heat treatment of two hours at 1150°C and tempering at 780°C for three hours. Experimental work has shown that boron nitride can be prevented from precipitating within the microstructure by changing the normalising conditions. Occasions may arise whereby a standard heat treatment is carried out instead of the optimised heat treatment, which could lead to the precipitation of boron nitride. It is therefore vital to understand how boron nitride which has previously precipitated can be subsequently dissolved.

A series of normalising trials were carried out on GAM 7 in the heat treated condition (N1150°C T780°C) with the use of dilatometry. The chemical composition of GAM 7 is shown in Table 3.2. The aim of the normalising trials was to identify if a heat treatment could be used to dissolve boron nitride, which had precipitated during previous heat treatments.

GAM 7 was normalised at the standard normalising temperature of 1150°C, and there was found to be significant precipitation of boron nitride. The thermodynamic calculations predict that boron nitride will not be present in the temperature range of 500°C – 1500°C, which is

thought to be due to the lower nitrogen of the second batch of steels manufactured (GAM 5 – 8). The thermodynamic calculations indicate that the stability of the nitrogen containing phases predicted to be present is very sensitive to the nitrogen content in MarBN.

A series of high temperature normalising heat treatments were carried out with the aim of dissolving boron nitride. An additional high temperature normalising heat treatment was applied to GAM 7. This alloy had already received a standard normalising and tempering heat treatment and therefore boron nitride was observed to be widely present initially as shown in Figure 6.16 a).

Two normalising heat treatments were carried out which consisted of heating the samples up to a normalising temperature of 1200^{o}C and holding for 10 and 30 minutes before cooling to room temperature. The full heat treatment parameters can be found in Section 3.6.5.

GAM 7 was chosen to investigate the dissolution of boron nitride because this alloy had the highest boron and nitrogen levels in the second batch of steels manufactured (GAM 5 – 8). The boron level in GAM 7 was measured to be 195 ppm and the nitrogen level was 160 ppm. The area percentage of boron nitride was examined in all of the steels manufactured in the second batch, and GAM 7 was found to have the highest level of boron nitride. A total of 103 nitrides were observed to be present in an area of 0.25 mm^{2}, which were found to have an average area of 3.50 μm^{2}.

The results show that after an additional normalising heat treatment at 1200^{o}C for 10 minutes no boron nitride was found to be present, as shown in Figure 6.16 b) and c). Therefore, the results indicate that a high normalising temperature can be used to dissolve boron nitride into solution. In addition, delta ferrite was not observed to be present after a normalising heat treatment at 1200°C in this particular alloy.

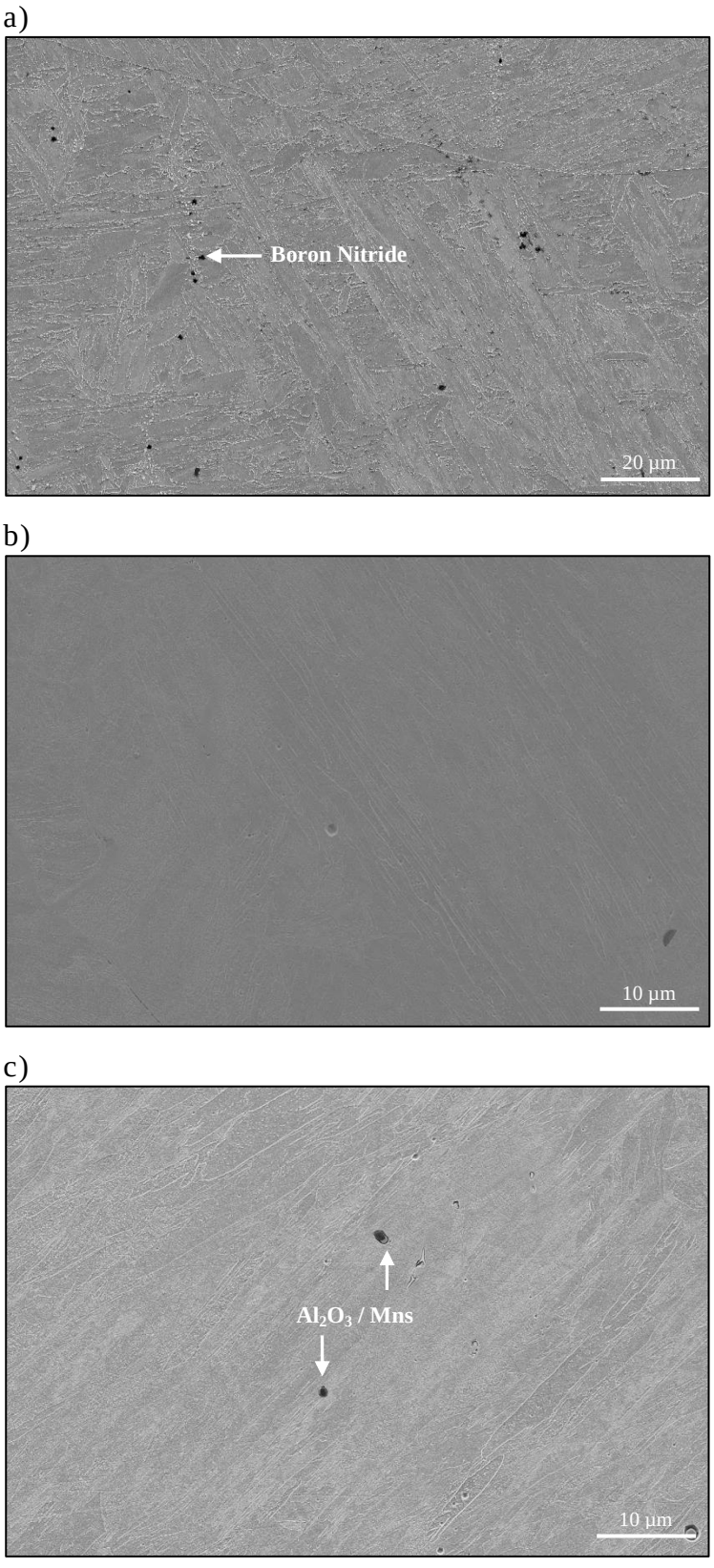

Figure 6.16: Three SEM micrographs of GAM 7 in the cast variant. a) The microstructure after a standard normalising and tempering heat treatment (N1150°C T780°C), b) and c) The microstructures after a standard normalising and tempering heat treatment and an additional normalising heat treatment at 1200°C for 10 minutes and 30 minutes respectively.

Previous normalising heat treatments have shown that boron nitride can be dissolved into solution using a normalising heat treatment at 1200°C. The heat treatments carried out on GAM 7 utilised a very fast cooling rate of 90°C/sec from the normalising temperature of 1200°C to room temperature. In industrial applications where large scale castings are manufactured the cooling rate is thought to be significantly slower and will depend on the size of the casting and cooling equipment used.

A series of heat treatments were therefore carried out to identify if boron nitride can be precipitated upon cooling after receiving a normalising heat treatment at 1200°C. Two heat treatments were carried out, one utilising a very fast cooling rate of 90ºC/sec and another utilising a slow cooling rate of 6ºC/min. Figure 6.17 a) and b) show the microstructures after the two heat treatments; no boron nitride appeared to be present in either microstructure, indicating that boron nitride does not precipitate upon slow cooling to room temperature.

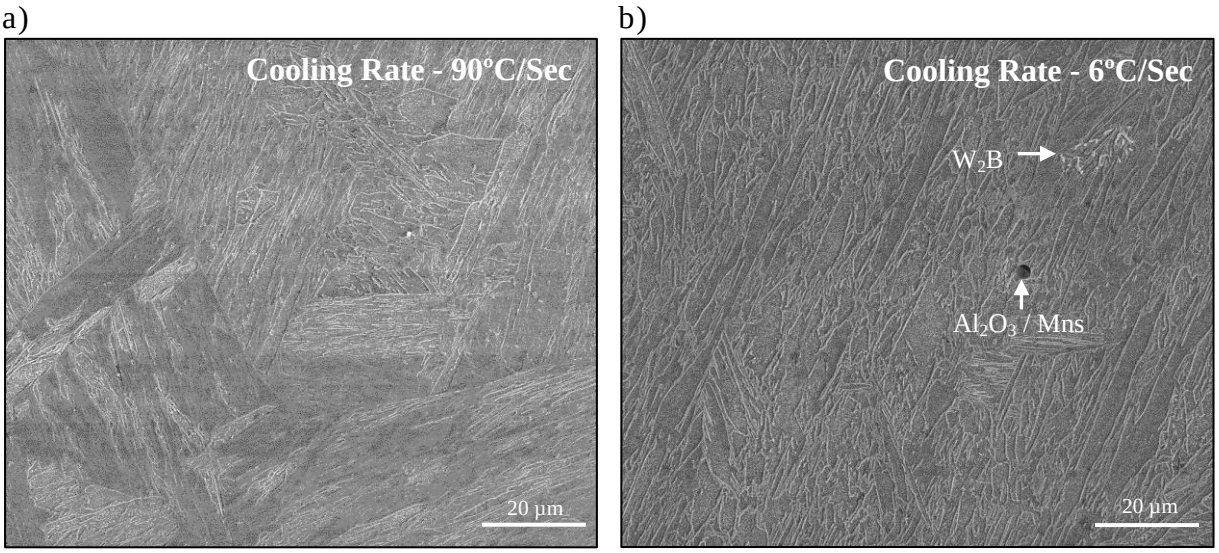

Figure 6.17: Two SEM micrographs of GAM 3 after a standard normalising and tempering heat treatment (N1150°C T780°C), plus an additional normalising heat treatment at 1200°C for 10 minutes. The samples were cooled at a rate of a) 90°C/sec and b) 6ºC/min.

6.4.2 Effect of the Starting Condition on the Dissolution of Boron Nitride

Previous characterisation has examined the microstructure of a number of cast alloys after different normalising heat treatments. The presence of boron nitride within the microstructure was validated with the use of EDX, then the nitrides were subsequently analysed using the method described in 3.9.2. The results have shown that the precipitation of boron nitride is very sensitive to the normalising temperature. Therefore, it is likely that in some situations a

non-optimised heat treatment may be applied to a MarBN steel, which could cause the precipitation of boron nitride.

Boron nitride was observed to be widely present in the cast materials after a standard normalising and tempering heat treatment. A high temperature normalising heat treatment at 1200°C for 10 minutes can be used to dissolve the boron nitride precipitates. However, in this particular investigation the dissolution of boron nitride was studied in the cast variant. The cast variant was found to have a significantly lower area percentage of boron nitride than the rolled variant.

Boron nitride has been observed to be present within the microstructure of GAM 3 after a normalising heat treatment between the temperature range of 1150°C - 1175°C. During the initial rolling process the alloy was preheated up to 1225°C, and the alloys were subsequently rolled, however, during the rolling process the temperature of the alloy decreased and therefore boron nitride is thought to have been precipitated. The precipitates were found to be elongated in the same orientation as the rolling direction, as shown in Figure 6.18 b). Therefore it is postulated that the precipitates were formed during the rolling process. The steels were rolled twice during the rolling process and this is thought to increase the amount of boron nitride which was found to have precipitated.

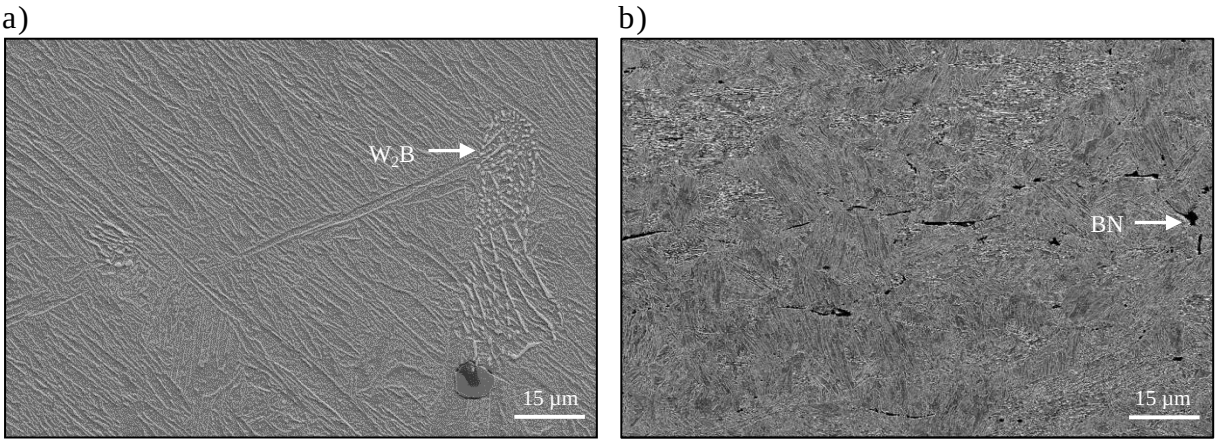

Figure 6.18: Two SEM micrographs of GAM 3 in different conditions, a) the as-cast condition and b) as-rolled condition.

After the rolling process the steel was normalised and tempered using the standard heat treatment parameters (N1150°C 1 hr & T780°C 3 hrs). The morphology of the precipitates was found to change from elongated precipitates in the as-rolled condition to a circular shape after a normalising and tempering heat treatment, as shown in Figure 6.19. The change in

morphology of the precipitates indicates that normalising at 1150°C can aid the dissolution of boron nitride in the rolled variant.

It is therefore vital to understand how the dissolution of boron nitride is affected by different pre service processing techniques. A series of normalising heat treatments were carried out on GAM 3 in the rolled condition at 1200°C for durations between 1 – 7 hours. The aim of the heat treatments was to determine a normalising heat treatment that could dissolve boron nitride in the rolled product. The heat treatment trials have shown that in order to dissolve all of the boron nitride in the rolled product, an extended normalising heat treatment at 1200°C for 7 hours is required. It was also observed that using a heat treatment at 1200°C for 4 hours was found to dissolve the majority of the boron nitride particles.

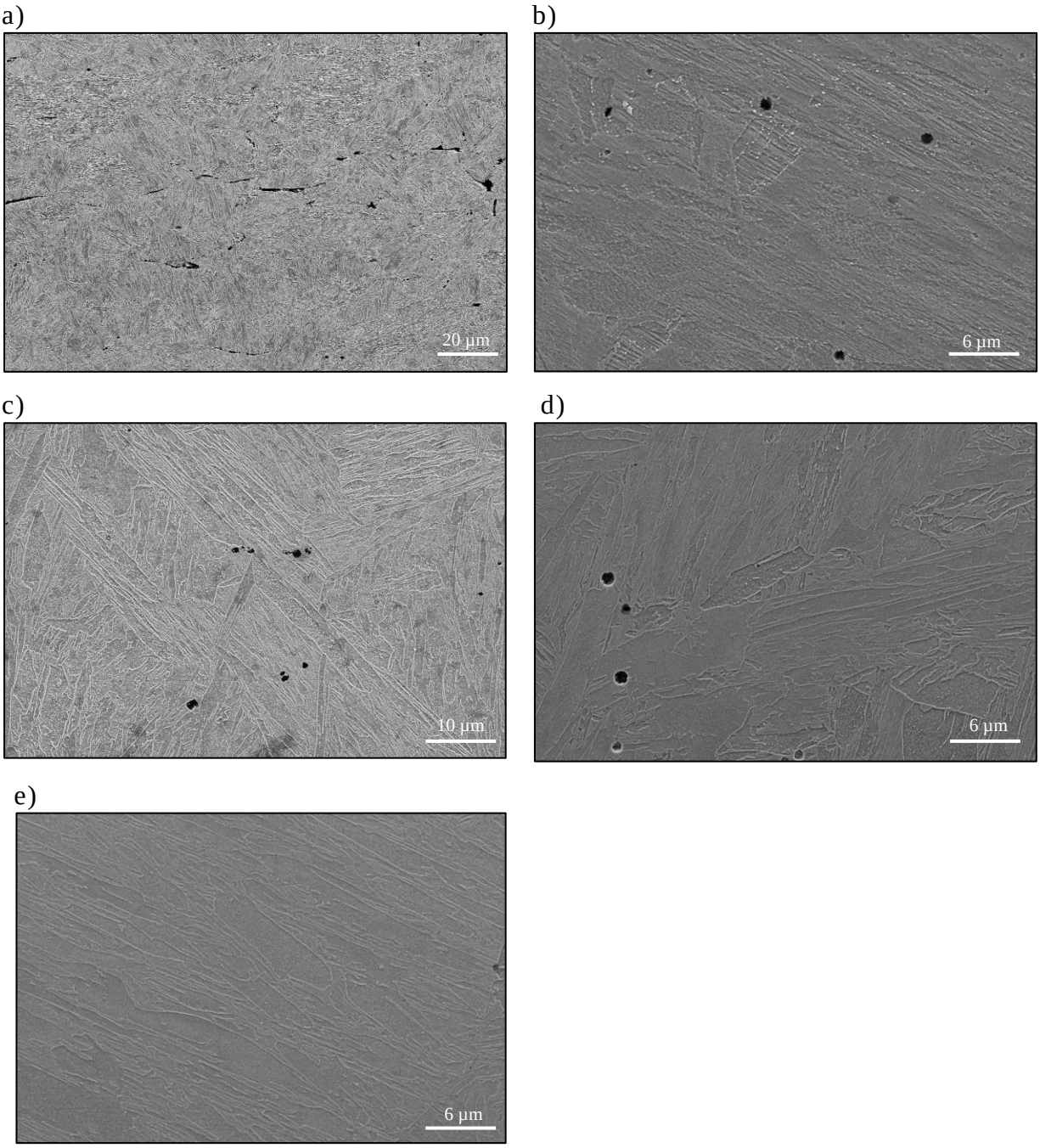

Figure 6.19: A series of SEM micrographs of GAM 3 in the rolled variant, after a series of different normalising heat treatments a) As-Rolled b) N1150°C 2 hr T780°C 3 hr c) N1175°C 1 hr d) N1200°C 4 hrs e) N1200°C 7 hrs.

Sakuraya *et al.* have reported that in P122, which has been reported to have a nitrogen content of ~600 ppm and a boron content of ~300 ppm, boron nitride can be dissolved using a normalising heat treatment at 1250°C for 0.5 hrs. It has also been reported that the boron nitride can be dissolved using a heat treatment at 1200°C for 50 hours[12]. The pre-service processing can have a significant effect on the amount of boron nitride precipitated; this has been observed to have an effect on the heat treatment parameters required to dissolve boron

nitride. The dissolution of boron nitride is thought to be relatively slow at 1200°C but is reported in literature to dissolve very quickly at 1250°C[26], probably due to the increase in the coefficient of diffusion of both boron and nitrogen at the higher temperature.

Figure 6.19 shows a series of micrographs which show the effect of the normalising temperature and duration on the dissolution of boron nitride within the rolled variant of GAM 3. The micrographs indicate that increasing the temperature to 1250°C can reduce the time required to dissolve boron nitride significantly.

6.4.3 Effect of the Normalising Temperature on the Precipitation of $M_{23}C_6$

The precipitation of $M_{23}C_6$ carbides within the microstructure has been reported in the available literature to decrease dislocation movement and act to strengthen the boundaries[10,70]. The $M_{23}C_6$ carbides have been reported to coarsen by several authors during long term, Abe *et al.* [7] have reported that a boron addition can be used to reduce the coarsening rate of the $M_{23}C_6$ carbides, and hence this helps reduce the recovery rate of the microstructure.

The initial precipitation of $M_{23}C_6$ carbides formed during the tempering heat treatment within is extremely important, and has been reported in literature to have a significant effect on the long term creep properties of the alloy. It has been reported in the literature that a boron addition can have a significant effect in aiding the precipitation of $M_{23}C_6$ carbides in a stainless steel alloy 316[71,72]. An investigation has been carried out on GAM 3 in the cast condition to identify if the boron addition can have an effect on the number, size and distribution of carbides precipitated. A comparison was made between the standard heat treatment, and between a sample which was normalised at 1200°C and then subsequently tempered at the standard tempering temperature of 780°C.

Figure 6.20 shows two micrographs produced with the use of ion beam imaging. Both micrographs reveal that the microstructure contains a number of precipitates, which have been observed to be present on the lath boundaries. Quantification of the carbides present within the microstructure of both the standard and optimised normalised heat treatments has been carried out. The micrographs were produced using a focussed ion beam and xenon difluoride gas in order to reduce the contrast differential between the matrix, as shown in Figure 6.21. Figure 6.21 indicates there were a higher number of precipitates in the samples that were normalised at 1200°C.

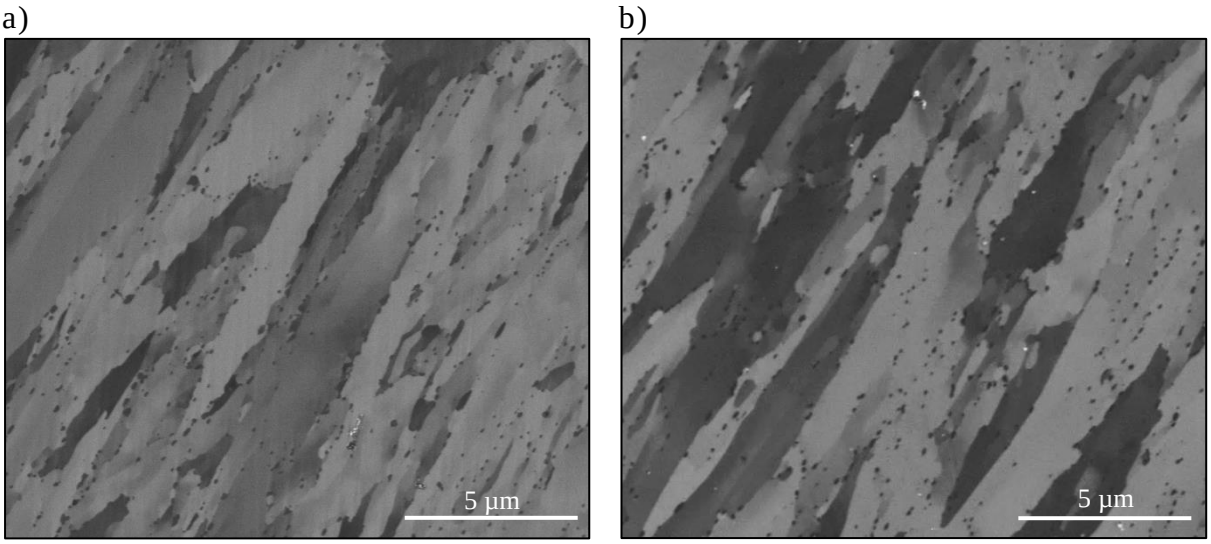

Figure 6.20: Two micrographs of GAM 3 produced using gallium ion beam imaging. Two cast variants were characterised in the conditions a) N1150°C 2 hrs T780°C 3 hrs b) N1200°C 4 hrs T780°C 3 hrs.

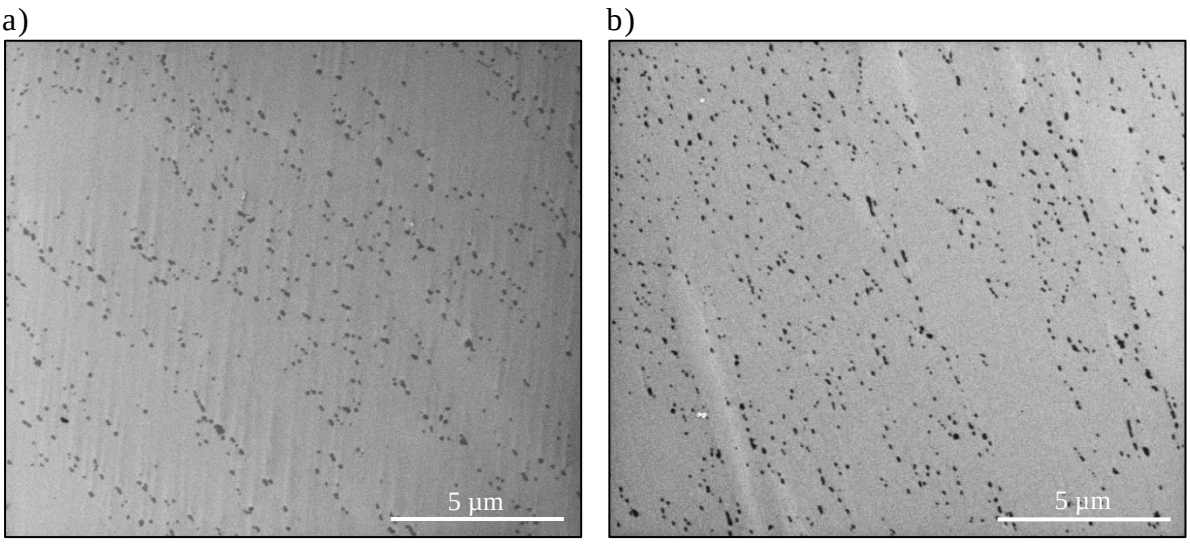

Figure 6.21: Two micrographs of GAM 3 produced using gallium ion beam imaging and a xenon difluoride gas. Two cast variants were characterised in the conditions a) N1150°C 2 hrs T780°C 3 hrs b) N1200°C 4 hrs T780°C 3 hrs.

Quantification of the carbides within an area of 692 µm² after a standard normalising and tempering heat treatment was carried out. 1750 $M_{23}C_6$ carbides were observed to be present. However, after a normalising at 1200°C and tempering at 780°C there were ~3000 M23C6 carbides present. The particles were found to be a similar size in both conditions, as shown in Figure 6.21.

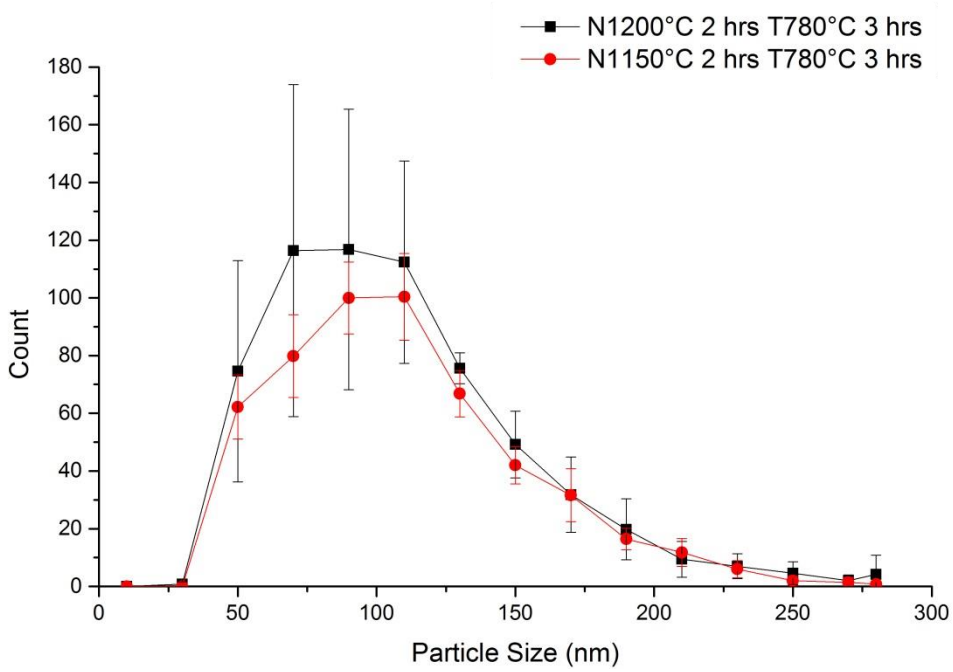

Figure 6.22: A graph showing the size distribution of the carbides observed to be present in GAM 3 after two different normalising heat treatments, a standard normalising heat treatment N1150°C 2 hrs T780°C 3hrs (Black Line) and after an optimised normalising heat treatment N1200°C 2hrs T780°C 3hrs (Red Line).

6.5 Optimising the Tempering Temperature

The tempering heat treatment is a critical process which precipitates carbides and MX carbonitrides throughout the microstructure. The precipitation of such particles can have a significant effect on the mechanical properties of the material. The standard tempering heat treatment for P92 has been reported to be between 750°C - 780°C for a duration of three hours. MarBN materials have a lower nitrogen content in comparison to P92, and therefore the heat treatment process becomes more complex to ensure that the carbonitrides are precipitated throughout the microstructure.

The number, size and inter particle spacing of $M_{23}C_6$ carbides within the steel have been reported to have a major impact on the creep strength of the material, and impede dislocation movement. A series of heat treatments have been carried out to investigate the effect of the tempering temperature. The steels were normalised at 1150°C for 15 minutes and were subsequently tempered at temperatures between 660°C to 780°C; full details of the heat treatment parameters can be found in section 3.6.7.

A significant difference was observed to be present in the hardness of the samples as a function of tempering temperature, as shown in Figure 6.23. There was found to be a linear

decrease in hardness between 660°C and 780°C. Two main mechanisms take place during the tempering heat treatment; the precipitation of $M_{23}C_6$ throughout the microstructure and the annihilation of dislocations within the structure[70]. It is postulated that the dominant mechanism for the linear decrease is the annihilation of dislocations within the structure. Maruyama *et al.* [10] have shown that lowering the tempering temperature to 750°C results in a higher dislocation density. A higher dislocation density was reported to have superior creep rupture properties at a high stress, however, this was reported to be reduce at a lower stress. When the steel was tempered above the Ae_1 temperature of 800°C a significant increase in the hardness was observed. This was due to the formation of un-tempered martensite upon cooling to room temperature.

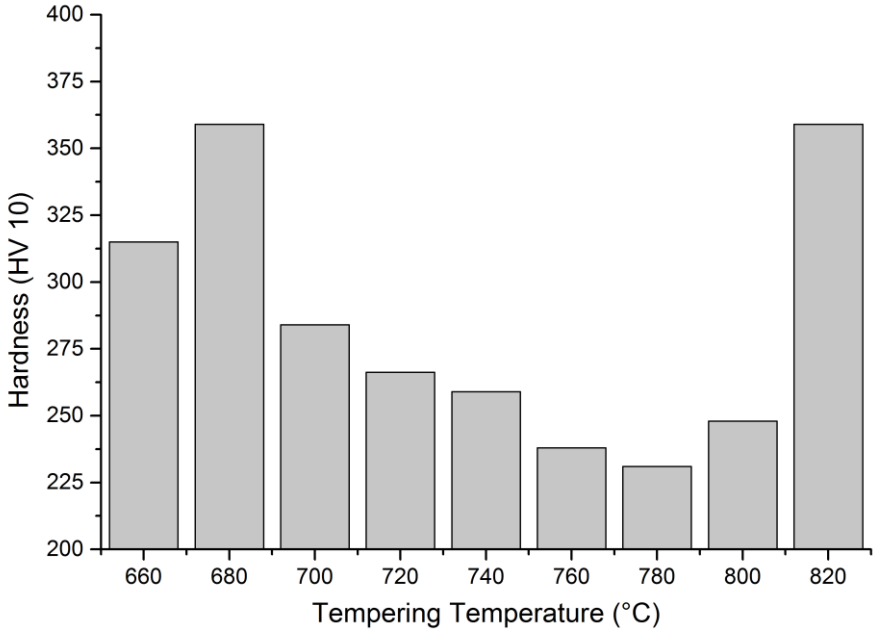

Figure 6.23: A graph showing the effect of the tempering temperature on the hardness of GAM 3. The samples were normalised at 1150°C for 15 minutes, then tempered in the range of 660°C to 820°C for three hours.

6.5.1 $M_{23}C_6$ Precipitation

The larger precipitates within the microstructure have been quantified as a function of tempering temperature. The larger precipitates have previously been identified as chromium rich $M_{23}C_6$ carbides with the use of TEM, as shown in Section 6.2. The precipitate distributions have been quantified using gallium ion beam imaging. This has shown that the precipitates are found to be present on the lath boundaries at all tempering temperatures in the range of 660°C to 820°C, as shown in Figure 6.24 a) & b). Quantification of the precipitates has been carried out as a function of tempering temperature to determine the number, size and

density of the particles within the microstructure. Figure 6.24 c) & d) shows two digitally enhanced images which have been used to quantify the $M_{23}C_6$ carbides in isolation. Quantification of the $M_{23}C_6$ carbides has shown that there were approximately 2250 precipitates per 1360 µm² when tempered between 660°C - 740°C. When the alloy was tempered in the temperature range of 760°C - 820°C, there was found to be a significant reduction in the number of particles present, as shown in Figure 6.25.

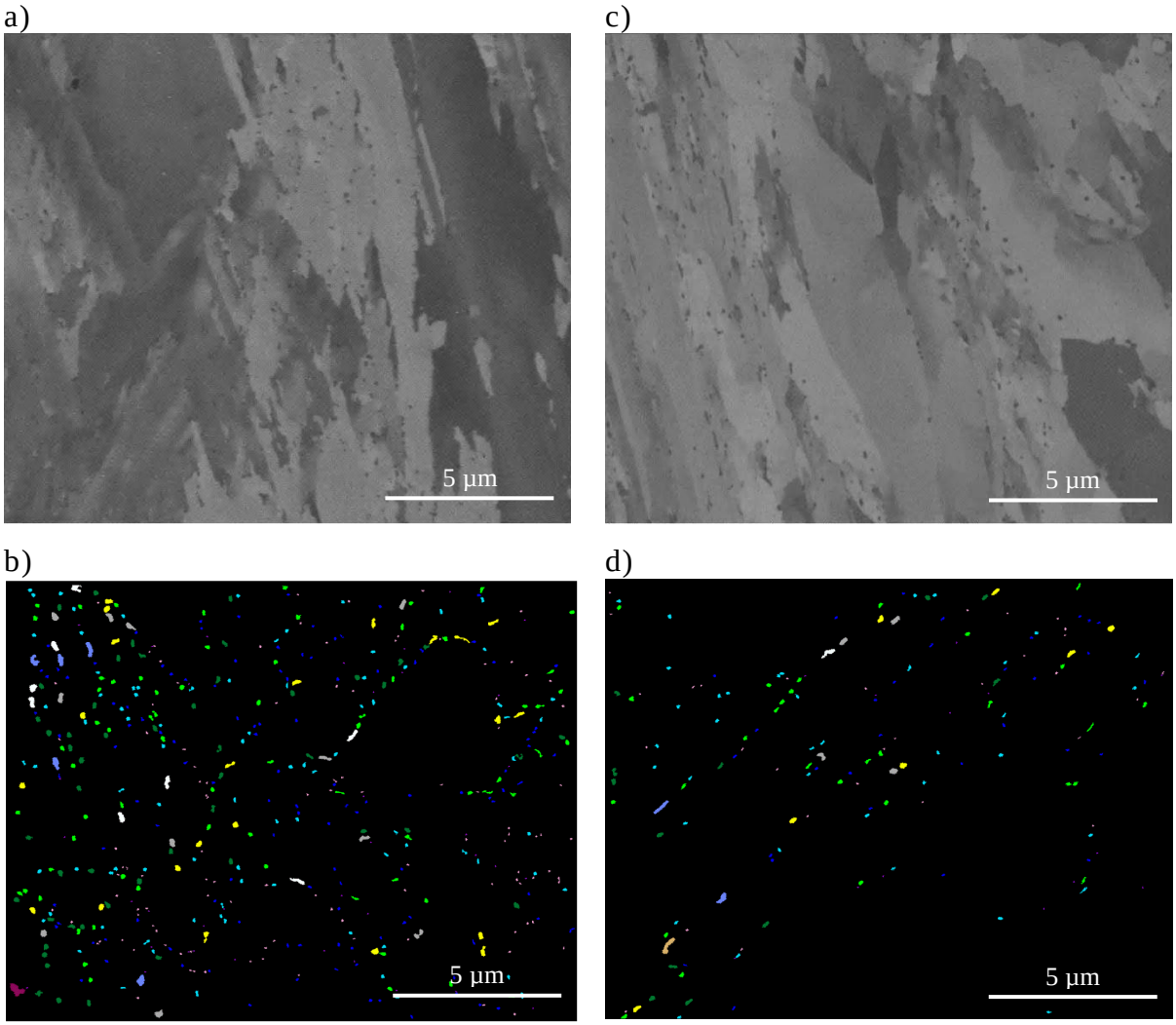

Figure 6.24: Two micrographs produced using gallium ion beam imaging of GAM 3 in the cast variant after normalising at a) 600°C and b) 780°C. The figure also shows two processed images, where the $M_{23}C_6$ precipitates have been isolated from the matrix the samples were normalised at 1150°C and tempered at c) 600°C d) 780°C.

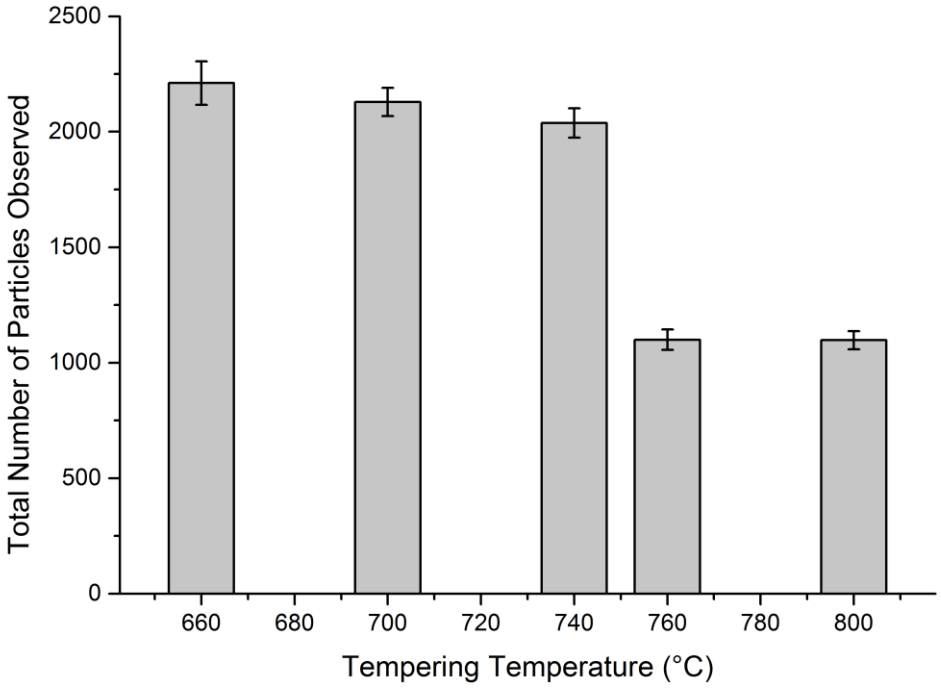

Figure 6.25: A graph illustrating the effect of the tempering temperature on the total number of particles observed to be present per 700 µm², in GAM 3 after the steel has been normalised at 1150°C and subsequently tempered.

The average particle size of the $M_{23}C_6$ precipitates has been quantified at each of the tempering temperatures. The smallest average precipitate size was found to be 86 nm, which was observed to be present at the lowest tempering temperature of 660°C. As the tempering temperature was increased, the average particle size was found to increase, and when the alloy was tempered at 780°C, the particle size was found to be 120 nm, as shown in Figure 6.25. The highest number density of particles present per 1 µm² was found to be at the lowest tempering temperature, which correlates to an increase in hardness. There are other mechanisms which have not been studied in this work which are thought to affect the overall increase in hardness such as the annihilation of dislocations within the structure. In section 6.6 the results are discussed in light of all the experimental findings.

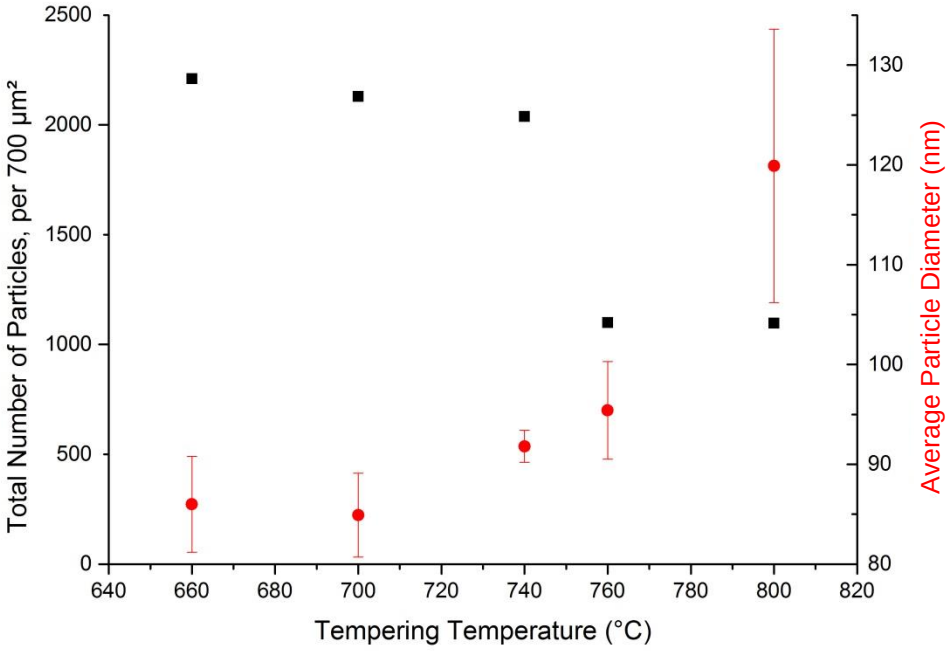

Figure 6.26: A graph illustrating the effect of the tempering temperature on the total number of particles observed to be present per 700 µm² and the average particle diameter, in GAM 3 after the steel has been normalised at 1150°C and subsequently tempered.

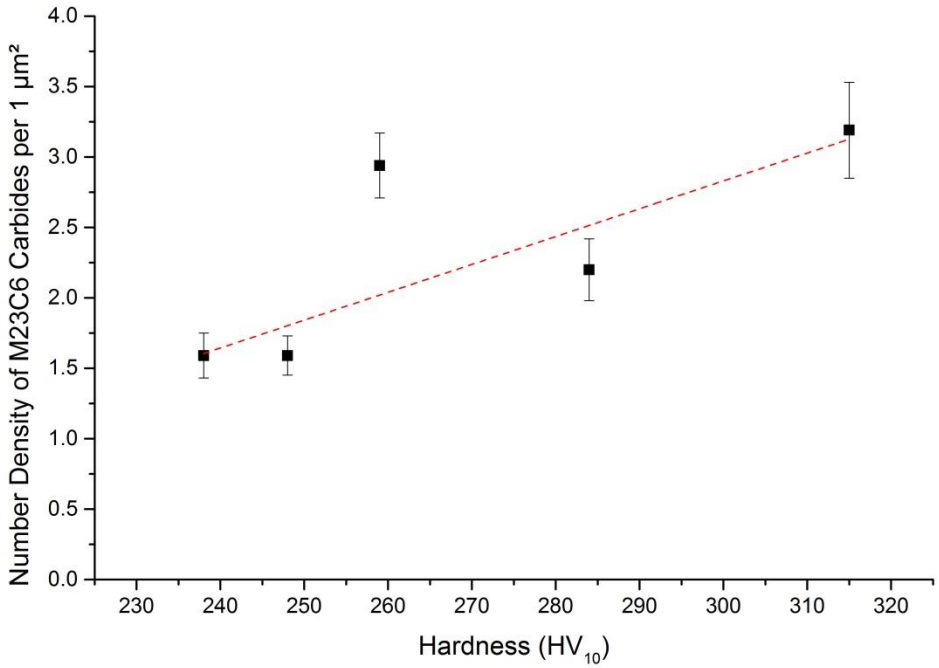

Figure 6.27: The effect of the number density of $M_{23}C_6$ carbides on the hardness of GAM 3 when normalised at 1150°C for two hours before tempering at between 600°C and 800°C.

To summarise the characterisation performed quantifying the $M_{23}C_6$ carbides within the microstructure of GAM 3 at a range of temperatures. The tempering temperature which is optimised for the precipitation of $M_{23}C_6$ was found to be 660°C, as this was observed to

precipitate the highest number density of smaller particles. Optimising the tempering temperature needs to also take into consideration the precipitation of MX.

6.5.2 MX Precipitation

The carbonitrides have been examined with the use of TEM. The precipitates present have been characterised after normalising at two different temperatures 1150°C and 1200°C. The steels were subjected to a tempering heat treatment which was carried out at four different temperatures; 700°C, 740°C, 760°C and 780°C.

Examination of the precipitates present after the different heat treatments has shown that there is a significant variation in the number of precipitates observed to be present. A visual examination of each micrograph has been carried out to provide an estimation of the number of precipitates present. When the samples were normalised at 1150°C and 1200°C then subsequently tempered at 700°C, the number of MX precipitates was observed to be very low, as shown in Figure 6.28 a) and b). There was observed to be slightly more precipitates in the sample normalised at 1200°C, which is thought to be due to the increased amount of available nitrogen after normalising at 1200°C. After normalising at 1150°C and 1200°C then subsequently tempered at 760°C there was observed to be a significant increase in the number of MX precipitates present. There was observed to be an increased amount of MX precipitates in the sample normalised at 1200°C in comparison to the sample normalised at 1150°C, as shown in Figure 6.28.

The chemical composition of the MX precipitates has been studied with the use of EDX. Approximately 50 particles were analysed per sample the chemical composition of the particles was subsequently plotted onto a ternary diagram, as shown in Figure 6.29. The ternary diagrams show the atomic percentage of niobium, chromium and vanadium.

The ternary diagrams show that there is a distinct shift in the types of particles observed to be present at different normalising and tempering temperatures. After normalising at 1200°C, at a lower tempering temperature the precipitates were observed to be chromium rich and therefore are likely to be Cr_2B or $M_{23}C_6$. As the tempering temperature was increased to 760°C there was observed to be a mixture of Cr_2B or $M_{23}C_6$ and vanadium nitride. As the tempering temperature was increased further to 780°C the precipitates were found to be predominantly vanadium nitride precipitates present. After normalising at 1200°C no boron nitride was precipitated and therefore there is more nitrogen available to form vanadium nitride during the tempering heat treatment.

After a normalising heat treatment at 1150°C boron nitride was found to be present, as previously discussed. Boron nitride has been observed to be precipitated during the normalising heat treatment. The precipitates present after tempering at 700°C were observed to be niobium carbides. As the tempering temperature was increased to 760°C, the type of precipitates was observed to change to vanadium nitride. As the tempering temperature was increased to 780°C the precipitates were predominantly niobium carbide.

Therefore to ensure that the microstructure contains a fine distribution of vanadium nitride particles to act as obstacles to dislocation motion and slow down the recovery of the microstructure[10], the optimum heat treatment is normalising at 1200°C followed by tempering at 780°C.

a)

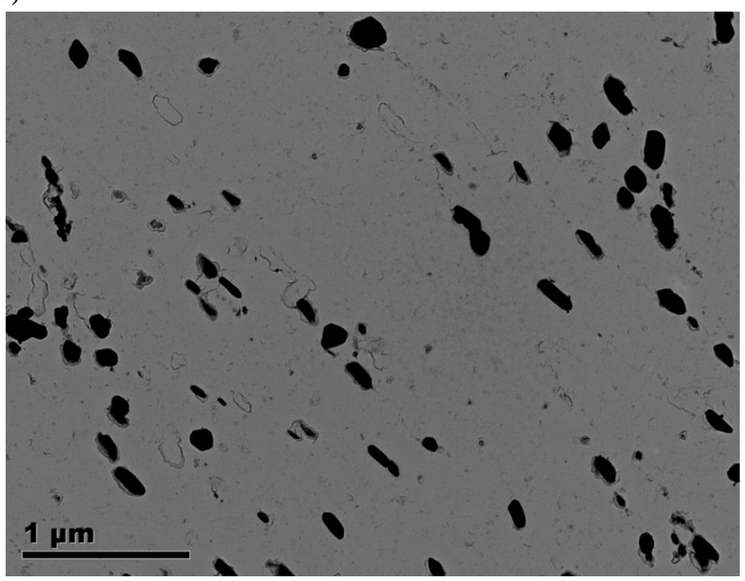

b)

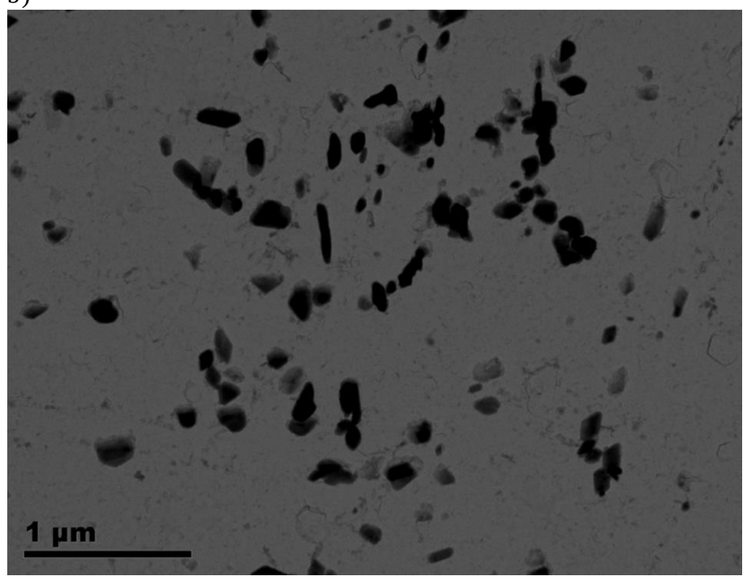

c)

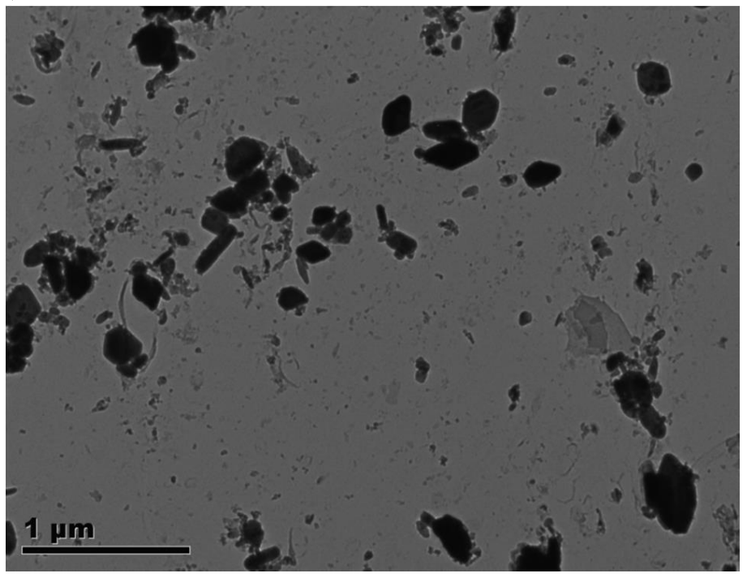

d)

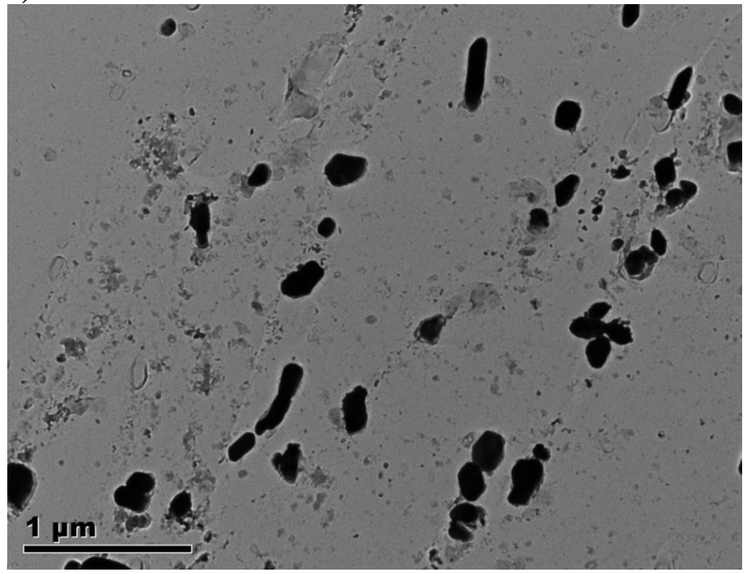

Figure 6.28: Carbon Extraction replicas showing the precipitation of $M_{23}C_6$ and MX in four conditions, a) N1150ºC T700ºC, b)N1150ºC T780ºC, c) N1200ºC T700ºC, d) N1200ºC T780ºC

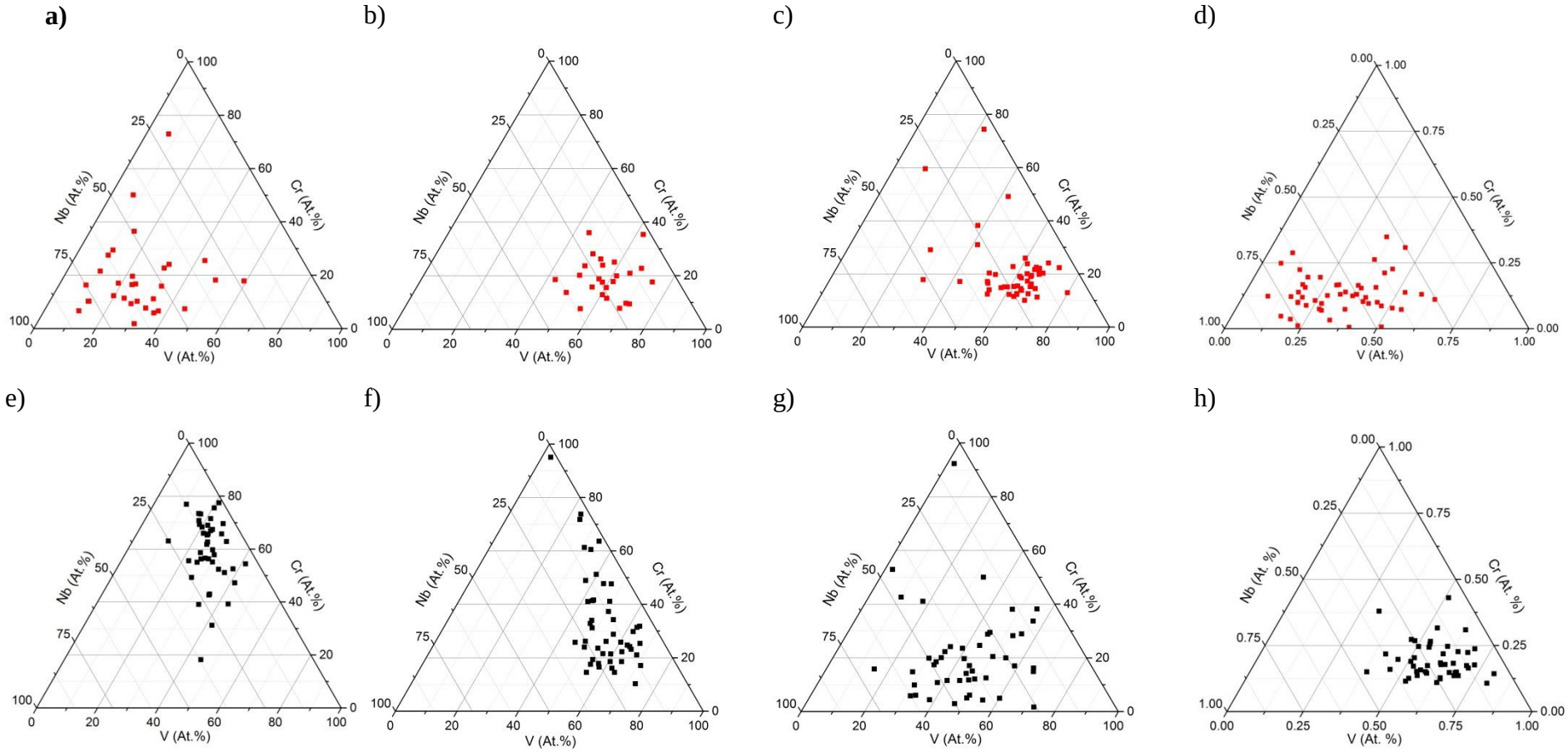

Figure 6.29: A series of ternary Diagrams to show the effect of normalising and tempering on the precipitation of VN, a) N1150ºC T700ºC, b) N1150ºC T740ºC,c) N1150ºC T760ºC, d) N1150ºC T780ºC, e) N1200ºC T700ºC, f) N1200ºC T740ºC, g) N1200ºC T760ºC, h) N1200ºC T780ºC.

6.6 Review of Pre-Service Normalising and Tempering

GAM 3 was chosen as the alloy to investigate the effect of the pre-service normalising and tempering heat treatment on the resulting microstructure. This alloy was chosen because it was designed with the use of thermodynamic calculations to have the highest boron (180 ppm) and nitrogen (150 ppm) level without precipitating boron nitride. GAM 3 was produced using an induction air melting process; during this process it was difficult to produce a melt with the target nitrogen content of 150 ppm. The final nitrogen content was 200 ppm which resulted in a small boron nitride peak being predicted between 1030°C to 1130°C using thermodynamic calculations.

Boron nitride which is considered to be a harmful phase in boron strengthened advanced 9 Cr power plant steels was found to be present after a standard normalising heat treatment in both the cast and rolled variants of GAM 3. The amount of boron nitride has been quantified in a number of conditions as-rolled, rolled HT and cast HT. The product with the highest area percentage of boron nitride was in the 'as-rolled' condition. In the as-cast variant no boron nitride was observed to be present, therefore it is postulated that in the cast variant boron nitride precipitates during the normalising heat treatment at 1150°C. The rolling process is a two stage process, this is thought to cause an increase in the amount of boron nitride precipitated within the microstructure.

Boron nitride was observed to precipitate in GAM 3 when normalised in the temperature range of 1000°C to 1150°C. However when the steel was normalised at 1175°C to 1200°C no boron nitride was found to be precipitated within the microstructure. The experimental results were found to be in very good agreement with the thermodynamic calculations which predicted that boron nitride would be present between 1031°C to 1130°C. The prior austenite grain size was measured as a function of normalising temperature, the grain size was found to be very constant at ~200 µm when normalised in the range of 1150°C (1 hr) to 1200°C (4 hrs).

In order to produce a microstructure free of boron nitride it is recommended the normalising heat treatment is carried out at 1200°C. Situations may arise whereby a non-optimised normalising heat treatment is applied to the steel which may precipitate boron nitride throughout the microstructure. It is vital that it is understood how boron nitride can be dissolved. It was observed that a normalising heat treatment at 1200°C for 10 minutes could dissolve boron nitride present in the cast variant of GAM 7. However after rolling GAM 3

significantly more boron nitride was observed to be present, a normalising heat treatment of 1200°C for four hours was found to produce a microstructure free of boron nitride.

Increasing the normalising temperature to 1200°C ensured all of the boron was in solution, which in theory should decrease the coarsening rate of the $M_{23}C_6$ carbides within the microstructure. Increasing the normalising temperature has been observed to have an effect on the number of $M_{23}C_6$ carbides precipitated within the microstructure. After normalising at 1200°C more precipitates were observed to present, which were smaller in size.

The pre-service tempering heat treatment consists of heat treating the steel within the ferrite phase field. This heat treatment precipitates chromium rich $M_{23}C_6$ carbides and MX carbonitrides throughout the microstructure. A series of heat treatments were carried out to determine the optimum tempering heat treatment. As the tempering temperature was increased from 660°C to 780°C the hardness was found to decrease, as the temperature was increased beyond 800°C the hardness was found to increase rapidly due to the formation of un tempered martensite. The total number of $M_{23}C_6$ precipitates observed to be present per 700 μm² was found to change significantly depending on the tempering temperature. When tempered between 660°C to 740°C, approximately 2200 particles per 700 μm² were observed to be present. However, when tempered between 760°C to 800°C there was only approximately 1000 precipitates per 700 μm². The precipitates were found to increase in size as the tempering temperature was increased.

The effect of the normalising and tempering temperature on the precipitation of MX has been investigated. Samples were normalised at both 1150°C and 1200°C, and were subsequently tempered between 700°C to 780°C.

The optimum normalising temperature based on microstructural characterisation was 1200°C. The tempering temperature was a balance between a number and type of MX precipitates and the size and number of $M_{23}C_6$ precipitates present. The optimum tempering temperature chosen to provide a balance between the precipitation of $M_{23}C_6$ and MX was 780°C.

Chapter 7

THE EFFECT OF PRE-SERVICE HEAT TREATMENTS ON THE LONG TERM PROPERTIES OF MarBN

7.1 Introduction

The effect of pre-service normalising and tempering heat treatments have been shown in chapter six to have a significant effect on the types of precipitates present within the microstructure of GAM 3. This chapter focuses on investigating the effect of the normalising heat treatment on the precipitation and evolution of the minor phases during subsequent long term thermal ageing at 650°C and 675°C. The chapter will primarily focus on studying the microstructural effects of isothermal ageing; however, in addition results will be reported on the effect of the pre-service heat treatments on the short term creep properties.

This chapter has been organised into four sections. The first main results section (Section 7.4) investigates the effect of the pre-service normalising temperature on the evolution of $M_{23}C_6$ and Laves phase after isothermal ageing. The second section (Section 7.5) characterises the microstructural degradation of the alloy after isothermal ageing, using Electron Backscatter Diffraction (EBSD). The third section (Section 7.6) characterises the stability of the boron containing phases such as boron nitride and M_2X during long term isothermal ageing. The final section (Section 7.7) chapter reports on the short term creep properties of the different pre-service heat treatments and reviews this in light of the microstructural characterisation.

7.2 Materials

GAM 3 was used as the material to investigate the effect of the normalising temperature on the long term microstructural evolution, and its chemical composition can be found in Table 3.1. The alloy was characterised after two different pre-service normalising heat treatments; a standard heat treatment, which consisted of normalising at 1150°C for 2 hrs followed by tempering at 780°C for 3 hrs, and also after an ‘optimised’ normalising heat treatment which consisted of normalising at 1200°C for 4 hrs followed by tempering at 780°C for 3 hrs. The samples were subsequently isothermally heat treated at 650°C and 675°C in a laboratory furnace for 2,500 hrs, 5,000 hrs and 10,000 hrs. The 8 tonne melt was used as a suitable alloy to carry out short term creep tests on due to the availability of material and this alloy was also

selected for a long term creep test programme within the IMPACT project. The chemical composition of the 8 tonne melt can be found in Table 3.4 and is broadly similar to GAM 3.

7.3 Review of Previous Findings

Chapter six has shown that increasing the normalising temperature to 1200°C dissolves all of the boron nitride particles and therefore implies that boron is instead in solution. Literature suggests that when boron is in solution it can decrease the coarsening rate of the $M_{23}C_6$ carbides within the microstructure[7]. Increasing the normalising temperature has also been observed to increase the number density of $M_{23}C_6$ precipitates present after a normalising and tempering heat treatment, as shown in Section 6.4.3.

The effect of modifying the tempering temperature was investigated in the previous chapter. The results have shown that after a standard normalising and tempering heat treatment at 1150°C and 780°C respectively, only niobium carbides were observed to be precipitated and very few vanadium nitrides observed to be present, as shown in Section 6.5.2. However, after normalising at 1200°C and tempering at 780°C the primary precipitate type was found to be vanadium nitride, in addition to a small amount of niobium carbides.

7.4 Idealised Microstructure Evolution in MarBN

The microstructure of MarBN prior to entering service consists of a martensitic microstructure with a high dislocation density and fine distribution of precipitates. In service applications, the material is subjected to a temperature of approximately 580°C for 20 years. During this time, the microstructure changes to reach an equilibrium state and therefore the microstructure changes dramatically. The martensitic microstructure shall transform to ferrite during long term exposure at the service temperature of 580°C, which is the thermodynamically stable phase. The precipitates present within the microstructure provide a pinning force on the grain boundaries which prevents the recovery of the microstructure to ferrite. Therefore the initial precipitation of carbides and carbonitrides can affect the rate in which the microstructure recovers to ferrite. It is postulated that the creep properties shall be improved by having a distribution of finer carbides and carbonitrides within the microstructure. During service the carbides coarsen so they become more thermodynamically stable and the carbonitrides transform into Z Phase, which is a coarse precipitate. Vanadium nitride and niobium carbide have been reported to be very stable and not coarsen easily at high temperature, due to their low solubility of vanadium and austenite in the ferrite phase

field. Therefore ensuring the initial microstructure of the material has a fine distribution of carbonitrides is critical to providing long term creep properties.

In MarBN the addition of boron has been added, with the aim of reducing the coarsening rate of the $M_{23}C_6$ carbides, as discussed in section 2.3.3. In order to prevent the precipitation of boron nitride throughout the microstructure the nitrogen content has been reduced, which shall reduce the amount of nitrogen available to precipitate carbonitrdes, such as vanadium nitride. Therefore it is essential that the normalising and tempering conditions are optimised to ensure there is an optimum distribution of fine carbides and carbonitrides.

7.5 The Effect of the Pre Service Normalising Heat Treatment Temperature on the Long Term Stability of $M_{23}C_6$ and Laves Phase

7.5.1 Long Term Stability of $M_{23}C_6$

Chromium rich $M_{23}C_6$ precipitates were observed to be present in GAM 3 after normalising at 1150°C and 1200°C followed by tempering at 780°C for three hours, as discussed in chapter six. Ion beam imaging was used to raster across the surface of the samples to characterise the grain structure in addition to the $M_{23}C_6$ precipitates within the microstructure. The $M_{23}C_6$ precipitates were found to be present on the lath boundaries in the normalised and tempered condition.

The $M_{23}C_6$ precipitates within the microstructure have been quantified after two pre-service normalising heat treatments. When GAM 3 was normalised at 1150°C boron nitride was precipitated throughout the microstructure. In contrast, when the material was normalised at 1200°C no boron nitride was precipitated and therefore boron is expected to be in solution.

Figure 7.1 shows a series of ion beam images which illustrate the effect of long term isothermal ageing at 650°C on the resulting microstructure. The micrographs show a comparison between the two different pre-service normalising heat treatments. The precipitates were observed to remain present on the lath boundaries after 10,000 hrs ageing at 650°C. The ion beam images provide an indication of the microstructural degradation that has taken place as a function of ageing. It is evident from examining the micrographs that both normalising heat treatment conditions remain fully martensitic after 10,000 hrs ageing at 650°C. The degradation of the microstructure has been quantified with the use of EBSD. The results and discussion can found in Section 7.5.3.

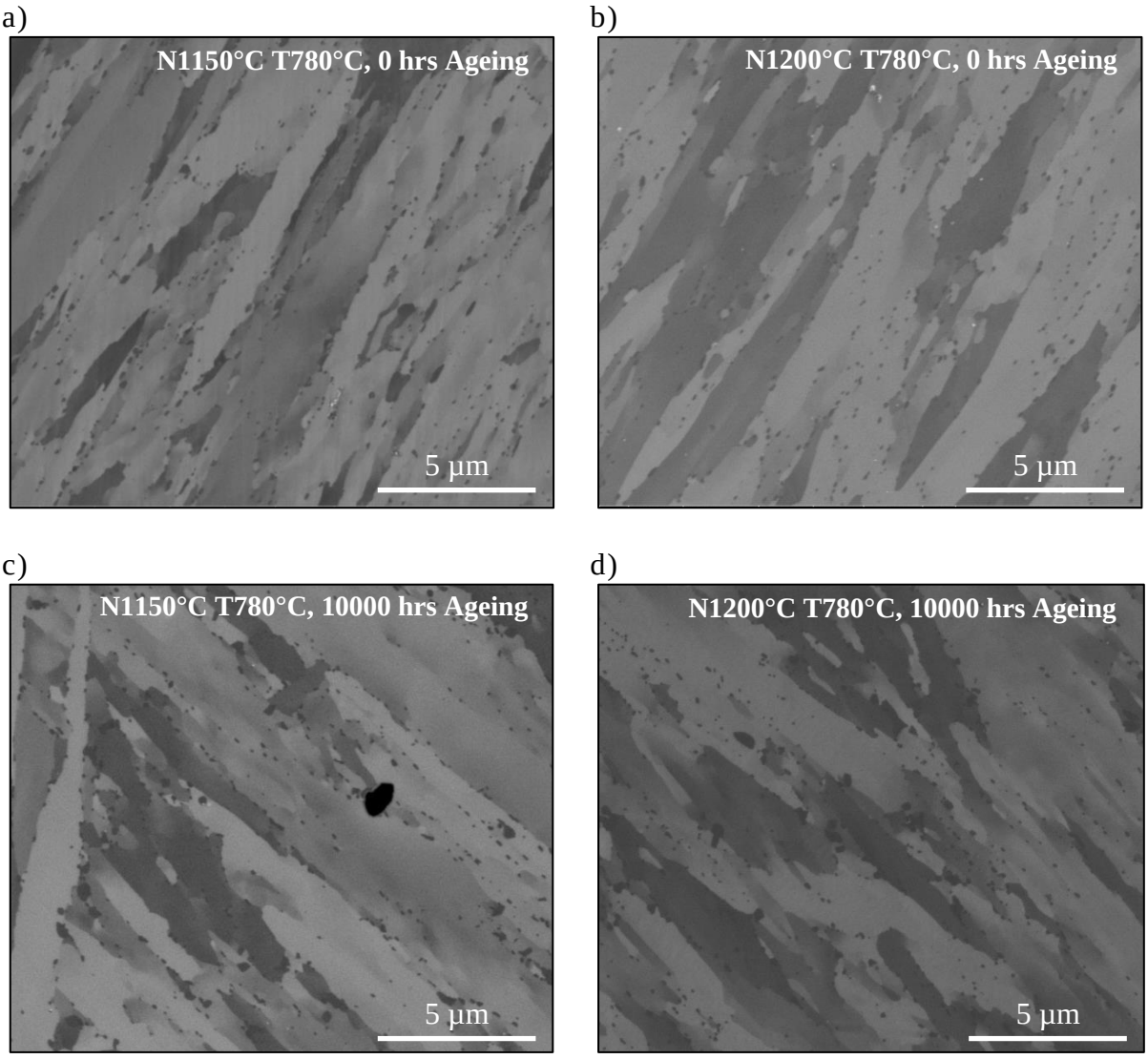

Figure 7.1: A series of high resolution micrographs produced using ion beam imaging. The micrographs were from samples normalised at 1150°C and 1200°C, which were all tempered at 780°C for 3 hours. The samples were aged at 650°C for between 0 – 10,000 hours. a) N1150°C 0 hours, b) N1200°C 0 hours, c) N1150°C 10,000 hours, d) N1200°C 10,000 hours.

Figure 7.1 provides invaluable information about the location of the precipitates within the microstructure. In order to quantify the $M_{23}C_6$ precipitates ion beam images were acquired with the use of a xenon difluoride gas to temporarily reduce the contrast differential between the matrix and the $M_{23}C_6$ precipitates to allow the $M_{23}C_6$ carbides to be quantified independently.

Quantification of the $M_{23}C_6$ carbides has been carried out as a function of ageing duration and the pre-service normalising temperature. The micrographs shown in Figure 7.2 clearly show that the $M_{23}C_6$ precipitates increase in size as a function of ageing duration after both

normalising heat treatments. Further quantification has been carried out with image analysis software to determine the changes in the precipitate size, number density and distribution.

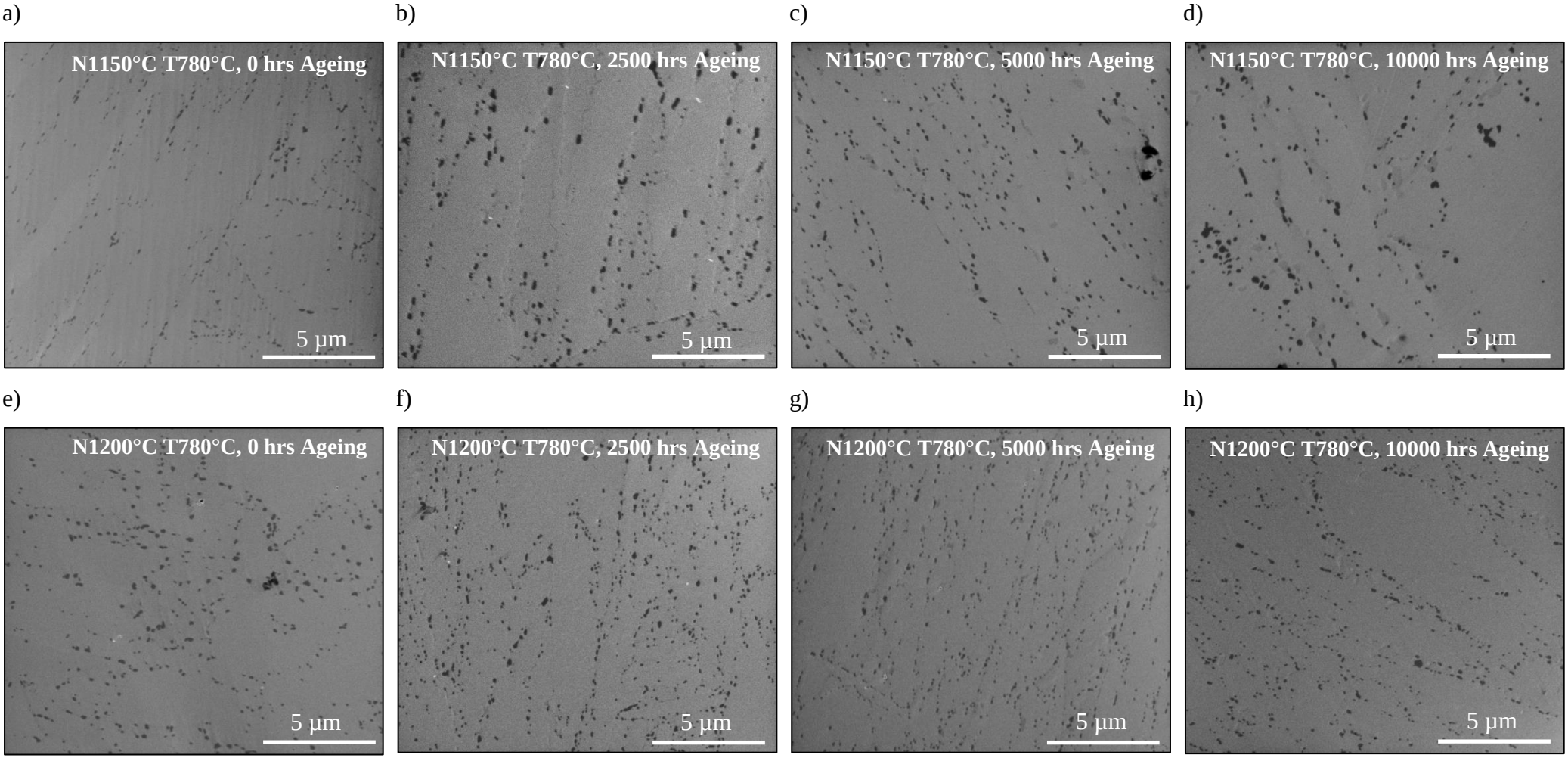

Figure 7.2: A series of high resolution micrographs produced using ion beam imaging in conjunction with a xenon difluoride gas etch. The micrographs were produced after normalising at 1150°C and 1200°Cand the samples were all tempered at 780°C. The samples were aged at 650°C for between 0 and 10,000 hours. a) N1150°C 0 hours, b) N1150°C 2,500 hours, c) N1150°C 5,000 hours, d) N1150°C 10,000 hours, e) N1200°C 0 hours, f) N1200°C 2,500 hours, g) N1200°C 5,000 hours and h) N1200°C 10,000 hours.

The samples normalised at 1200°C were observed to have a higher number density of $M_{23}C_6$ precipitates than the samples which were normalised at 1150°C. Figure 7.3 shows the number density of precipitates per 1 µm² as a function of ageing duration. After normalising at 1200°C the number density of the precipitates was observed to increase from ~4.5 per µm² after 0 hrs ageing to ~4.7 per µm² after 10,000 hrs ageing. After normalising at 1150°C the number density of precipitates was observed to be significantly lower before any ageing was carried out. After ageing at 650°C the number density was found to increase from ~2.6 per µm² after 0 hrs ageing to ~2.7 per µm² after 10,000 hrs ageing.

Figure 7.3 also indicates the total number of particles per 692 µm². It can be seen that there is an increase in the number density of precipitates observed to be present after ageing for 2,500 hours due to the increased precipitation of $M_{23}C_6$. After further ageing between 2,500 hours – 10,000 hours the number density of precipitates was observed to remain approximately constant for both pre-service conditions.

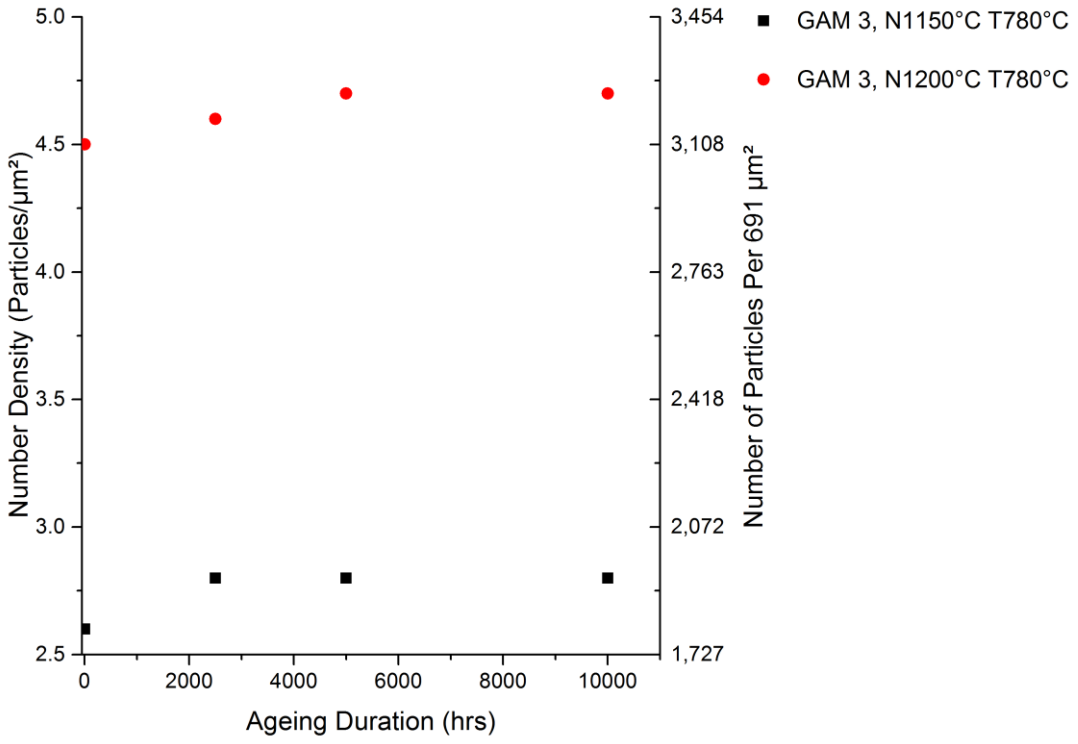

Figure 7.3: A graph showing the number density of $M_{23}C_6$ particles per micron^2 present in GAM 3 after normalising at 1150°C and 1200°C. The samples were tempered at 780°C for 3 hours and aged at 650°C. The left hand axis shows the number density of particles, and the axis on the right shows the total number of particles analysed per condition.

The size of the precipitates has been observed to change as a function of ageing duration and pre service normalising heat treatment. The samples normalised at 1150°C were found to

have an increased average particle size of ~125 nm after 2,500 hours ageing at 650°C. However, between 2,500 hours and 10,000 hours the average particle size was found to remain relatively constant between 122 – 127 nm. After a pre-service normalising heat treatment at 1200°C, the average particle size was observed to decrease after 2,500 hours to approximately 95 nm. The average particle size was then found to remain constant from 2,500 – 5,000 hours. After 10,000 hours the particle size was found to significantly increase to approximately 110 nm. The particle sizes in the samples normalised at 1200°C were always significantly less than those in the samples normalised at 1150°C.

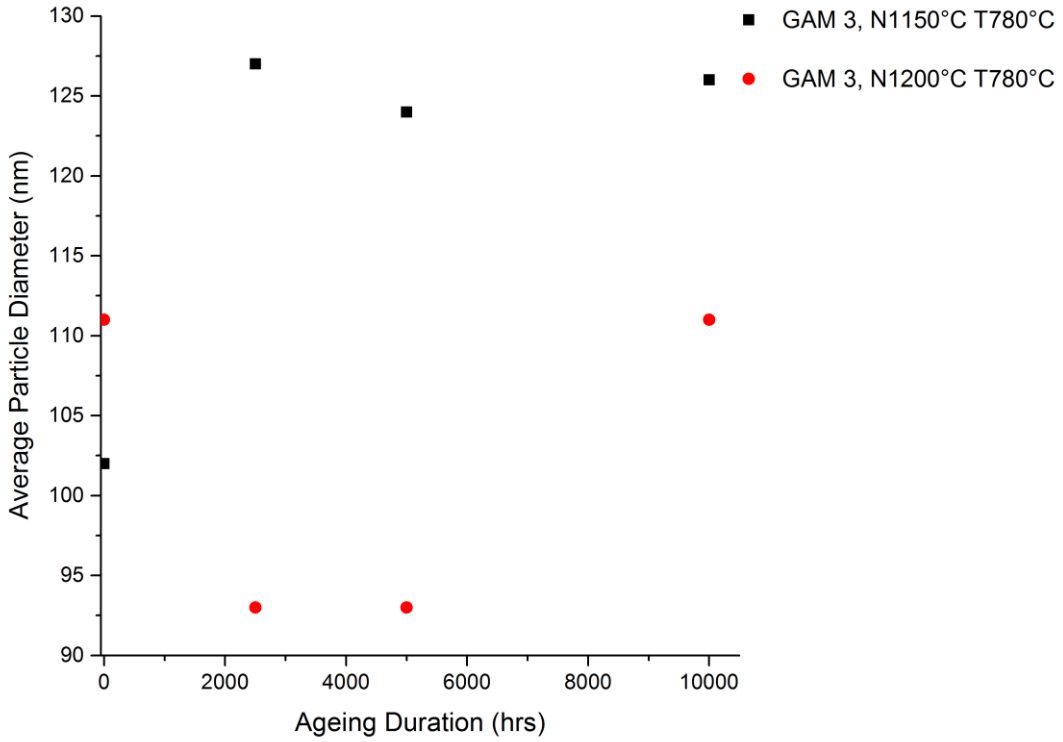

Figure 7.4: A graph showing the average particle diameter of the $M_{23}C_6$ particles present in GAM 3 after normalising at 1150°C and 1200°C. The samples were subsequently tempered at 780°C and aged at 650°C.

Figure 7.5 shows the distribution of $M_{23}C_6$ precipitates observed to be present after normalising at 1150°C and 1200°C and subsequent ageing at 650°C, as shown in the figure by the dotted and solid lines respectively. The distribution shows that normalising at 1200°C increases the number density of particles significantly and after ageing for up to 5,000 hours, the mean particle size is smaller than observed in the samples normalised at 1150°C. The distribution highlights that there is an increased number of coarser particles in the sample normalised at 1200°C after 10,000 hours at 650°C in comparison to the samples aged for up to 5,000 hours.

a)

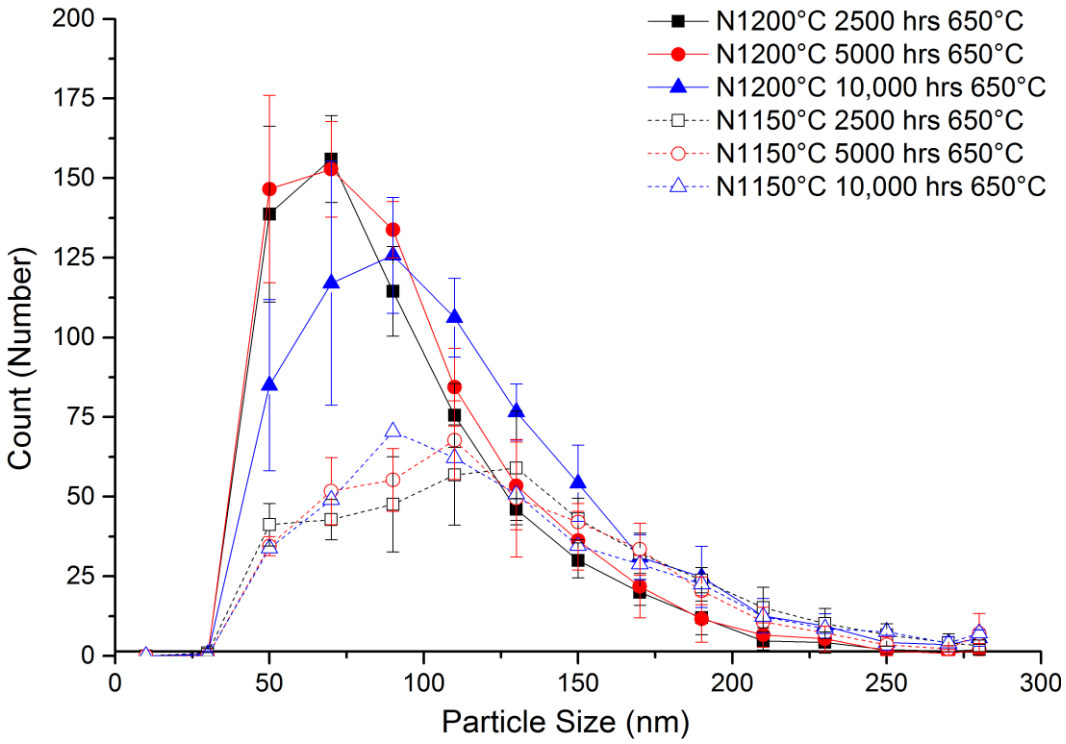

b)

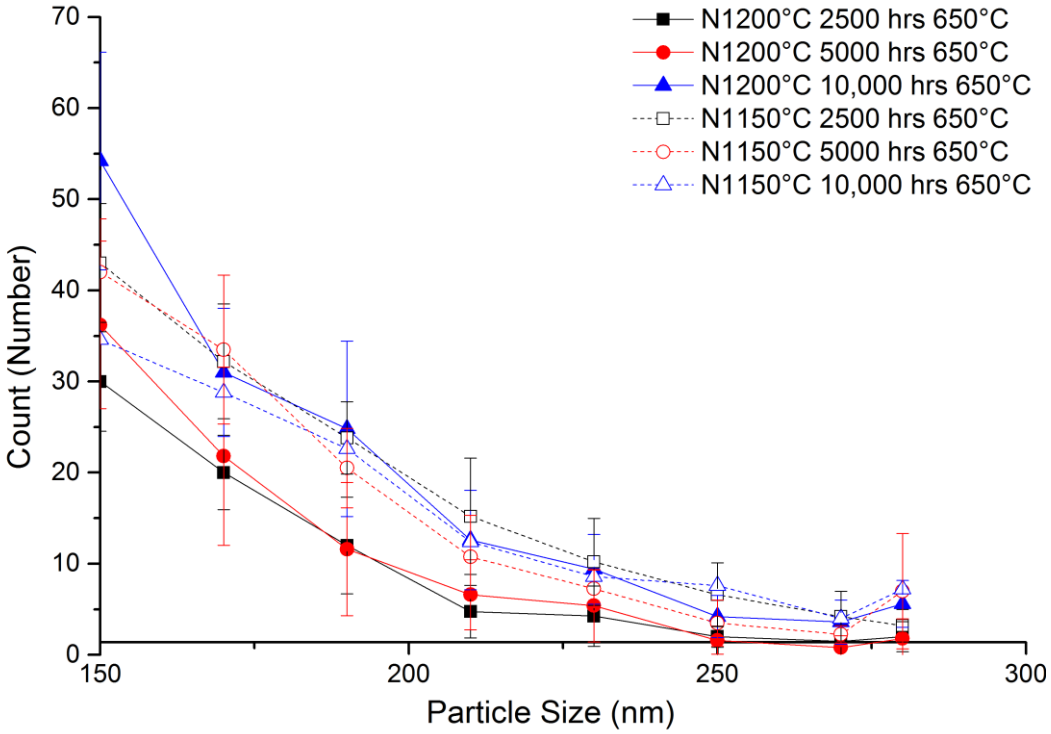

Figure 7.5: A graph showing the size distribution of $M_{23}C_6$ particles present in GAM 3 after normalising at 1150°C and 1200°C. The samples were subsequently tempered at 780°C and aged at 650°C for various durations, a) shows the distribution of particles between 0 nm to 300 nm whereas b) shows the distribution between 150 nm to 300 nm.

7.5.2 Long Term Stability of Laves Phase

Laves phase is an intermetallic compound with a chemical composition of either Fe_2W or Fe_2Mo. This phase has been reported in the literature to have a detrimental effect on the creep properties of 9 wt. % chromium power plant steels. Section 2.4.2 reviewed the current literature on Laves phase.

Laves phase has been reported to be precipitated in 9 wt. % chromium steels after long term exposure at the service temperature. This is also true for MarBN alloys in which Laves phase has been observed to be present in GAM 3 after 2,500 hours at 675°C. Quantification of Laves phase has been carried out after long term ageing at 675°C, after both of the two pre-service normalising heat treatments at 1150°C and 1200°C.

Thermodynamic calculations were carried out to assess if the pre service heat treatment may have an effect on the type of phases predicted to be present and their subsequent amount. Two calculations were carried out using the composition of GAM 3. The first calculation carried out used the actual composition of GAM3. The second calculation used the composition of GAM 3 with a modified nitrogen content of 20 ppm. The second calculation was carried out to try and simulate the effect of boron nitride precipitated within the microstructure. The calculations are shown in Figure 7.6 a) and b).

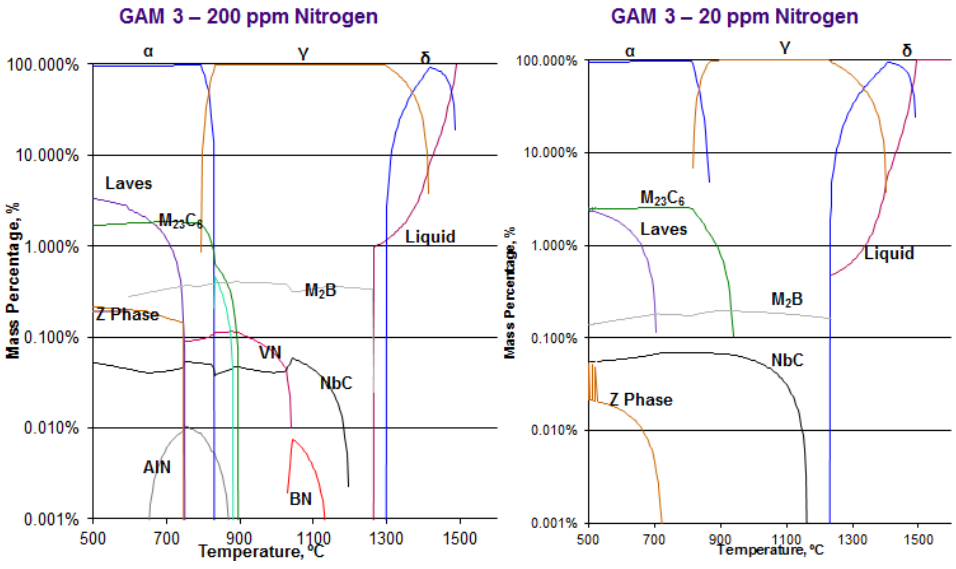

Figure 7.6: Thermodynamic calculations using the bulk composition of GAM 3; calculations were carried out using two nitrogen contents a) 200 ppm and b) 20 ppm.

The thermodynamic calculations carried out under equilibrium conditions have shown that increasing the nitrogen content increases the mass percentage of Laves phase predicted to be

present. Calculations that were performed using a nitrogen content of 200 ppm found that Laves phase was predicted to have a maximum mass percentage of 3.2% and was predicted to be present until 747°C, whereas calculations that were performed using a nitrogen content of 20 ppm were found to have a maximum mass percentage of 2.4% and Laves phase was predicted to be present until 697°C. The thermodynamic calculations indicate therefore that when boron nitride is present the mass percentage of Laves phase will be lower than when boron is in solution at equilibrium.

Figure 7.7 shows a series of images produced using a backscatter detector after ageing at 675°C after two different pre-service normalising heat treatments of 1150°C and 1200°C. Examination of the images shows that the precipitates are present on the grain and sub grain boundaries. Quantification of Laves phase has been carried out with the use of image analysis software.

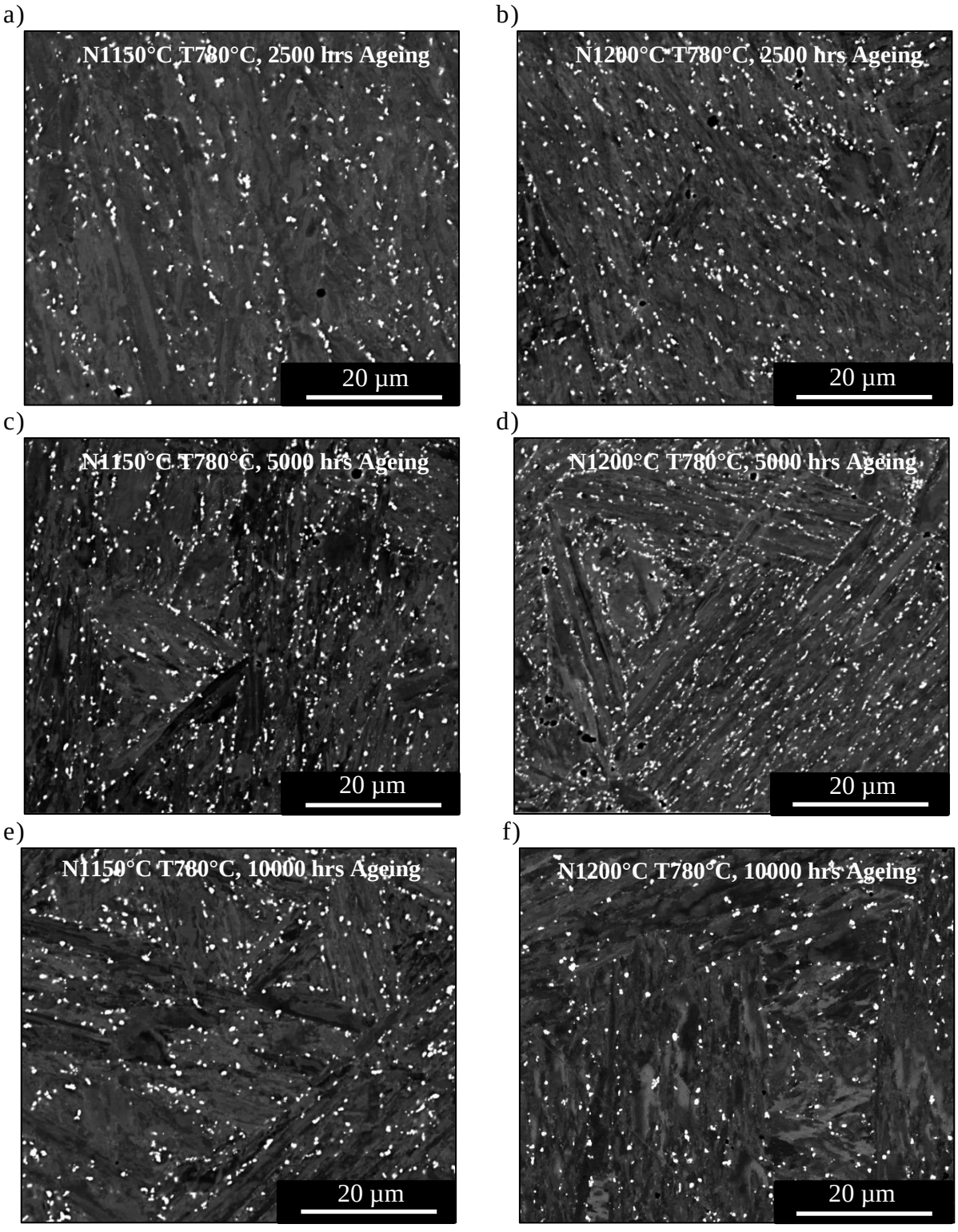

Figure 7.7: A series of micrographs produced using a backscatter detector in the SEM. The micrographs were produced after normalising at 1150°C and 1200°C and the samples were all tempered at 780°C. The samples were aged at 650°C for between 2500 – 10,000 hours. a) N1150°C 2500 hours, b) N1200°C 2500 hours, c) N1150°C 5000 hours, d) N1200°C 5000 hours, e) N1150°C 10,000 hours, f) N1200°C 10,000 hours.

The average particle diameter of the Laves phase has been observed to be slightly larger in the samples which received the pre-service normalising heat treatment at 1200°C, in

comparison to the samples which were heat treated at 1150°C. The total number of Laves phase particles per 849 μm² has been quantified and shows that the samples normalised at 1150°C have a higher number density, in comparison to those normalised at 1200°C, as shown in Figure 7.9.

Figure 7.10 shows the distribution of Laves phase as a function of ageing and the pre service normalising heat treatment. The diagram clearly shows that by increasing the pre-service normalising heat treatment temperature the number of smaller precipitates present increases after ageing for less than 5,000 hours. The increase in the number of smaller precipitates was observed to decrease to a similar level to those samples normalised at 1150°C, after 10,000 hours ageing. The distribution of particles was found to change as a function of ageing duration for both pre service normalising heat treatments. As the ageing duration increased the number of smaller particles decreased whilst the number of larger particles increased.

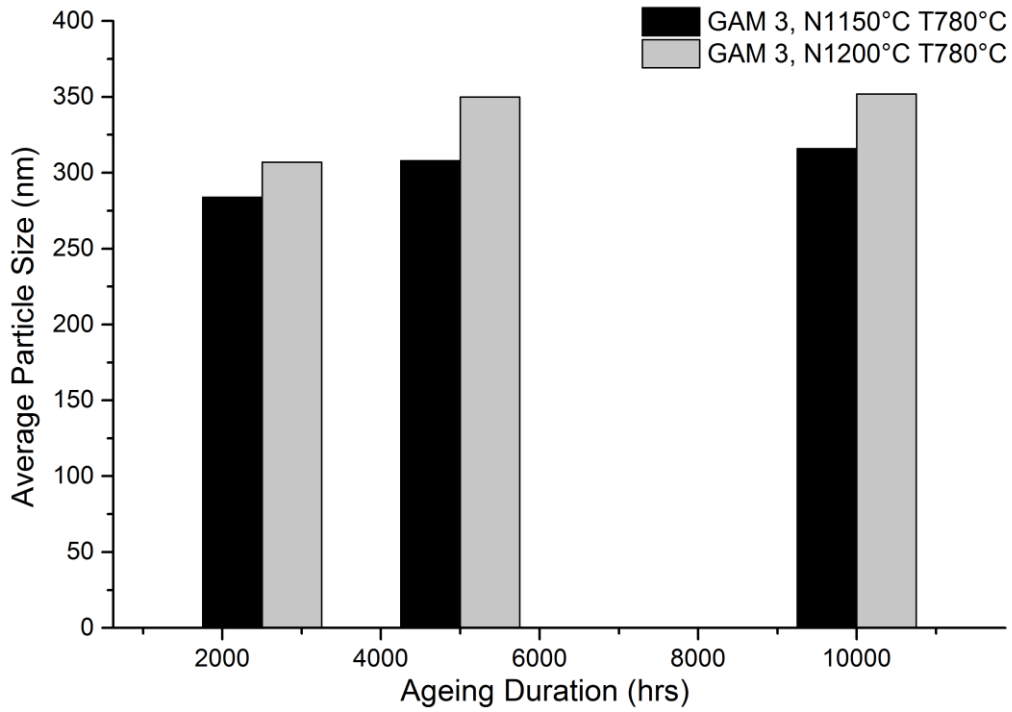

Figure 7.8: A graph showing the average diameter of Laves phase precipitates after ageing at 675°C for between 2500 – 10,000 hours. The samples were normalised at two different temperatures 1150°C (Black) and 1200°C (Red), and subsequently tempered at 780°C.

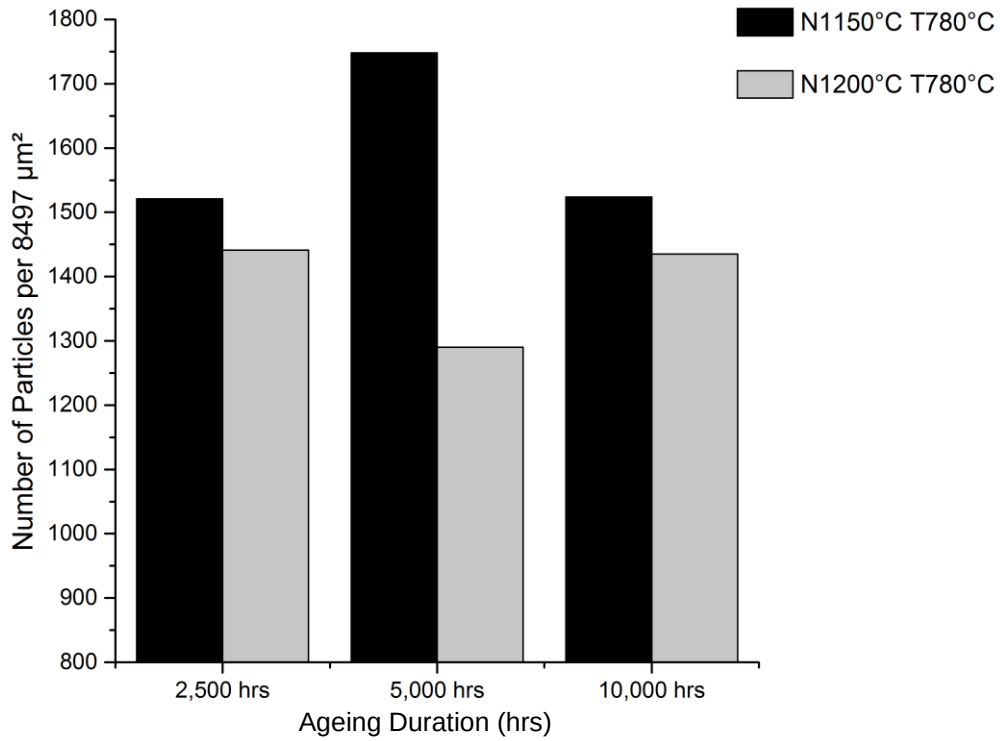

Figure 7.9: A graph showing the total number of Laves phase precipitates observed to be present per 8497 µm² after ageing at 675°C for between 2500 – 10,000 hours. The samples were normalised at two different temperatures 1150°C (Black) and 1200°C (Red), and subsequently tempered at 780°C.

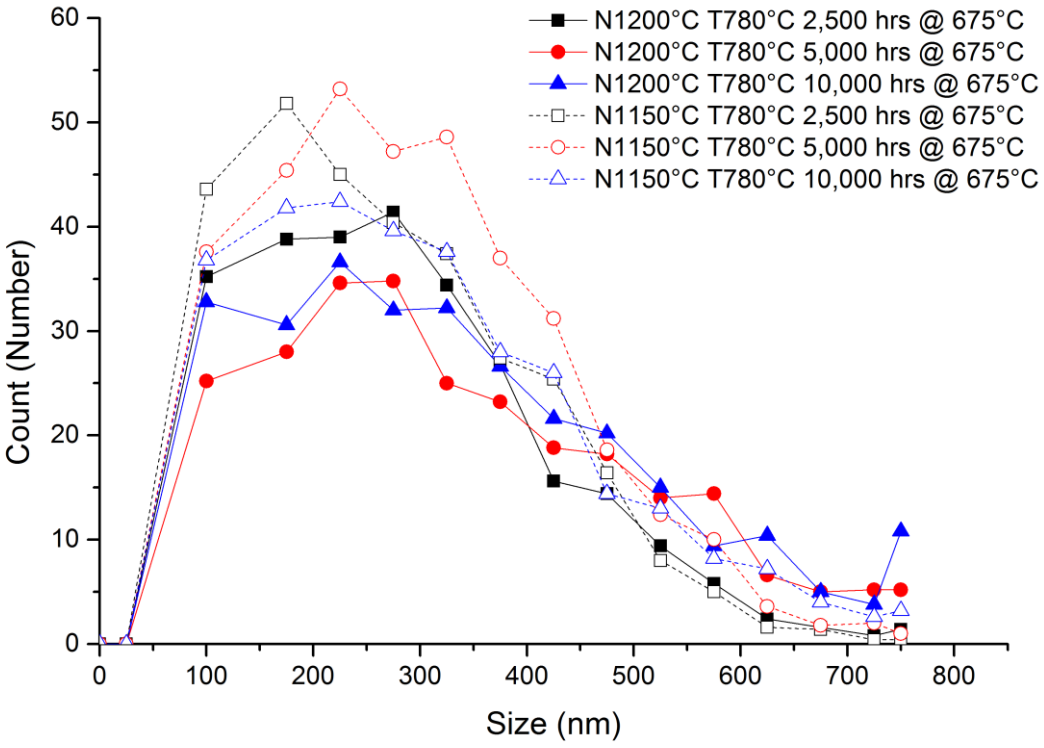

Figure 7.10: A graph showing the size distribution of Laves phase precipitates present in GAM 3 after normalising at 1150°C and 1200°C. The samples were subsequently tempered at 780°C and aged at 675°C for between 2500 – 10,000 hours.

7.5.3 Microstructure Evolution of the Martensitic Matrix During Isothermal Ageing

Microstructural evolution in earlier 9 wt. % chromium steels such as P91 and P92 is extremely well documented. The fine martensitic matrix has been reported in P91 and P92 to transform into a ferritic matrix after long term ageing[19, 52]. The newly developed MarBN alloy is expected to have similar microstructural degradation because ferrite is thermodynamically stable within the ageing temperature range of 650°C to 675°C.

The microstructural evolution of the matrix after ageing has been characterised with the use of electron back scatter diffraction (EBSD). The samples characterised were normalised at both 1150°C and 1200°C and subsequently tempered at 780°C then aged at 675°C.

This technique has been used for a number of years to quantify the microstructural degradation in P91 and P92[69,73,74]. MarBN is a very different alloy because it has a very large prior austenite grain size due to the higher normalising temperature and the fact that much of this work originated in the cast material. It is vital to understand if this has an effect on the results obtained using this technique and if the results are consistent.

An initial study was carried out to determine the experimental parameters required to produce consistent EBSD results on MarBN. Particular attention was paid to the variance produced when a number of different prior austenite grains were analysed. In addition to this, the variance between scans within the same prior austenite grain was also investigated. This has enabled the accuracy of the results to be determined and allows the results to be interpreted with confidence.

During the first part of this study, an EBSD map with the dimensions of 5 mm x 4 mm was collected with a large step size of 0.4 microns to identify the location of the prior austenite boundaries, as shown in Figure 7.11. Five grains were selected for analysis; two scans were carried out per grain with a scan dimension of 200 µm x 200 µm and a step size of 0.15 µm. The grain boundaries were classified using their associated mis-orientation angle. The boundaries were defined into high angle boundaries and low angle boundaries. High angle boundaries were defined as those with a mis-orientation greater than 15°; these boundaries represent the prior austenite and martensite lath boundaries. Low angle boundaries were defined as those with a mis-orientation angle of between 2° - 15°; these boundaries represent the substructure dislocations.

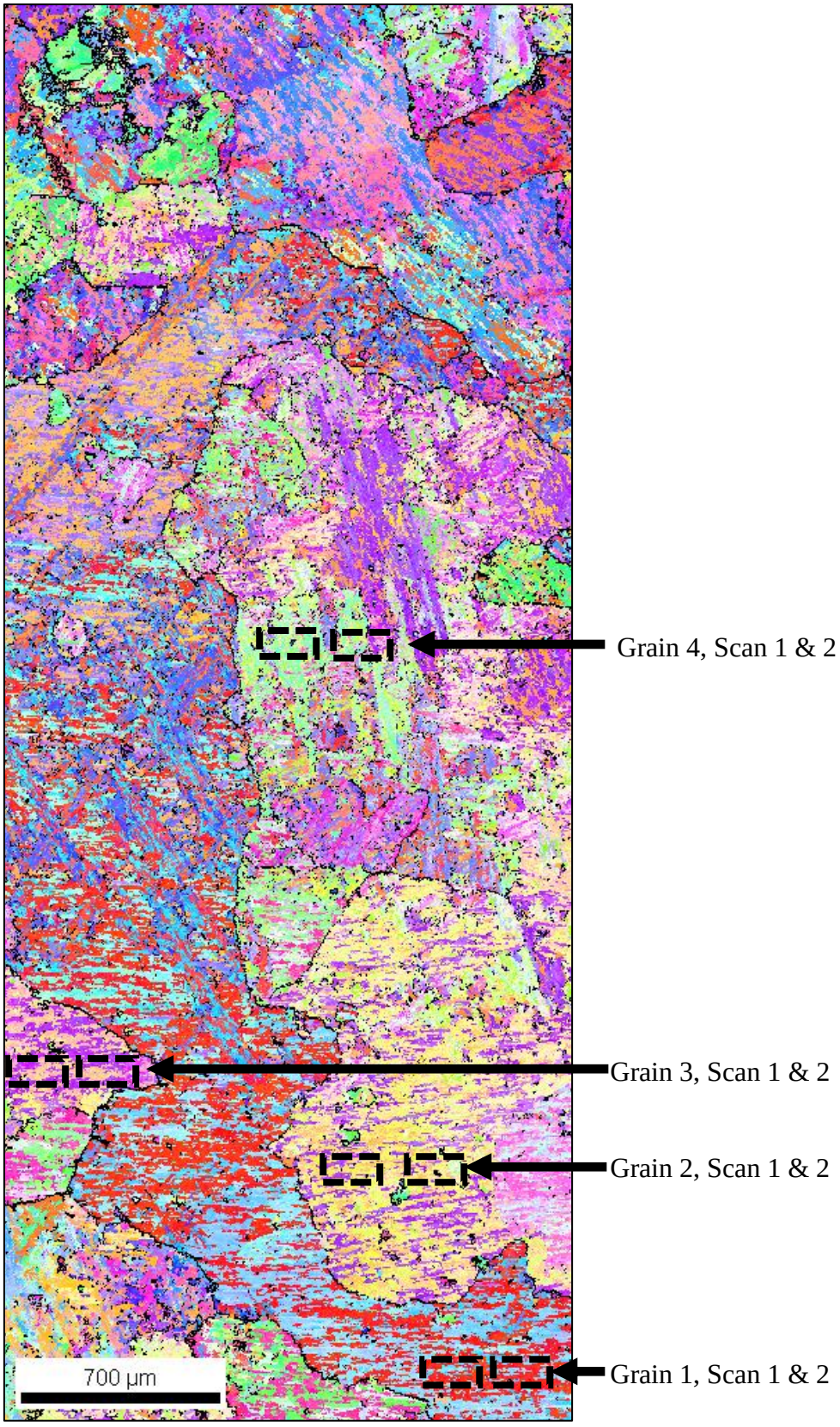

Figure 7.11: An EBSD derived inverse pole figure map of GAM 3 after normalising at 1150°C and tempering at 780°C. The boundaries with a mis-orientation angle between 15° - 40° are shown by the black line. The scan was acquired using a step size of 0.4 µm.

Figure 7.11 also shows the locations of the specific scans carried out within each grain. The total grain boundary length has been plotted as a function of grain number as shown in Figure 7.12. The error bars show the variance between the two scans within the same grain; this variance is approximately 5% and is deemed within the tolerance of this technique. In contrast the variation between the different prior austenite grains is significantly higher. The percentage error for the boundaries with a mis-orientation in excess of 15° was quantified as 18%, as shown in Table 7.1.

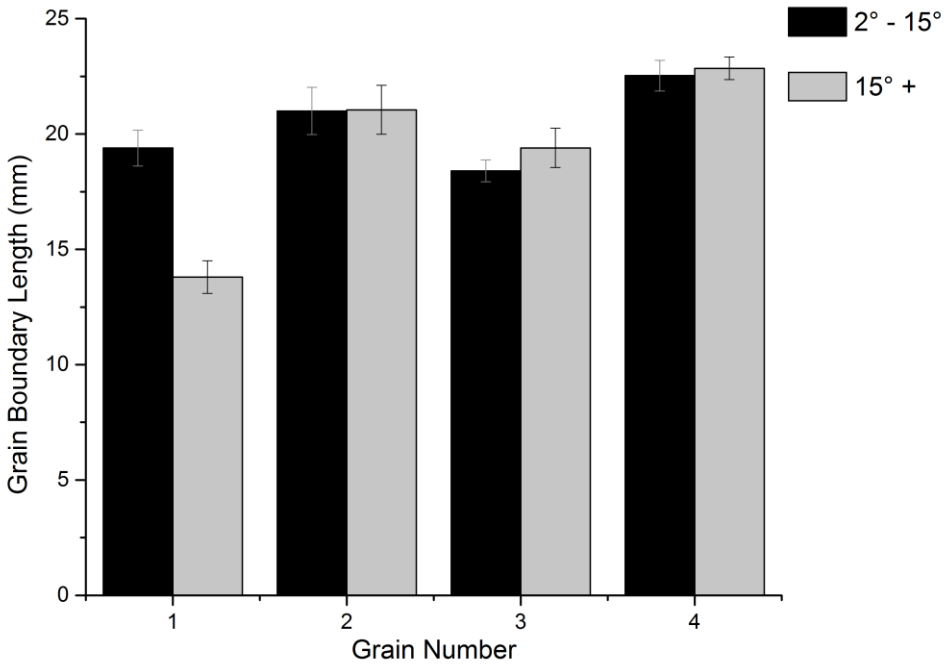

Figure 7.12: A graph of the grain boundary length of two types of mis-orientation angles quantified with the use of EBSD. The two mis-orientation angles quantified were between 2° - 15° and >15°. The analysis was carried out on GAM 3 normalised at 1150C and tempered at 780°C, five individual grains were analysed, the error bars show the variation between the two areas analysed within the same grain.

Table 7.1: The average grain boundary length, between two mis-orientation angles of 2° - 15° and > 15° and shows the associated errors.

	2° - 15°	**15° +**
Average	20.4 mm	19.5 mm
Standard Deviation	1.6 mm	3.4 mm
Percentage Error	7.8%	17.6%

Unfortunately there is no practical way of reducing the error using this particular technique. Therefore it is important to understand that small changes in the microstructural degradation may be difficult to quantify accurately using EBSD.

Figure 7.13 shows the grain boundary maps for the samples normalised at 1150°C and 1200°C, after normalising and tempering and subsequent ageing up to 10,000 hours. The maps show that there is a very small change in the microstructure after 10,000 hours ageing and both microstructures remain fully martensitic.

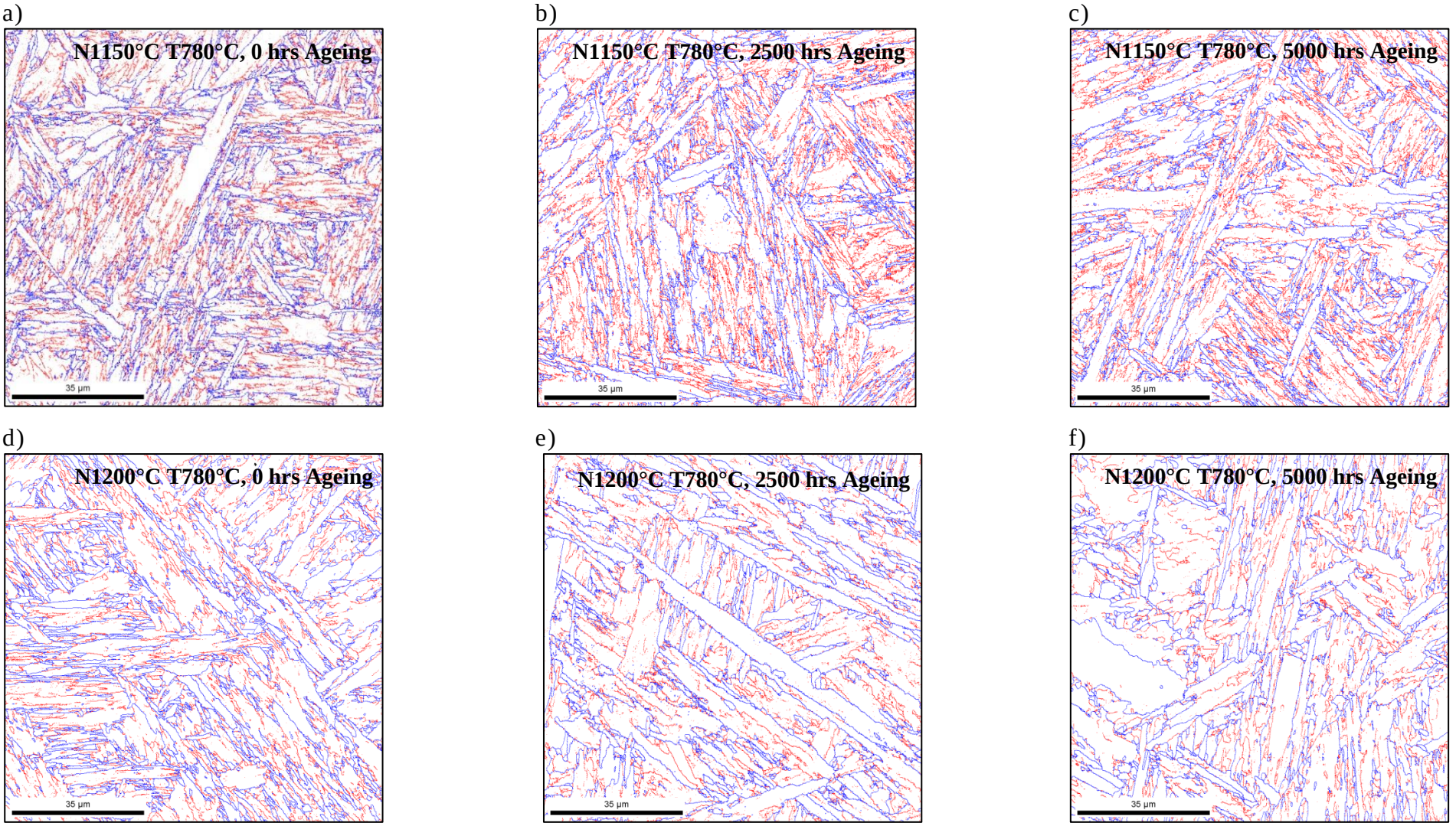

Figure 7.13: A series of grain boundary maps obtained using EBSD. The maps were produced from GAM 3 after N1150°C T780°C, and the samples were aged at 675°C for between 0 – 10,000 hours. The boundaries with a mis-orientation between 2° - 15° are shown in red and those with a mis-orientation above 15° are shown in blue. a) N1150°C 0 hrs, b) N1150°C 2500 hrs, c) N1150°C 5000 hrs, d) N1200°C 0 hrs, e) N1200°C 2500 hrs, f) N1200°C 5,000 hrs.

Quantification of the mis-orientation maps has been carried out. The total length of grain boundaries has been quantified, as a function of normalising temperature and ageing duration, as shown in Figure 7.14. Figure 7.14 shows there is a gradual decrease in the total length of grain boundaries as a function of ageing after normalising at 1150°C and 1200°C. The results have also been plotted in terms of a ratio between the length of the high and low mis-orientation angles, as shown in Figure 7.15. The results show some fluctuation and there is no clear trend. Due to the error involved in acquiring EBSD on this particular MarBN alloy as previously discussed it is deemed impossible to accurately interpret the results because they are all within the range of ±20%. However, it can be concluded that the difference in normalising temperature between 1150°C and 1200°C does not appear to have a significant influence on the recovery on the martensitic matrix.

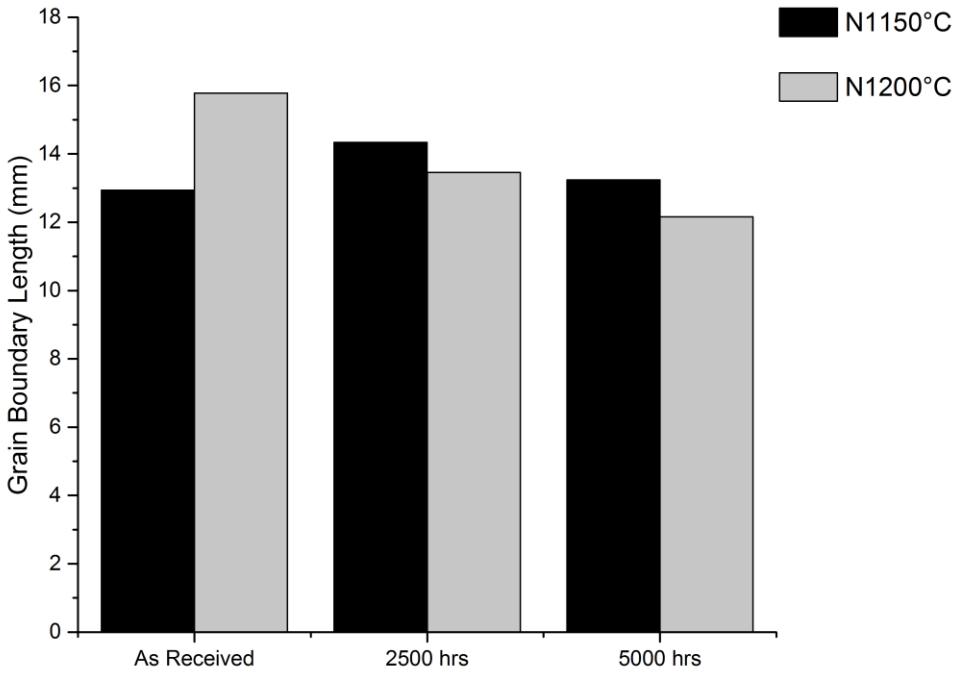

Figure 7.14: A graph showing the total grain boundary length of GAM 3 when normalised at 1150°C and 1200°C. The samples were isothermally aged at 650°C for between 2,500 – 5,000 hours.

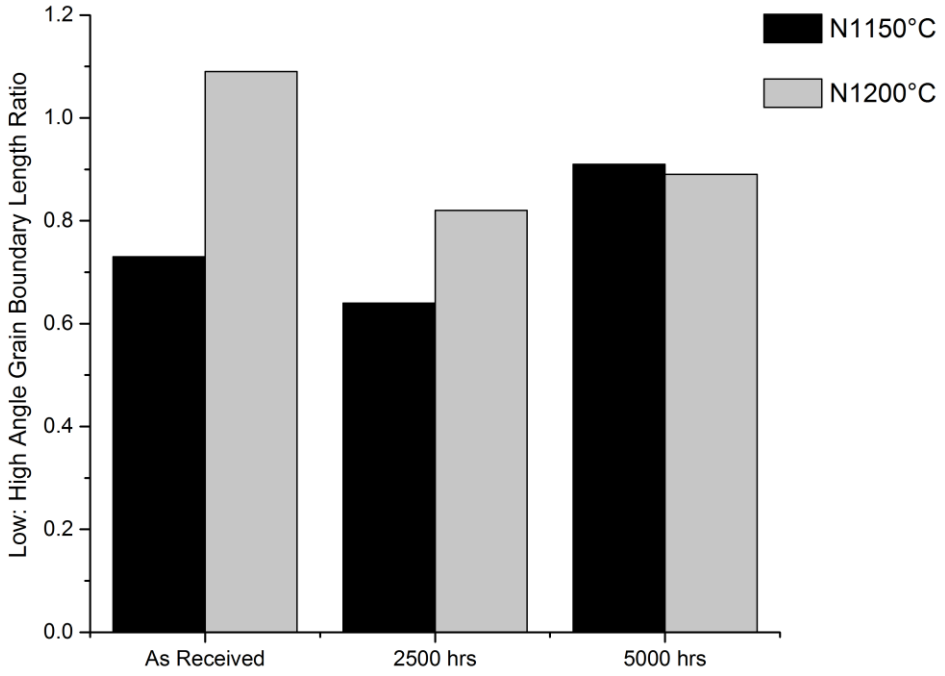

Figure 7.15: A graph showing the ratio between angles with a mis-orientation between 2° - 15°, and boundaries is a mis-orientation > 15°. The analysis was carried out on GAM 3 after normalising at 1150°C and 1200° when aged for between 2,500 – 5,000 hours.

7.5.4 Effect of Long Term Ageing on the Precipitation of Boron Containing Phases

The results from Chapter six have shown that a higher normalising heat treatment of 1200°C can be used to dissolve boron nitride. This pre-service normalising heat treatment has been observed to have a significant effect on the precipitation and evolution of $M_{23}C_6$ and, to some extent, Laves phase. The current theory of utilising the boron addition is that the element reduces the coarsening rate of the $M_{23}C_6$ carbides because the element is located at the interface near the $M_{23}C_6$ particles and is therefore able to prevent the coarsening of the carbides by occupying free vacancies.

It is therefore vital to understand if during long term ageing, boron is subsequently removed from solution and is precipitated out within a phase, such as boron nitride or tungsten boride. GAM 3 has been characterised after two pre-service normalising heat treatments 1150°C and 1200°C after ageing at 675°C for 10,000 hours. EDX mapping has been utilised to identify if any boron containing phases were precipitated as a function of ageing.

Boron Nitride

It is evident from analysing the boron and nitrogen EDX maps obtained from the samples normalised at 1150°C that there is a significant number of boron nitrides present in the

normalised and tempered condition as shown in Figure 7.16 a) – c). Figure 7.16 g) – i) also shows EDX maps after ageing for 10,000 hours at 675°C. The maps show that there is no indication that boron nitride precipitates as a function of ageing.

Samples were also examined after a pre-service normalising heat treatment at 1200°C. Very few boron nitride particles were observed to be present in the normalised and tempered condition as shown in Figure 7.17 a) – c). There is again no evidence to suggest that boron nitride precipitates as a function of isothermal ageing, as shown in Figure 7.17 d) – i).

Boron nitride is predicted to be present using thermodynamic calculations between 1030 - 1130°C. Therefore, the experimental findings are in line with the thermodynamic calculations.

Tungsten Borides

Tungsten boride (M_2B) was predicted to be present using thermodynamic calculations between 610°C – 1255°C under equilibrium conditions. The experimental findings were observed to be different from the thermodynamic calculations. In the as-cast condition M_2B was found to be widely present, however, after normalising only a few residual particles were found to remain. The stability of this precipitate at the service temperature is the main concern as this could have a detrimental effect on the long term properties of a MarBN alloy.

EDX maps were acquired from multiple areas to investigate if M_2B precipitates during long term isothermal ageing. Figure 7.17 a) – i), show the maps for boron, nitrogen and tungsten. In the normalised and tempered condition there is evidence to suggest the majority of the boron it associated with nitrogen and there is only a small number of W_2B particles present in normalised and tempered condition. After ageing at 675°C Laves phase is precipitated which has a high tungsten content. The boron maps do not show any areas of high concentration as a function of isothermal ageing and therefore this indicates that M_2B does not appear to precipitate as a function of ageing up to 10,000 hours, when examined using EDX maps with a field of view of 194 µm x 143 µm.

The thermodynamic predictions for the M_2B phase do not appear to be completely accurate. The isothermal heat treatments carried out for 10,000 hours may not have reached the equilibrium state and therefore the possibility that M_2B may precipitate after very long exposure in a similar manner to Z-phase cannot be excluded.

a)

Boron

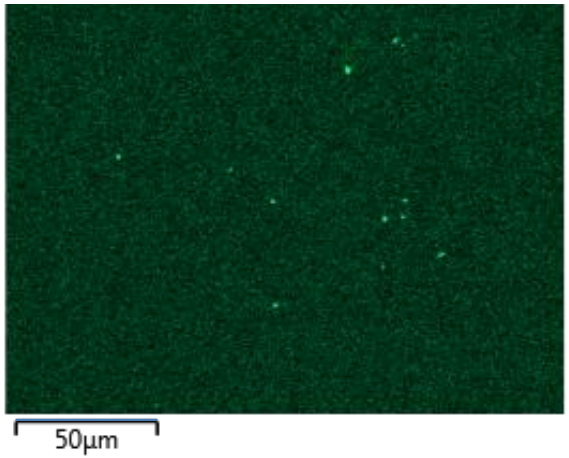

b)

Nitrogen

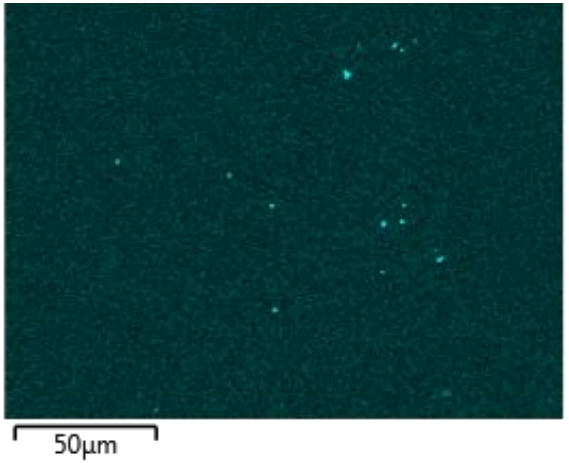

c)

Tungsten

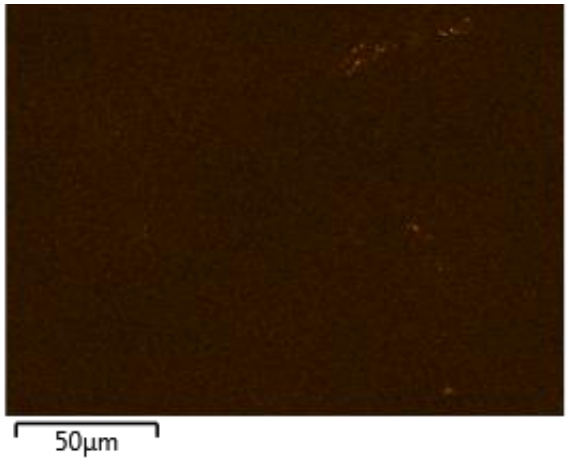

d)

Boron

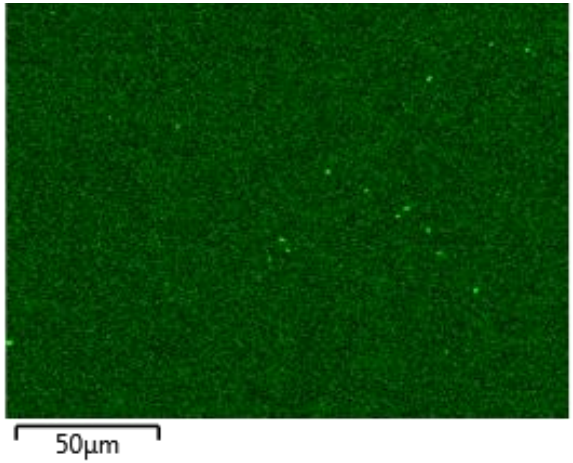

e)

Nitrogen

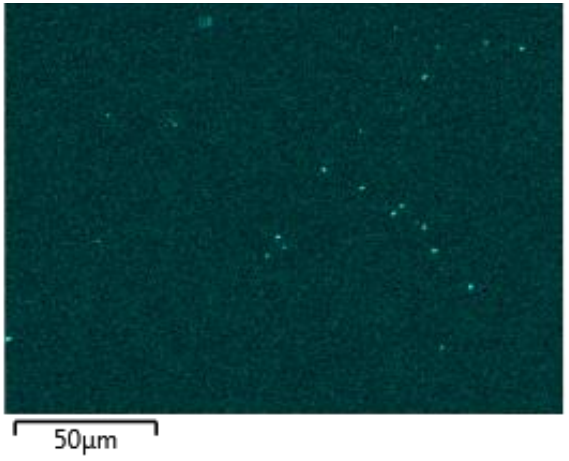

f)

Tungsten

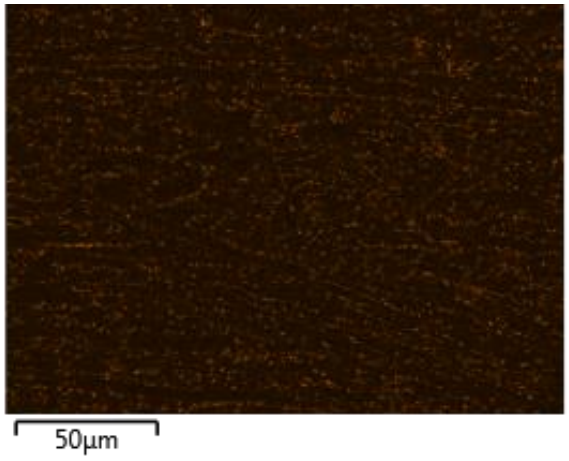

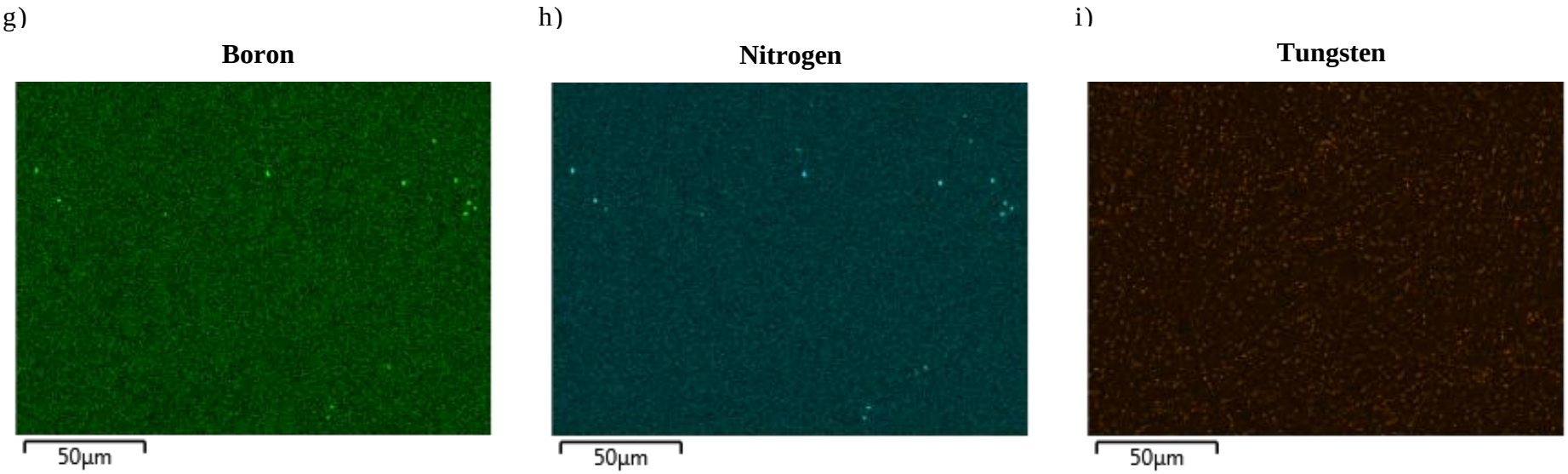

Figure 7.16: EDS maps of GAM 3 after N1150°C T780°C heat treatment, the samples were aged for a) – c) 0 hours, d) – f) 2,500 hrs, g) – i) 5,000 hrs. The figures show the individual elemental maps for boron, nitrogen and tungsten respectively.

a)

Boron

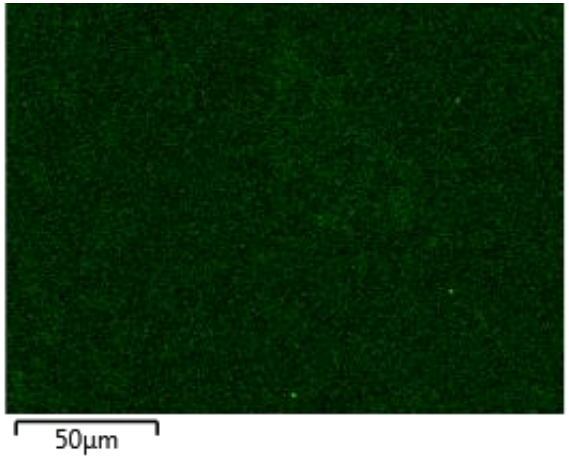

b)

Nitrogen

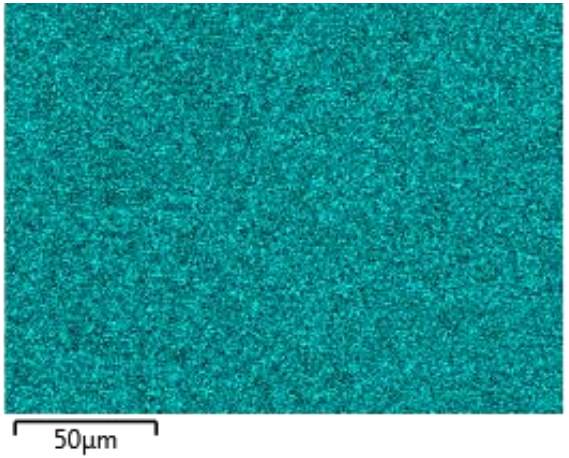

c)

Tungsten

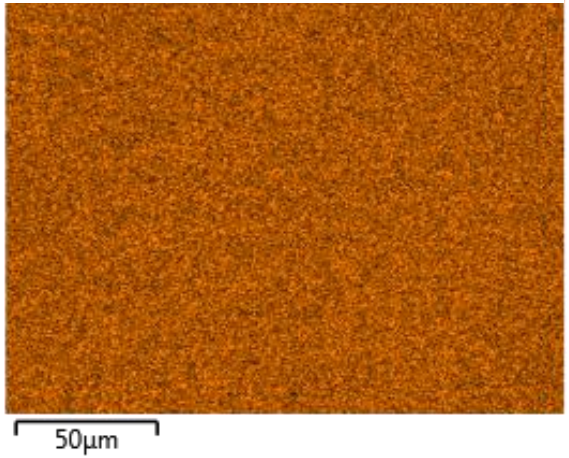

d)

Boron

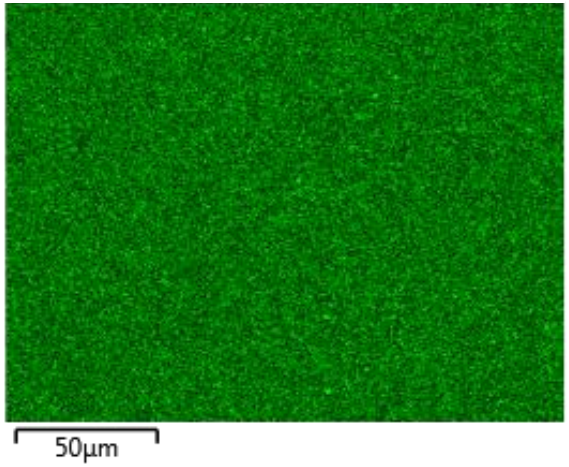

e)

Nitrogen

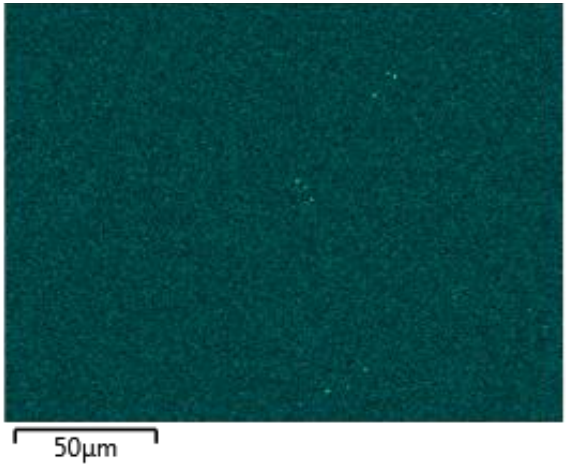

f)

Tungsten

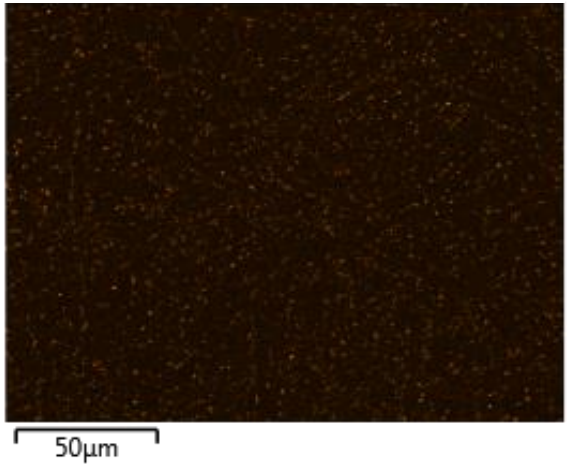

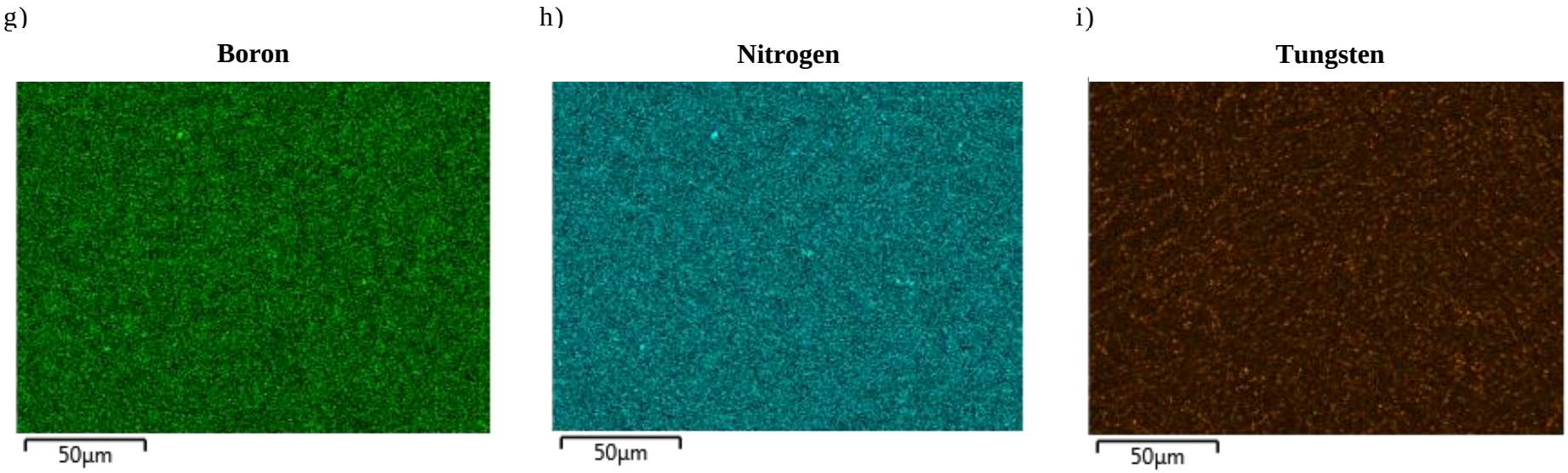

Figure 7.17: EDS maps of GAM 3 after N1200°C T780°C heat treatment, the samples were aged for a) – c) 0 hours, d) – f) 2,500 hrs, g) – i) 5,000 hrs. The figures show the individual elemental maps for boron, nitrogen and tungsten respectively.

7.6 Analysis of Mechanical Properties

Figure 7.18 shows the effect of long term ageing at 650°C on the hardness of GAM 3, after two pre-service normalising heat treatments at 1150°C and 1200°C. The results show that in the normalised and tempered condition, the samples normalised at 1150°C and tempered at 780°C are approximately 11 HV harder than those normalised at 1200°C. The difference in hardness is thought to be related to the change in the number density and size of both the $M_{23}C_6$ and carbonitrides within the microstructure. After normalising at 1200ºC there was an increase in the number density of finer $M_{23}C_6$ precipitates. The type of carbonitride precipitate also changes from niobium carbide to vanadium nitride and niobium carbide at the higher normalising temperature and this is likely to contribute to the change in the hardness. After 2,500 hrs there is still a significant difference in the hardness of 8 HV, which is thought to be related to the change in the MX and $M_{23}C_6$ precipitates.

Between 5,000 and 10,000 hours a significant decrease in the hardness of both conditions has been observed. This is thought to be related to the significant precipitation of Laves phase which has resulted in a loss in solid solution strengthening. There is also likely to be some recovery of the dislocation structure, which has contributed to the decrease in hardness.

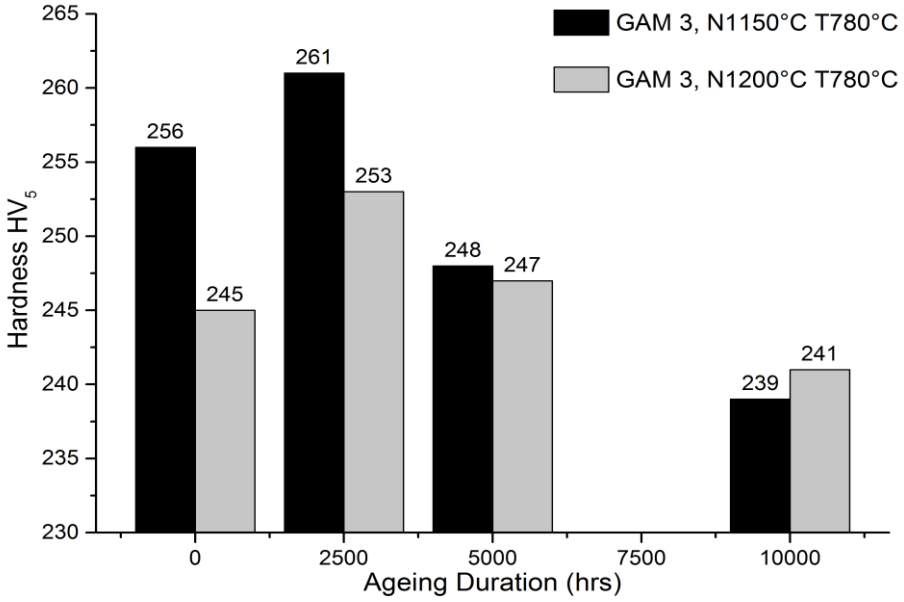

Figure 7.18: A graph showing the hardness of GAM 3 as a function of ageing at 650°C for between 0 – 10,000 hours. The samples were normalised at 1150°C and 1200°C.

Short term creep tests were carried out on the 8 tonne melt, in conjunction with a number of different normalising and tempering heat treatment parameters. The creep tests were carried out at a test temperature of 675°C. The standard temperature used for creep testing 9 wt. %

chromium steels is 650ºC. The IMPACT consortium increased the creep test temperature by 25ºC. This justification was based on results from microstructural characterisation of the precipitates within the microstructure from isothermal heat treatment trials up to 5,000 hours on GAM 2. The results have shown that coarser $M_{23}C_6$ carbides were found after 2,500 hours and 5,000 hours in the condition aged at 675ºC, as shown in Figure 7.19. Furthermore ageing at 675°C was found to accelerate the formation of coarser Laves phase precipitates within the microstructure as shown in Figure 7.19.

In addition, the short term creep tests were carried out at three stresses ranging from 142 – 114 MPa. The stresses chosen are high in comparison to other long term creep test programmes carried out on 9 wt. % chromium steels. This was another method which was utilised to accelerate the degradation of the microstructure and ultimately reduce the time to rupture.

Figure 7.20 shows the creep properties of the short term tests carried out (<3000 hours). It is very clear that the heat treatment parameters have a significant effect on the time to rupture. Changing the heat treatment from N1150°C T780°C to N1200°C T710°C was found to approximately double the time to failure.

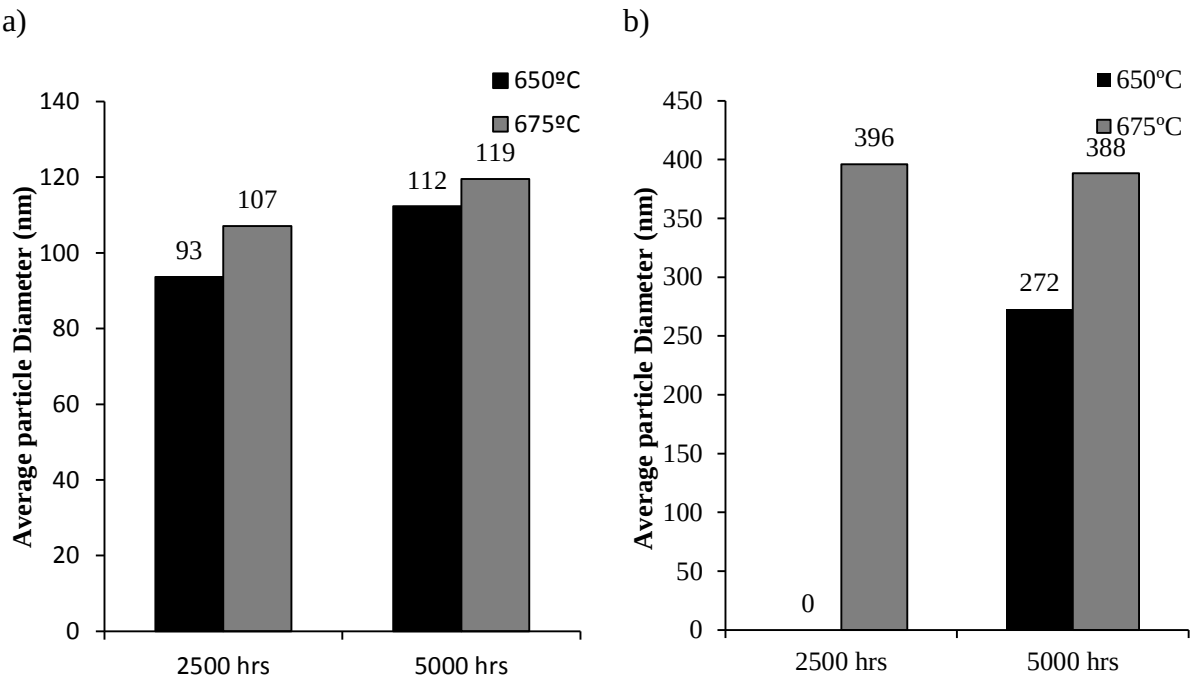

Figure 7.19: A graph illustrating the effect of isothermal ageing up to 5000 hours at two temperatures, 650°C and 675°C on GAM 2 and the resulting average size of a) $M_{23}C_6$ and b) Laves phase.

Increasing the normalising temperature from 1150°C to 1200°C has been shown to increase the number density of $M_{23}C_6$ precipitates and also results in the precipitation vanadium nitride rather than niobium carbide. This has been found to increase the time to rupture significantly. However normalising at 1200°C and tempering at 710°C has been observed to have the 'optimum' properties in the short term, this is thought to be related to the increased precipitation of $M_{23}C_6$ and the possible precipitation of M_2X at the lower tempering temperature.

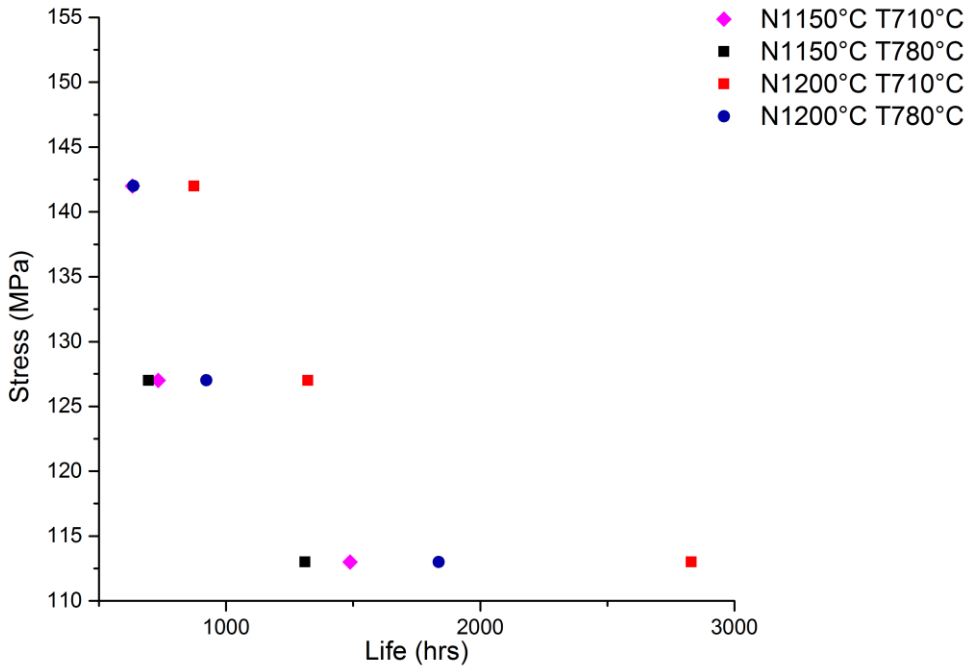

Figure 7.20: A graph showing the short term creep results, giving the time to rupture in hours versus stress in MPa. The creep tests were carried out at a temperature of 675ºC on the 8 tonne melt in conjunction with a number of different normalising and tempering heat treatments.

Figure 7.20 shows a visual representation of the short term creep properties carried out on the 8 tonne melt, in which the results are shown as the time to rupture in hours versus the stress which the test was carried out at. The figure highlights that this particular MarBN alloy has significantly higher creep properties when normalised at 1200°C, the creep properties were observed to improve further by tempering the alloy at 710°C in comparison to the standard temperature of 780°C.

7.7 Summary

The alloys characterised within this chapter were GAM 3 and the 8 tonne melt. Long term isothermal ageing heat treatments were carried out at 650°C and 675°C for up to 10,000 hours, in conjunction with a number of different normalising and tempering heat treatments.

Microstructural characterisation was carried out on GAM 3 to study the evolution of the minor phases and the degradation of the microstructure. Mechanical creep tests were carried out on the 8 tonne melt for a number of different normalising and tempering heat treatments.

The $M_{23}C_6$ precipitates were analysed with the use of image analysis software to identify the size, number and distribution of precipitates, as a function of isothermal ageing. The number density of precipitates was observed to be significantly higher after normalising at 1200°C in comparison to 1150°C. After 10,000 hours ageing the relative difference between the number density of precipitates was found to remain present. The size of the precipitates has been observed to change as a function of isothermal ageing, and it has been observed that there are a high number of coarser precipitates when normalised at a lower temperature of 1150°C.

The effect of the pre-service normalising heat treatment on the precipitation of Laves phase after isothermal heat treatments has been studied. The results have shown that the precipitates were found to be marginally smaller after a normalising heat treatment at 1150°C in comparison to those carried out at 1200°C. In contrast the number of particles per 8497 μm^2 was found to be significantly lower in the samples normalised at 1200°C in comparison to those normalised at 1150°C.

It is vital to understand if during long term ageing if boron is removed from solution and is subsequently precipitated out within a phase, such as boron nitride or tungsten boride. EDX maps have been analysed for boron, nitrogen and tungsten after normalising at 1150°C and 1200°C. The samples were subsequently tempered at 780°C followed by isothermal ageing for 10,000 hours. Boron nitride was observed to be present in the 1150°C normalised and tempered condition. There was no increase in the amount of boron nitride after ageing for 10,000 hours. After normalising at 1200°C there were no boron nitride particles or tungsten borides observed to be precipitated as a function of ageing.

The hardness has been measured as a function of ageing and normalising heat treatment. In the short term heat treatments the samples normalised at a lower temperature of 1150°C were found to be harder than those normalised at 1200°C. However, after an isothermal heat

treatment greater than 5,000 hours the difference between the hardness of the two pre service normalising heat treatments was found to decrease significantly. A gradual decrease in hardness was observed to be present as a function of ageing duration for both pre service normalising heat treatments.

Short term creep tests were carried out on the 8 tonne melt, in conjunction with a number of different normalising and tempering heat treatment parameters. The creep tests were carried out at a test temperature of 675°C, at three stresses ranging from 142 – 114 MPa. Figure 7.24 shows the creep properties of the short term tests carried out. It is very clear that the heat treatment parameters can have a significant affect on the time to rupture. The heat treatment parameters that provided the highest strength were normalising at 1200°C for two hours followed by tempering at 710°C for three hours. The short term creep properties have shown that, depending on the heat treatment, the properties can be improved between 124 – 142% of the strength of P92. This is a very significant result and indicates a potential success in designing and optimising the cast MarBN material.

Chapter 8

THE EFFECT OF COBALT ON THE EVOLUTION OF THE MICROSTRUCTURE IN MarBN

8.1 Introduction

A detailed exploration of the use of cobalt within 9 – 12 wt. % chromium steels to improve the creep properties has not been carried out on a commercial scale. The latest two commercial 9 wt. % chromium steels, T/P91 and T/P92 have not been reported to have an addition of cobalt [21], where "T" denotes Tube and "P" denotes Pipe. The latest 9 wt. % chromium steel developed, known as MarBN, initially developed by NIMS, has a cobalt addition of between 2.5 – 3 wt.% [22].

A research study has been carried out by Helis *et al.* [29] using a 9Cr - 3W - 0/5Co - 0.2V - 0.05Nb - 0.08C - 0.05N steel series to understand the effect of the cobalt addition on the initial pre-service microstructure. This research study has reported that as the cobalt addition is increased, there is a significant increase in the precipitation of $M_{23}C_6$ and MX. The study also confirmed that as the cobalt content is increased, the Ms temperature also increased. Increasing the Ms temperature resulted in less residual austenite after a normalising heat treatment, because the cobalt addition suppressed the delta ferrite formation temperature[29].

A detailed study was carried out by Li *et al.* [69] who investigated the effect of the cobalt addition on the microstructure of a 9 wt. % chromium steel, known as P92. The study investigated the effect of a change of 2 wt. % cobalt on the precipitates present within the microstructure after a pre-service heat treatment and also after isothermal ageing for 5,000 hours. The study was reported to be carried out on a P92 base and showed that an increase in the cobalt addition could have a significant effect on the precipitation of $M_{23}C_6$. The study also reported that cobalt had no significant effect on the precipitation and evolution of Laves phase.

To date all the results presented in literature investigating the effect of a cobalt addition have not been carried out on a MarBN base. It is important to understand if the cobalt addition has a similar effect on a MarBN alloy as the work reported within literature by Helis *et al.* [29] and Li *et al.* [69] on a P92 alloy base. Cobalt is one of the most expensive alloying additions in a 9 wt. % chromium steel and therefore it is essential to determine if it has a beneficial effect on

the long term creep properties of the alloy. An investigation has been carried out to identify if a small change in the cobalt content (0.4 wt. %) can have an effect on the initial precipitation and evolution of phases within the microstructure. Investigating a small change in the cobalt content will help enhance the understanding of MarBN alloys, with particular emphasis on understanding the effect that the cobalt content at the minimum or maximum of the alloy's specification has on the resulting microstructure. This information is vital in order to produce a standard specification for producing this alloy on a commercial scale.

In summary, this chapter will present the characterisation of the effect of a change of 0.4 wt. % cobalt on the precipitates present in the normalised and tempered condition. In addition the effect of isothermal ageing for up to 18,000 hrs on the evolution of the precipitates and the degradation of the martensitic matrix will also be investigated as a function of cobalt content.

8.2 Materials

In this chapter two 9 wt. % chromium steels were characterised which had different additions of cobalt, as shown in

Table 8.1. Two MarBN alloys were characterised, GAM 2 and GAM 3. The two alloys had a variation of 0.4 wt. % cobalt and 80 ppm boron. The influence of the difference in boron concentration will also need to be considered as part of this research. To provide simplification for the reader the alloys have been denoted as 'GAM 2 – HiCo' and 'GAM 3 – LoCo' throughout this chapter of the thesis.

The materials examined were in the cast condition and were subjected to a normalising heat treatment of 1150ºC for 2 hours, followed by tempering at 780ºC for three hours. The alloys were also examined after isothermal ageing after 5,000 hours, 10,000 hours and 18,000 hours. The isothermal heat treatments were carried out at 650°C and 675°C.

Table 8.1: Chemical composition of GAM 2 and GAM 3 steels manufactured by Goodwin Steel Castings, Weight %, balance Fe.

	C	**Si**	**Mn**	**P**	**S**	**Cr**	**Mo**	**Ni**	**Al**
GAM 2 - HiCo	0.09	0.31	0.46	0.007	0.007	8.70	<0.01	0.06	0.01
GAM 3 - LoCo	0.09	0.46	0.54	0.007	0.006	8.65	<0.01	0.06	0.02

	As	**B (ppm)**	**Co**	**Cu**	**Nb**	**Sn**	**V**	**W**	**N (ppm)**
GAM 2 - HiCo	<0.01	100	3.18	0.01	0.06	<0.01	0.22	2.51	200
GAM 3 - LoCo	<0.01	180	2.84	0.01	0.06	<0.01	0.22	2.49	200

8.3 Thermodynamic Calculations

Thermodynamic calculations have been carried out to predict the phases present at thermodynamic equilibrium in both GAM 2 - HiCo and GAM 3 - LoCo. Both alloys were predicted to have a ferritic matrix in addition to ~2% of $M_{23}C_6$ carbides (chromium rich), which were predicted to be stable between a temperature range of 500°C to 750°C. Two types of MX carbonitrides were predicted, niobium carbide and vanadium nitride. Niobium carbide was predicted to be stable between a temperature range of 500°C to 1200°C, with an approximate mass percentage of 0.07%. Vanadium nitride was predicted to be stable between 750°C to 1050°C, with an approximate mass percentage of 0.1%.

The addition of boron and nitrogen in MarBN has led to three boron containing phases predicted to be present, which are boron nitride, W_2B and Cr_2B. Boron nitride was predicted to be present between 1030ºC and 1140ºC and W_2B was predicted to be present between 500ºC and the liquid formation temperature. Cr_2B was predicted between 500°C and 600°C.

Figure 8.1 and 8.2 show the predicted phase diagrams for GAM 2 – HiCo and GAM 3 – LoCo respectively.

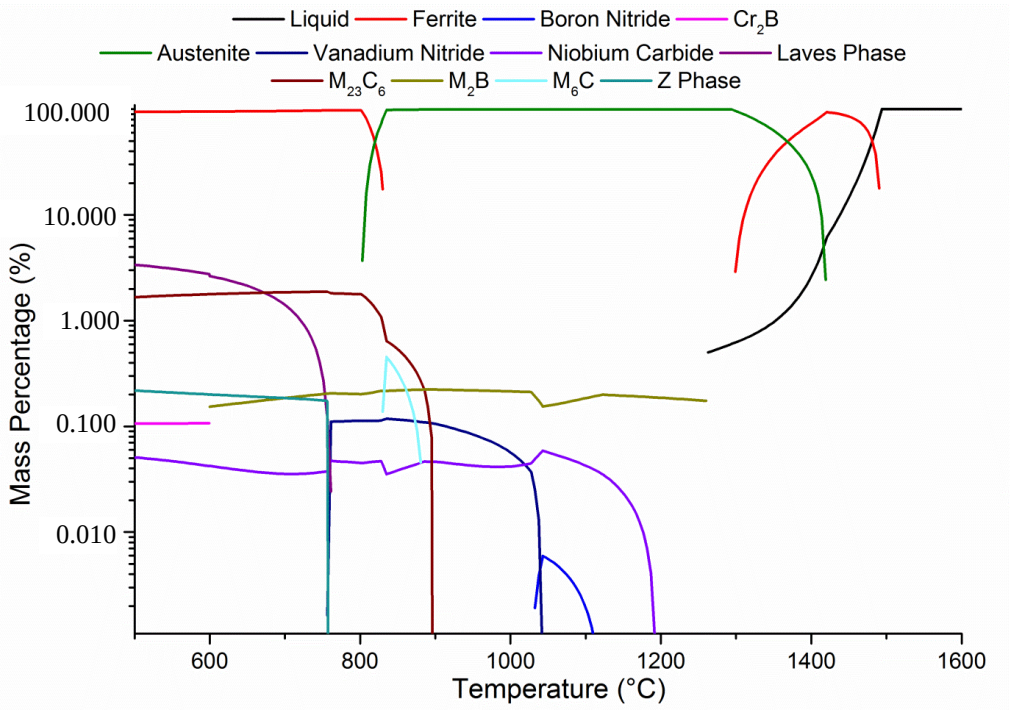

Figure 8.1: A phase diagram predicted under equilibrium conditions, indicating the phases predicted to be present as a function of temperature for GAM 2 – HiCo.

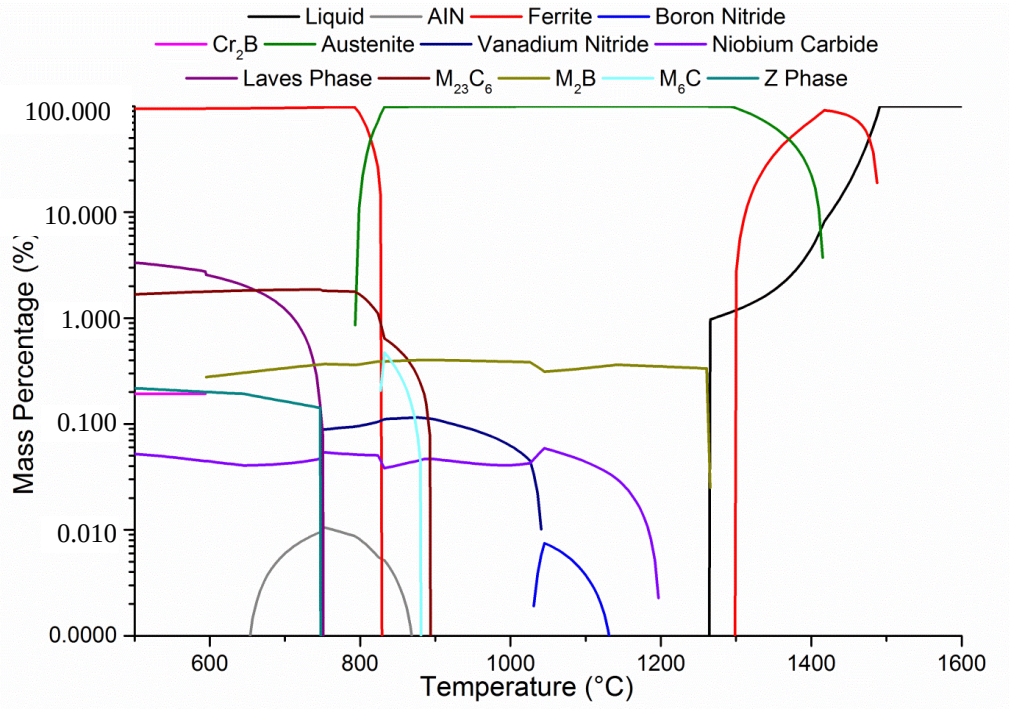

Figure 8.2: A phase diagram predicted under equilibrium conditions, indicating the phases predicted to be present as a function of temperature for GAM 3 – LoCo.

8.3.1 Specific Variations between the Thermodynamic Calculations for GAM 2 – HiCo and GAM 3 LoCo

There are a number of small differences between Figure 8.1 and 8.2. GAM 3 – LoCo has a boron content, which is 80 ppm higher than GAM 2 HiCo. This has led to a small variation in the stability and mass percentage of the boron containing phases predicted to be present. Due to the higher boron content of GAM 3 – LoCo, thermodynamic calculations have predicted a higher mass percentage of Cr_2B, W_2B and boron nitride. The phase stability range of boron nitride was predicted to increase by approximately 20°C in GAM 3 – LoCo. An increased mass percentage of Cr_2B and W_2B were predicted to be present in GAM 3 – LoCo due to the higher boron addition.

It was identified that there are no other key variations in the phase transformation temperatures or mass percentage of phases predicted to be present for GAM 2 – HiCo and GAM 3 LoCo, as shown in Table 8.2.

Table 8.2: Phase transformation temperatures determined using thermodynamic calculations, Temperatures in degrees celsius.

Material	**Ae_1**	**Ae_3**	**BN Range**	**$M_{23}C_6$ dissolution**	**Delta ferrite formation on heating**	**Liquid formation on heating**
GAM 2 'HiCo'	801°C	835°C	1032°C - 1107°C	900°C	1299°C	1263°C
GAM 3 'LoCo'	793°C	832°C	1031°C - 1140°C	898°C	1300°C	1265°C

Cobalt was predicted to be mainly distributed within alpha ferrite; a small amount was predicted to be distributed in M_6C, $M_{23}C_6$ and Laves phase. Within literature cobalt has been reported to have a significant effect on the delta ferrite temperature. The thermodynamic calculations performed using the composition of GAM 2 – HiCo and GAM 3 – LoCo does not show the same increase in the delta ferrite temperatures when there was only a small change in cobalt content.

8.3.2 Thermodynamic Sensitivity Study – Delta Ferrite

A sensitivity study was carried out using the chemical composition of GAM 2 - HiCo to fully understand the effect of the cobalt addition on the delta ferrite formation temperature. During the study a number of thermodynamic calculations were carried out in conjunction with the MarBN base of GAM 2 – HiCo in a systematic manner. The cobalt content was modified by ± 30% at the expense of iron. Figure 8.3 shows a summary of the results, which show the

effect of the cobalt content on the delta ferrite formation temperature. The results show that as the cobalt content is increased the delta ferrite formation temperature subsequently increases in a fairly linear manner.

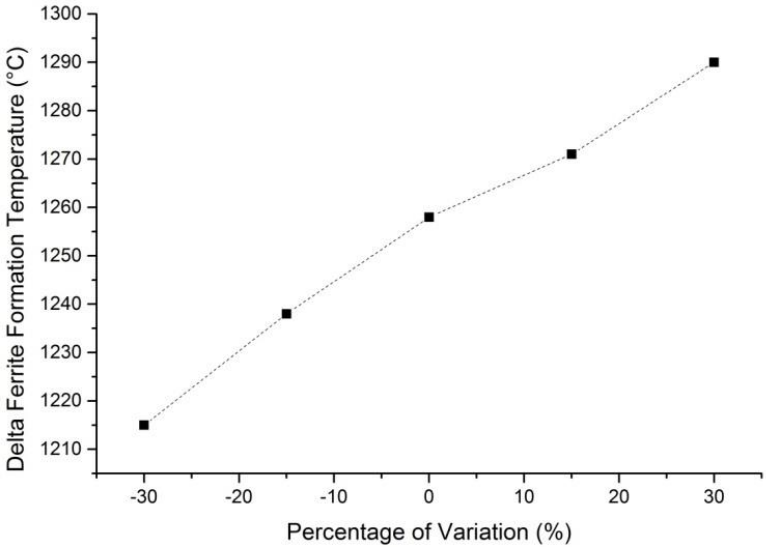

Figure 8.3: A graph showing the effect of cobalt addition on the delta ferrite formation temperature, predicted using thermodynamic calculations utilising the chemical composition of GAM 2 - HiCo.

8.4 The Effect of Cobalt on the Initial Microstructure

The microstructures of GAM 2 - HiCo and GAM 3 - LoCo in the normalised and tempered condition were observed to be fully martensitic, as shown in Figure 8.4. The hardness of the samples was found to be 275 HV_{10} and 256 HV_{10} respectively.

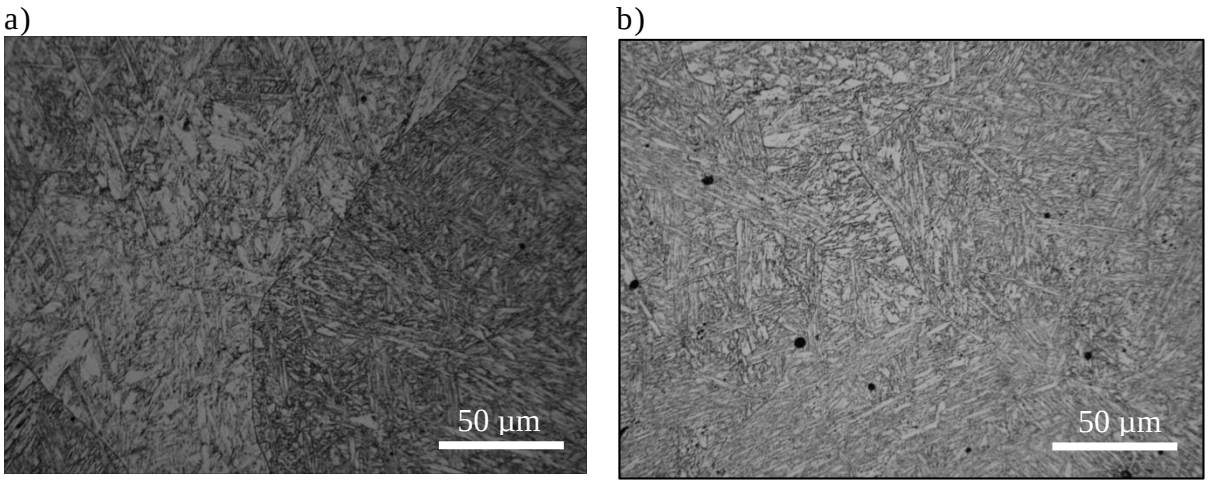

Figure 8.4: Two optical micrographs after normalising at 1150°C and tempering at 780°C for a) GAM 2 – HiCo and b) GAM 3 – LoCo.

An advanced silicon drift detector was used to identify the boron containing phases present within the microstructure. Boron nitride (BN) and tungsten boride (W_2B) were found to be present and are marked in Figure 8.5. EDS analysis was carried out on both types of particles and Figure 8.6 confirms that the particle is boron nitride. Figure 8.7 shows an EDS spectrum on a particle with a high contrast differential between the particle and the matrix. This provides further evidence that this type of particle is a tungsten boride.

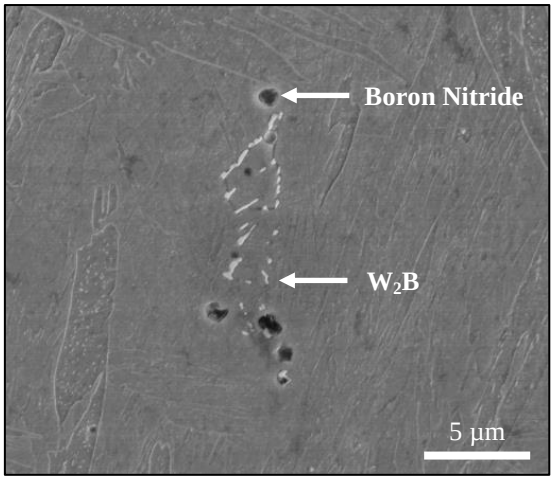

Figure 8.5: A backscatter electron micrograph of GAM 3 in the cast variant, showing boron nitride and W_2B. Both samples received a standard normalising and tempering heat treatment.

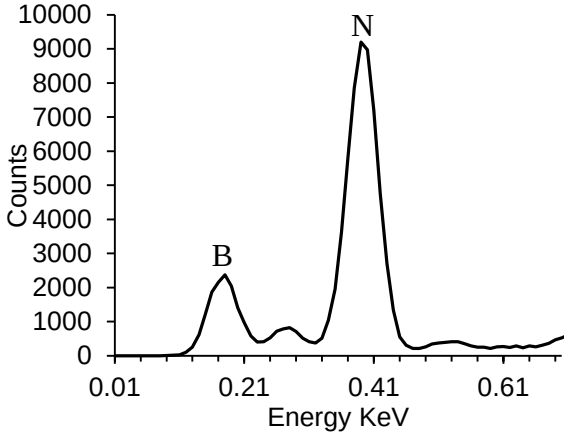

Figure 8.6: An EDS Spectrum of a boron nitride particle in the cast variant of GAM 3. The sample received a standard normalising and tempering heat treatment.

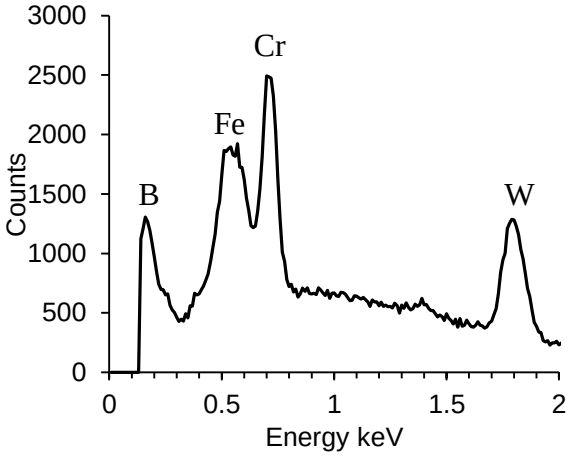

Figure 8.7: An EDS Spectrum of a W_2B particle in the cast variant of GAM 3. The sample received a standard normalising and tempering heat treatment.

Boron nitride was observed to be present in both GAM 2 - HiCo and GAM 3 - LoCo. It is therefore postulated that the change in the boron addition between the GAM 3 - HiCo and GAM 2 - LoCo of 80 ppm will not have a significant impact on the analysis within this

chapter. This assumption has been made because both alloys have widespread precipitation of boron nitride, removing boron from solution and therefore making less boron available to reduce the coarsening rate of the $M_{23}C_6$ carbides, as shown in Figure 8.8. Therefore it is postulated that when comparing GAM 2 - HiCo and GAM 3 - LoCo in the standard heat treated condition, the key difference can be thought of as the chemical composition change of 0.4 wt. % cobalt.

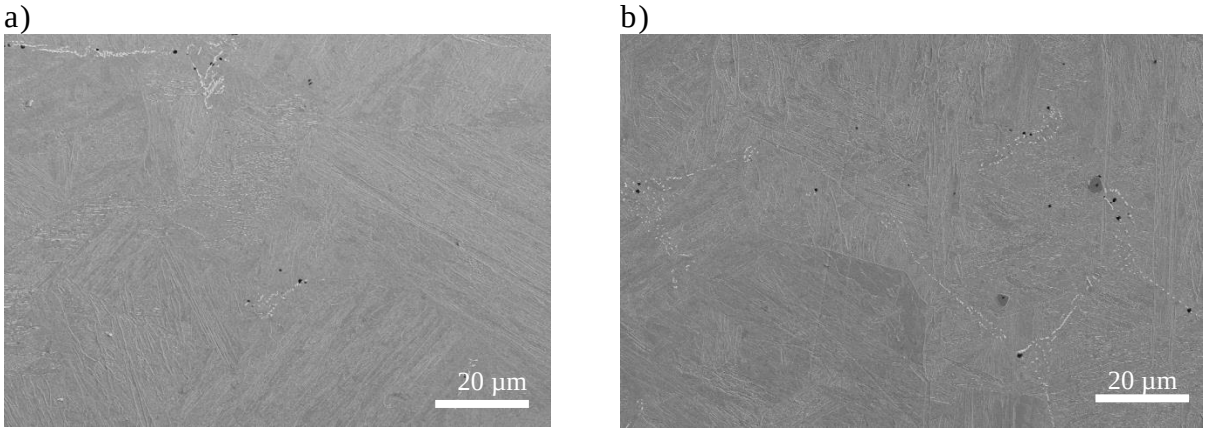

Figure 8.8: Two micrographs produced using a secondary electron detector, the images show the widespread presence of boron nitride after a standard normalising and tempering heat treatment (N1150°C T780°C) in a) GAM 2 – HiCo and b) GAM 3 – LoCo.

The effect of cobalt on the precipitation of $M_{23}C_6$ carbides has been studied in the normalised and tempered condition. Ion beam imaging was used as it provides an excellent opportunity to image and quantify the $M_{23}C_6$ precipitates within the alloy, whilst also allowing the opportunity to image the grain structure of the steel.

Examination of the images shown in Figure 8.9 a) and b) show that the carbides are precipitating on the martensite grain boundaries in GAM 2 - HiCo and GAM 3 - LoCo. The micrographs indicate the number of $M_{23}C_6$ precipitates is different in the normalised and tempered condition for GAM 2 – HiCo and GAM 3 - LoCo. Quantification of the $M_{23}C_6$ carbides has been carried out using the ion beam images and image analysis software. A series of five micrographs were analysed per sample condition analysing a total area of 1000 µm² and the size of each particle was analysed. The number density of $M_{23}C_6$ precipitates per micron² was found to be 3.4 and 2.6 for the GAM 2 - HiCo and GAM 3 - LoCo steels respectively. The average size of the $M_{23}C_6$ was found to be 95 µm and 102 µm for the GAM 2 - HiCo and GAM 3 - LoCo steels respectively.

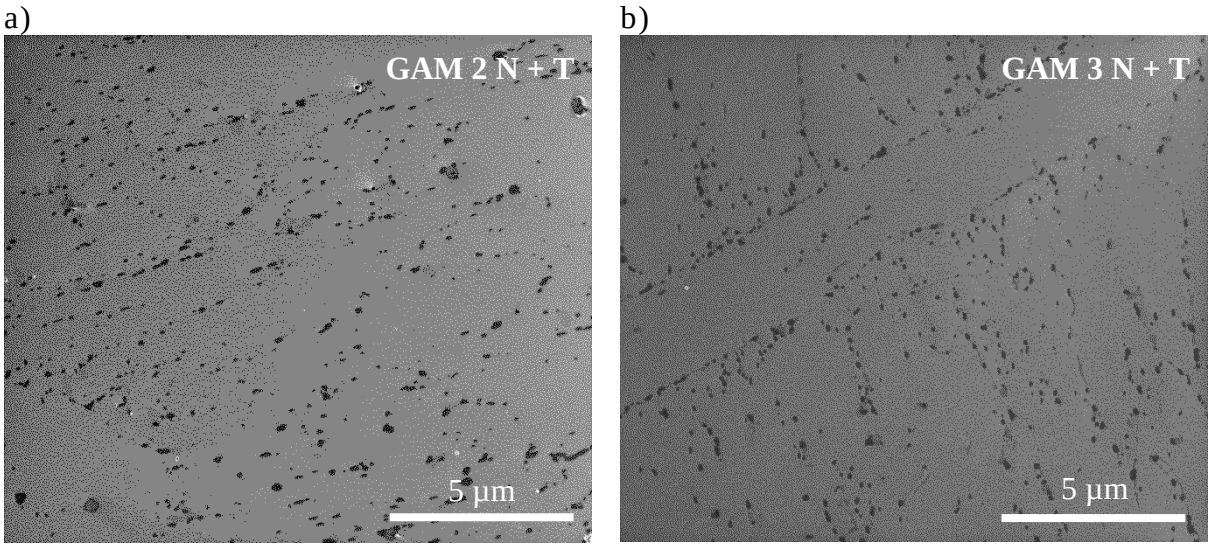

Figure 8.9: A series of micrographs produced using gallium ion beam imaging, a) and b) show the cast variants of GAM 2 - HiCo and GAM 3 - LoCo respectively in the normalised and tempered condition.

8.5 The Stability of $M_{23}C_6$ and Laves Phase as a function of Isothermal Ageing

The phase stability of $M_{23}C_6$ and Laves Phase were investigated as a function of isothermal ageing at two temperatures 650°C and 675°C, for up to 18,000 hours. Two types of samples were characterised, 'GAM 2 – HiCo' and 'GAM 3 – LoCo'. Extensive microstructural characterisation has been carried out to identify the size, number and particle size distribution of $M_{23}C_6$ and Laves Phase. The $M_{23}C_6$ precipitates were characterised after isothermal ageing at 650°C, to ensure that the results were consistent with those presented in Chapter 7. The characterisation was performed using a focussed ion beam; the ion beam was used to raster across the sample in order to produce ion beam images. A xenon difluoride gas etch was used to reduce the contrast of the matrix to allow the precipitates to be independently quantified. In comparison the characterisation of Laves phase was performed on the samples which were isothermally aged at 675°C; this characterisation was carried out using a backscatter detector.

8.5.1 Quantification of $M_{23}C_6$ as a Function of Isothermal Ageing

Detailed quantification of the $M_{23}C_6$ precipitates present after ageing between 0 to 18,000 hours at 650°C was carried in GAM 2 - HiCo and GAM 3 - LoCo. Figure 8.10 shows the evolution of $M_{23}C_6$ carbides for both alloys. After isothermal ageing up to 10,000 hours the average particle size was observed to increase in both GAM 2 – HiCo and GAM 3 – LoCo. GAM 2 – HiCo was observed to have a smaller average particle size after normalising and this difference between the two alloys was maintained during isothermal ageing, as shown in

Figure 8.11. After long term ageing between 10,000 – 18,000 hours the particle size was found to found to coarsen in both alloys, as shown in Figure 8.12.

The number density of carbides as a function of ageing has also been investigated. The number density of carbides was found to be significantly higher in GAM 2 – HiCo, between 0 – 10,000 hours isothermal ageing. After 18,000 hours isothermal ageing both alloys were found to have a similar number density of carbides present.

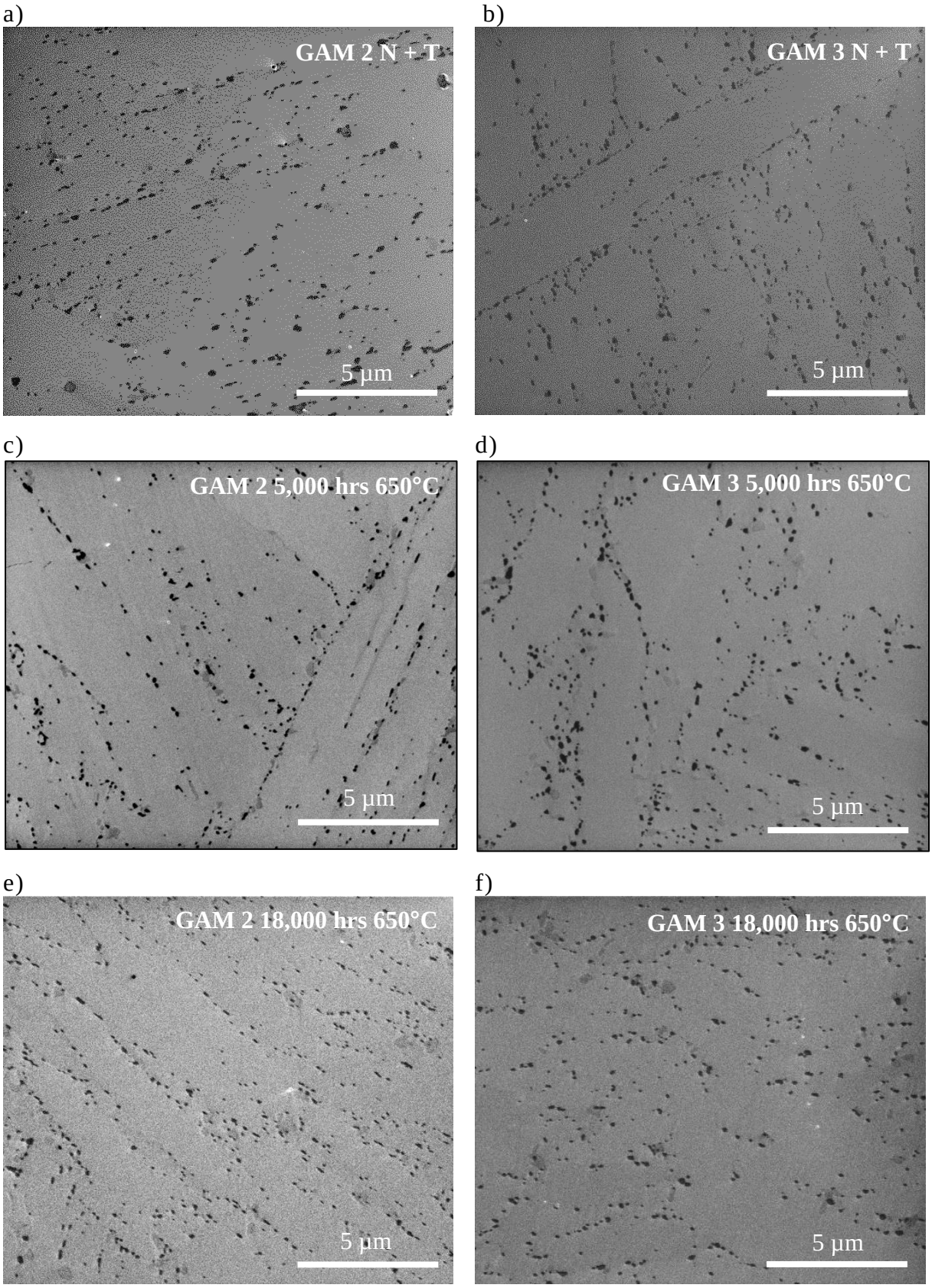

Figure 8.10: A series of micrographs produced using gallium ion beam imaging, a) and b) show the cast variants of GAM 2 and GAM 3 respectively in the normalised and tempered condition, c) and d) show the cast variants of GAM 2 and GAM 3 after 5,000 hours ageing at 650°C.

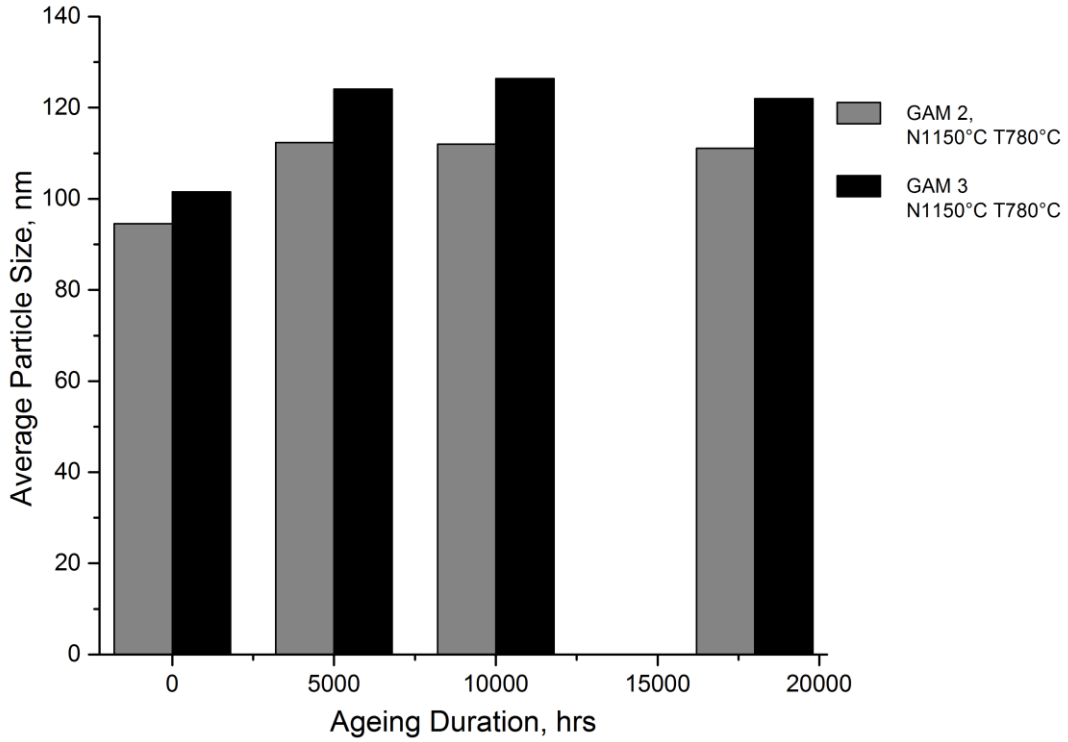

Figure 8.11: A graph showing the average particle diameter of the $M_{23}C_6$ preciptates in the normalised and tempered condition and aged condition for GAM 2 and GAM 3.

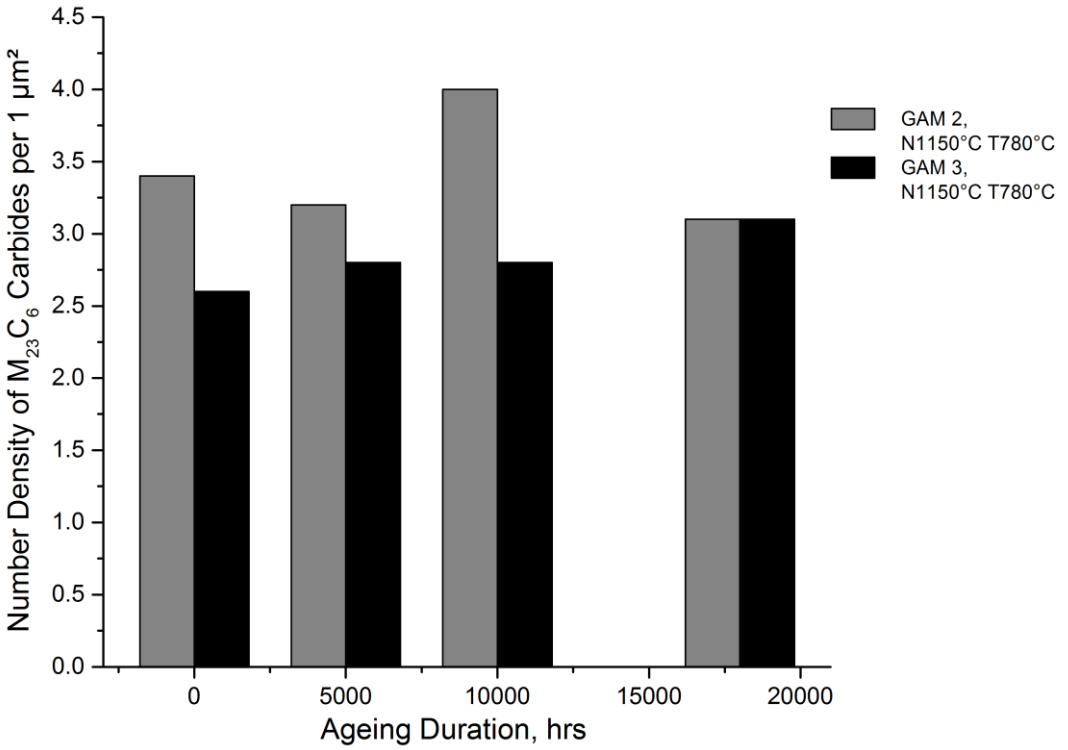

Figure 8.12: A graph showing the number density of $M_{23}C_6$ preciptates in the normalised and tempered condition and aged condition for GAM 2 and GAM 3.

To summarise, in MarBN a small change of 0.4 wt. % cobalt has been observed to have a significant effect on the number of $M_{23}C_6$ precipitates precipitated and their associated size. GAM 2 – HiCo was found to aid the precipitation of smaller $M_{23}C_6$ precipitates after a pre-service normalising and tempering heat treatment. The higher cobalt content was also found to aid the precipitation of $M_{23}C_6$ after short term ageing (2500 hours) at 650°C. The increased precipitation in GAM 2 – HiCo was maintained until approximately 10,000 hours as shown in Figure 8.13. However after long term ageing (~18,000 hours) the beneficial effect of the cobalt addition was reduced, the total number of carbides and average particle size was reduced significantly in to a similar quantity and size in GAM 3 – LoCo. This therefore indicates that the cobalt addition aids the precipitation of $M_{23}C_6$ in the short term; however the element does not prevent the coarsening of the carbides in the long term and therefore its long term benefit is minimal.

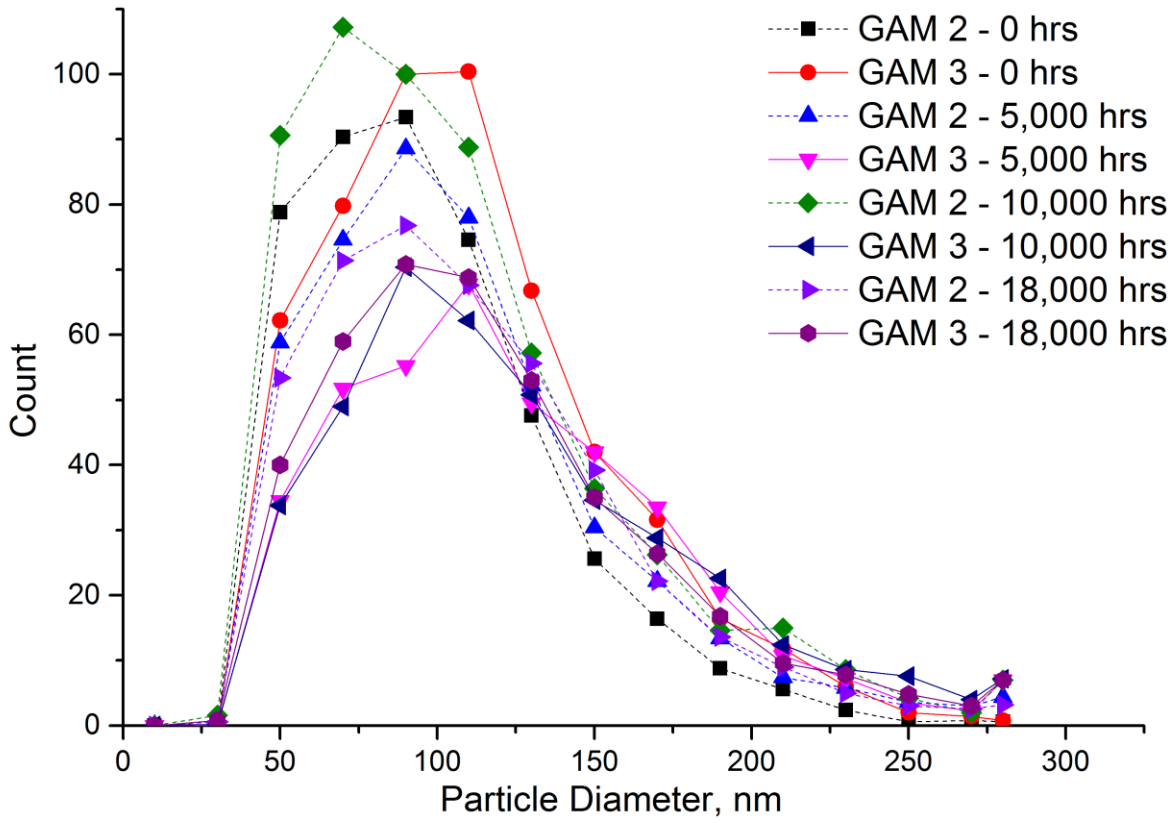

Figure 8.13: *Distribution of $M_{23}C_6$ particles for both the HiCo and LoCo MarBN steels as a function of heat treatment.*

A distribution of the number and associated size of the $M_{23}C_6$ carbides after a pre-service normalising and tempering heat treatment and after long term ageing is shown in Figure 8.13 for the HiCo and LoCo variants. The figure shows that after a pre-service heat treatment, the

high cobalt addition aids the precipitation of $M_{23}C_6$. After ageing at 650ºC for 5000 hours, the MarBN alloy with the HiCo addition was found to have a significant increase in fine $M_{23}C_6$ precipitates, in comparison to the MarBN alloy which had a lower addition of cobalt. The distribution shows that after 10,000 hours GAM 2 – HiCo was still found to maintain a higher number of finer precipitates in comparison to GAM 3 – LoCo. However, after 18,000 hours the difference between the HiCo and LoCo variants was significantly reduced

8.5.2 Quantification of Laves Phase as a Function of Isothermal Ageing

Quantification of Laves Phase as a function of isothermal ageing at 675°C, up to 18,000 hours has been carried out on two alloys 'GAM 2 – HiCo' and 'GAM 3 – LoCo'. The aim of this work is to identify if a change in the cobalt content has an effect on the initial precipitation and evolution of Laves phase. Laves phase was not reported to be present after an initial pre-service normalising and tempering heat treatment. However, the phase was observed to be present after isothermal ageing for 2,500 hours at 675°C. The number, size and particle size distribution was quantified for those samples aged between 2,500 hours – 18,000 hours.

Figure 8.14 shows a series of SEM micrographs of GAM 2 - HiCo and GAM 3 - LoCo after isothermal ageing; the images were acquired using a backscatter detector. The images show that there is a high contrast differential between the particles and the matrix. These particles have been previously identified in Chapter 7 to be Laves phase.

The micrographs indicate by visual observation that there is very little difference between the two alloys 'GAM 2 – HiCo' and 'GAM 3 – LoCo' after isothermal ageing up to 18,000 hours. Figure 8.14 shows that in both alloys there are significantly more precipitates after a short term isothermal ageing heat treatment of 2,500 hours which are smaller in comparison to the samples aged for 18,000 hours which are significantly coarser.

Quantification of the Laves phase present after isothermal ageing has been carried out with image analysis software to determine the number, size and size distribution of the precipitates present. Figure 8.15 shows the total number of Laves phase precipitates per 8497 μm², for both GAM 2 – HiCo and GAM 3 - LoCo. The figure shows that the general trend for both alloys is that the number of precipitates increases until 5,000 hours isothermal ageing. After 10,000 hours ageing the number of precipitates was observed to decrease as a function of ageing duration. It was observed that there were some variations in the total number of particles between GAM 2 – HiCo and GAM 3 – LoCo after the different isothermal ageing

heat treatments. After 2,500 hours and 10,000 hours there was observed to be an increased number of Laves phase particles, as shown in Figure 8.15. After 18,000 hours isothermal ageing the total number of particles observed to be present in both alloys were very similar.

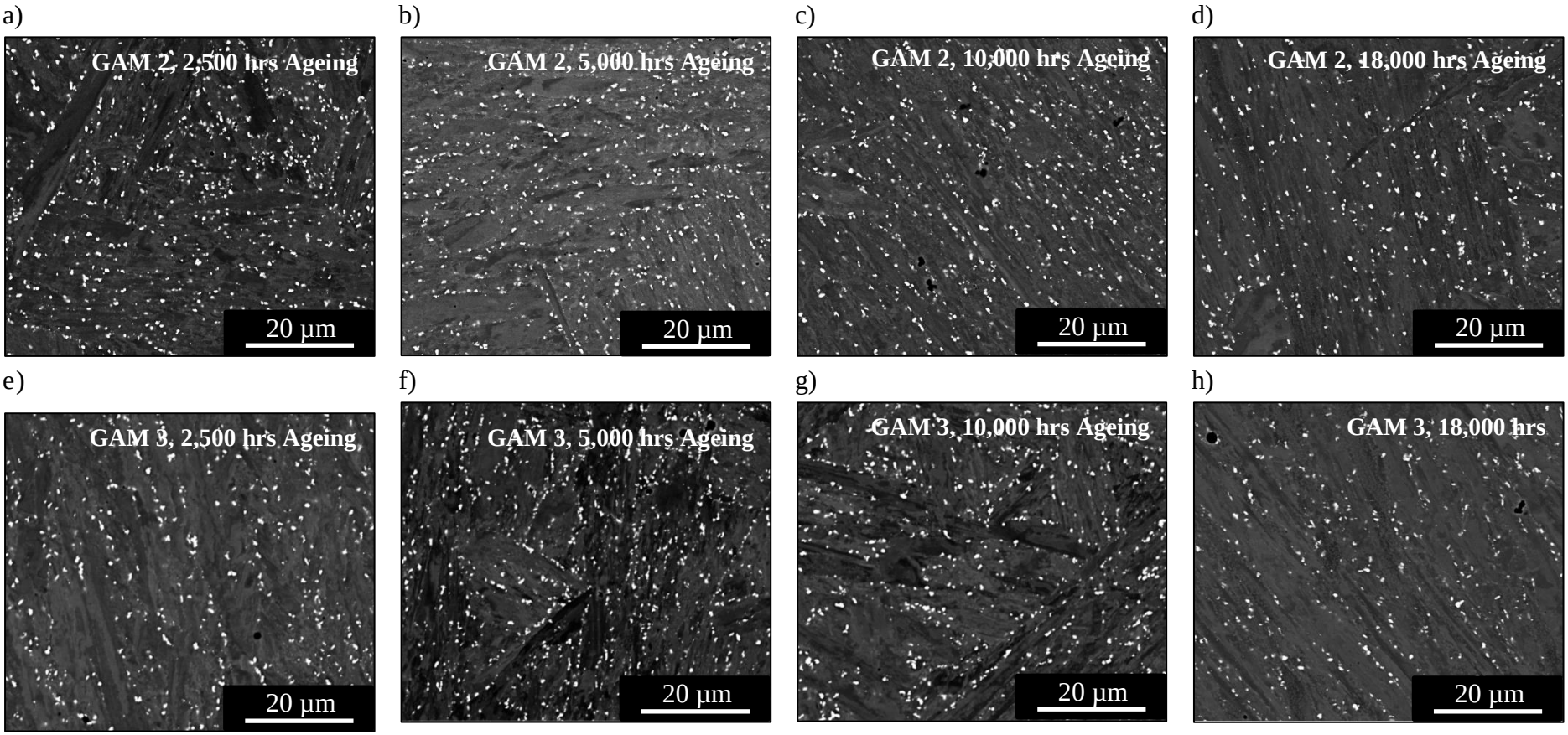

Figure 8.14: A series of micrographs produced using a backscatter detector. The micrographs were produced after normalising at 1150°C tempering at 780°C. The samples were aged at 675°C for between 2,500 – 18,000 hours. a) GAM 2 – HiCo 2,5000 hours, b) GAM 2 – HiCo 5,000 hours, c) GAM 2 – HiCo 10,000 hours, d) GAM 2 – HiCo 18,000 hours, e) GAM 3 – LoCo 2,500 hours, f) GAM 3 – LoCo 5000 hours, g) GAM 3 – LoCo 10,000 hours, h) GAM 3 – LoCo 18,000 hours.

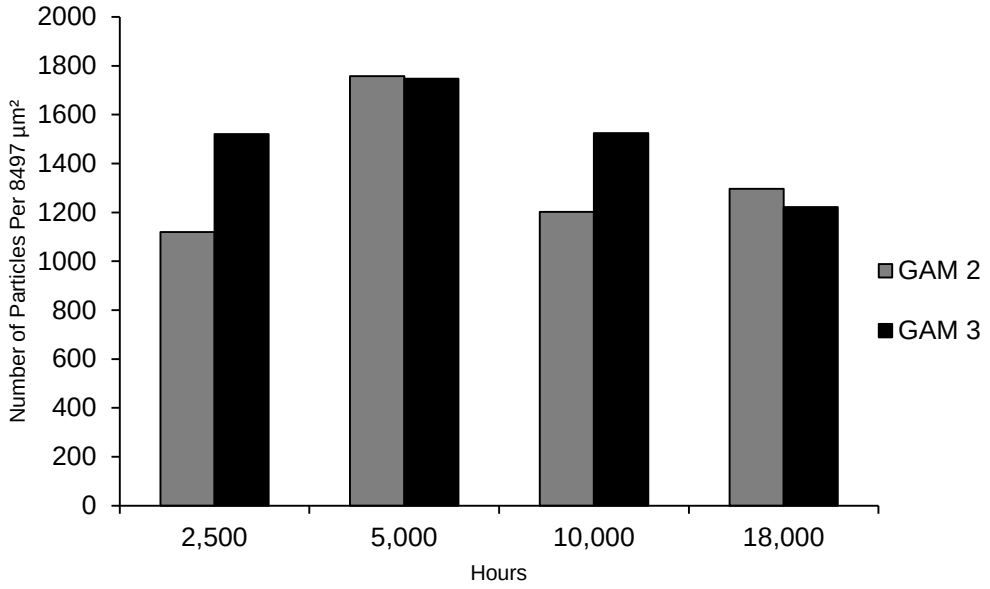

Figure 8.15: A graph showing the total number of Laves phase precipitates observed per 8497 µm² for GAM 2 – HiCo and GAM 3 - LoCo, after isothermal ageing at 675°C for 18,000 hours.

The average size of the precipitates was quantified for both alloys, GAM 2 – HiCo and GAM 3 – LoCo. The particles in both alloys were found to increase in size as a function of ageing duration. It was observed that there were small variations in the average particle size between the two alloys aged at the different ageing durations. The variations were observed to be less than 30 nm. In contrast to this SEM based technique is not deemed possible to analyse such small changes in particle dimensions.

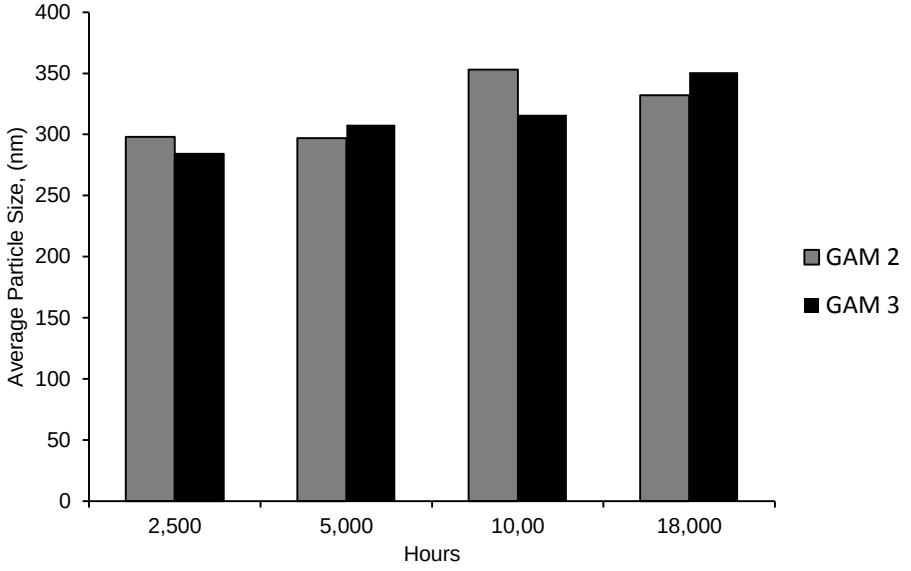

Figure 8.16: A graph showing the average particle size of Laves phase precipitates in GAM 2 – HiCo and GAM 3 - LoCo observed after isothermal ageing at 675°C for 18,000 hours.

Further quantification of the size and number of Laves phase precipitates present at the different ageing durations has been carried out for the two alloys and different ageing durations. These data have been used to plot a distribution which shows the number of precipitates against the precipitate size, as shown in Figure 8.17.

Figure 8.17 shows that there are a number of key differences in the distribution of particle size for the two alloys. The figure shows that the key change occurs in the number of smaller particles, whereas above 500 nm the number of coarser particles in all alloys was found to be very similar. After 2,500 hours ageing there was observed to be significantly more precipitates in GAM 3 – LoCo in comparison to GAM 2 – HiCo. After 10,000 hours ageing there was a difference in the number of smaller precipitates for the two alloys, GAM 3 – LoCo was observed to have a higher number of smaller precipitates.

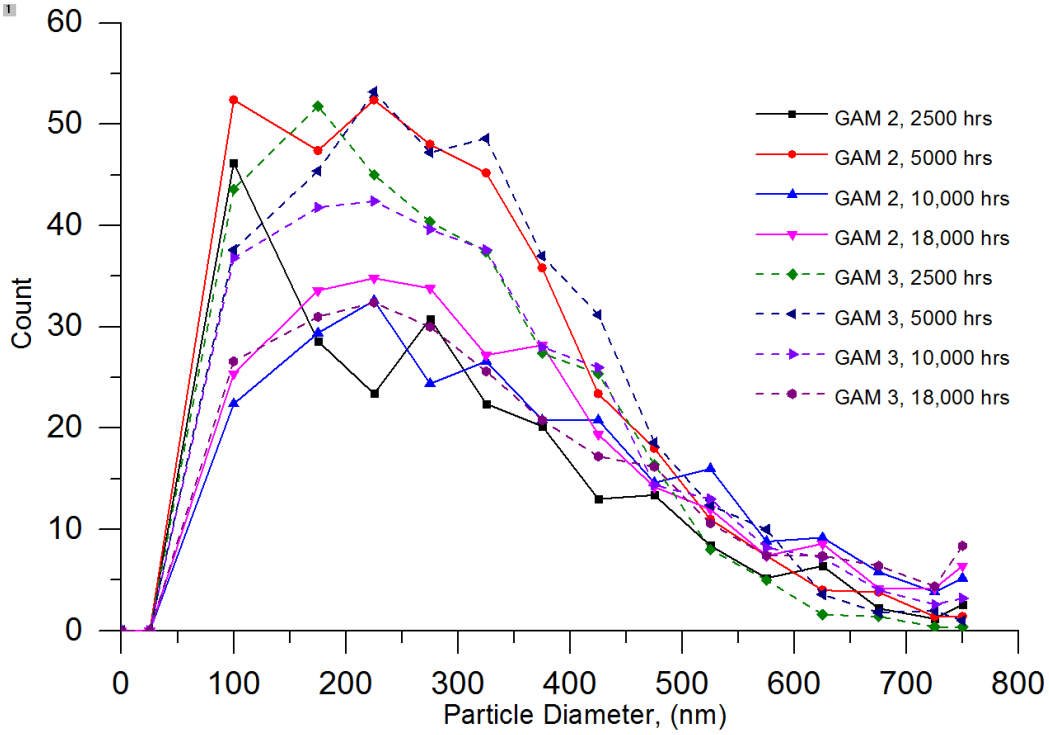

Figure 8.17: A graph showing the distribution of Laves phase particles for both GAM 2 - HiCo and GAM 3 - LoCo as a function of isothermal ageing.

The investigation examining the effect of cobalt on precipitation and evolution of Laves phase has revealed that a change of 0.4 wt. % cobalt can have an effect on the number precipitates in the short term (less than 10,000 hours). The samples with lower cobalt were observed to have a higher number of precipitates present in some aged conditions. However after long term ageing (~18,000 hours) there was observed to be very little difference between the number and size of Laves phase. This is similar to that reported by Li *et al.* [69] who investigated the effect the effect of a change of 1.5 wt.% cobalt in a P92 alloy, and the results reported that cobalt was observed to have no effect on the evolution of Laves Phase.

8.6 Microstructural Evolution of the Martensitic Matrix

Electron back scatter diffraction has been used as a technique for a number of years to quantify the microstructural degradation in P91 and P92[69,73,74]. A study was carried out in Chapter 7 to investigate if the martensitic matrix could be quantified using EBSD due to the prior austenite grain size been larger than 400 µm. The results from the study carried out in chapter 7 have shown that results have a larger error than typical EBSB scans carried out on materials with a prior austenite grain size. However the study has shown that repeatable results can be produced but care needs to be taken when interpreting quantified results.

The microstructural evolution of the matrix after ageing has been characterised with the use of electron back scatter diffraction (EBSD). Two alloys were characterised GAM 2 – HiCo and GAM 3 – LoCo after isothermal ageing up to 18,000 hours.

The grain boundaries were classified using their associated mis-orientation angle. The boundaries were defined into high angle boundaries and low angle boundaries. High angle boundaries were defined as those with a mis-orientation >15°. These boundaries represent the prior austenite and martensite lath boundaries. Low angle boundaries were defined as those with a mis-orientation angle of between 2° - 15°. These boundaries represent the substructure dislocations.

Figure 8.18 shows the grain boundary maps for GAM 2 – HiCo and GAM 2 – LoCo after a pre-service heat treatment and after 18,000 hours isothermal ageing at 675°C. The series of grain boundary maps show that the matrix is fully martensitic, and indicate that the laths are coarsening as a function of ageing.

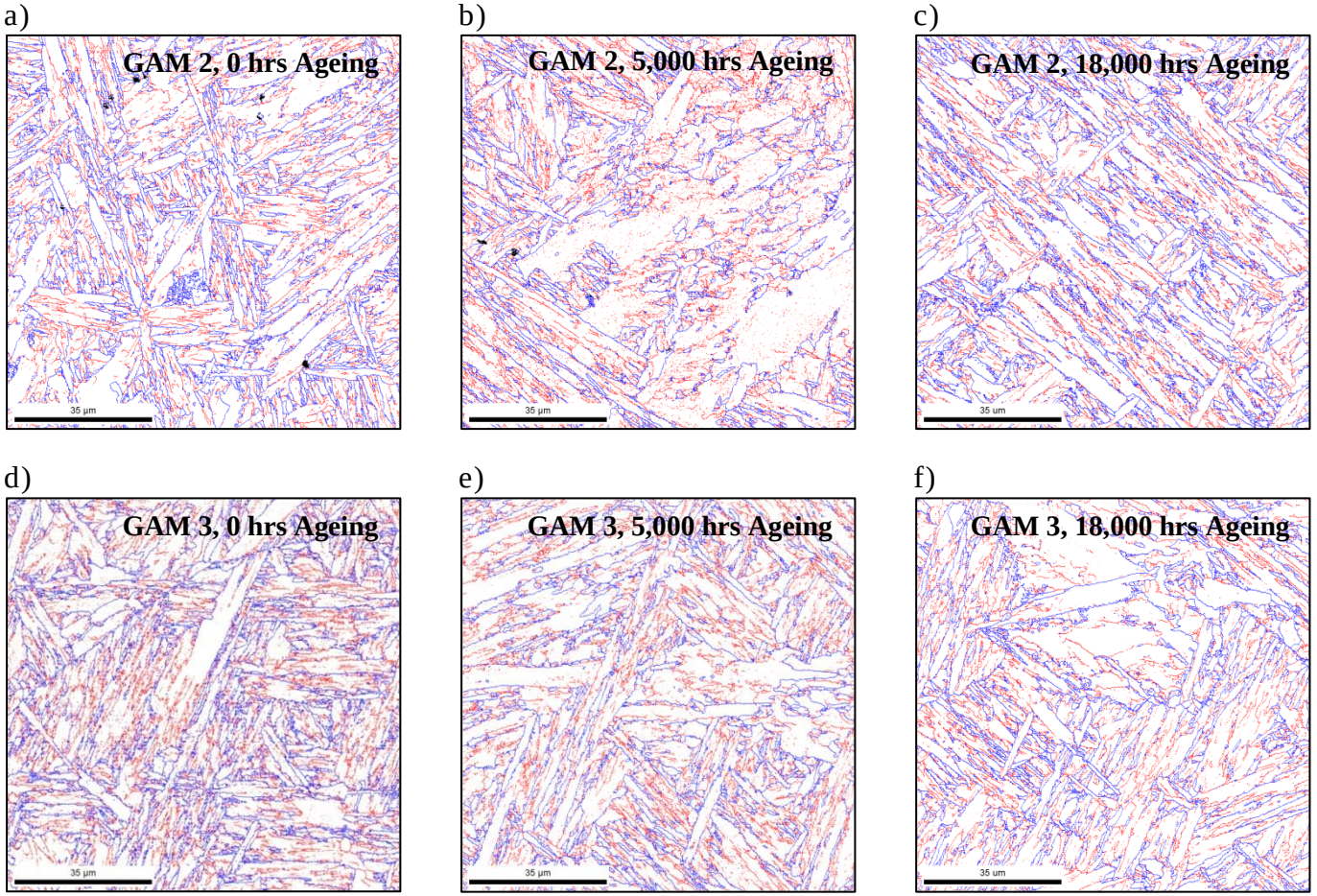

Figure 8.18: A series of grain boundary maps produced using EBSD. The maps were produced after a pre-service heat treatment of N1150°C T 780°C, the samples were aged at 675°C for between 0 – 18,000 hours. The boundaries with a mis-orientation between 2° - 15° are shown in red and those with a mis-orientation above 15° are shown in blue. a) GAM 2 0 hrs b) GAM 2 5,000 hrs c) GAM 2 10,000 hrs d) GAM 3 0 hrs e) GAM 3 5,000 hrs f) GAM 2 – LoCo 10,000 hrs.

Quantification of the mis-orientation maps has been carried out. The total length of grain boundaries has been quantified, as a function of ageing duration for GAM 2 – HiCo and GAM 3 LoCo, as shown in Figure 8.20. Figure 8.20 shows that there is a gradual decrease in the total length of grain boundaries as a function of ageing, after normalising for both alloys. The results need to be interpreted with care, as the typical error on MarBN with a large grain size in the region of 600 µm is ±20%.

Figure 8.18 shows the grain boundary maps as a function of isothermal ageing, it is evident from examining the maps that all the structures remain fully martensitic, which demonstrates that the recovery to ferrite has not taken place in place in either alloy. This helps provide an indication that the improved creep properties shall be maintained after long term testing.

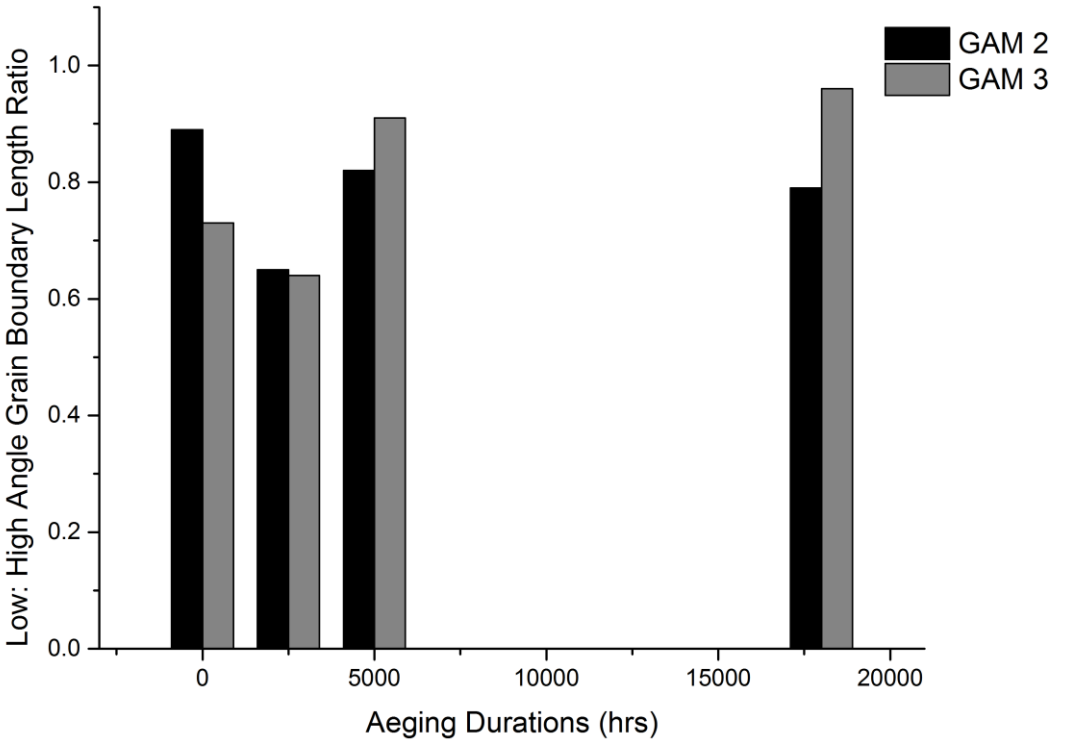

Figure 8.19: A graph showing the ratio between angles with a mis-orientation between 2° - 15°, and boundaries is a mis-orientation > 15°. The analysis was carried out on GAM 3 after normalising at 1150°C when aged for between 2,500 – 18,000 hours.

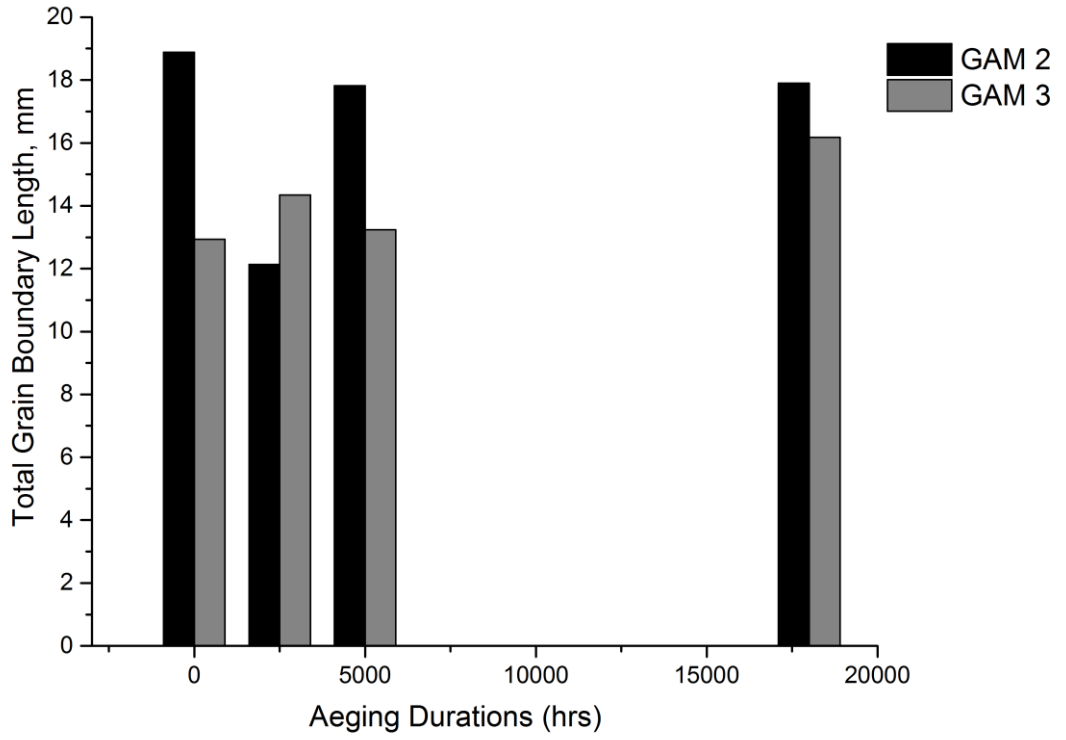

Figure 8.20: A graph showing the total grain boundary length for GAM 2 – HiCo and GAM 3 - LoCo when normalised at 1150°C and tempered at 780°C. The samples were isothermally aged at 650°C for between 0 – 18,000 hours.

8.7 Summary

Two alloys were characterised in this chapter to investigate the effect of Cobalt on the evolution of the precipitates as a function of time. The alloys had a difference of 0.4 wt. % cobalt, in addition to a small change of 80 ppm boron. These alloys were denoted as GAM 2 – HiCo and GAM 3 – LoCo. Microstructural characterisation was carried out on these two alloys to identify if a small change in cobalt has an effect on the initial precipitation and evolution of the minor phases and degradation of the microstructure after long term ageing.

After a pre-service normalising heat treatment at 1150°C and subsequent tempering at 780°C, boron nitride precipitates were observed to be widely present in both alloys. However in GAM 2 HiCo there was observed to be a higher number density of $M_{23}C_6$ precipitates which were smaller in size after a pre-service heat treatment.

The stability of $M_{23}C_6$ and Laves phase was investigated as a function of isothermal ageing up to 18,000 hours. The characterisation has shown that the $M_{23}C_6$ coarsen at a similar rate in both alloys. There was observed to be a difference in the number density of $M_{23}C_6$ precipitates in samples which were aged for less than 10,000 hours. A higher number density of carbides was observed to be present in GAM 2 – HiCo. This indicates that cobalt may aid the precipitation of $M_{23}C_6$ carbides; however this result is not conclusive, because of the change in the boron composition which has been linked in chapter 7 to increasing the precipitation of $M_{23}C_6$. However after 18,000 hours isothermal ageing the number density of $M_{23}C_6$ carbides was observed to be similar in both alloys which indicates that cobalt may not have a beneficial effect on increasing the creep properties in the long term.

The effect of a change in cobalt content on the precipitation and evolution of Laves phases was investigated. It was observed that after isothermal ageing, the average particle size was found to increase in both alloys and the particle sizes were similar in both GAM 2 – HiCo and GAM 3 - LoCo. The characterisation has shown that after short term ageing of less than 10,000 hours there is a higher number density of Laves Phase in GAM 3 – LoCo in comparison to the GAM 2 – HiCo. However, after 18,000 hours ageing the number density and size of Laves Phase was found to be similar which indicates that beneficial effect of the cobalt addition reducing the number density in the short term may not affect the long term creep properties of MarBN.

The evolution of the martensitic matrix as a function of ageing in both alloys with different cobalt contents was investigated. Grain boundary maps were produced using EBSD for both alloys which were aged for up to 18,000 hours. The grain boundary maps show that both variants are fully martensitic and there is marginal recovery of the microstructure after long term ageing. The grain boundary maps do not show any significant change in the recovery of the microstructure after long term ageing, between the two alloys with different cobalt contents.

This chapter has shown that cobalt may aid the precipitation of $M_{23}C_6$ in the short term and in contrast cobalt may also reduce the number density of Laves phase in the short term. During this project it was identified that boron can have a significant effect on aiding the precipitation of precipitates within the microstructure. Therefore further work is required to confirm the short term properties with an alloy that only has a 0.4 wt. % change in the cobalt content. However, in the long term the precipitation of $M_{23}C_6$ and Laves phase was observed to be similar in both alloys.

The microstructural characterisation has shown that in the long term the cobalt has very little effect. However, the hardness of GAM 2 – HiCo is significantly higher than GAM 3 – LoCo and the creep properties are significantly higher for GAM 2 – HiCo. Cobalt therefore does have a very important role in increasing the mechanical properties in MarBN, but it has little impact on the phases within the microstructure. This finding indicates that the increased strength observed from Cobalt is obtained from solid solution strengthening.

Chapter 9

THE IMPLICATIONS OF THE RESEARCH ON THE INDUSTRIAL DEPLOYMENT OF MarBN

9.1 Introduction

The first eight chapters of this thesis have reported results from extensive microstructural characterisation on a number of small scale trial melts, which were less than 50 kg. A total of eight alloys were manufactured using an induction furnace, which is not a commercial manufacturing route for 9 wt. % chromium steels. The two alloys with the optimum chemical composition, which were denoted as GAM 2 and GAM 3, were used to carry out heat treatment trials in order to determine the optimum pre-service normalising and tempering heat treatment. The effect of long term isothermal ageing on the microstructural stability of MarBN was investigated up to a duration of 10,000 hours. In order to quantify the effect of microstructural changes on the mechanical properties of the alloy, a short term creep testing program was carried out whereby the maximum test duration was 4,000 hours. This testing was carried out to identify which alloy produces the best creep properties in the short term.

This research project has demonstrated that MarBN is a potential candidate material for use within a coal fired power plant. In order for this alloy to be used within a power plant in the UK, extensive testing must be carried out by an external body such as the HSE and ASME to ensure the mechanical properties are accurate and that the material is fit for purpose. In order for an alloy to be considered by an external body, a substantial amount of mechanical property data is required to verify that the material meets the specified mechanical properties and that these will not rapidly deteriorate as a function of time. A typical long term creep testing programme requires creep testing on individual samples in excess of 100,000 hours. Therefore it is imperative that long term mechanical property data are generated on an alloy that has been optimised and has also been manufactured using an appropriate commercial process. A long term creep testing programme has significant time and financial constraints and therefore it is not usually possible to carry out such a programme on a number of variants and then subsequently decide which variant will be used in a commercial power plant.

The scope of this research project was to provide an understanding into the optimisation of MarBN steel, with the overall goal of improving the creep properties of the alloy. The

previous chapters have highlighted that by using the changes proposed, the creep strength can be increased by approximately 20% by optimising the chemical composition and pre-service heat treatment.

During this research project a number of findings have an influence on the ability to deploy this alloy within industrial applications, this chapter reflects on the findings. The research project has not provided solutions to all the issues which could prevent the deployment of this alloy. However, the key areas where further work need to be carried out are identified in Chapter 11.

The ability to manufacture this material on a commercial scale will ultimately determine if MarBN shall be utilised within a power plant. The alloy needs to provide improved properties but it is essential that the supply chain can manufacture this alloy using standard manufacturing methods. It is critical that the supply chain has a 'range' in which the enhanced properties, this is applicable to both the chemical composition and heat treatment parameters.

The first step identifying if it is possible to manufacture MarBN on a commercial scale was carried out, an 8 tonne MarBN was manufactured during this project. This shall help to identify if it possible has the potential to be manufactured on a commercial scale, and shall help reduce the risk in funding a long term creep testing program.

9.2 The Key Objectives

The key objective of this chapter was to identify if MarBN steel could be manufactured using a commercial casting technique and if the mechanical properties could be similar to that achieved in the small scale trials manufactured using an air melting induction technique. The typical melting route for manufacturing 9 wt. % chromium steels such as P91 and P92 is using Argon oxygen decarburization (AOD), therefore this was chosen as the melting route to manufacture an 8 tonne MarBN casting.

In order to verify the overall objective of identifying if similar mechanical properties could be achieved on the 8 tonne casting this overall objective this chapter has been split into three sections: -

- The effect of small changes in the chemical composition to identify the effect of batch to batch variation. The aim is to understand which elements are most likely to affect

the creep properties of MarBN and are therefore most important to control during manufacture.

- To provide verification that MarBN can be manufactured on a commercial scale using an AOD process or similar without a decrease in mechanical properties.
- Understand the effect of heat treating a large scale MarBN casting and the subsequent effect on the precipitation of secondary phases within the microstructure.

9.3 The Effect of Chemical Composition Variation on the Mechanical Properties

It is important to understand what effect small changes in the chemical composition have on the creep properties of MarBN. The chemical composition of MarBN is reported within literature; however, they all specify a specific boron and nitrogen composition. It is vital for steel makers to have a range for each alloying element to allow this alloy to be manufactured on a commercial scale which still shall ensure that the minimum acceptance properties can be achieved. Furthermore it is critical to understand the effect that each element has on the mechanical properties of MarBN. This is important because it will increase the theoretical understanding into MarBN but will also provide a practical understanding by tightening the specifications on elements which shall provide a variance in the creep properties produced. This shall allow the casting manufacturers to put process in place for elements which have a tighter specification.

The chemical composition of the small scale trial melts were optimised using thermodynamic calculations, as shown in Chapter 4. The melts made a systematic change in the chemical composition, however a melt was not manufactured to study the effect of each alloying element in MarBN. Therefore it is not possible to determine the effect of each alloying element on the creep properties in MarBN. However, the results have shown which alloying elements can affect the creep properties produced.

The alloys were manufactured with the aim of optimising the creep properties of MarBN, using a maximum of twelve melts. A short term creep testing program was carried out on eight of the trial melts (GAM 1 – 8) at an elevated temperature of 675°C, as discussed in section 7.6. The alloys were creep tested at three stresses 142 MPa, 127 MPa and 113 MPa. Figure 9.1 shows the time to rupture versus test stress for GAM 1 – 8 in addition to the mean behaviour for P92 derived from ECCC 2005 published data at test temperature of 675°C. The figure shows that GAM 5 is weaker than P92 and GAM 1 has marginally better creep properties than P92. GAM 2 was found to be the alloy with the highest creep properties,

which was closely followed by GAM 3, 7 and 8. The four alloys have a variation of 50 ppm nitrogen, 0.5 wt. % tungsten, 0.3 wt. % cobalt and 80 ppm boron. This shows that MarBN can achieve substantially higher creep properties than P92. However, the material specification will need to be tighter for specific elements to ensure the improved mechanical properties are achieved.

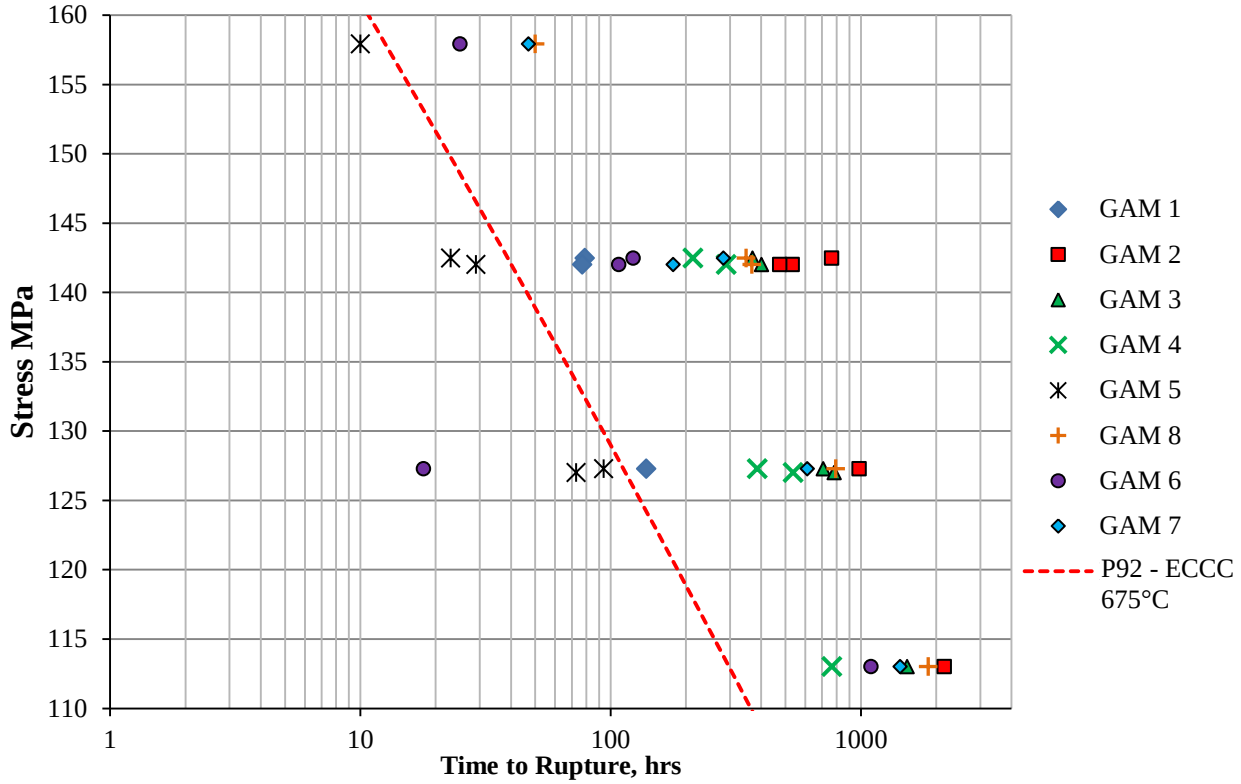

Figure 9.1: A graph showing the time to rupture versus stress for GAM 1 – GAM 8, the samples were normalised at 1150°C and tempered at 780°C and creep tested at 675°C. The data is compared with mean behaviour for P92 derived from ECCC 2005 published data.

The key difference between GAM 2 and GAM 3 was a variation of 80 ppm boron and 0.5 wt. % cobalt. The change in chemical composition has been observed to have a significant effect on the creep properties; GAM 2 was found to have an increased time to rupture in comparison to GAM 3 as shown in Figure 9.2. The microstructural characterisation which was carried out in Chapter 6 in order to understand the difference between GAM 2 and GAM 3, showed that increasing the boron chemical addition was found to increase the precipitation of $M_{23}C_6$ after a pre-service normalising and tempering heat treatment. It is postulated that boron could provide a long term benefit by reducing the coarsening rate of $M_{23}C_6$ carbides. The addition of cobalt is not thought to have a significant effect on the long term stability of phases, but provide improved properties through solid solution

strengthening. Further creep testing is required to determine the beneficial effect of the cobalt addition populated to be provided by solid solution strengthening, is maintained after long term creep testing.

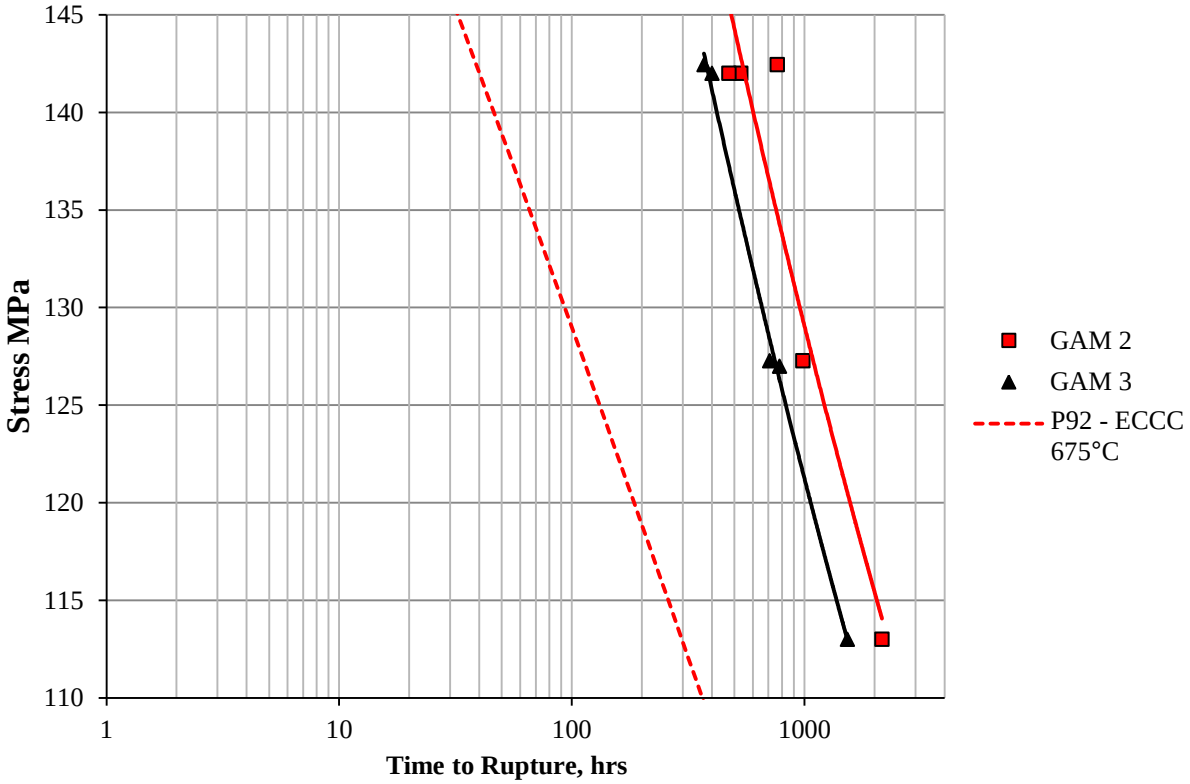

Figure 9.2: A graph showing the time to rupture versus stress for GAM 2 (Red) and GAM 3 (Black), the samples were tested at a temperature of 675°C. The samples were normalised at 1150°C and tempered at 780°C. The data is compared with mean behaviour derived from ECCC 2005 published data.

Figure 9.1 shows that GAM 8 was found to have improved creep properties in comparison to GAM 4. The only change in the chemical composition was a variation of 60 ppm nitrogen. GAM 4 was observed to have a higher nitrogen content of 210 ppm, whereas GAM 8 was observed to have a nitrogen content of 150 ppm. This indicates that in the short term the effect of a small change of boron, cobalt, nitrogen and tungsten produces a large scatter in the creep properties which would not be acceptable to end user of the material. The addition of cobalt is an element which can be well controlled during the steel making process. However it has been identified that the boron and nitrogen contents can have a significant effect on the creep properties, based on short term data. These elements are very low within MarBN, and if the elements are significantly increased the creep properties of the alloy can be reduced. Therefore steel makers need to carefully control both the boron and nitrogen contents to

ensure they are within specification to ensure there is no significant deviation in the mechanical properties of the alloy manufactured.

It should be noted that the interpretation of creep data within this chapter is based on short term data up to 2,200 hours and therefore long term creep testing will be required to verify the results obtained to date. A long term creep testing is now in progress and will extend beyond the completion of this work.

Microstructural characterisation was carried out in chapter 6, and has shown that the addition of boron can have a significant effect on the size and number of precipitates, present after a pre-service heat treatment and also after long term isothermal ageing. The size and number of precipitates was found to change as the ageing duration was increased up to 10,000 hours, there it is essential that long term creep testing is carried out in order to confirm the effect of each element on the creep properties of the alloy.

During the definitive stage of this research project an 8 tonne casting was manufactured. A number of components were manufactured from the 8 tonne melt:-

- 150 mm x150 mm ingots - Forging and rolling trials for the manufacture of wrought products
- Large ‘O2’ Ingot – Manufacture of pipe for demonstrator applications
- Three tonne ‘bonnet’ shaped casting – To simulate a typical manufacture of a turbine component
- Cast material test plates and weld plates – to allow for microstructural and welding trials to be carried out.

A long term creep testing program using a number of ingots from the eight tonne melts in various conditions, manufactured using a commercial steel making technique is now in progress. However, the results are outside the scope of this work.

9.4 Ability to Manufacture MarBN on a Commercial Scale

It is vital to understand whether or not MarBN can be manufactured commercially using a similar melting practice as other 9 wt. % chromium steels such as P9, P91, P92 and E911. The previous section has shown that a number of elements can have a significant effect on the mechanical properties which can be achieved. Nitrogen was identified as an element which can have a significant effect on the creep properties of MarBN. It was therefore vital to

understand a process that could be integrated into the melting practice to ensure that steel makers could manufacture the steel within specification.

An AOD melting method was used to manufacture an eight tonne melt, which is one commercial manufacturing route for such alloys. Section 9.3 has identified in order to control the creep properties the nitrogen content of the melt needs to be carefully controlled. In order to ensure that alloys can be consistently produced with a controlled nitrogen content, Goodwin Steel Castings Ltd have implemented the process of utilising argon purging when products are poured from the ladle into the mould. This process has been found to minimise the nitrogen pickup when the melt is poured from the ladle into the mould.

This process has allowed the Goodwin Steel Castings to consistently produce melts which have a nitrogen content which is approximately 100 – 150 ppm. Figure 9.3 shows two photographs of the pouring of the 8 tonne melt into a mould used to manufacture the ‘O2’ ingot, in conjunction with argon purging.

The implementation of argon purging has provided steel makers with the confidence that it is possible to manufacture MarBN with a consistent nitrogen content. It has also provided steel makers with the confidence that argon purging can be used without having a detrimental effects on the creep properties of the alloy.

a)

b)

Figure 9.3: Two photographs showing the pouring of the eight tonne melt into the individual moulds.

The chemical composition of GAM 2 was very similar to that of the eight tonne melt. GAM 2 was manufactured using a small induction furnace and the final products were ~50 kg. In contrast the eight tonne melt was manufactured using an AOD melting method and the final products were between 200 kg and 4,000 kg. Both alloys were creep tested using the same parameters and it was observed that in the short term the 8 tonne melt has slightly lower creep properties than GAM 2 and GAM 3. The creep properties were found to be similar to GAM 8 and still substantially higher than that achieved by P92, as shown in Figure 9.4.

This confirms that this alloy can be manufactured on a commercial scale and the creep properties obtained are similar to other MarBN small scale trial melts with similar heat treatment parameters.

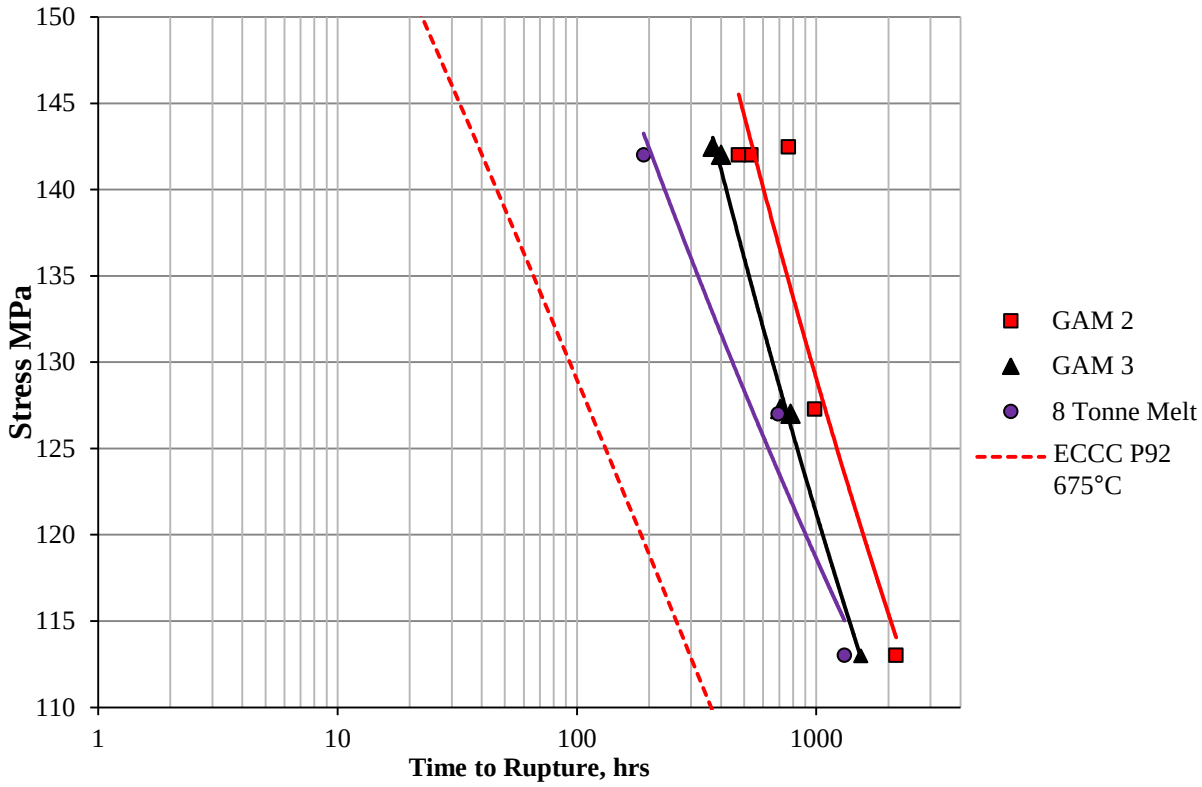

Figure 9.4: A graph showing creep rupture data at 675°C of both GAM2, GAM 3 and the 8 tonne melt bonnet casting after a standard normalising heat treatment at 1150°C followed by tempering at 780°C, compared with mean behaviour derived from ECCC 2005 published data.

9.5 The Implications of Heat Treating Large Scale Castings

The research presented in the first eight chapters of this thesis has investigated the effect of pre-service heat treatment conditions on the secondary phases observed to be present. This information has been used to predict the likely effect on the mechanical properties. The

research has significant implications on the heat treatment required for a commercial casting. Previous work has shown that modifying the normalising and tempering temperatures can have a significant effect on the creep properties of the alloy as shown in Figure 4.3.

The composition of the eight tonne melt manufactured was slightly different from the composition of the GAM melts. Therefore, it was essential to optimise the normalising heat treatment to ensure boron nitride was not precipitated. The microstructure of the as-cast material was examined in both the largest and smallest section sizes of the bonnet casting, and was observed to be fully martensitic. Both microstructures were found to have wide spread precipitation of tungsten borides and no boron nitride was observed to be present, as shown in Figure 9.5. A series of normalising heat treatments were carried out to examine if the precipitation of boron nitride in this alloy followed a similar trend to the work carried out on GAM 3 presented in Chapter 6. The microstructures produced after a normalising pre-service heat treatment at 1200°C indicate that boron nitride is precipitated between 1150°C and 1175°C and therefore in contrast at 1200°C the microstructure is free of boron nitride, as shown in Figure 9.5. This indicates that the precipitation of boron nitride in this alloy follows a similar trend to GAM 3. The bonnet casting manufactured from the eight tonne melt has been normalised at 1200°C after small scale heat treatment trials, and this shall be the material which shall be used for a future long term creep testing programme.

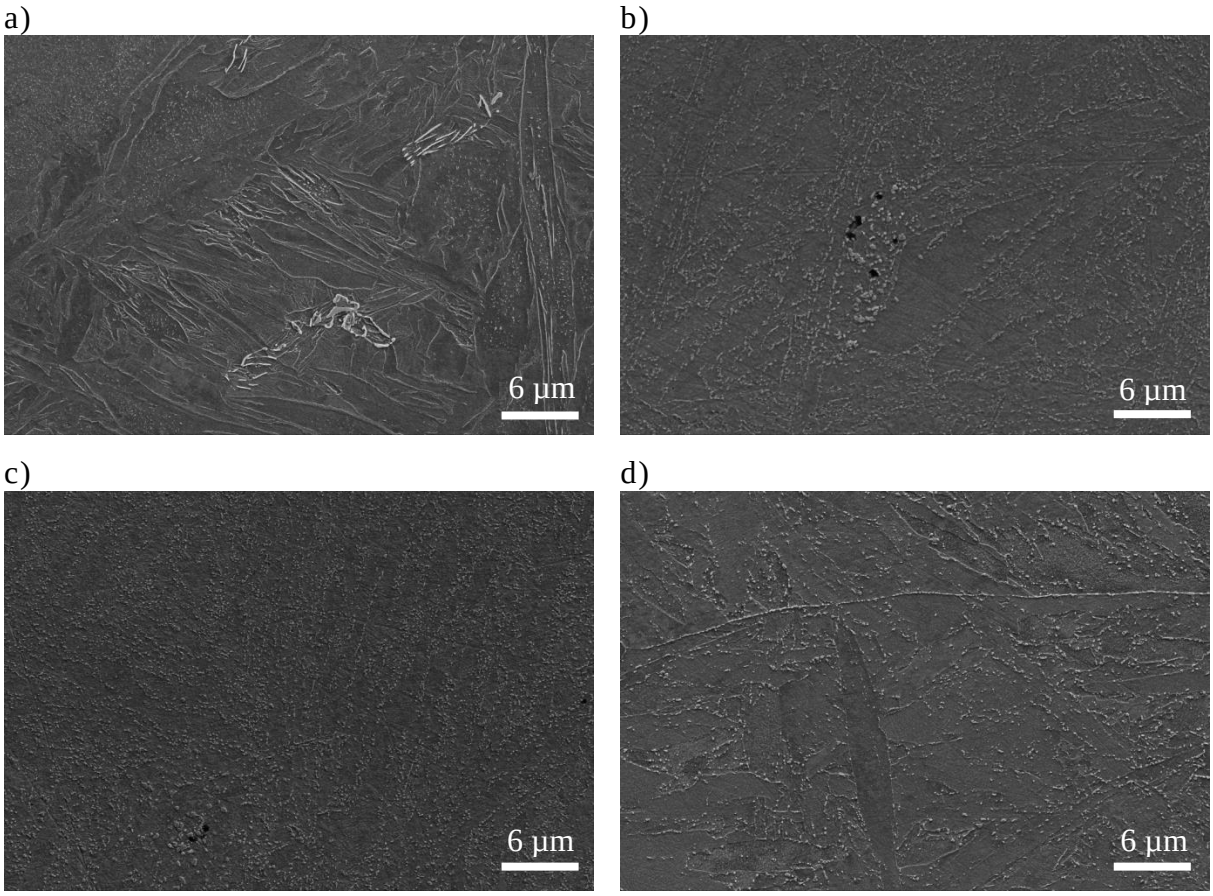

Figure 9.5: A series of SEM micrographs of the cast variant of the 8 tonne melt in a number of conditions a) as-cast, b) N1150°C T780°C, c) N1175°C T780°C, d) 1200°C T780°C.

Short term creep testing was carried out on the eight tonne melt at two different pre-service normalising temperatures, 1150°C and 1200°C. The aim of this testing program was to determine if the increased creep properties obtained on small scale trial melts could be replicated on a larger commercial casting. A total of three samples per heat treatment condition were creep tested at three stresses 142 MPa, 127 MPa and 113 MPa. The longest time to rupture was approximately 2,000 hours. Figure 9.6 shows the creep properties for two different normalising heat treatment conditions, in addition to the mean creep properties for P92 at a test temperature 675°C calculated using the ECCC standard creep results for P92. There is an increase in the creep properties when the alloy is normalised at a higher normalising temperature, which is a similar finding to those reported from the small scale melts.

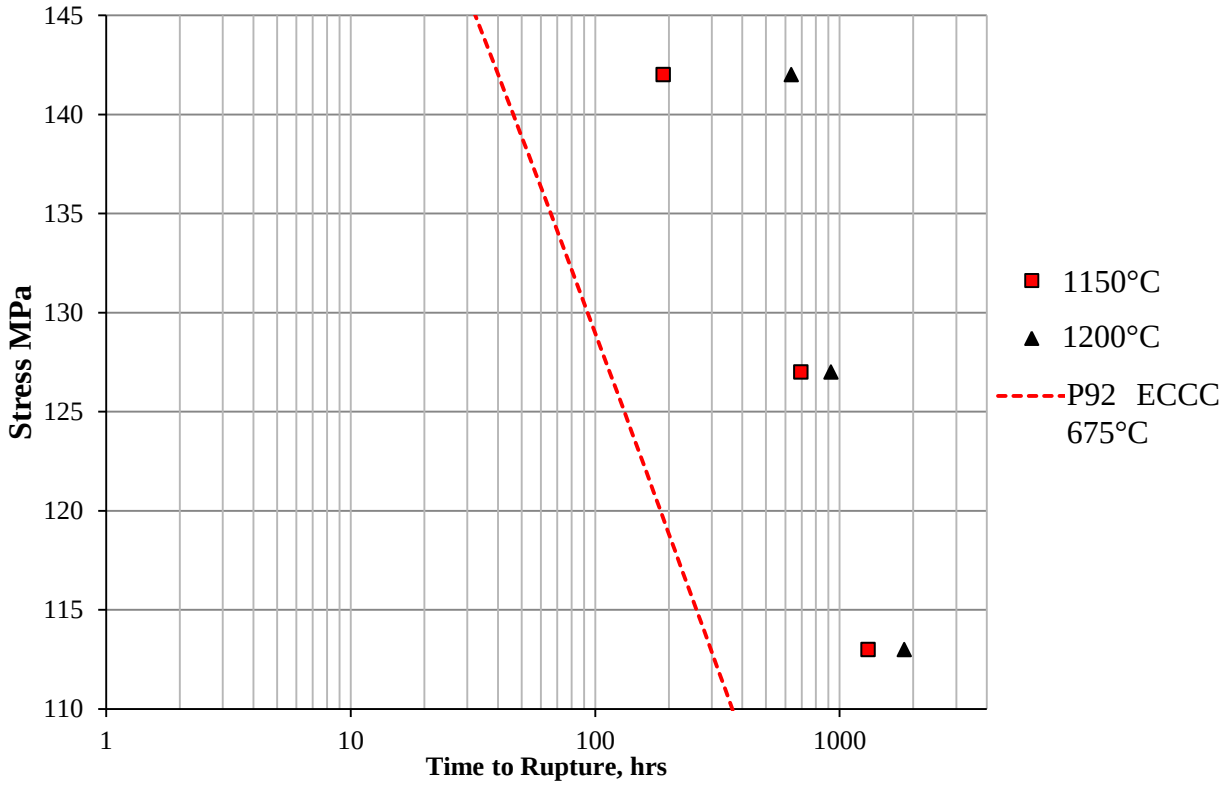

Figure 9.6: A graph showing the effect of normalising at 1150°C and 1200°C on the creep properties of the 8 tonne melt.

When a large casting is cooled from the normalising temperature, the cooling rate can be sufficiently slow that pro eutectoid ferrite is produced upon cooling. This has been observed in previous 9 wt. % chromium steels, such as P91 and P92. Trials have been carried out to determine what cooling rate is required to produce ferrite upon cooling. Two different cooling rates were utilised 11°C/hour and 2°C/hour.

The micrographs from the heat treatment trials are shown in Figure 9.7. The figures show a comparison between GAM 8 and P92 for both cooling rates used. It is evident that in the MarBN alloy the microstructure remains fully martensitic after both heat treatments, whereas in P92 both microstructures contain a proportion of ferrite. The alloys were normalised at 1200°C and therefore this implies that boron is within solution, which indicates that the boron addition has a beneficial effect in terms of preventing the transformation to ferrite upon cooling. This has a significant benefit to steel makers when manufacturing large castings.

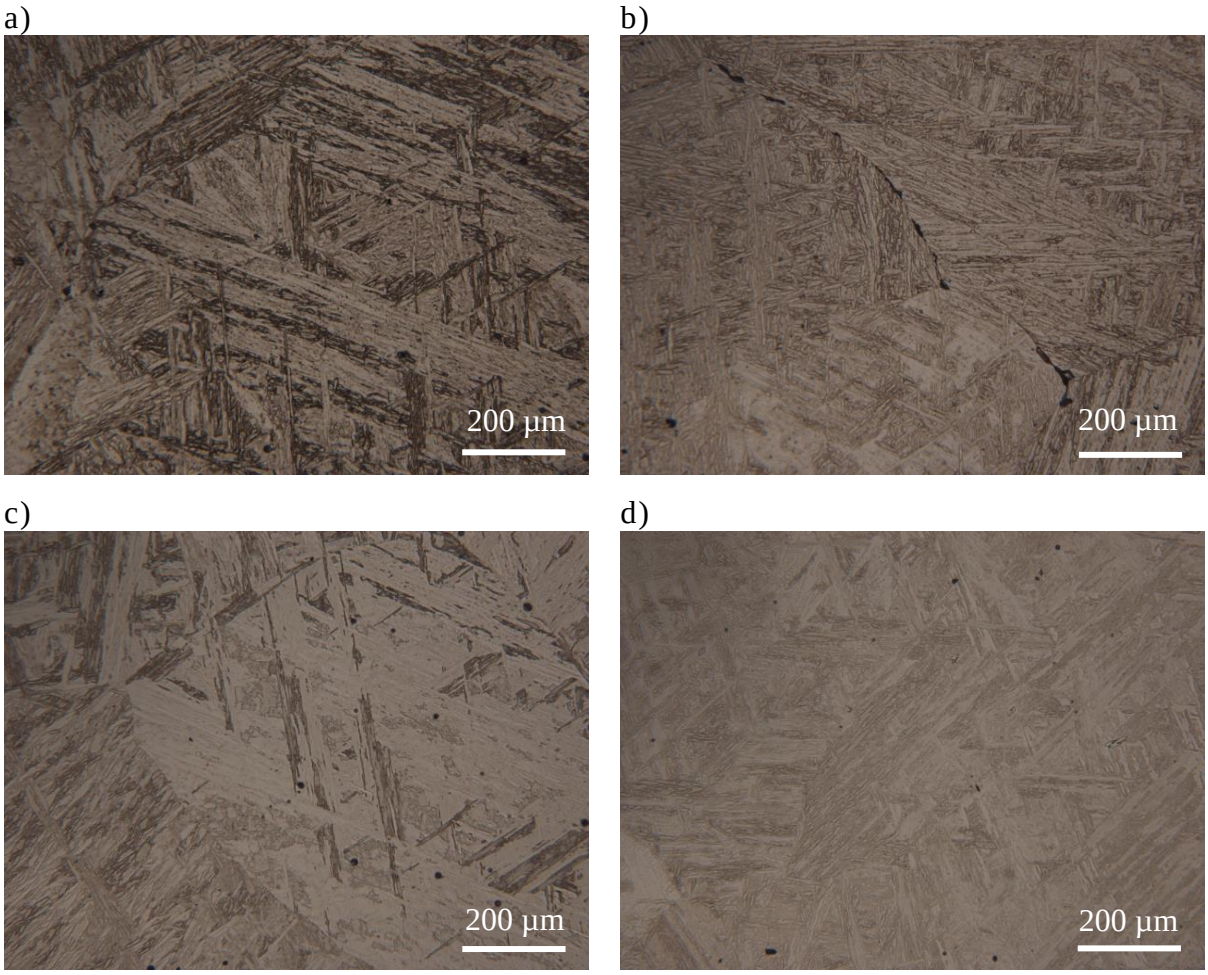

Figure 9.7: A series of optical micrographs of GAM 1 and GAM 4 after different cooling rates from 1200°C. Two different cooling rates were utilised 0.8°C/hour and 0.2°C/hour. a) GAM 1, 0.2°C/hr, b) GAM 4, 0.2°C/hour, c) GAM 1, 0.8°C/hour and d) GAM 4 0.8°C/hour.

An implication of normalising MarBN at a higher normalising temperature of 1200°C is that a very thick oxide is produced during the normalising heat treatment. This scale is approximately 1 mm thick. There is, however, a clear beneficial effect to the creep properties. However, the production of a very thick scale has serious commercial implications which may require the processing to be adapted. Further work is required to determine the effect of the initial oxide formation on the oxidation resistance within service applications.

9.6 Installation of MarBN into an Operating Power Plant

The long term aim of the research project was to install a section of MarBN into an operating power plant. This goal was achieved in June 2014 and is a significant milestone for the research project. This development will help develop and understanding of how this material will behave during service conditions.

Figure 9.8: A photograph showing a section of MarBN material installed within an operating coal fired power plant in June 2014, Photograph Courtesy of Dr C.Degnan, EON

9.7 Summary

Within this chapter a brief study has been carried out to identify if MarBN can be manufactured on a commercial scale using a similar production method to previous 9 wt. % chromium steels, such as P91 and P92. It has been identified that similar creep properties can be obtained on a commercial scale in comparison to the small scale trial melts manufactured during this research project.

This chapter has confirmed that the heat treatment optimisations recommended for GAM 3 in Chapter 6, can be replicated on a larger scale. The boron addition has been identified to

provide a significant increase against the transformation of ferrite upon slow cooling. This is a significant finding which will aid manufactures ensure that large castings are fully martensitic.

It has been identified that when MarBN is normalised at 1200°C a very thick oxide is produced, this will have an effect on the processing that is subsequently required.

This section of work has demonstrated that further work should be carried out into developing MarBN and there are significant energy saving benefits to the utilities by utilising such technology. This driver has this alloy has been recognised by the utilised who have subsequently installed a section of MarBN into a coal fired power plant for demonstration purposes.

Chapter 10

CONCLUSIONS

The key objective of this research was to optimise a MarBN alloy to increase the creep properties of the alloy. A range of techniques was used, from thermodynamic modelling through to quantification of the precipitates within the microstructure. Thermodynamic modelling was extensively used to predict the chemical composition which would produce optimum creep properties. Detailed characterisation of the microstructure of the alloys manufactured was carried out to identify a pre-service heat treatment which would provide optimum long term creep properties. Further characterisation was performed after long term isothermal ageing in order to assess the pre-service heat treatment, and gain an understanding how this material would perform within service. The final chapter assesses the ability to manufacture MarBN on a commercial scale and the implications that this may have on the resulting microstructure.

This research project has increased the understanding into MarBN alloys, the results have provided evidence to understand the effect of the chemical composition and microstructural features on the creep properties of the alloy. This understanding will help provide manufacturers and end users with the confidence that MarBN has the potential to be used within a future power plant and further testing should be considered in future projects.

Thermodynamic modelling was performed to determine a chemical composition which would produce optimum creep properties. A sensitivity study was initially carried out to determine the effect of each alloying element within MarBN. A systematic study was carried out to predict the limits of the boron and nitrogen without predicting boron nitride to be present. A further study was showed that the mass percentage of Z phase cannot be significantly reduced by modifying the chemical composition and retaining the creep properties.

The results from the thermodynamic modelling helped predict the chemical composition which would provide the optimum creep properties. The chemical composition was selected with the following rational of reducing the tungsten content, and maximising the nitrogen and boron contents, but the formation of boron nitride was avoided.

The major finding from the research was understanding the critical role of boron in MarBN and relating the microstructural changes to the creep properties of the alloy. Boron nitride is a

detrimental phase which forms during a standard normalising heat treatment at 1150°C. This phase consumes nitrogen which could otherwise be utilised within the system to precipitate carbonitrides, which would increase the creep strength of the alloy.

Boron nitride was found to be present in a number of conditions which are, as-rolled, rolled HT and cast HT. The method in which the alloys were processed was found to influence the amount of boron nitride precipitated within the microstructure and hot working was found to have the highest area percentage of boron nitride precipitated within the microstructure. Normalising trials have demonstrated that normalising these alloys at a higher temperature of 1200°C, provides a microstructure which is free of boron nitride. Furthermore, after the boron is solution, trials have shown that the material can be cooled using a slow cooling rate and boron nitride will not precipitate within the microstructure.

When a higher normalising temperature was utilised it was postulated that boron was within solution. In addition a significantly higher number of smaller $M_{23}C_6$ precipitates were observed within the microstructure. The presence of soluble boron was postulated to aid the precipitation of $M_{23}C_6$.

MarBN has a lower nitrogen content in comparison to other commercial 9 wt. % chromium steels and therefore these alloys have a reduction in the mass percentage of carbonitrides. Thermodynamic calculation has predicted that niobium carbide will be present when the alloy is normalised and tempered. However, vanadium nitride will only be precipitated at a high tempering temperature and low normalising temperature.

When MarBN was normalised at the standard temperature of 1150°C and then subsequently tempered at 780°C, the majority of the carbonitrides were observed to be niobium carbides. In contrast, after a high temperature normalising heat treatment at 1200°C, then tempered at 780°C, the carbonitride observed to be present was vanadium nitride.

The effect of tempering temperature between 700°C to 780°C was investigated further after a high temperature normalising heat treatment. There was found to be a change in the type of precipitates observed at different tempering temperatures. At a low tempering temperature of 700°C there was found to be a distribution of chromium rich precipitates but as the tempering temperature was increased to a medium tempering temperature of 740°C there was observed to be a distribution of vanadium nitride and niobium carbide and as the tempering

temperature was increased further to 780°C the distribution was found to only contain vanadium nitrides.

Therefore based on microstructural characterisation the optimum normalising temperature is 1200°C, because during tempering it aids the precipitation of fine $M_{23}C_6$ carbides and also the precipitation of vanadium nitride.

The long term creep properties of MarBN are linked to the stability of the microstructure, when exposed to an elevated temperature and stress. During this research microstructural characterisation was carried out to investigate the effect of isothermal ageing on the evolution of the minor phases and the degradation of the microstructure to provide an understanding of how the alloys will behave within service. Samples were isothermally aged after two different pre-service heat treatments:

- Normalising at 1150°C followed by tempering at 780°C
- Normalising at 1200°C followed by tempering at 780°C

After long term isothermal ageing at 650°C, for up to 10,000 hours, the size of the precipitates was observed to change. It was observed that there was a higher density of $M_{23}C_6$ precipitates in the samples normalised at 1200°C. There was observed to be a higher number of coarser precipitates in the samples normalised at 1150°C, which confirms that the stabilisation of $M_{23}C_6$ is only effective when boron stays in solid solution.

The samples were isothermally heat treated using a higher pre-service normalising heat treatment and were characterised to identify if boron was removed from solution as a function of isothermal ageing. Elemental mapping was carried out on samples aged up to 15,000 hours and there was no boron nitride particles or tungsten borides observed to be precipitated as a function of ageing. This provides evidence that boron is within solution and therefore will help to reduce the coarsening rate of the $M_{23}C_6$ carbides.

The microstructural characterisation indicated that boron has a critical role in changing the distribution of precipitates within the microstructure. Short term creep tests were carried out on material manufactured from the 8 tonne AOD melt and various samples were tested using different heat treatment parameters. It was evident from the creep test results that the heat treatment parameters have a significant effect on the time to rupture. The heat treatment parameters that provided the highest strength were normalising at 1200°C for two hours followed by tempering at 710°C for three hours and therefore this validates the

microstructural findings. This is a very significant result which indicates a potential in optimising the mechanical properties of MarBN. Further creep testing is required to determine if the mechanical properties can be maintained during long term ageing.

Extensive microscopy characterisation has been carried out on two alloys, GAM 2 and GAM 3. These alloys had a difference in cobalt content of 0.4 wt. %, along with a small variation in boron. The alloys were denoted as GAM 2 – HiCo and GAM 3 – LoCo. Microstructural characterisation was carried out on these two alloys to identify if a small change in cobalt has an effect on the initial precipitation and evolution of the minor phases and degradation of the microstructure after long term ageing. After a pre-service normalising and tempering heat treatment there was observed to be a difference in the number of $M_{23}C_6$ carbides present. However, after long term isothermal ageing there was very little difference in the number and size of the $M_{23}C_6$ and Laves phase precipitates. Cobalt is a very expensive alloying element and therefore there is a need to reduce this addition, without reducing the creep properties. This research indicates that cobalt provides an increase to the long term creep properties by solid solution strengthening and therefore the addition of this element into MarBN is considered beneficial to the long term creep properties.

The implication of the research on the commercialisation of MarBN has been investigated. An 8 tonne casting was manufactured using a commercial manufacturing melting technique known as AOD. This alloy was creep tested to demonstrate that similar creep properties could be achieved to the small trial melts previously manufactured during this project. The mechanical properties were found to be in a similar range to the small trial melts. The creep properties were significantly higher than other alloys, such as P92, which are currently used within coal fired power plants in the UK. This has shown that this alloy could potentially allow power plants to operate at a higher temperature and therefore operate more efficiently.

Chapter 11

FURTHER WORK

The key objective of this research was to optimise MarBN to increase the creep properties of the alloy. A range of techniques were used to achieve this goal. Thermodynamic modelling was used to investigate the effect of the chemical composition under equilibrium conditions and microstructural characterisation was used to help gain an understanding into the microstructure produced, as a function of pre-service heat treatment and long term isothermal ageing.

The initial aims of this research project were achieved during this project; however, there are a number of areas where further work should be carried out to help improve the understanding into MarBN. This information will ultimately help determine if this alloy can be used within a power plant in the future.

The suggested areas for further work have both a practical and theoretical interest. It has been highlighted that the boron addition has a significant effect on the ferrite transformation upon slow cooling. It would be highly desirable to generate a CCT diagram using a dilatometer on both MarBN and P92 to understand how the two alloys compare.

The research project has shown that the presence of soluble boron increases the precipitation of $M_{23}C_6$ during tempering. In addition to this, the presence of soluble boron has been thought to reduce the coarsening rate of the $M_{23}C_6$ carbides during isothermal ageing. The theory presented within the literature has not been confirmed by experimental results. Therefore it is essential to determine if boron is located at the interface of the $M_{23}C_6$ carbides using atom probe. Identifying the role of boron on a nano-scale would validate the mechanism which reduces the coarsening rate of $M_{23}C_6$ in MarBN.

The effect of 18,000 hours isothermal ageing on the microstructural evolution of both the matrix precipitates was investigated during this project. It is essential that further long term microstructural characterisation is carried out to further develop an understanding of how the microstructure of MarBN will evolve during long term ageing.

During the research project a number of welding trials were carried out to investigate if MarBN retains its improved mechanical properties after welding. These results are not

reported within the thesis. However, it is essential further work microstructural characterisation is carried out to optimise MarBN welds in a similar way to that of the parent material. In the first instance it is essential that matching welding filler is developed and a series of welding trials are carried out to determine the optimum heat treatment parameters to optimise the precipitates present within the microstructure. Secondly it is important that the pre-service heat treatment prior to welding is optimised along with the welding parameters to optimise the microstructure.

It would be desirable to quantify the size of the MX precipitates present after a pre-service heat treatment and after isothermal ageing. This information would provide a complete understanding about how all the phases evolve as a function of time.

The microstructural characterisation data acquired during this project has been invaluable in optimising MarBN. In the future this data should be linked with the creep data also generated during this project on multiple alloys, to produce a model to predict the long term creep properties. In order to develop and effective model it would be desirable to characterise the microstructure of MarBN alloys which have been creep tested in order to understand the effect of stress on the evolution of precipitates within the microstructure.

REFERNCES

1. Ennis, P. J. Recent advances in creep-resistant steels for power plant applications. *Sadhana Academy Proceedings in Engineering Sciences*, **28**, 709–730 (2003).

2. Abe, F. Utilization of Added B in 9Cr Heat-Resistant Steels Containing W. *ISIJ International* **42**, 67–71 (2002).

3. Vanstone, R. & Kern, T. Goals and market-expectations for fossil fired power plants and consequences on material development and research. *KMMVIN Consortium Meeting, Linz, 2011*

4. Shirane, T. *et al.* Ferrite to austenite reverse transformation process in B containing 9%Cr heat resistant steel HAZ. *Science and Technology of Welding and Joining* **14**, 698–707 (2009).

5. Miller, B. Clean Coal Engineering Technology, (2011), *Butterworth Heinemann*

6. J, Selwin Rajadurai. Thermodynamics and Thermal Engineering, (2003), *New Age International Publishers*

7. Abe, F. Behavior of Boron in 9Cr Heat Resistant Steel during Heat Treatment and Creep Deformation. *Key Engineering Materials* **345-346**, 569–572 (2007).

8. Abe, F., Tabuchi, M., Kondo, M. & Tsukamoto, S. Suppression of Type IV fracture and improvement of creep strength of 9Cr steel welded joints by boron addition. *International Journal of Pressure Vessels and Piping* **84**, 44–52 (2007).

9. Hald, J. Microstructure and long-term creep properties of 9–12% Cr steels. *International Journal of Pressure Vessels and Piping* **85**, 30–37 (2008).

10. Maruyama, K., Sawada, K. & Koike, J. Strengthening Mechanisms of Creep Resistant Tempered Martensitic Steel. **41**, 641–653 (2001).

11. Abe, F. Precipitate design for creep strengthening of 9% Cr tempered martensitic steel for ultra-supercritical power plants. *Science and Technology of Advanced Materials* **9**, 013002 (2008).

12. Sakuraya, K., Okada, H. & Abe, F. BN type inclusions formed in high Cr ferritic heat resistant steel. *Energy Materials: Materials Science and Engineering for Energy Systems* **1**, 158–166 (2006).

13. Masuyama History of power plants and progress in heat resistant steels. *ISIJ International* **41**, 612–625 (2001).

14. Honeycombe, R.W.K. & Bhadeshia, H.K.D.H. Steels: Microstructure and Properties, (2006), *Butterworth-Heinemann*.

15. Metastable Iron-Carbon (Fe-C) Phase Diagram. *http://www.calphad.com/iron-carbon.html.* Visited on 01/02/2013.

16. Huntz, A.M. *et al.* Effect of silicon on the oxidation resistance of 9% Cr steels. *Applied Surface Science* **207**, 255–275 (2003).

17. Richardot, D., Vaillant, J., Arbab.A, Bendick.W. The T92/P92 Book. Vallourec & Mannesmann Tubes, (2000).

18. Sanderson, S. J. Mechanical Properties and Metallurgy of 9%Cr 1%Mo Steel. *American Society for Metals 1:87 (1983)*

19. L.Li, "Microstructural Evolution of 9Cr Power Plant Steels", *PhD Thesis, Loughborough University, 2013*

20. Abe, F. Creep rates and strengthening mechanisms in tungsten-strengthened 9Cr steels. *Materials Science and Engineering: A* **319-321**, 770–773 (2001).

21. Taneike, M., Sawada, K. & Abe, F. Effect of Carbon Concentration on Precipitation Behavior of M 23 C 6 Carbides and MX Carbonitrides in Martensitic 9Cr Steel during Heat Treatment. **35**, (2004).

22. Semba, H. & Abe, F. Alloy design and creep strength of advanced 9%Cr USC boiler steels containing high concentration of boron. *Energy Materials: Materials Science and Engineering for Energy Systems* **1**, 238–244 (2006).

23. Abe, F., Kern, T. & Viswanathan, R. *Strengthening mechanisms in steel for creep and creep rupture*. *Creep-resistant steels* 279–301 (Woodhead Publishing Limited: 2008).

24. Klotz, U. E., Solenthaler, C. & Uggowitzer, P. J. Martensitic–austenitic 9–12% Cr steels—Alloy design, microstructural stability and mechanical properties. *Materials Science and Engineering: A* **476**, 186–194 (2008).

25. Hatterstrand, M. & Andre, H. Boron distribution in 9 – 12 % chromium steels. *Materials Science and Engineering A* **270**, 33–37 (1999).

26. Sakuraya, K., Okada, H. & Abe, F. Influence of Heat Treatment on Formation Behavior of Boron Nitride Inclusions in P122 Heat Resistant Steel. *ISIJ International* **46**, 1712–1719 (2006).

27. Yamada, K., Igarashi, M., Muneki, S. & Abe, F. Effect of Co Addition on Microstructure in High Cr Ferritic Steels. *ISIJ International* **43**, 1438–1443 (2003).

28. Kipelova, a. Y., Belyakov, a. N., Skorobogatykh, V. N., Shchenkova, I. a. & Kaibyshev, R. O. Structural changes in steel 10Kh9K3V1M1FBR due to creep. *Metal Science and Heat Treatment* **52**, 118–127 (2010).

29. Helis, L., Toda, Y., Hara, T., Miyazaki, H. & Abe, F. Effect of cobalt on the microstructure of tempered martensitic 9Cr steel for ultra-supercritical power plants. *Materials Science and Engineering: A* **510-511**, 88–94 (2009).

30. Mayer, K. & Masuyama, F. The development of creep-resistant steels. *in Creep-resistant steels* **Woodhead P**, 15–70 (2008).

31. Abe, F., Taneike, M. & Sawada, K. Alloy design of creep resistant 9Cr steel using a dispersion of nano-sized carbonitrides. *International Journal of Pressure Vessels and Piping* **84**, 3–12 (2007).

32. Petty E.R. Martensite: Fundamentals and Technology, Longman Publishing, 1970

33. Hu, P. *et al.* Study on Laves phase in an advanced heat-resistant steel. *Frontiers of Materials Science in China* **3**, 434–441 (2009).

34. Abe, F. Bainitic and martensitic creep-resistant steels. *Solid State and Materials Science* **8**, 305–311 (2004).

35. Rodak, K., Hernas, A. & Kiełbus, A. Substructure stability of highly alloyed martensitic steels for power industry. *Materials Chemistry and Physics* **81**, 483–485 (2003).

36. Bhadeshia, H.K.D.H. Design of Ferritic Creep-resistant Steels. *ISIJ International.* **41**, 626–640 (2001).

37. Ennis, P.J. & Zielin, A. The Influence of heat treatments on microstructural parameters and mechanical properties of P92 steel. *Materials Science and Technology.* **16**, 1226-1233 (2000).

38. Taneike, M., Abe, F. & Sawada, K. Creep-strengthening of steel at high temperatures using a dispersion of nano-sized carbonitrides. *Nature* **424**, 294–296 (2003).

39. Sawada, K., Taneike, M., Kimura, K. & Abe, F. Effect of Nitrogen Content on Microstructural Aspects and Creep Behavior in Extremely Low Carbon 9Cr Heat-resistant Steel. *ISIJ International* **44**, 1243–1249 (2004).

40. Sawada, K., Kubo, K. & Abe, F. Creep behavior and stability of MX precipitates at high temperature in 9Cr – 0 . 5Mo – 1 . 8W – VNb steel. *Materials Science and Engineering: A* **321**, 784–787 (2001).

41. Cipolla, L. *et al.* Conversion of MX nitrides to Z-phase in a martensitic 12% Cr steel. *Acta Materialia* **58**, 669–679 (2010).

42. Hald, J., Korcakova, L., Danielsen, H. K. & Dahl, K. V. Thermodynamic and kinetic modelling: creep resistant materials. *Materials Science and Technology* **24**, 149–158 (2008).

43. Korcakova, L., Hald, J. & Somers, M. a. . Quantification of Laves phase particle size in 9CrW steel. *Materials Characterization* **47**, 111–117 (2001).

44. Prat, O., Garcia, J., Rojas, D., Carrasco, C. & Inden, G. Investigations on the growth kinetics of Laves phase precipitates in 12% Cr creep-resistant steels: Experimental and DICTRA calculations. *Acta Materialia* **58**, 6142–6153 (2010).

45. Lee, J. S., Armaki, H. G., Maruyama, K., Muraki, T. & Asahi, H. Causes of breakdown of creep strength in 9Cr–1.8W–0.5Mo–VNb steel. *Materials Science and Engineering: A* **428**, 270–275 (2006).

46. Danielsen, H. K. & Hald, J. On the nucleation and dissolution process of Z-phase Cr(V,Nb)N in martensitic 12%Cr steels. *Materials Science and Engineering: A* **505**, 169–177 (2009).

47. Golpayegani, A., Andrén, H.-O., Danielsen, H. & Hald, J. A study on Z-phase nucleation in martensitic chromium steels. *Materials Science and Engineering: A* **489**, 310–318 (2008).

48. Sawada, K., Suzuki, K., Kushima, H., Tabuchi, M. & Kimura, K. Effect of tempering temperature on Z-phase formation and creep strength in 9Cr–1Mo–V–Nb–N steel. *Materials Science and Engineering: A* **480**, 558–563 (2008).

49. Kim, H. & Kim, I. S. Effect of Austenitizing Temperature on Microstructure and Me chanical Properties of 12% Cr Steel. *ISIJ International* **34**, 198–204 (1994).

50. Barraclough, D.R., D.J.Gooch. Effect of Inadequate Heat Treatment on Creep Strength of 12Cr-Mo-V Steel. *Materials Science and Technology*, 1:961 (1985).

51. Totemeier, T., Tian, H., Simpson, J. Effect of Normalising Temperature on the Creep Strength of Modified 9Cr-1Mo Steel. *Metallurgical and Materials Transactions A*. 37(5) 1519-1525 (2006).

52. Sanchez-Hanton, J. "Microstructural evolution in Grade 91 power plant steels," *PhD Thesis, Loughborough University*, 2007.

53. Tamura, M., IidaT, Kusuyama, H., Shinozuka, K. & Esaka, H. Re-dissolution of VN during Tempering in High Chromium Heat Resistant Martensitic Steel. *ISIJ International* **44**, (2004).

54. Shen, Y. Z. *et al.* Vanadium nitride precipitate phase in a 9% chromium steel for nuclear power plant applications. *Journal of Nuclear Materials* **374**, 403–412 (2008).

55. ASM Handbook Vol. 9. *ASM International* 621–625 (2004).

56. Callister, W.D. Materials Science and Engineering: An Introduction. *John Wiley & Sons* (2007).

57. TA Instruments - Thermo physical Properties DIL 805A/D. . *http://thermophysical.tainstruments.com/instruments/dilatometers/dil-805ad-quenching-and-deformation-dilatometer/ visited on 01/04/2010*

58. P, S. & Sundman, B. Thermo-Calc Software system. *(Thermodynamic Framework and Data)* **Thermocalc**, 2.27–2.29 (2008).

59. "Thermo-Calc software AB, TCFE6-TCS Steels/Fe-Alloys Database Version 6.2," 2010. http://www.thermocalc.com/res/pdfDBD/tcfe6fromtcfe5.pdf. Visited on 01/05/2010.

60. J. Goldstein, C. Lyman, D. Newbury, E. Lifshin, P. Echlin, L. Sawyer, D. Joy, and J. Micheal, Scanning Electron Microscopy and Microanalysis. *Kluwer Academic/Plenum Publishers*, 2003.

61. Dimmler, G., Weinert, P., Kozeschnik, E. & Cerjak, H. Quantification of the Laves phase in advanced 9–12% Cr steels using a standard SEM. *Materials Characterization* **51**, 341–352 (2003).

62. Orloff, J., Utlaut, M. & Swanson, L. High Resolution Focused Ion Beams: FIB and its Applications. *Kluwer Academic/Plenum Publishers* (2003).

63. Oxford Instruments Principal System Components. . http://www.ebsd.com/index.php/ebsd-explained/basics-of-ebsd/principal-system-components. Visited on 10/09/2013.

64. Dyson, D. X-Ray and Electron Diffraction Studies in Materials Science. *Maney Publishers*, 2004.

65. MacKenzie, D., & Totten, G. Analytical Characterization of Aluminium, Steel and Superalloys. *Taylor & Francis Publishers*, 2005.

66. Mayr, P. *et al.* Experience with 9Cr3W3CoVNbBN Base Material and Crosswelds at 650°C for Implementation in USC Power Plants. *3rd Symposium on heat Resistant Steels and Alloys for High Efficiency USC Power Plants 2009,* National Institute of Materials Science, Tsukuba, Japan (2009).

67. Albert, S. K. *et al.* Improving the Creep Properties of 9Cr-3W-3Co-NbV Steels and their Weld Joints by the Addition of Boron. **36**, 333–343 (2005).

68. Danielsen, H. K., Hald, J., Grumsen, F. B. & Somers, M. A. J. On the Crystal Structure of Z-Phase Cr (V , Nb) N. **37**, 2633–2640 (2006).

69. L.Li, "Microstructural Evolution of 9Cr Power Plant Steels", *PhD Thesis, Loughborough University, 2013*

70. Li, S. *et al.* Effect of thermo-mechanical treatment on microstructure and mechanical properties of P92 heat resistant steel. *Materials Science and Engineering: A* **559**, 882–888 (2013).

71. Sourmail, T. Precipitation in creep resistant austenitic stainless steels. *Materials Science and Technology*, **17**, (2001).

72. Steel, A. review of precipitation behaviour in A. type 316 stainless A review of precipitation behaviour in AISI type 316 stainless steel. *Materials Science and Engineering A* **61**, 101–109 (1983).

73. Li, L., Zhu, P., West, G. and Thomson, R. C. The effect of duration of stress relief heat treatments on microstructural evolution and mechanical properties in Grade 91 and 92 power plant steels. *ASM International* 14, 679 - 692 (2011)

74. Výrostková, a., Homolová, V., Pecha, J. & Svoboda, M. Phase evolution in P92 and E911 weld metals during ageing. *Materials Science and Engineering: A* **480**, 289–298 (2008).

LIST OF TABLES

LIST OF FIGURES